ACCESSIBILITY

OSLO METROPOLITAN UNIVERSITY
STORBYUNIVERSITETET

Master's Degree in

Structural Engineering and Building Technology

Department of Civil Engineering and Energy Technology

THESIS TITLE	DATE
Structural model updating of a historical stone masonry tower considering soil-structure interactions	06.08.2021
	NUMBER OF PAGES 107/40
AUTHOR(S) Mohyeddin Feyzabadi	SUPERVISOR(S) AmirHosein Shabani and Mahdi Kioumarsi

SUMMARY

Operational modal analysis (OMA) has been utilized in this thesis to extract the modal parameters of a historic masonry tower, "Slottsfjelltårnet," located in Tønsberg, Norway. “Slottsfjelltårnet” case study is a part of the Hyperion Project funded by the European Union’s Horizon 2020. In this study, the modal parameters identification has been carried out using ambient vibration test (AVT) data of some sensors installed on the tower. Also, the finite element model of the Slottsfjell tower has been modified to meet the requirements of this project. A complete sensitivity analysis has been carried out to investigate the most sensitive parameters of the structure before doing the model updating. The final purpose was to update the structure with and without considering soil-structure interaction effects to optimize the finite element model regarding reliable dynamic characteristics of the structure for future structural analysis.

3 KEYWORDS
Model updating
Operational modal analysis
Soil-structure interaction

Abstract

This thesis has been performed to investigate the dynamic properties of a historic masonry tower, "Slottsfjelltårnet," located in Tønsberg, Norway, to update the finite element model with and without considering the soil-structure interaction effects. The Slottsfjelltårnet" case study is a part of the Hyperion Project funded by the European Union's Horizon 2020.

Some operational modal analyses have been used to identify the main natural frequencies and corresponding mode shapes based on available AVT test results done by Agon Ademi [1]. Applying these methods helps to improve the understanding of the tower's dynamic structural behavior.

Moreover, different soil-structure interaction modeling techniques have been studied and used in modeling to investigate the effects of soil-structure interaction on the structure's dynamic characteristics. Three different models, one without and two with soil-structure interaction effects, have been used in the analysis.

Finally, the sensitivity analysis and the model updating of finite element models have been done. Sensitivity analysis has been carried out to investigate the most sensitive parameters of the structure before model updating. Then, the finite element model updating has been done, resulting in optimal material properties for each model. Model updating helps to have an accurate finite element model for future analysis of the Slottsfjell tower.

Foreword

This thesis has been conducted during the spring semester of 2021 to complete the master's program in Structural Engineering and Building Technology at Oslo Metropolitan University. The thesis aims to evaluate the dynamic properties and model updating of a historic masonry tower, "Slottsfjelltårnet," located in Tønsberg, Norway, considering soil-structure interaction.

I would like to express my sincere gratitude to my supervisors, Amirhosein Shabani and Mahdi Kioumarsi, for their valuable guidance and encouragement during this thesis. My warm thanks also goes to Eddy Dascotte from the Dynamic Design Solutions company for collaboration and technical support on FEMtools software. I would like to extend my thanks to Padova University for their cooperation in conducting laboratory tests on masonry stones.

Last but not least, I am deeply grateful to my family for their emotional support. Words cannot express how grateful I am to my beloved wife, Maryam, for her tremendous understanding, constant encouragement, and sacrifices. I also appreciate my lovely daughters, Salma and Samar, for tolerance and patience and for putting up with me being a part-time dad during my study. I sincerely thank my dear parents, grandmother, and sister for their love and prayers. Special thanks to my uncle for his motivation, cheerful mood, and continuous support during this adventure.

Finally, I am thankful to my classmates and teachers at Oslo Metropolitan University for making my two years of studying enjoyable.

June 8, 2021

Mohyeddin Feyzabadi

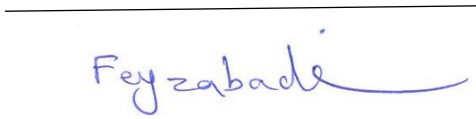

Table of Contents

List of Figures

List of Tables

Abbreviations

Artemis Modal	Artemis
E	Elasticity modulus
E_x	Elasticity modulus in x-direction
E_y	Elasticity modulus in y-direction
E_z	Elasticity modulus in z-direction
FB model	Fixed-based model
FE	Finite element
Floor1	Floor of the first story
Floor2	Floor of the second story
Floor3	Floor of the third story
G	Shear modulus
G_{xy}	Shear modulus in plane XY
G_{xz}	Shear modulus in plane XZ
G_{yz}	Shear modulus in plane YZ
NU	Poisson’s ratio
NU_{xy}	Poisson’s ratio in plane XY
NU_{xz}	Poisson’s ratio in plane XZ
NU_{yz}	Poisson’s ratio in plane YZ
Parameter-s	Sum of the parameters
Response-s	Sum of the responses
RHO	Density
Soil1	First part of the soil
Soil2	Second part of the soil
Soil3	Third part of the soil
Soil4	Fourth part of the soil
SB model	Soil-box model

SS model	Soil-spring model
UnquakeSuite	Unquake
Wall1B	Back wall of the first story
Wall1F	Front wall of the first story
Wall1L	Left wall of the first story
Wall1R	Right wall of the first story
Wall2B	Back wall of the second story
Wall2F	Front wall of the second story
Wall2L	Left wall of the second story
Wall2R	Right wall of the second story
Wall3B	Back wall of the third story
Wall3F	Front wall of the third story
Wall3L	Left wall of the third story
Wall3R	Right wall of the third story

Problem Statement

In this thesis, operational modal analysis (OMA) has been utilized to extract the modal parameters of a historic masonry tower, "Slottsfjelltårnet," located in Tønsberg, Norway. The modal parameters identification has been carried out using ambient vibration test (AVT) data of some sensors installed on the tower. Also, the available finite element model of the Slottsfjell tower has been modified to meet the requirements of this project. A sensitivity analysis has been carried out to investigate the most sensitive parameters of the structure before doing the model updating. The final purpose was to update the structure with and without considering the soil-structure interaction effects to optimize the finite element model regarding reliable dynamic characteristics of the structure for future structural analysis.

Chapter 1: Introduction

Nowadays, modern societies are very careful about historical buildings due to the importance of historical structures that reflect nations' history. They are representative of the religious, collective, and cultural history of human development which should be kept and transferred to the next generations. These heritage structures, such as mosques, cathedrals, and other historical monuments, are the best teachers of human being's culture, history, and civilization [2]. Masonry materials are one of the oldest materials for constructing historic structures [3]. Continuous protection and monitoring of human heritage regarding necessary precautionary activities should be done to preserve them against natural hazards and destructive phenomena like floods, earthquakes, fire, erosion, tornadoes, etc. [2].

Thanks to the significant development of computer software and hardware, new techniques for monitoring historical heritage have been used in recent years. Researchers have developed new methods such as operational modal analysis and ambient vibration testing to investigate the dynamic properties of historical masonry structures [2].

1.1 Objectives

The primary purpose of this study is to evaluate the dynamic properties and finite element model updating of a historic masonry tower, "Slottsfjelltårnet," located in Tønsberg, Norway.

To this aim, extracting the experimental modal parameters and identifying the main natural frequencies and related modes has been regarded as the first. It has been done through some operational modal analysis (OMA) techniques applied to the ambient vibration test (AVT) data using some accelerometers installed on the masonry tower case study. Agon Ademi, who has done the test data, reported in his master thesis that the experimental modal test has been performed accurately. It is essential for the modal analysis to accurately extract the dynamic parameters of the structure through the test data.

Modification of the available finite element model and extraction of numerical modal parameters have been regarded as the second part of the study. The available finite element model of the tower has been prepared using a 3D laser scanner, Autodesk Revit software, and Diana FEA software. To do the sensitivity analysis, model updating, and investigating the soil-structure interaction effects, some modifications have been made on the FE model of the tower to meet the requirements of the intended study's tasks adequately.

Two main soil-structure interaction modeling techniques have been studied as the third objective of this study to investigate the effects of soil-structure interaction on the structure's dynamic characteristics. Two different modeling scenarios, with and without soil-structure interaction effects, including two models considering soil-structure interaction effects (SB and SS models) and one without (FB model), have been used for analysis.

The last part of the thesis consists of sensitivity analysis and model updating of finite element models. Sensitivity analyses have been carried out to investigate the sensitivity of natural frequencies and corresponded mode shapes to a change in different material properties of the structure before doing model updating. Model updating results in obtaining optimal material properties, helps us have an accurate finite element model for future analysis of the tower.

1.2 Thesis Procedure

As shown in the below flow chart, the thesis consists of the following main steps:

1. Extracting the experimental modal parameters:

Identifying the main natural frequencies and corresponded mode shapes has been carried out using operational modal analysis (OMA) techniques applied to the ambient vibration test (AVT) results using some accelerometers installed on the masonry tower.

2. Extracting the numerical modal parameters:

Modifying the finite element model and extracting numerical modal parameters, including frequencies and mode shapes, have been regarded as the second step of the study.

3. Modeling the soil-structure interaction effects:

Two different soil-structure interaction modeling techniques, including the direct method and the subtructure method, have been studied and modeled in the third step of this study. The soil-structure interaction effects have been applied on two of three models to evaluate how the soil-structure interaction affects the structure's dynamic characteristics.

4. Doing sensitivity analysis:

A series of sensitivity analyses have been carried out to investigate the sensitivity of natural frequencies and corresponded mode shapes to a change in different material properties of the structure before doing model updating. Material properties considered in this study include modulus of elasticity, density, Poisson's ratio, shear modulus, and spring stiffness.

5. Model updating:

Based on the sensitivity analysis findings, model updating has been carried out to obtain optimal material properties. The updated finite element model will help us have an accurate finite element model for future analysis of the Slottsfjell tower.

Figure 1 flow chart provides a visual overview of the thesis procedure, including the main steps of the study.

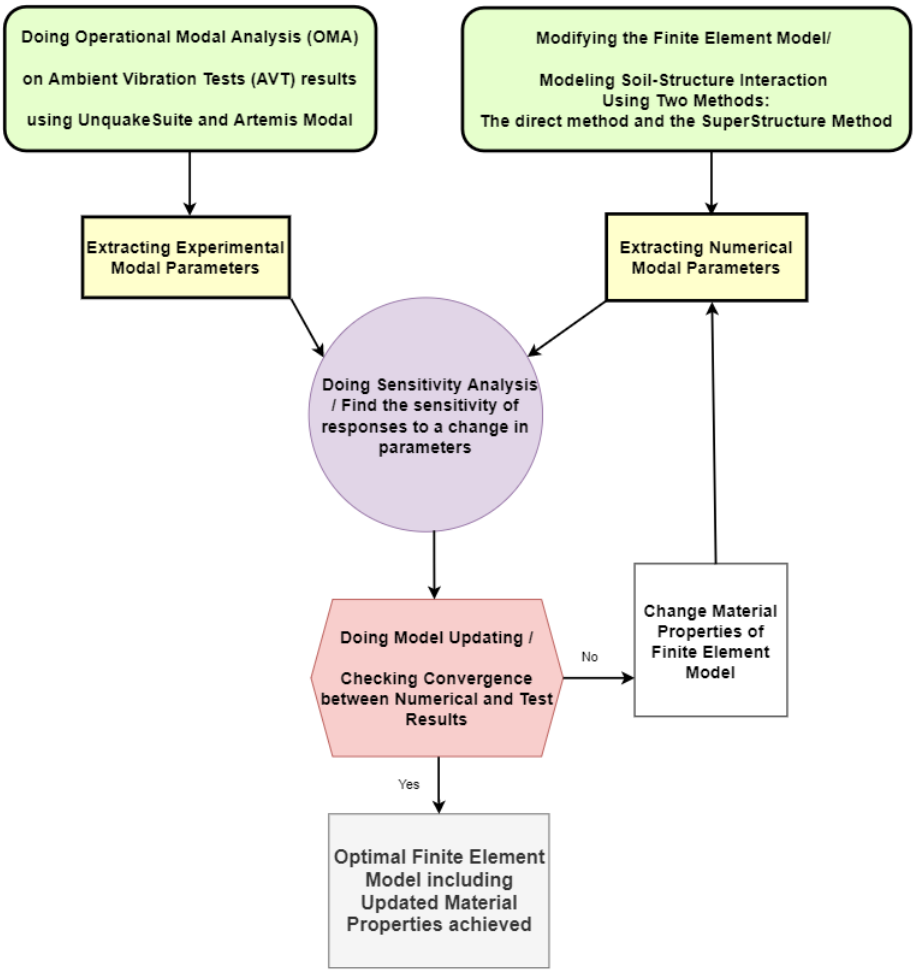

Figure 1 Flow chart of thesis procedure

1.3 Thesis Structure

The thesis consists of eight chapters and three appendixes. A short description of each chapter and appendix has been presented in the following.

Chapter 1: Introduction

In the first chapter, a description of the thesis objectives, thesis procedure, and thesis structure has been presented.

Chapter 2: Background

The second chapter summarizes the theoretical basis and the literature related to the thesis subject. This chapter first describes finite element analysis and modal analysis, followed by a description of operational modal analysis and some techniques. Furthermore, the soil-structure interaction effect and its main methods, including direct and substructure methods, have been shortly presented. Lastly, model updating has been described in this chapter.

Chapter 3: Case Study and Geometrical Survey

The third chapter provides an overview of the Slottsfjell tower and the 3D geometrical survey done on the case study.

Chapter 4: Numerical Modeling

The fourth chapter describes how the numerical modeling has been made and imported into different software. Also, a detailed explanation of computational modeling, including general descriptions as well as material properties, boundary conditions, structure sets, modeling of soil-structure interaction effects, and numerical modal analysis, have been given.

Chapter 5: Operational Modal Analysis

The fifth chapter gives explanations on how AVT has been done on the structure. Also, the chapter includes the software and the results of modes identification, including natural frequencies and corresponded mode shapes.

Chapter 6: Sensitivity Analysis

In the sixth chapter, sensitivity analysis with its steps, procedures, results, and related discussions have been presented.

Chapter 7: Model Updating

The seventh chapter covers the model updating procedure and results.

Chapter 8: Conclusion and Future Works

The conclusion of this study with future works has been described in the eighth chapter.

Appendix 1:

Appendix 1 presents the FFT results of Unquake software for different sensors in x and y directions.

Appendix 2:

In appendix 2, the time histories of twelve measured channels, including six accelerometers in x and y directions, have been shown.

Appendix 3:

Sensitivity graphs of frequencies and corresponded mode shapes to a change in material properties, including elasticity modulus, Poisson's ratio, density, shear modulus, and spring stiffness, have been presented in appendix 3.

Chapter 2: Background

2.1 Finite Element Analysis

To investigate the performance of structures under different conditions, numerical modeling of complex models has become an essential topic of structural design in engineering sciences. The finite element method is generally considered a reliable technique for numerical modeling in engineering design [4]. The finite element method is the best and the most versatile tool for modeling complex structures [5], [6]. In today's engineering society, the finite element is the most popular numerical simulation since it is a flexible method with a considerable capability to check how accurate the model is [7].

Finite element as computational modeling consists of four main procedures, including geometrical modeling, meshing process, defining the material properties, and identifying the load and boundary conditions [8].

In the finite element method, geometrical discretization and dividing the structure into elements with known dynamic responses are done through meshing. The dynamic behavior of structures can be estimated using the response of these elements [8].

Dynamic parameters of the structure consist of natural frequency, mode shape, and damping ratio. The structure tends to vibrate at its natural frequencies with corresponded vibration patterns called mode shapes which may change for every frequency. The damping ratio defines how the vibrations of the structure decay. Dynamic properties evaluation can be done using modal analysis methods.

Although the engineers try to make the most accurate models they can, the accuracy of the finite element models still demands greater importance. Therefore, to model the dynamic behavior of structures, the approximation assumptions should adjust the structural characteristics with keeping the model accuracy. These approximations involve all the modeling procedures, from geometrical modeling to boundary conditions. The engineers should validate the accuracy of finite element modeling with the experimental data done on the structure [7].

2.2 Modal Analysis

As already mentioned, modal analysis is used to define the dynamic properties of a structure, including natural frequencies and corresponding mode shapes.

Two main modal analysis methods include operational modal analysis (OMA) and experimental modal analysis (EMA). EMA method obtains dynamic characteristics of the structure using artificial input forces by vibrating tools such as hammers or shakers to excite the structure and measure the response. EMA method is called the input-output method for the identification of structural modal parameters [9].

EMA has many limitations to be applied to actual structures, from high cost to difficulties in artificially exciting large physical projects regarding their dimensions and operating conditions. It was originally regarded as a laboratory-based experiment where one can get the responses from artificial excitations using different signal processing techniques. In this sense, due to differences in laboratory and field conditions, researchers and engineers preferred to proceed with a new method that reflects the real operational situations called OMA [10].

OMA had been introduced as an output technique, a modal identification method based on only the measured response regardless of inputs [11]. It is also called the ambient response method, which can be done using ambient vibration testing (AVT) results [12]. Since AVT is a non-destructive testing method, it has turned into the most suitable experimental method of dynamic assessment of historic structures. No external vibration affects the structure in the AVT method, and it only uses environmental excitations such as the passage of vehicles and wind [13].

2.2.1 Operational Modal Analysis (OMA)

Based on AVT results, OMA procedures can be used to identify dynamic parameters of the structure. OMA procedures can be one using both frequency and time domains from which stochastic subspace identification (SSI), principal component (PC), unweight principal component (UPC), and random decrement (RD) methods are the most famous techniques of the time domain. Also, there are some well-known techniques in the frequency domain platform, such as frequency domain decomposition (FDD), enhance frequency domain decomposition (EFDD), curve-fitted enhanced frequency domain decomposition (CFDD), and peak picking (PP) methods.

2.2.1.1 Frequency Domain Decomposition (FDD)

The Frequency Domain Decomposition (FDD) method is one of the frequency domain techniques of operational modal analysis proposed by Brincker et al. [14].

Developing two previous techniques, including primary frequency domain and peak picking methods, the frequency domain decomposition method has been introduced by defining a series of single degree freedom systems related to different structure modes as different responses. Using singular value decomposition (SVD) of varying power spectral density (PSD) matrix applied on the output response, other modes of vibrating of the structure can be obtained. This method gives more accurate results in some cases, such as geometrically orthogonal spacing of mode shapes, small damping values, and white noise loading of the structures. However, in cases where the above conditions are not met, this method is still more accurate than previous techniques [14].

2.2.1.2 Enhanced Frequency Domain Decomposition (EFDD)

Following the previous research, Brincker et al. introduced an updated FDD technique named the enhanced frequency domain decomposition (EFDD) method to obtain the damping ratio value of the structure in addition to the natural frequencies and mode shapes [15].

In this method, the natural frequencies and mode shapes can be found in a more accurate way besides the damping ratio from the power spectral density (PSD) function, which turns into the time domain by using the inverse discrete Fourier transform (IDFT). In this method, the crossing times are used to estimate the natural frequencies. Also, the initial value of the correlation function and the logarithmic decrement would be used to estimate the damping ratio of the structure using the EFDD technique [15].

2.2.1.3 Curve-Fitted Enhanced Frequency Domain Decomposition (CFDD)

An enhanced FDD method named Curve-Fitted Enhanced Frequency Domain Decomposition (CFDD) has been defined to incorporate the harmonic excitation in the system. A frequency response function estimation of a single degree of freedom is used with linear interpolation of harmonic components through a singular value decomposition plot to obtain modal parameters of the system by the CFDD technique [16].

2.2.2 OMA Studies on Historical Structures

Many studies on applying different OMA techniques to identify modal parameters of historical structures have been reported in the literature. Some of them have been shortly reviewed in this section.

Jaishi et al. have used the peak picking (PP) and stochastic subspace identification (SSI) methods to obtain modal parameters of ten multi-tiered masonry temples in Nepal. The ambient vibration test (AVT) has been used to find the dynamic properties of three masonry towers due to wind excitations and updated the finite element model of the towers to find the optimum parameters of the FE model and proposed an empirical formula for natural period estimation of the towers [17].

Ramos et al. have investigated the structural health monitoring of the Saint Torcato church in Guimaraes, Portugal, where many in-situ tests were done, and FDD, EFDD, and CC-SSI techniques were used to find modal parameters of the building. Based on obtained parameters from the experimental test results, they updated the FEM model of the church for further simulations of the structure model [18].

Min et al. investigated the dynamic properties of a historical wooden castle using FDD and SSI modal parameters identification methods on AVT results. A story stiffness method for structural health monitoring has been proposed in their research that would apply to all other historical structures [19].

Compan et al. used ambient vibration tests on the historical masonry building in Germany. The SSI and EFDD techniques of operational modal analysis were applied to find the modal parameters of the structure. A good MAC range for the two methods was gained, and the results were presented [20].

Cimellaro et al. studied the dynamic characteristics of a historical masonry palace in Italy with data from some ambient vibration tests. The FDD, RD, NExT combined with ERA methods were applied to identify the modal parameter of the structure, followed by calibration of the finite element model [21].

Reviewing the literature reveals that many studies have used FDD, EFDD, and CFDD techniques of operational modal analysis to identify modal parameters. It has been proven that these techniques can be used to estimate the modal parameters of the historical structures accurately and adequately.

2.3 Soil-Structure Interaction

It is common to use fixed-based boundary conditions in either initial design and analysis of the structures or when there is not enough information about the geotechnical situation of the structure [22]. Since the buildings are usually laid at the ground supported by a foundation, it has been reported in the literature that the soil properties of the ground affect the structural behavior of the buildings [23]. Therefore, it is essential to investigate and consider the effects of the soil-structure interaction on the dynamic properties of the structure.

Different approaches for dealing with soil-structure interaction effects, from the time-domain vs. frequency domain, linear vs. nonlinear, discrete vs. continuum to direct and substructure method. The last method which is based on the fundamental differences of considering soil-structure interaction effects can be regarded as a reference method studying these effects [24].

2.3.1 Direct Method

In the direct method, three main parts of the system, including the soil, the structure, and the foundation (if considered), form a complete simulation model. Using finite elements for simulating the soil layers needs appropriate properties for soil deposit and proper boundary conditions for the soil part [23].

Although the direct method is the most accurate method of modeling the soil-structure interaction effects, it has some difficulties in simulations. It may need high computational cost and time, which should be considered when analyzing complex case studies. It has also been reported that this method can better model the complex geometries and various loading conditions in the structure than other methods [23].

2.3.2 Substructure Method

The system's main parts have been regarded to be modeled and analyzed separately in the substructure method. The soil layers in this method would be modeled using springs and dashpots. Using the substructure method, one should equivalence the soil properties by the spring and dashpot inputs using proposed formulas in the literature [23].

2.4 Model Updating

Providing an accurate numerical model for a structure is essential when an engineer wants to simulate the actual situation of the structure in the design and analysis. There would be some uncertainties in every numerical model, including boundary conditions, geometries, and material properties. The models should be calibrated with the experimental test results to remove uncertainties and increase accuracy [7]. Specifically for the heritage structures, it is essential to have an updated numerical model according to the current situation of the structures [25].

A flow chart of model updating procedures reported in the literature has been presented in Figure 2 [26].

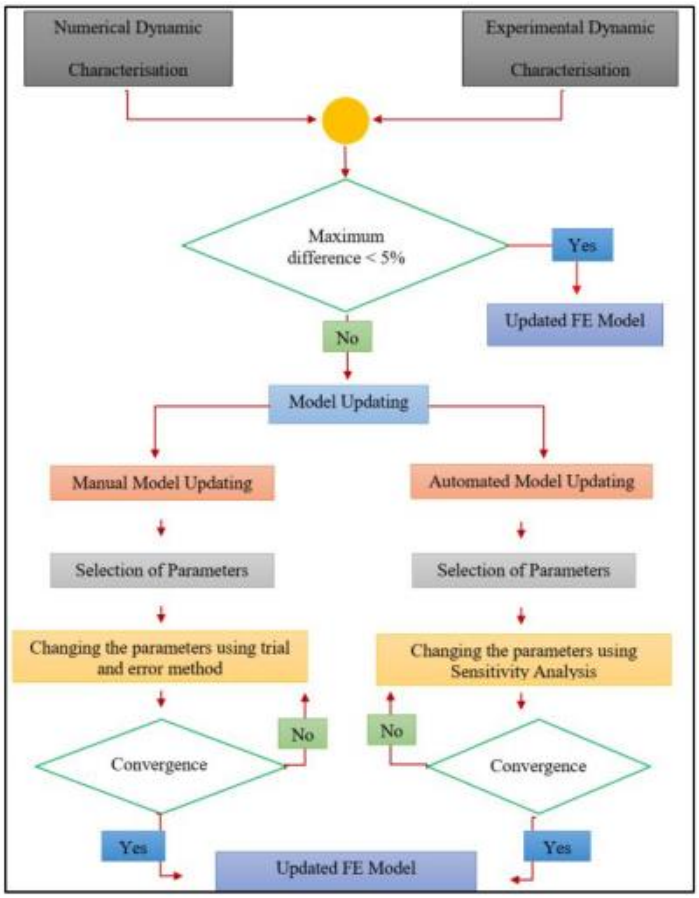

Figure 2 Flow chart of model updating using AVT and OMA techniques [26]

Using automated model updating with selected parameters from sensitivity analyses is the most common way of doing model updating reported in the literature, which is the basis of the following studies.

Votsis et al. used AVT results to update the finite element model of two monuments in Cyprus. The elasticity modulus has been found as the most influential parameter on the responses [27].

Foti et al. performed AVT on a historical tower in Italy to do model updating. Using sensitivity analysis, they regarded the elasticity modulus and density of different zones as the most influential parameters on the structure’s responses. Different updated values for each zone's elasticity modulus and structure density have been found and presented [28].

Ramos et al. conducted structural health monitoring research at a historical church in Portugal. The elasticity modulus of the structure and soil underneath has been regarded as updating parameters, and optimized values have been presented [29].

Also, Conde et al. performed some non-destructive experimental testing, sensitivity analysis, and model updating of the finite element model of a masonry arch bridge in Spain. The elasticity modulus of different bridge parts has been considered as updating parameters, and the updated values have been presented [30].

Chapter 3: Case Study and Geometrical Survey

3.1. The Slottsfjell Tower Case Study

The Slottsfjell tower is a high masonry tower situated in Tønsberg, a city in the municipality of Vestfold and Telemark county [31].

Figure 3 The Slottsfjell tower [32]

Tønsberg has a population of 53,018 in 2020, which is the most populous city in the Vestfold and Telemark county. Tønsberg is also the tenth-largest urban area and the seventeenth largest city of Norway. Also, Tønsberg is the headquarters for the municipality of Vestfold and Telemark county. The municipality borders are on Horten and Holmest in the north, on the municipalities of Sandefjord and Larvik in the west, and the Færder in the south. The Oslo Fjord is in the East of Tønsberg is and the middle fjord borders the municipality of Moss, Råde, and Fredrikstad. The Vestfold and Telemark county is located in the south of Norway and approximately 100 kilometers in the southwest part of Oslo, the capital of Norway [31].

Tønsberg houses Tønsberg Fortress on Castle Mountain, which contains Castrum Tunsbergis, Norway's largest castle in the 13th century. Also, Tønsberg is home to the Oseberg Mound, where a well-preserved Viking ship named Oseberg ship was excavated in the 9th century [31].

Based on what has been mentioned in the Slottsfjell Museum, which is responsible for the daily operation and dissemination of the Slottsfjell Tower, the tower itself is from 1888. Still, it symbolizes the Castle Mountain area's connection to the Middle Ages. The tower is centrally located in ruin park and is one of the largest medieval castles in the Nordic countries [32].

The Slottsfjell tower was the center of the royal power and the country's government for several years during the Middle Ages period [32].

3.2 Geometrical Survey

Gentile et al. (2015) mentioned that investigating the ongoing health condition of the historical buildings is the first step of doing successful structural health monitoring. This stage consists of the following activities [33]:

- Study the history of the case study in addition to investigating the current on-site condition of the case study to gather knowledge management-based documentation of all geometrical changes in the building regarding the construction technology
- Investigating the preservation situation of the structure through visual inspections. Visual inspections help to check the health condition of the structure concerning the possible crack pattern and scrutinizing the discontinuities in the materials and the overall structure
- Carrying out some non-destructive tests (NDT) on the structure's materials in the laboratory or at the site to find out the material's characteristics

Visual inspection is an important step of the geometrical survey, which helps to obtain information about the current condition and the history of the structure [34]. In this sense, visual inspection of the Slottsfjell tower case study has already been done before doing ambient vibration testing (AVT) (Figure 4), and the overall health condition of the building is well detected. No visible cracks or discontinuities have been detected. Also, a good connection between the masonry unit and mortar has been observed [1].

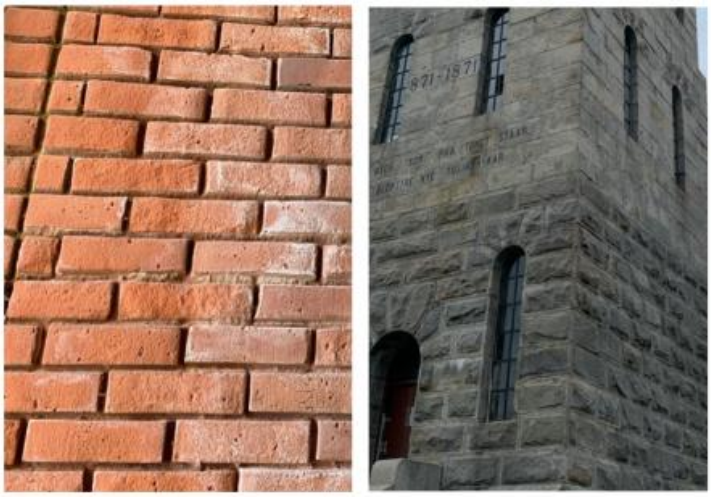

Figure 4 Internal and external material layout of the Slottsfjell tower [1]

Performing 3D geometrical surveys using laser scan and point clouds technologies, the structure has been appropriately modeled in FE Diana software by Agon Ademi in his master thesis [1]. The procedure has been shown in Figure 5.

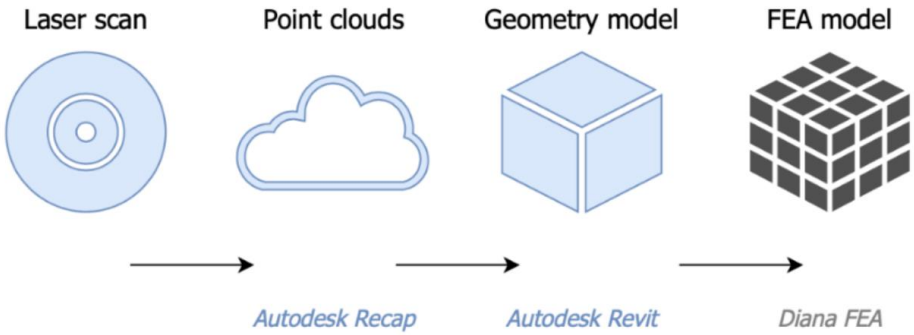

Figure 5 Laser scan and point clouds technologies [1]

GLS-2000 series 3D laser scanner has been used to do laser scanning of the structure as the first step of the geometrical survey (Figure 6).

Figure 6 3D laser scanner calibrated on the outside of the Slottsfjell tower [1]

In the second step, the point clouds were then imported and merged into the Autodesk Recap to produce the complete 3D model.

Figure 7 3D model of the Slottsfjell tower in Recap [1]

Importing the built point cloud model into Autodesk Revit forms the third step of work as shown in Figure 8.

Figure 8 Point clouds imported from Recap into Revit [1]

The last step comprises importing the Revit file into Diana FEA software [1]. The final 3D Revit model with measured dimensions has been shown in Figure 9, which illustrates that the structure is symmetric and quadratic.

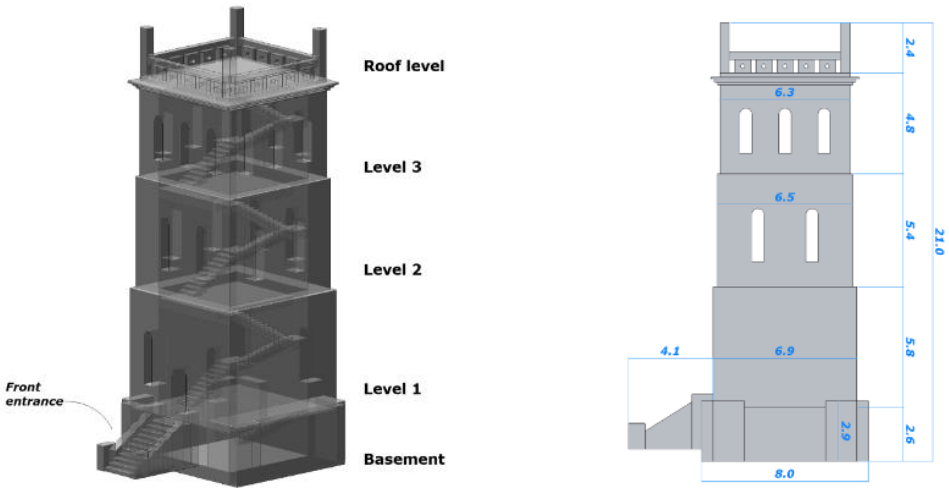

Figure 9 Final 3D Revit model with dimensions [1]

Based on Figure 9, the main dimensions of the tower have been stated in Table 1.

Table 1 Main dimensions of the Slottsfjell tower

Element	Plan Area (m^2)	Height (m)
Roof	6 x 6	2.4
Level 3	6.3 x 6.3	4.8
Level 2	6.5 x 6.5	5.4
Level 1	6.9 x 6.9	5.8
Basement	8 x 8	2.6

Chapter 4: Numerical Modeling

4.1 Importing the Model from Autodesk Revit into Diana FEA

The following procedure has been followed in Agon's thesis to import the model from Autodesk Revit into Diana FEA [1].

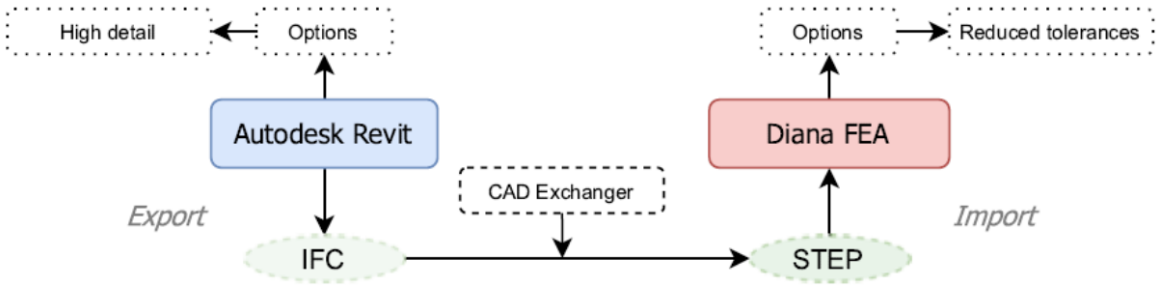

Figure 10 Model importing procedure from Autodesk Revit into Diana FEA [1]

Some modifications have been done on the available finite element model to create better-shaped mesh elements before proceeding with the model in the second step.

Secondly, the finite element models have been imported to FEMtools using a program script designed by the FEMtools support team named "impdiana.bas". This script contains the reader's source code, which helps import the finite element model from Diana to FEMtools. The script then has been modified and extended as needed for incorporating the soil-structure interaction effects.

4.2 Computational Modeling

4.2.1 Model Types

Two scenarios have been investigated and compared to investigate the soil-structure interaction effects on the simulations. The first scenario is related to models without soil-structure interaction effects, while the second scenario includes soil-structure interaction effects. As a result, three different models have been used in this study as follows:

Model 1: The first model, called the fixed-base model (FB model), does not include soil-structure interaction effects. In this case, the structure is fixed at the base of the model against movement and rotation.

Model 2: The second model, called the soil-box model (SB model), considers the soil-structure interaction effects using a direct analysis approach as soil-structure interaction methodology.

Model 3: Vertical springs as the representative of the soil behavior in the substructure method have been included in the third model, called the soil-spring model (SS model).

A schematic of three models has been shown in Figure 11.

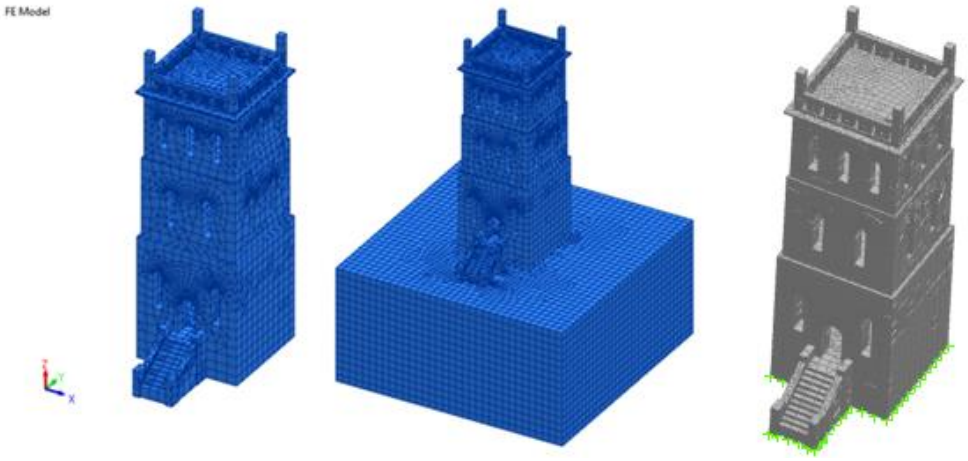

a) *b)* *c)*

Figure 11 Different model types used in the study, a) FB model, b) SB model, and c) SS model

4.2.2 Axis Definition

The orientation of the axes is shown in Figure 12. The x and y axes are horizontal, and the z-axis is vertical. It should be mentioned that x, y, and z refer to global x, y, and z directions.

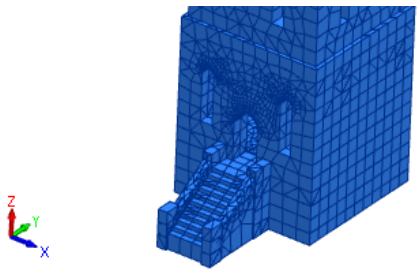

Figure 12 Definition of axes

4.2.3 Discretization

Regarding the mesh size, which controls the number of elements in the finite element method, an optimal element mesh size of 0.65 m was chosen for all the models. This mesh size was determined after comparing the modal analysis results on the models with variations of less than 5%.

3D modeling of the structure, foundation, and soil has been made using solid Diana and FEMtools software elements.

The tower has been modeled using different types of 3D solid elements, including 4-node tetrahedron (TETR4), 8-node hexahedron (HEXA8), and 6-node pentahedron (PENT6) elements (Figure 13). The FB, SB, and SS models consist of 66676, 93832, and 66286 elements. The number of different element types used for each model has been presented in Table 2.

Table 2 Number of different element types used in the models

Model / Element	FB model	SB model	SS model
TETR4	60655	68013	60119
HEXA8	4128	23820	4336
PENT6	1893	1999	1831
Total	66676	93832	66286

For modeling the soil layers in the SB model, 28819 out of 93832 is used, consisting of 18844 HEXA8 elements, 3026 PENT6 elements, and 6949 TETR4 elements.

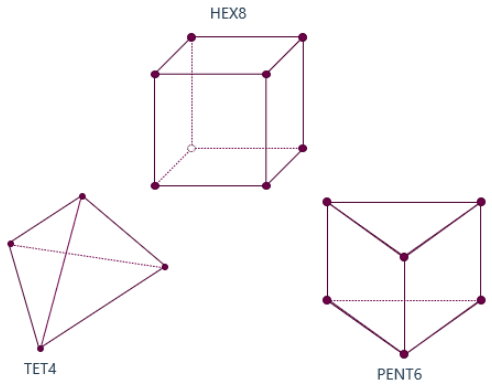

Figure 13 Different 3D solid element types used in the FE models [35]

4.2.4 Material Properties

Although masonry is an inhomogeneous material composed of mortar joints and individual masonry units, it has been assumed as homogenous material in this study. Based on the obtained findings in the model updating chapter, orthotropic elastic behavior has been considered for the masonry structure in all three models. The results of the testing samples on the masonry unit of the Slottsfjell tower have been discussed in the next section.

4.2.4.1 Masonry Stone Results

Elastic-mechanical characteristics of the syenite masonry stone as an intrusive rock have been measured by non-destructive tests using ultrasonic testing at the Padova University. Ultrasonic

waves were transmitted in the three perpendicular directions of the cubic samples (edge: 50 mm) using an EPOCH650® ultrasonic flaw detector (olympus) to find the propagation velocities V_p (compression pulse) and V_s (shear pulse). Figure 14 shows the instrumentation tool and masonry stone sample.

Measurements were performed with transducers of 0.5 MHz over a circular contact surface of 3 cm in diameter. A viscoelastic couplant (an ultrasound eco-gel) was used for effective coupling between the transducers and the sample surfaces.

a) *b)*

Figure 14 a) Masonry syenite stone samples, b) EPOCH650® ultrasonic flaw detector (olympus)

The propagation velocities Vp1, Vp2, and Vp3 (compression pulses) were measured along the three perpendicular directions of the cube-shaped samples (50 mm edge, Figure 15) to determine structural anisotropies as follows:

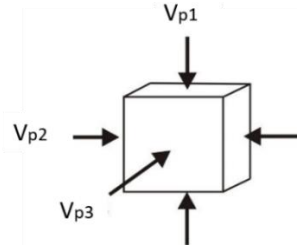

Figure 15 A scheme of the propagation velocities Vp1, Vp2, and Vp3 (compression pulses) along with the three perpendicular directions of a cube-shaped sample.

where Vp1 is the maximum propagation velocity, Vp2 is the mean propagation velocity, and Vp3 is the minimum propagation velocity.

Measurements were performed with transducers of 0.5 MHz over a circular contact surface of 3 cm in diameter. A viscoelastic couplant (an ultrasound eco-gel) was used for good coupling between the transducers and the brick surfaces. Poisson's ratio (ν), and elasticity modulus (E), shear modulus (G), and bulk modulus (K) were then calculated from measured wave velocities V_p and V_s, according to the following equations:

$$\text{Poisson's coefficient } (\nu) = \frac{(\frac{V_p}{V_s})^2 - 2}{2\,[(\frac{V_p}{V_s})^2 - 1]} \quad \text{(Eq.1)}$$

$$\text{Elasticity modulus } (E) = 2\rho_b V_s^2\,(1+\nu) \quad \text{(Eq.2)}$$

$$\text{Shear modulus } (G) = \frac{E}{2(1+\nu)} \quad \text{(Eq.3)}$$

$$\text{Bulk modulus } (K) = \frac{E}{3(1-2\nu)} \quad \text{(Eq.4)}$$

where ρ_b is the bulk density (Kg/m^3) (according to the values determined by mercury intrusion porosimetry).

Porosity (open porosity, P_o in %) and density (bulk and skeletal densities, ρ_b and ρ_{sk}, respectively) were determined by Mercury Intrusion Porosimetry (MIP) on a Thermo Scientific Pascal 140-240 apparatus on freshly cut samples of approximately 1.5 cm^3.

Table 3 shows the results obtained for the physical and elastic-mechanical parameters.

Table 3 Obtained results for masonry stone sample

Property	Value
ρ_b	2720
ρ_{sk}	2745
P_o	0.455
Vp1	4777
Vp2	4824
Vp3	4986
ΔM	3
Δm	3
Vp	4862
Vs	2874
ν	0.23
E	56.08
G	22.77
K	34.81

where ρ_b is the bulk density (Kg/m^3), ρ_{sk} is the skeletal density (Kg/m^3), Po is the open porosity (%), Vp1 is the maximum propagation velocity, Vp2 is the mean propagation velocity, and Vp3 is the minimum propagation velocity, ΔM is the total anisotropy, Δm is the relative anisotropy, Vp is the average compressional propagation velocity of ultrasonic pulses, Vs is the average shear propagation velocity of ultrasonic pulses, ν is the Poisson's ratio (GPa), E is the elasticity modulus (GPa), G is the shear modulus (GPa), and Kis the bulk modulus (GPa).

4.2.4.2 Material Properties of Masonry and Soil

According to the laboratory test results, the approximate elasticity modulus and density have been regarded as 60 Gpa and 2700 Kg/m^3.

The proposed elasticity modulus value for strong mortar of flagstone reported by Felix [36] equal to 11,3 Gpa has been regarded as the elasticity modulus of the mortar part in this study.

Using the following formulas proposed by Ciesielski et al. representing the correlation between the elasticity modulus of the masonry, the mortar, and the unit [37], the elasticity modulus of the masonry unit has been assumed to be around 40 Gpa.

$$E_{mas} = \frac{1{,}20.E_b.E_m}{0{,}2.E_b+E_m} \quad \text{(Eq.5)}$$

$$\frac{1}{E_{mas}} = \frac{0{,}86}{E_b} + \frac{0{,}14}{E_m} \quad \text{(Eq.6)}$$

where E_m is the elasticity modulus of mortar, E_b is the elasticity modulus of the masonry unit, and E_{mas} is the elasticity modulus of the masonry.

Therefore, the initial material properties for masonry and soil parts have been illustrated in Table 4.

Table 4 Material properties of a) masonry, b) soil

a)

Property	Sign	Value
Mass density	RHO	2700 Kg/m3
Young's modulus in direction X	EX	40 Gpa
Young's modulus in direction Y	EY	40 Gpa
Young's modulus in direction Z	EZ	40 Gpa
Shear modulus in plane XY	GXY	13.33 Gpa
Shear modulus in plane XZ	GXZ	13.33 Gpa
Shear modulus in plane YZ	GYZ	13.33 Gpa
Poisson's ratio in plane XY	NUXY	0.2
Poisson's ratio in plane XZ	NUXZ	0.2
Poisson's ratio in plane YZ	NUYZ	0.2

b)

Property	Sign	Value
Mass density	RHO	2700 Kg/m3
Young's modulus in direction X	EX	6 Gpa
Young's modulus in direction Y	EY	6 Gpa
Young's modulus in direction Z	EZ	6 Gpa
Shear modulus in plane XY	GXY	2 Gpa
Shear modulus in plane XZ	GXZ	2 Gpa
Shear modulus in plane YZ	GYZ	2 Gpa
Poisson's ratio in plane XY	NUXY	0.25
Poisson's ratio in plane XZ	NUXZ	0.25
Poisson's ratio in plane YZ	NUYZ	0.25

4.2.5 Boundary Conditions

There are two scenarios for modeling the boundary conditions in this study, models with and without soil-structure interaction effects. The models considering soil-structure interaction effects consist of two different models arising from the direct and substructure methods of modeling the soil-structure interaction effect.

4.2.5.1 Model without Soil-Structure Interaction Effects

The model's base has been constraint against movement and rotation, as shown in Figure 16.

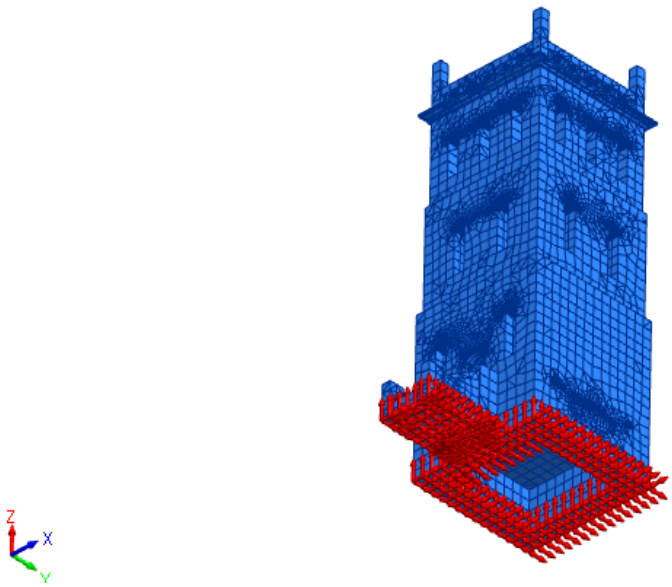

Figure 16 Boundary conditions / FB model

4.2.5.2 Model with Soil-Structure Interaction Effects

4.2.5.2.1 Direct Method

Regarding the dimension of the soil box, the depth and the length have been considered larger than 1,5 and 3 times the dimension of the foundation according to the recommendation by Choiniere et al. [38]. In this case, the depth and length of the soil box have been taken as 11 m and 22 m, respectively (Figure 17). Also, fixed base boundary conditions were applied to the base of the soil box and roller boundary conditions for the vertical sides based on Awlla et al. [39].

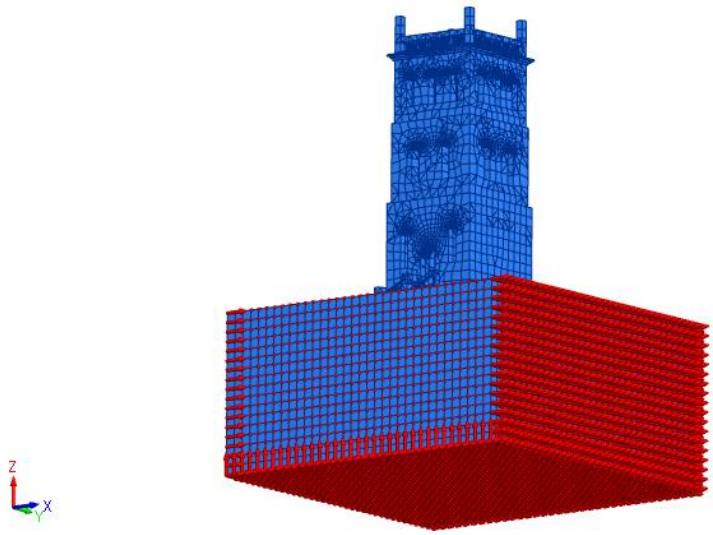

Figure 17 Boundary conditions / SB model

4.2.5.2.2 Substructure Method

Applying the Winkler model method for soil-structure interaction modeling in the finite element model, the springs are modeled beneath the superstructure with subgrade reaction modulus (k) in three different directions. The subgrade reaction modulus (k) calculated from the following formula [40] equals 0.8 Gpa.

$$k = \frac{E_s}{B.(1-\nu_s{}^2)} \qquad \text{(Eq.7)}$$

where E_s is the elasticity modulus of soil, B is the foundation length, and ν_s is the Poisson's ratio.

The boundary conditions of substructure method models have been shown in Figure 18.

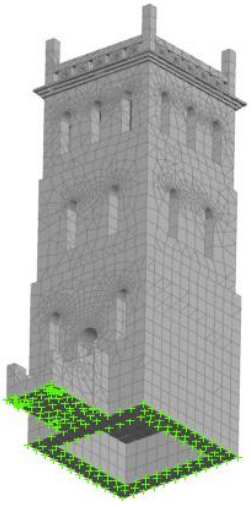

Figure 18 Boundary conditions / SS model

4.2.6 Sets

Different sets have been created for the FB, SB, and SS models, as shown in Figure 19 to Figure 24, so that model updating can be done successfully. The importance of sets will be discussed later in the model updating chapter.

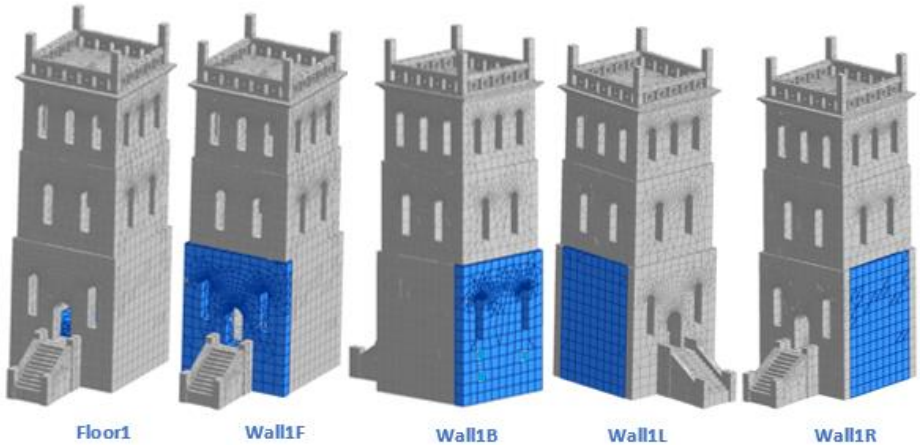

Figure 19 Sets of the first floor / all models

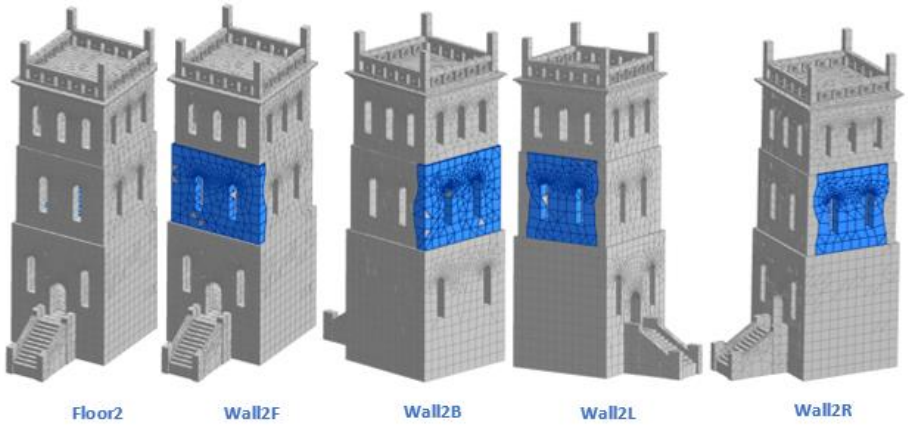

Figure 20 Sets of the second floor / all models

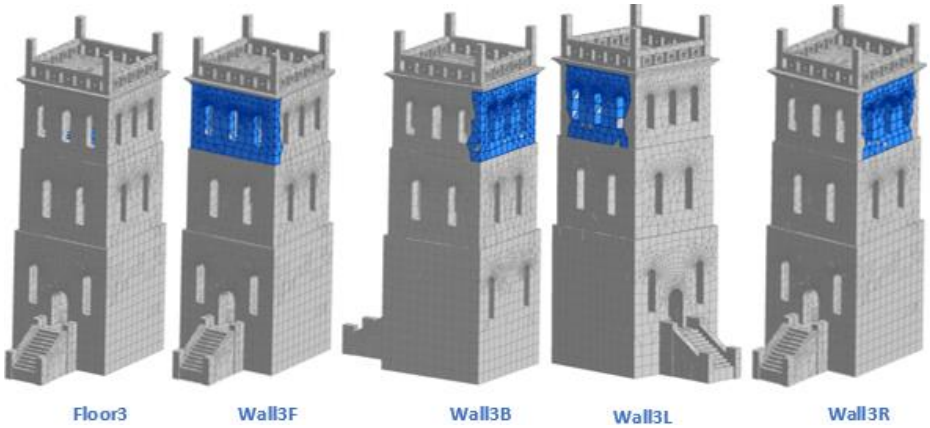

Figure 21 Sets of the third floor / all models

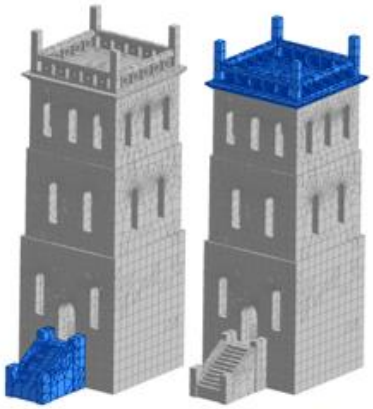

Figure 22 Sets of entrance and roof / all models

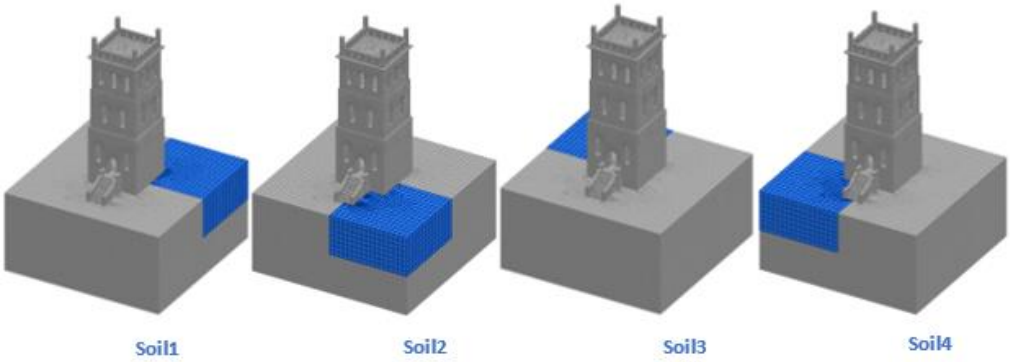

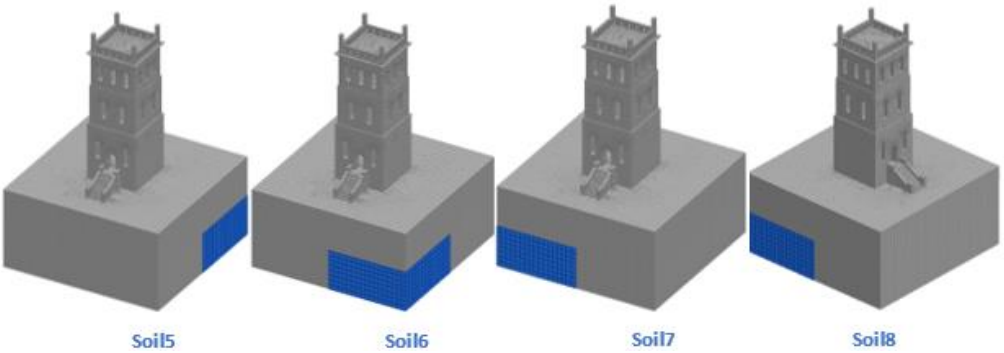

Figure 23 Sets of soil / SB model

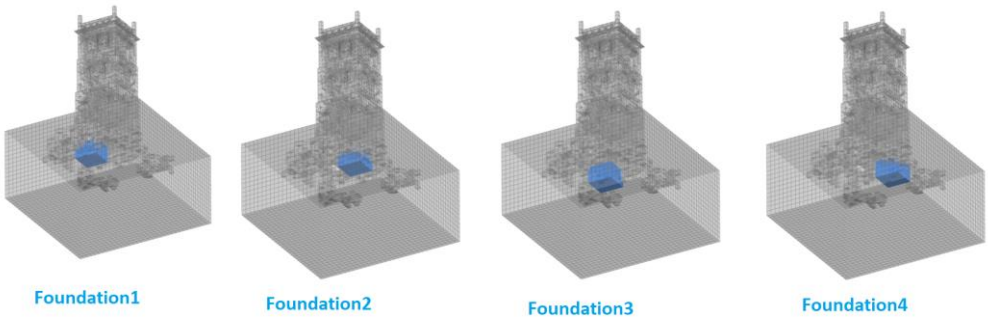

Figure 24 Sets of foundation / SB model

4.3 Modal Analysis

The modal analysis can be used in numerical and experimental methods to determine the modal properties of the structure, like natural frequencies and related modes. The gained modal parameters can be a basis for further correlation analysis between FE and test models, sensitivity analysis, and model updating procedures. The concluded equations types from the modal analysis are the same as eigensystems. In FEMtools, modal analysis using different solvers like FEMtools, Abaqus, Nastran, etc., can be done with Lanczos and modal Hessenberg methods to find modal parameters of structure.

4.3.1. Modal Analysis Results

The results of modal analysis done on the models in FEMtools using the Lanczos method have been presented in this section. Material properties for masonry and soil can be found in Table 4.

4.3.1.1 FB Model

The first five natural frequencies and related mode shapes of the FB model are Figure 25 and Figure 26.

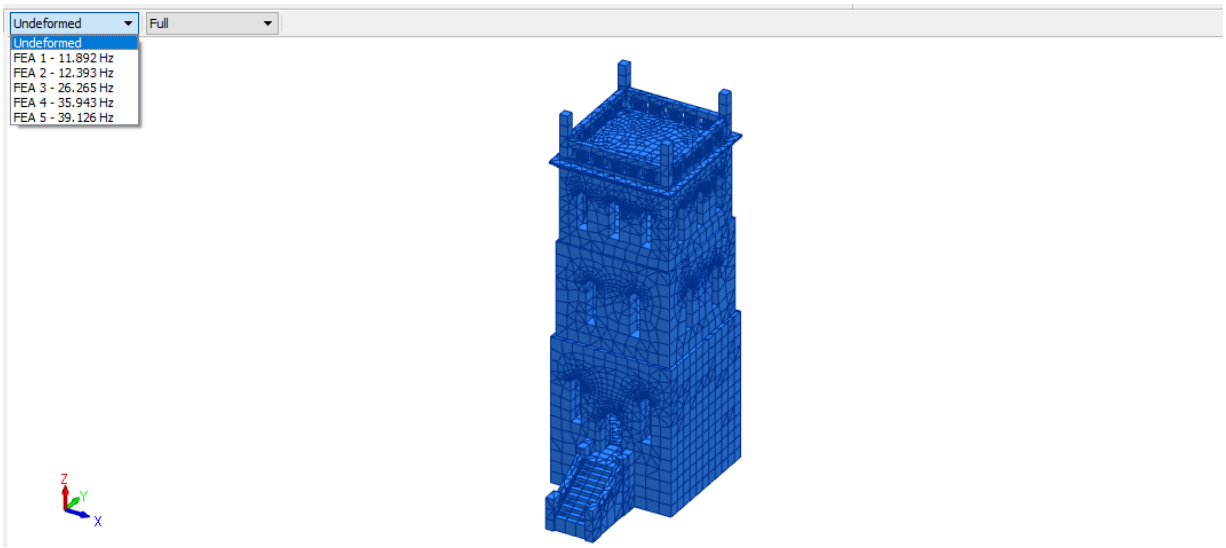

Figure 25 Natural frequencies / FB model

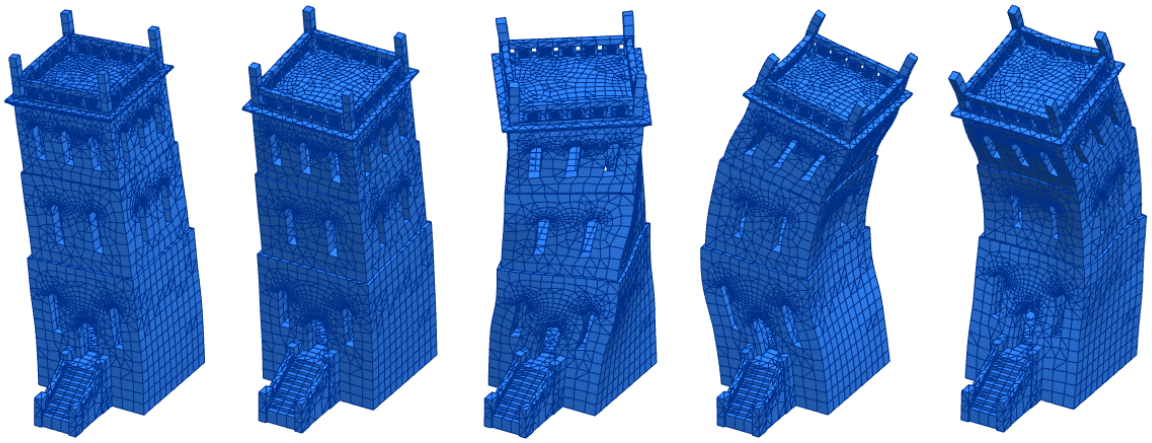

Figure 26 First five mode shapes / FB model

4.3.1.2 SB Model

The first five natural frequencies and related mode shapes of the SB model have been illustrated in Figure 27 and Figure 28.

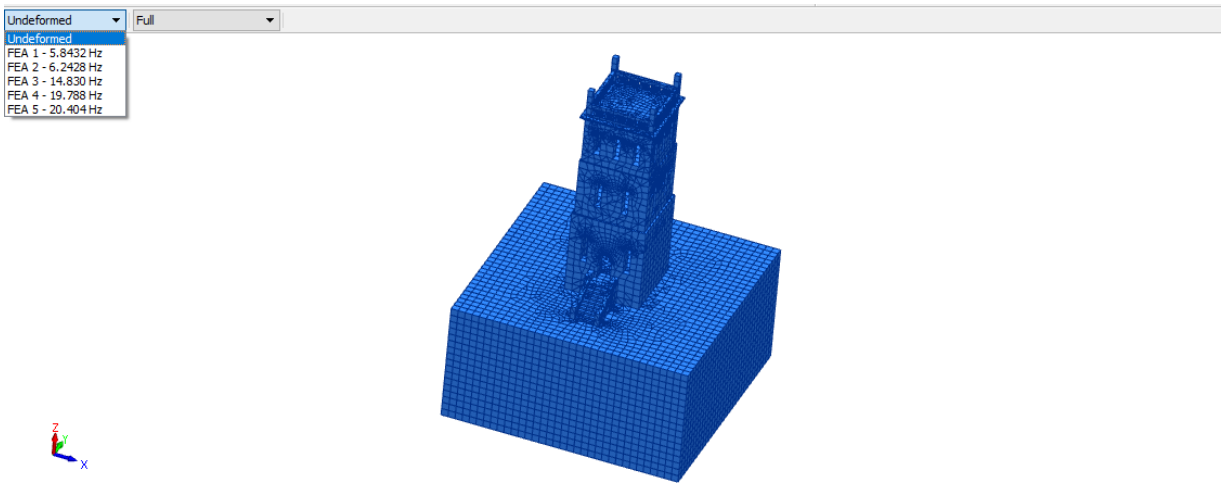

Figure 27 Natural frequencies / SB model

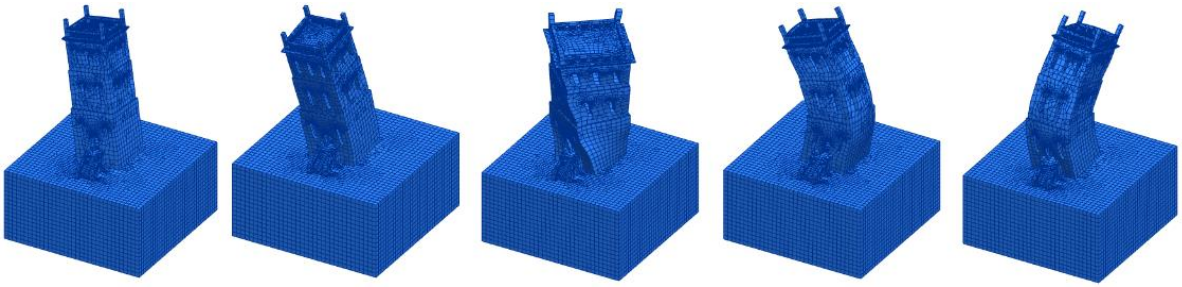

Figure 28 First five mode shapes / SB model

4.3.1.3 SS Model

The first five natural frequencies and associated mode shapes of the SS model are shown in Figure 29 and Figure 30.

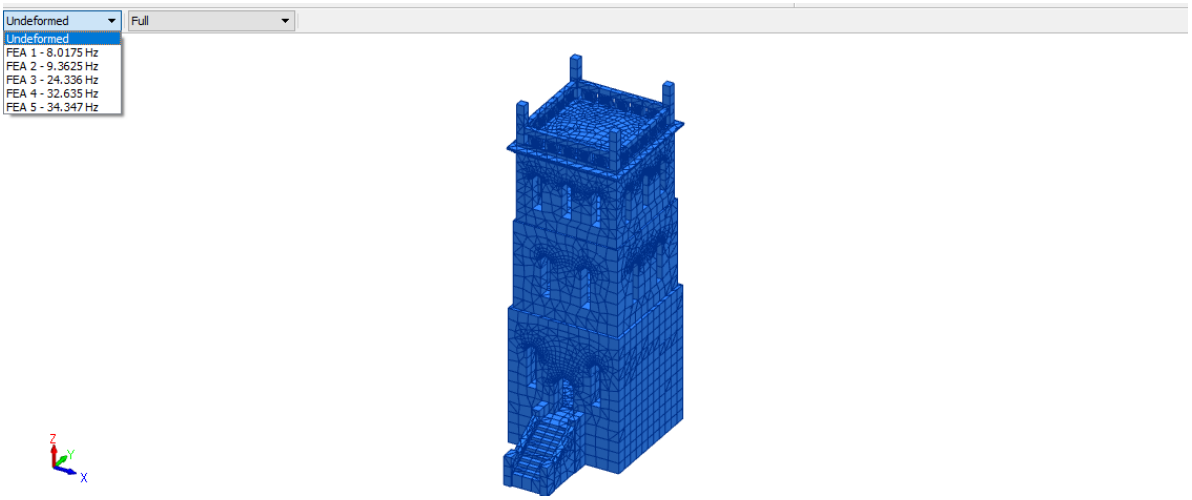

Figure 29 Natural frequencies / SS model

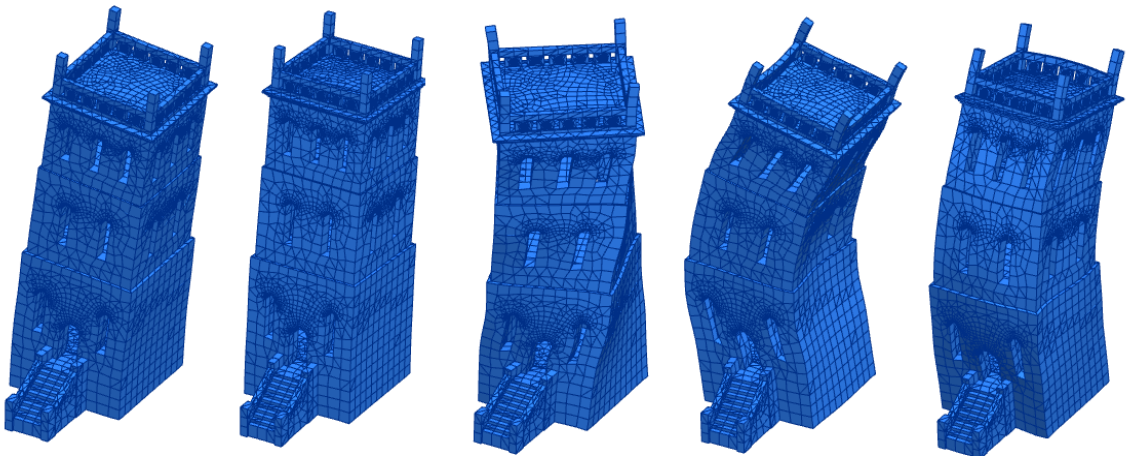

Figure 30 First five mode shapes / SS model

4.3.2 Comparison of the Modal Analysis Results

The results of modal analysis for different models have been summarized in Table 5 as follows.

Table 5 Results of modal analysis for different models

Model	Property	Mode1	Mode2	Mode3	Mode4	Mode5
FB model	f (Hz)	11.89	12.39	26.27	35.94	39.13
SB model	f (Hz)	5.84	6.24	14.83	19.79	20.41
SS model	f (Hz)	8.02	9.36	24.34	32.64	34.35

Control of the obtained values revealed a remarkable difference between the natural frequencies of models with and without soil-structure interaction effects. The frequencies of SB and SS models are smaller than the frequencies of the FB model. The results are consistent with previous researches and confirms the impacts of considering soil-structure interaction on the numerical modeling of structures.

4.3.3 Modal Analysis Results of the FB Model Used in Model Updating

It will be further discussed in section 7.2.1 that the FB model cannot be updated using the Table 4 material properties. Based on model updating simulations, The FB model can be updated with the material properties of Table 10. The first five natural frequencies, in this case, are shown in Figure 31.

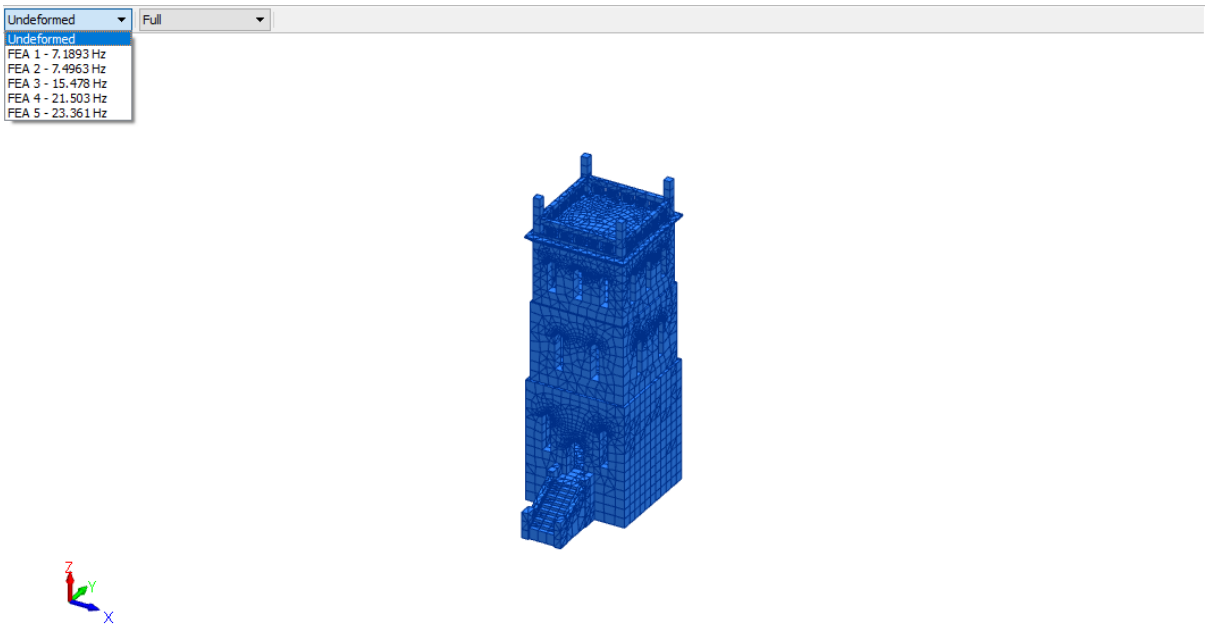

Figure 31 Natural frequencies (Based on Table 9 material properties) / FB model

The associated mode shapes are as for Figure 26.

Chapter 5: Operational Modal Analysis

5.1 Overview

Concerning the previous site AVT investigations done by Agon Ademi [1], the tower has been monitored for five days. All recorded data have been analyzed for different time durations to ensure the same results to achieve the structure's natural frequencies. The frequencies and mode shapes were obtained from 24-hours data in the middle of the recorded data.

5.2 Accelerometer

Six accelerometers have been placed along with the height of the masonry tower to record the structure's dynamic properties. The accelerometers were 20-bit 3-axis MEMS digital ones with the sample rate of 250 Hz placed at levels 2, 3, and 4 of the Slottsfjell tower.

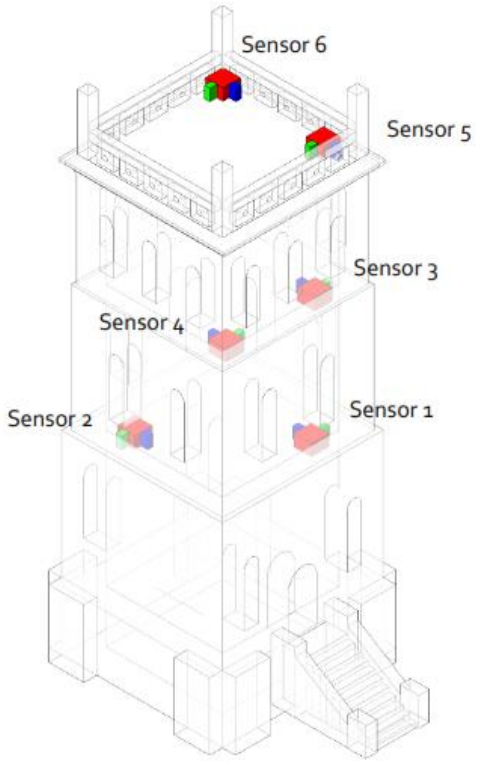

Figure 32 Schematic of accelerometers placement [1]

a) *b)*

Figure 33 (a) Instrumented sensor3 on the third floor, (b) Instrumented sensor1 on the second floor [1]

Fore noise decrease and easier installation, the sensors have been put in separate casings from the supplier. Each accelerometer has a GNSS receiver and an antenna GPS to stamp time stamps and synchronize the instruments [41].

As shown in Figure 33, all sensors are data-driven accelerometers with their GPS antenna and power source. Placing the sensor magnet on a steel plate and gluing the plate on the ground kept the sensor away from movements [1].

The sampling rate of measurements was 250 Hz registered in separate files of 20 min duration in the microSD card of the datalogger.

It is essential to have an effective sensor placement plan and careful installation of sensor networks to obtain good quality measurements. Due to noise problems in acquired measurement data from the initial execution of sensors, the AVT work has been done again with new sensors placement following the supplier's suggestions. Also, one of the sensors which were out of order was removed during the second execution [1].

5.3 Software

UnquakeSuite v1.4 software is a MATLAB-based dedicated software to process the raw data obtained from AVT measurements of accelerometers. The software does the operational modal analysis using FFT and FDD methods in MATLAB software. Many OMA methods, such as Frequency Domain Decomposition (FDD), Enhanced Frequency Domain Decomposition (EFDD), Curve-fitted Enhanced Frequency Domain Decomposition (CFDD), etc., can be implemented in other OMA software such as Artemis Modal.

5.4 Modes Identification

The raw data accumulated in separate 20 min duration files were first combined and then synchronized through GPS synchronization in Unquake. The combined and synchronized data can then be analyzed in Unquake and then exported to Artemis for modal extraction.

5.4.1 Unquake Results

The following results from modal parameters extraction of AVT data using the FFT and FDD methods have been presented.

5.4.1.1 FFT Method

The results of sensor1 in both x and y directions using the FFT method have been presented in Figure 34. Other sensors' results have been presented in appendix 1.

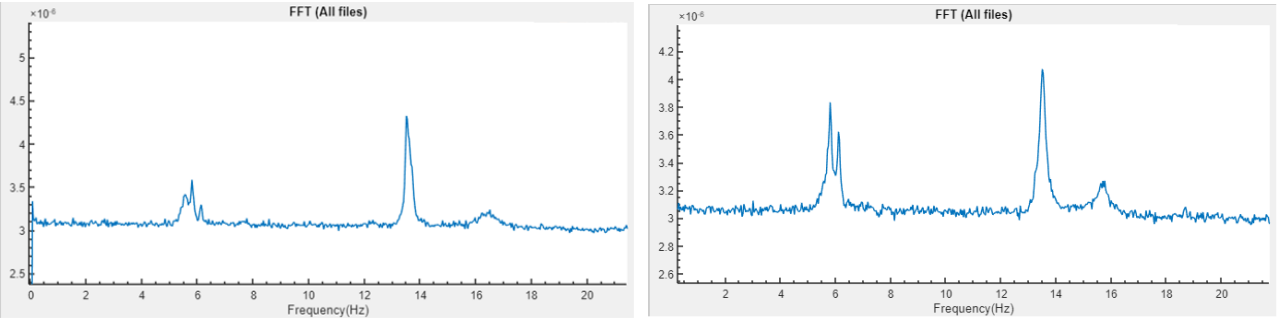

(a) *(b)*

Figure 34 FFT results of sensor1, (a) the x-direction (b) the y-direction

5.4.1.2 FDD Method

The results obtained from the FDD method of modal extraction have been presented in this section.

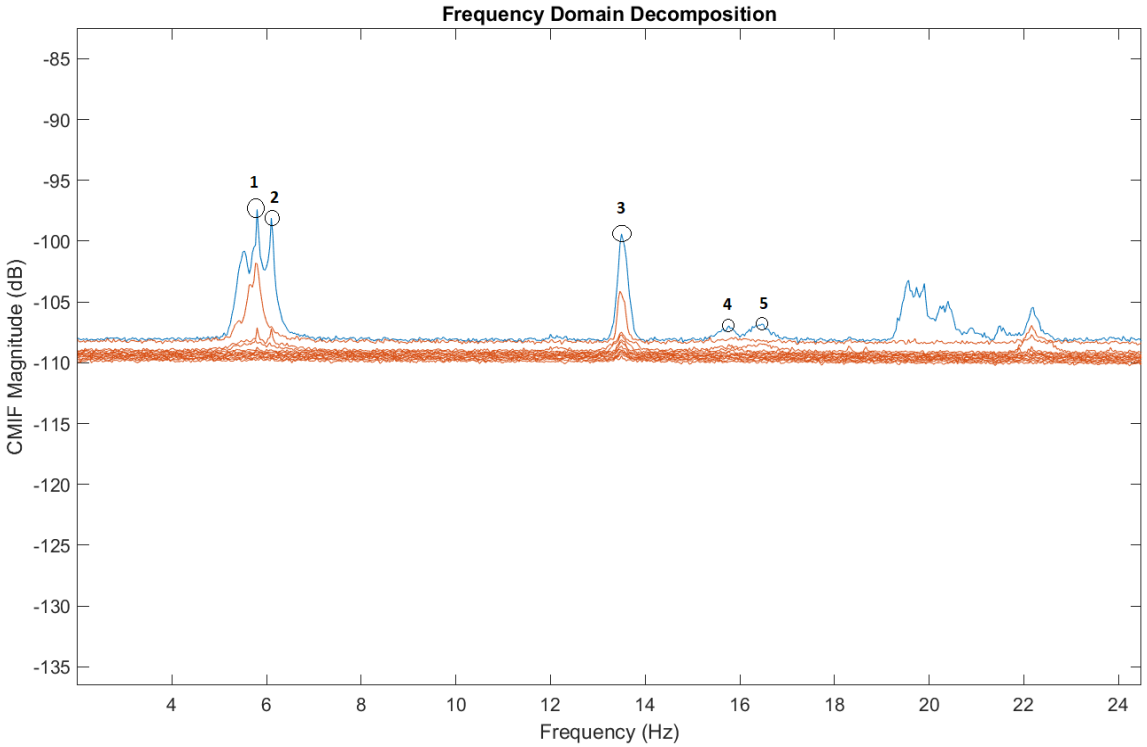

Figure 35 FDD results obtained from Unquake

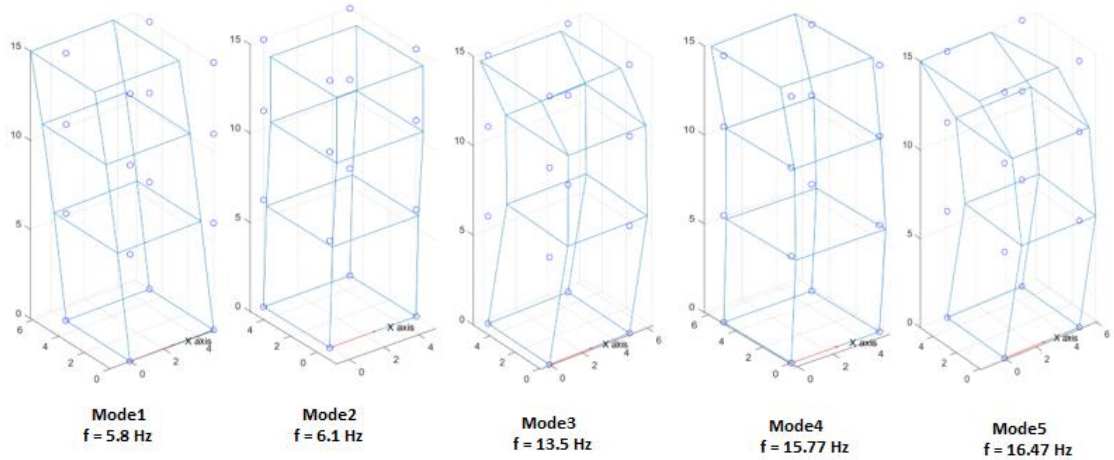

Figure 36 Mode shapes related to FDD results obtained from Unquake

While checking the above modes obtained from two methods of operational modal analysis in Unquake, the torsional mode cannot be found.

5.4.2 Artemis Modal 7.0 Results

The extracted modal parameters, natural frequencies, and associated mode shapes obtained from different OMA methods have presented in Figure 37 to Figure 42.

5.4.2.1 Frequency Domain Decomposition (FDD) Method

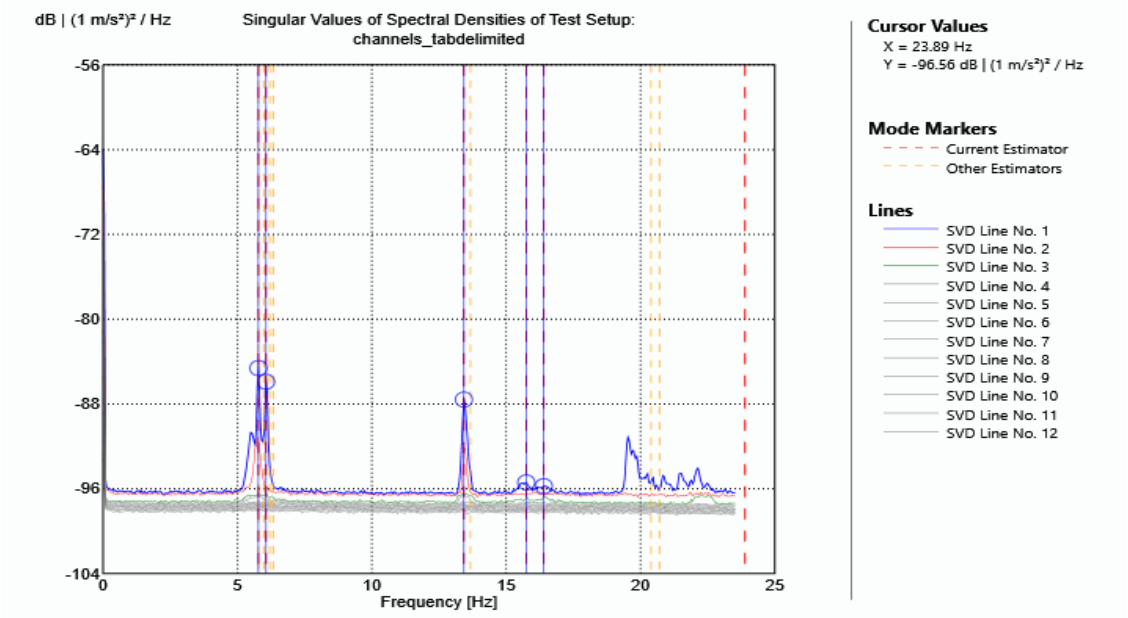

Figure 37 FDD results in Artemis

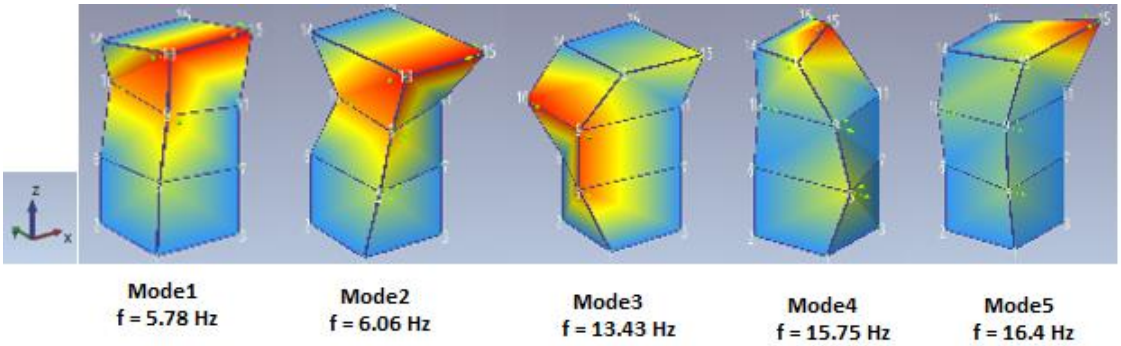

Figure 38 Obtained mode shapes from FDD method in Artemis

5.4.2.2 Enhance Frequency Domain Decomposition (EFDD) Method

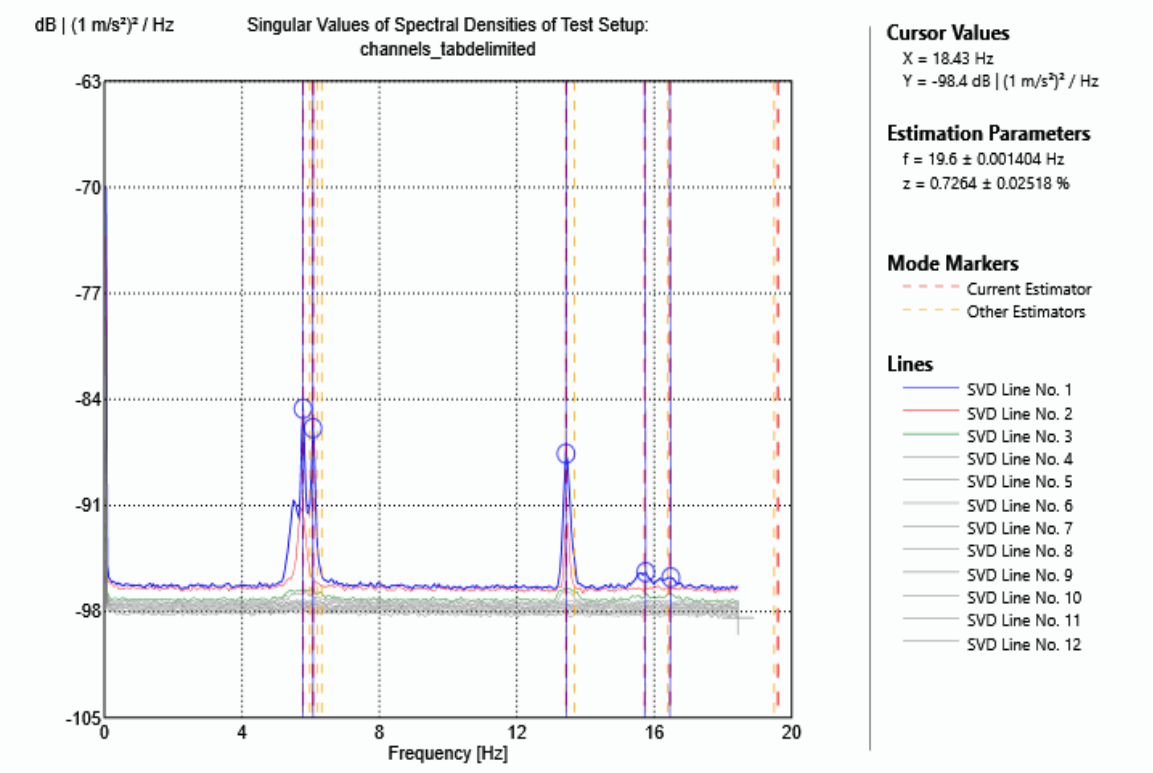

Figure 39 EFDD results in Artemis

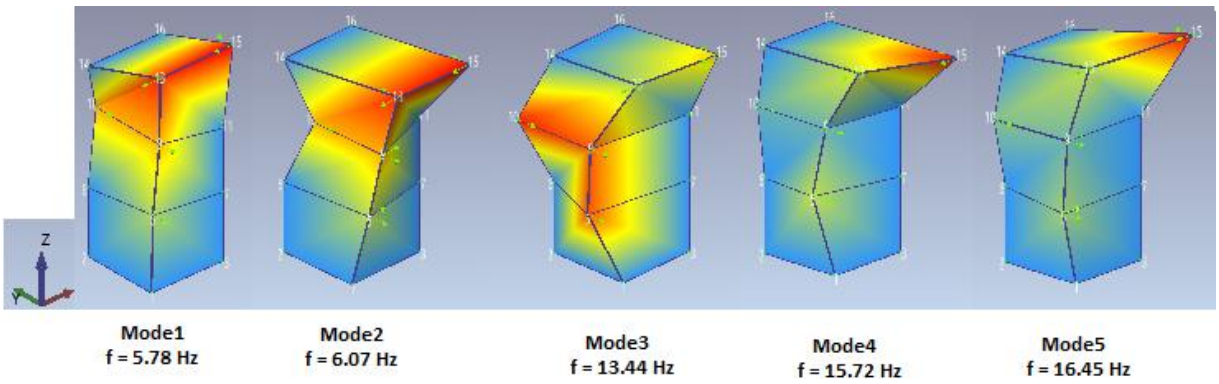

Figure 40 Obtained mode shapes from EFDD method in Artemis

5.4.2.3 Curve-Fitted Enhanced Frequency Domain Decomposition (CFDD) Method

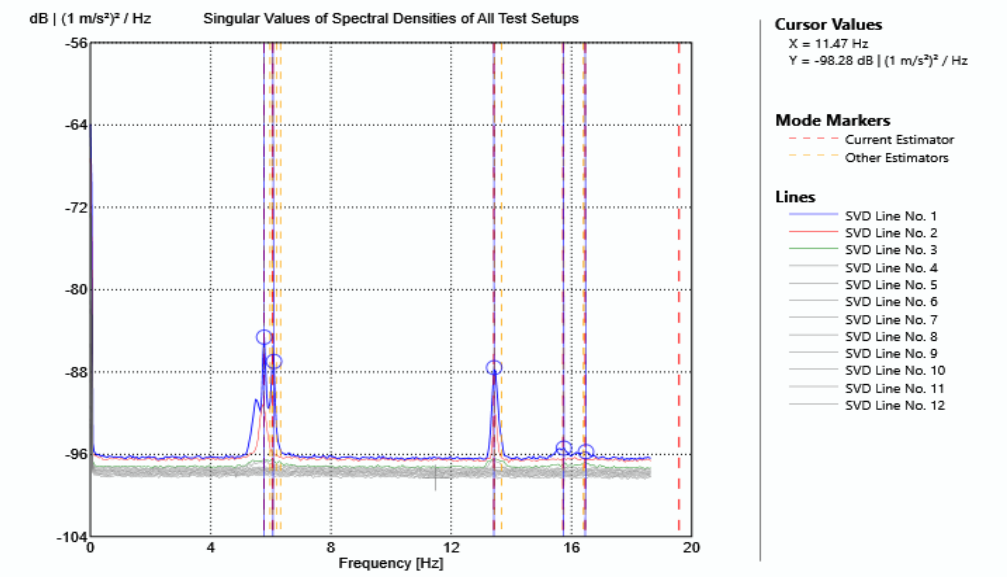

Figure 41 CFDD results in Artemis

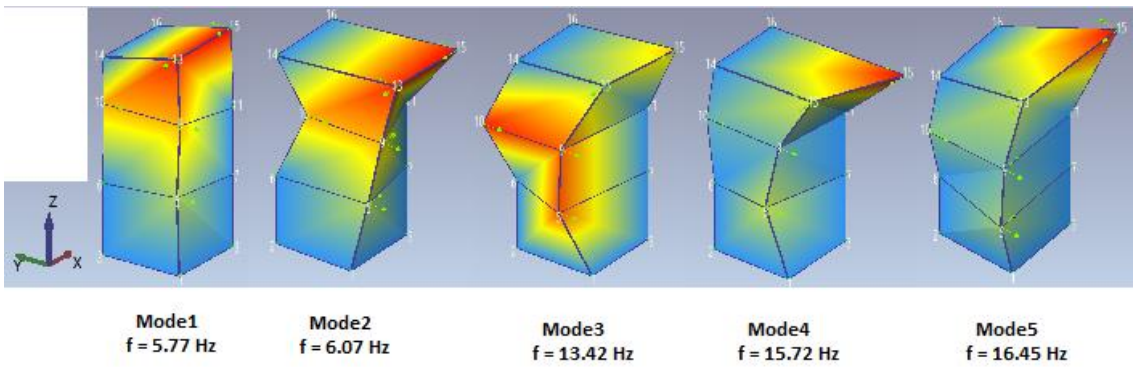

Figure 42 Obtained mode shapes from CFDD method in Artemis

5.4.3 Comparing the Results and Discussion

The mode shapes associated with the first five modes obtained from both Unquake and Artemis had been compared. Although the bending mode shapes did not show significant differences with the numerical ones in Unquake and Artemis, the torsional mode shape of test data in Unquake cannot be found. It means that the identification of all modal parameters in Unquake was not identical to the numerical ones. In this regard, it was understood that the extracted modal parameters carried out in Artemis should be followed.

It should be stated that a good correlation between the dynamic characteristics of the tower resulted from the finite element modal analysis, and the test data was obtained from FDD, EFDD, and CFDD was observed in Artemis. The mode shapes figure pointed out that the first,

second, fourth, and fifth modes are translational while the third mode is rotational, according to the numerical mode shapes. The first and fifth modes are in the x-direction, while the second and third modes are in the y-direction.

While comparing the results of different OMA methods in Artemis, it became clear that FDD, EFDD, and CFDD methods provide approximately the same frequencies as summarized in Table 6. Obtained frequencies from different OMA methods in Artemis have been presented in Table 6.

Table 6 Obtained frequencies from different OMA methods in Artemis

Method	Property	Mode1	Mode2	Mode3	Mode4	Mode5
FDD	f (Hz)	5.78	6.06	13.43	15.75	16.40
EFDD	f (Hz)	5.78	6.07	13.44	15.72	16.45
CFDD	f (Hz)	5.77	6.07	13.42	15.72	16.45

Therefore, FDD results have been chosen for sensitivity and model updating analysis. More specifically, it concluded that the five main frequencies are as for Figure 43.

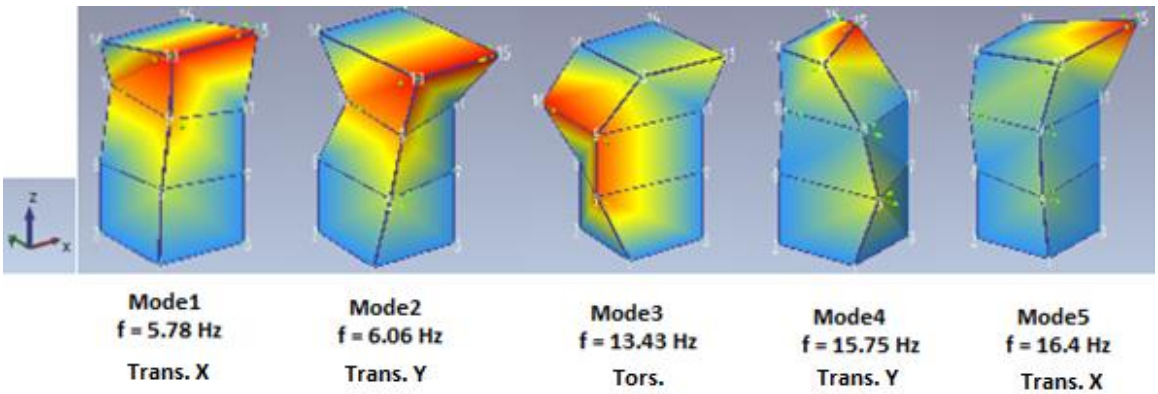

Figure 43 Intended five main modal parameters based on Artemis results

Figure 44 shows the imported mode shapes in FEMtools.

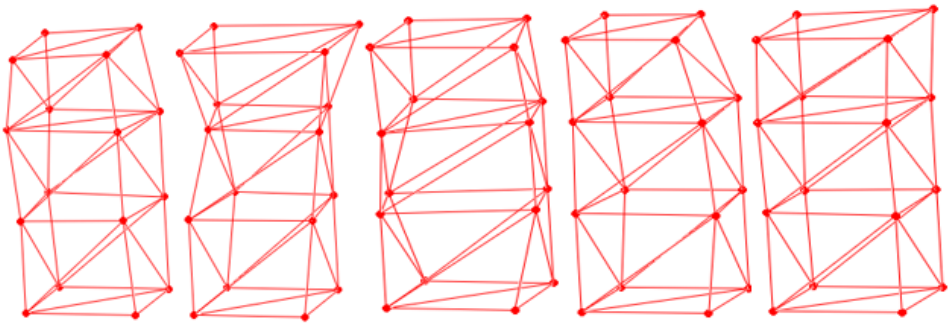

Figure 44 First five mode shapes imported from Artemis into FEMtools

Chapter 6: Sensitivity Analysis

6.1 Overview

Before model updating of the structure, a sensitivity analysis has been carried out using FEMtools 4.2.0 software to investigate the sensitivity of responses (frequencies and corresponding mode shapes) to a change in parameters (material properties).

6.2 Sensitivity Analysis Steps

As Figure 45 depicts, a sensitivity analysis consists of some steps in FEMtools. The sensitivity analysis flow chart has been illustrated in Figure 45.

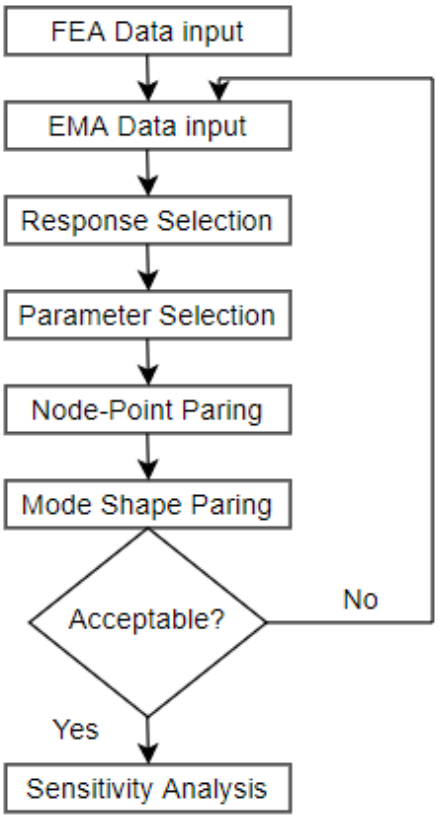

Figure 45 Sensitivity analysis flow chart

First, the FEA and EMA data should be imported. Then node-point paring and mode shape pairing should be done, followed by a response and parameter selection.

The node-point paring procedure for the three models has been shown in Figure 46.

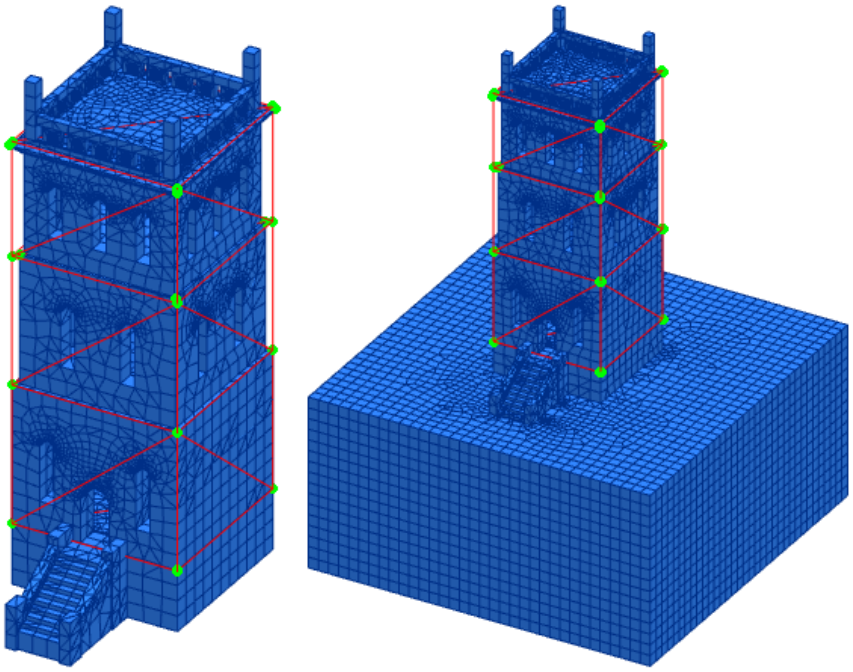

a) *b)*

Figure 46 Node-point paring, a) FB and SS models, b) SB model

Also, mode shape paring figures for the FB, SB, and SS models have been presented in Figure 47 to Figure 49. Mode shapes would be paired based on MAC criteria and the maximum error on the natural frequency.

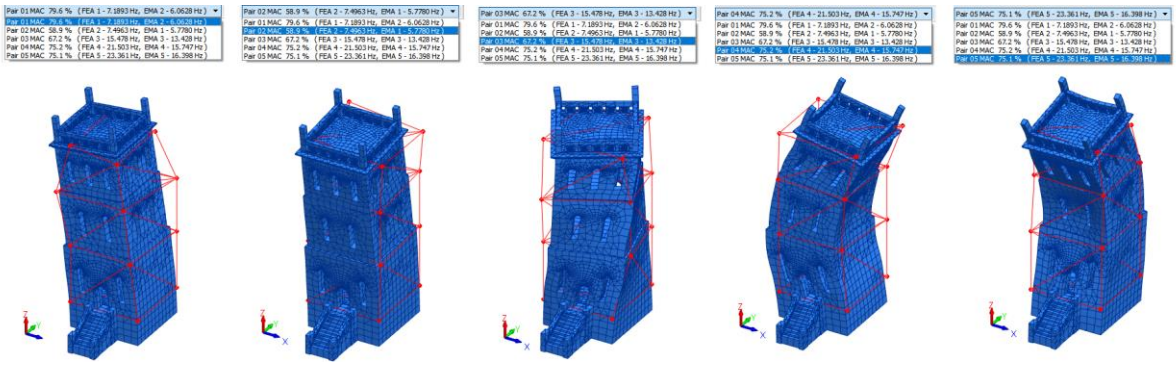

Figure 47 Mode shape pairing figures / FB model

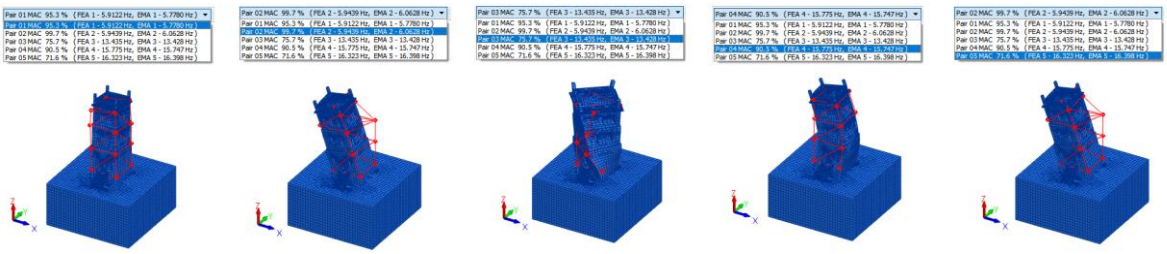

Figure 48 Mode shape pairing figures / SB model

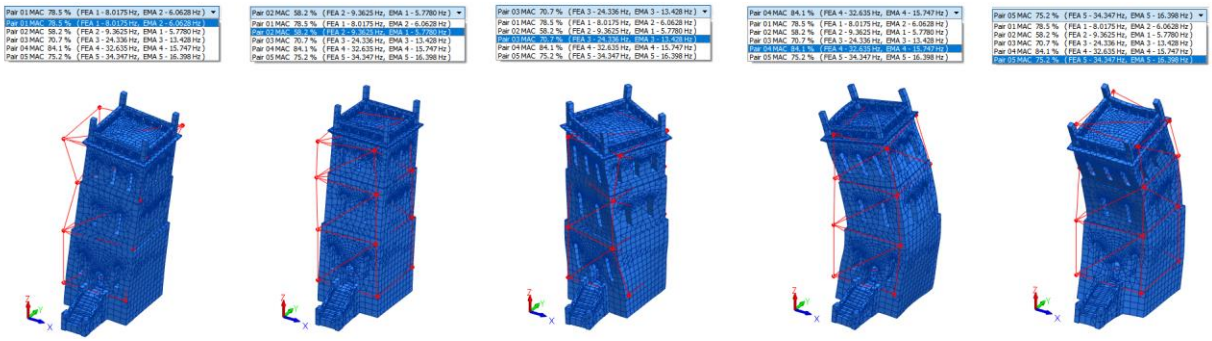

Figure 49 Mode shape pairing figures / SS model

Response selection is the next step of doing a sensitivity analysis. In this case, obtained modal parameters, including frequencies and associated mode shapes, have been selected as target responses for sensitivity analysis and model updating. In other words, ten responses have been regarded in this study. It is essential to underline that only the responses corresponding to FE through mode shape paring would be effective.

Different groups of global parameters named "set" have been selected to decrease the number of elements. The target parameters are the sets that have been created as Figure 50 reports. These parameters have been selected for sensitivity analysis to find out how much the target responses are sensitive. Creating more sets will help to have a successful convergence.

ID	Title
1	Entrance
2	Floor1
3	Wall1F
4	Wall1B
5	Wall1L
6	Wall1R
7	Floor2
8	Wall2F
9	Wall2B
10	Wall2L
11	Wall2R
12	Floor3
13	Wall3F
14	Wall3B
15	Wall3L
16	Wall3R
17	Roof

a)

Set ID	Title
101	Entrance
102	Floor1
103	Wall1F
104	Wall1B
105	Wall1L
106	Wall1R
107	Floor2
108	Wall2F
109	Wall2B
110	Wall2L
111	Wall2R
112	Floor3
113	Wall3F
114	Wall3B
115	Wall3L
116	Wall3R
117	Roof
118	Foundation1
119	Foundation2
120	Foundation3
121	Foundation4
122	Soil1
123	Soil2
124	Soil3
125	Soil4
126	Soil5
127	Soil6
128	Soil7
129	Soil8

b)

ID	Title
1	Entrance
2	Floor1
3	Wall1F
4	Wall1B
5	Wall1L
6	Wall1R
7	Floor2
8	Wall2F
9	Wall2B
10	Wall2L
11	Wall2R
12	Floor3
13	Wall3F
14	Wall3B
15	Wall3L
16	Wall3R
17	Roof
18	Spring

c)

Figure 50 Sets of different models, (a) FB model, (b) SB model, (c) SS model

Since selecting more parameters will provide more freedom for the system to obtain convergence [7], the structure has been divided into 17, 29, and 18 sets for FB, SB, and SS models, respectively.

6.3 Sensitivity Analysis Results

The sensitivity of the parameters to a change in elasticity modulus, density, shear modulus, and Poisson's ratio has been studied and discusses in this chapter.

As already discussed, orthotropic material has been used in this study for all different models. Also, to perform successful model updating simulations, 17, 29, and 18 parameters have been used in the sensitivity analysis simulations, as mentioned in Table 4. It will be discussed more in detail in the model updating chapter. Therefore, regarding the x, y, and z directions, 51 sets of FB model parameters have been regarded in the analysis. The number of sets of parameters for the SB and SS models is 87 and 54, respectively. There are ten target responses which consist of five frequencies with five associated mode shapes.

Parameters may have positive, negative, or zero effects on the responses. A positive sensitivity indicates that an increase in the parameter value leads to rising in the selected response. A negative sensitivity reflects unequal variations in response on one side and parameters on the other side. For instance, if parameter 1 has positive sensitivity to a change in both the first frequency and the first mode shape, increasing parameter 1 will increase the first frequency. Also, the positive effect on the mode shape makes the first test, and finite element mode shapes becoming more like each other.

The vertical axis in the sensitivity graphs shows the normalized sensitivity values. For example, the normalized value equal to "2.00E-2" for a specific parameter means that a 1% increase in the parameter value leads to a 0.02% increase in the target response. Similarly, the "-2.00E-2" normalized sensitivity value for a parameter is interpreted as a 0.02% decrease in that response.

In this section, the sensitivity graphs have been presented only for the first frequency and associated mode shape to avoid many graphs. The sensitivity graphs related to other responses have been presented in appendix 3.

6.3.1 Sensitivity to a Change in Elasticity Modulus

6.3.1.1 FB Model

The sensitivity graph to a change in elasticity modulus for the FB model has been presented in Figure 51.

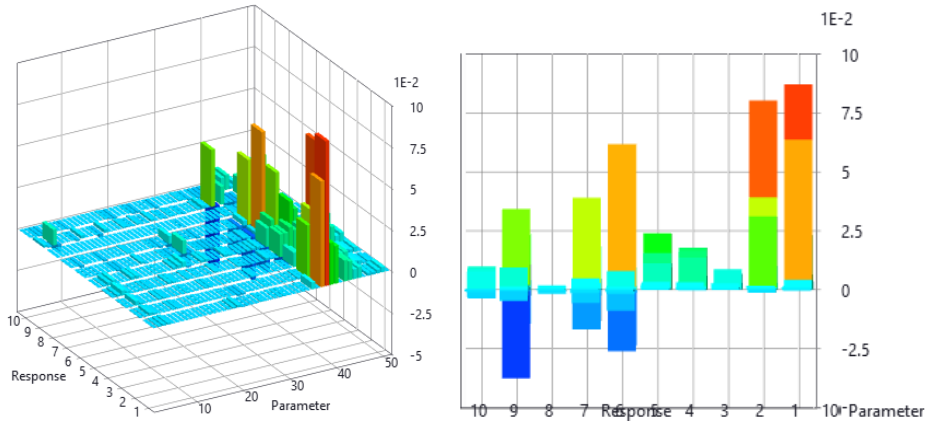

Parameters	
1-17	Ex
18-34	Ey
35-51	Ez

Responses	
1-5	Frequencies
6-10	Mode shapes

Figure 51 Sensitivity graph to a change in elasticity modulus / FB model

Analyzing the sensitivity graph shows that the frequencies have positive sensitivity to a change in increase in E_z. In contrast, the mode shapes have both positive and negative sensitivity to a change in E_z. The graph shows that the target responses do have sensitivity only to a change in E_z. In other words, they do not have sensitivity to a change in E_x and E_y. The most negative sensitivity is for the fourth mode shape, while the most positive is for the first frequency. The effect of different parameters on the first frequency and mode shape has been shown below.

In Figure 52, the effects of different parameters on the first response have been shown. The maximum sensitivity is related to parameter 38 (E_z of Wall1B). No negative sensitivity to a change in elasticity modulus for the first response has been found.

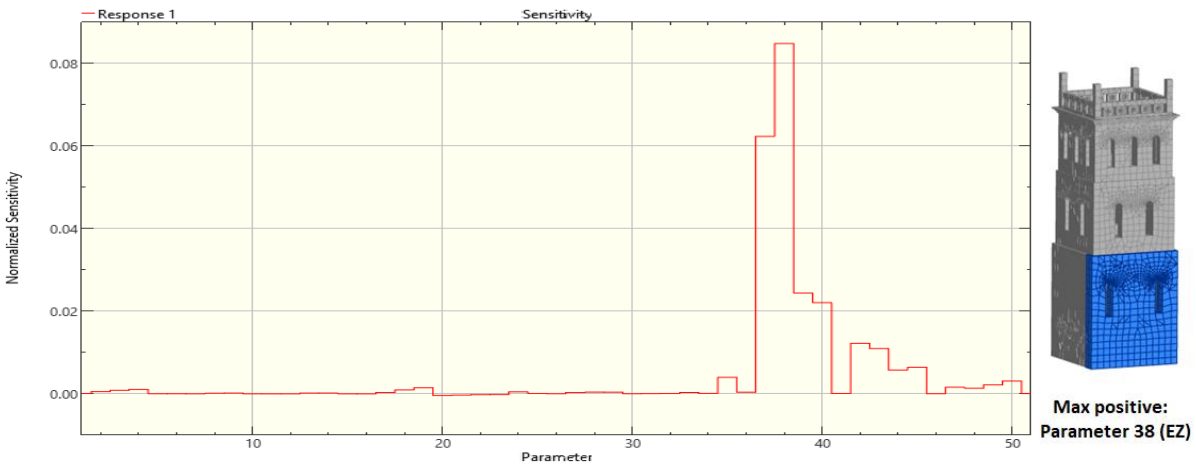

Figure 52 Sensitivity graph of the first frequency to a change in elasticity modulus / FB model

The first frequency has shown the highest sensitivity to a change in parameters 36 to 40 (E_z of the first floor sets); then parameters 41 to 45 (E_z of second-floor sets), and parameters 46 to 50 (E_z of third-floor sets). The first frequency has the lowest sensitivity to a change in the third-floor sets than other floor sets.

As one can see in Figure 53, which shows the sensitivity graph of the first mode shape to a change in elasticity modulus, the first mode shape has the most positive and negative sensitivity to a change in parameter 39 (E_z of Wall1L) and parameter 37 (E_z of Wall1F).

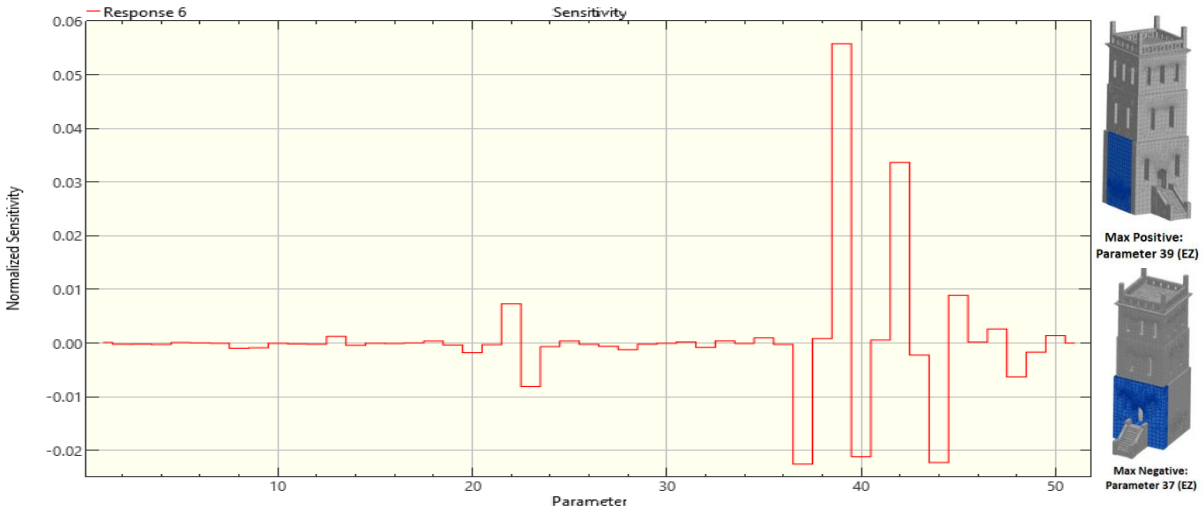

Figure 53 Sensitivity graph of the first mode shape to a change in elasticity modulus / FB model

Figure 54 is the sensitivity graph related to the sum of responses to a change in elasticity modulus. The sum of responses is most positively sensitive to parameter 39 (E_z of Wall1L) among defined parameters. Also, maximum negative sensitivity has been observed to a change in parameter 23 (E_z of Wall1R).

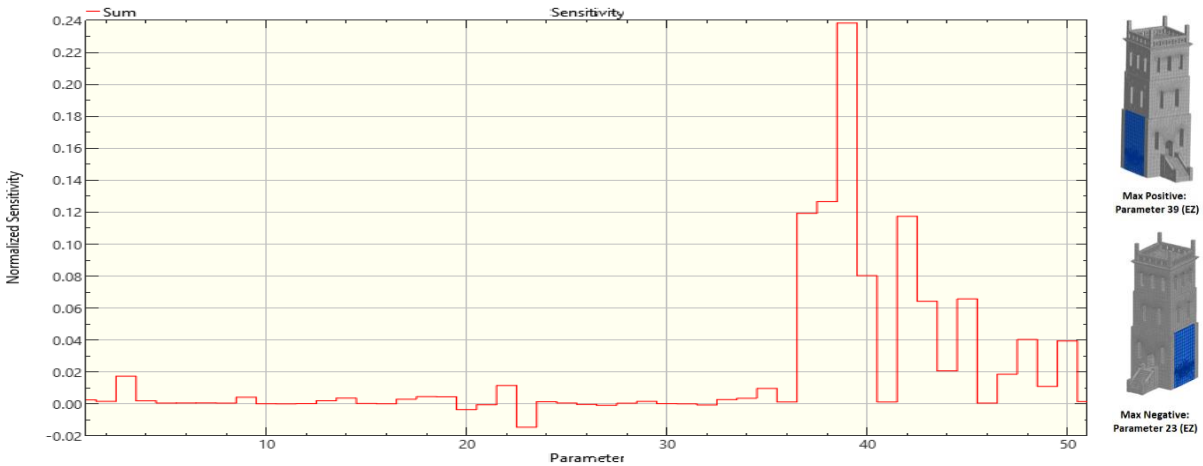

Figure 54 Sensitivity graph of the sum of responses to a change in elasticity modulus / FB model

It should also be mentioned that higher sensitivity has been observed for the first-floor sets than sets of the second and third floors for the sum of responses. Normalized sensitivity values for the first, second, and third floors are 0.566, 0.269, and 0.11, respectively. The values show a 145% increase in the sensitivity values from the third floor to the second floor and a 110% increase from the second floor to the first one.

A sensitivity graph of responses to a change in the sum of parameters has been presented in Figure 55. As can be seen, all responses have positive sensitivity to a change in the sum of parameters.

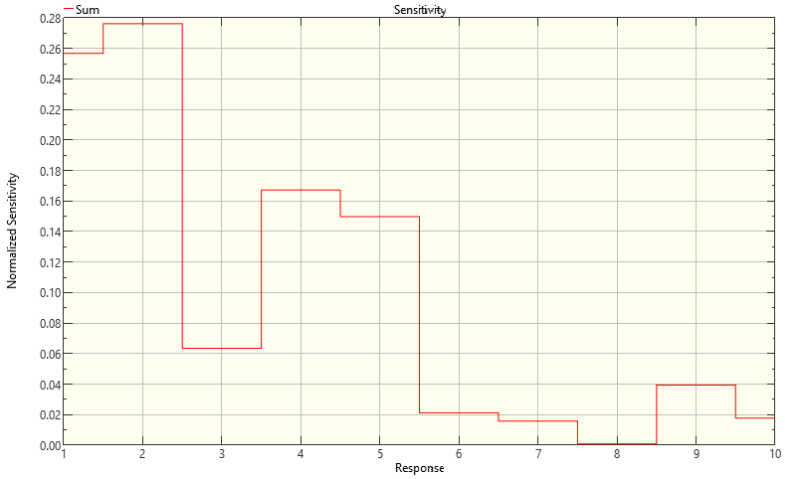

Figure 55 Sensitivity graph of all-responses to a change in elasticity modulus for the sum of parameters / FB model

Figure 55 also depicts that the second frequency is the most sensitive response to a change in the elasticity modulus.

6.3.1.2 SB Model

Figure 56 concludes that the responses have more sensitivity to a change in E_z.

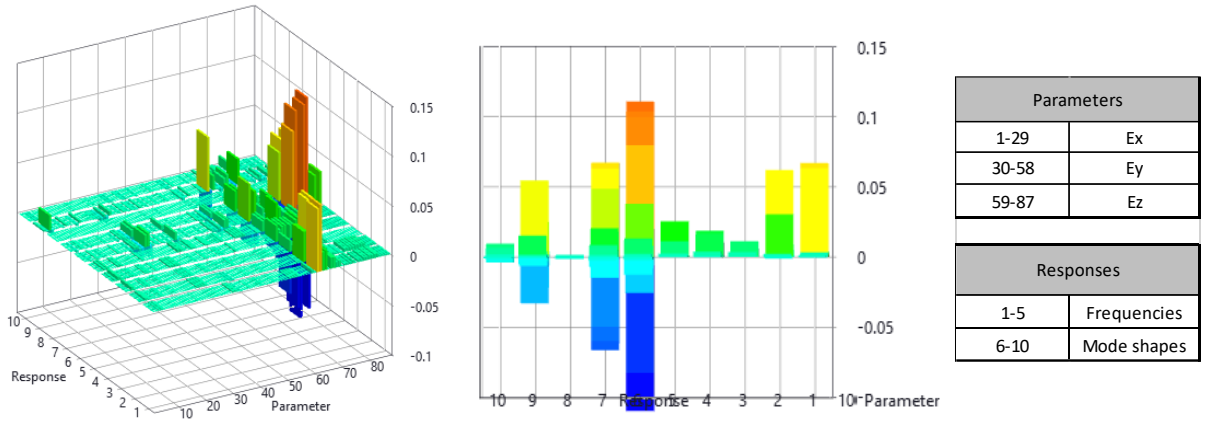

Figure 56 Sensitivity graph to a change in elasticity modulus / SB model

As Figure 56 shows, frequencies have positive sensitivity to a change in elasticity modulus, while the corresponding mode shapes have positive and negative sensitivities. The most negative and positive sensitivity have been observed for the first mode shape.

Figure 57 shows that the first frequency is more sensitive to a change in parameter 62 (E_z of Wall1B) than other parameters. No negative sensitivity has been observed to a change in elasticity modulus for the first response.

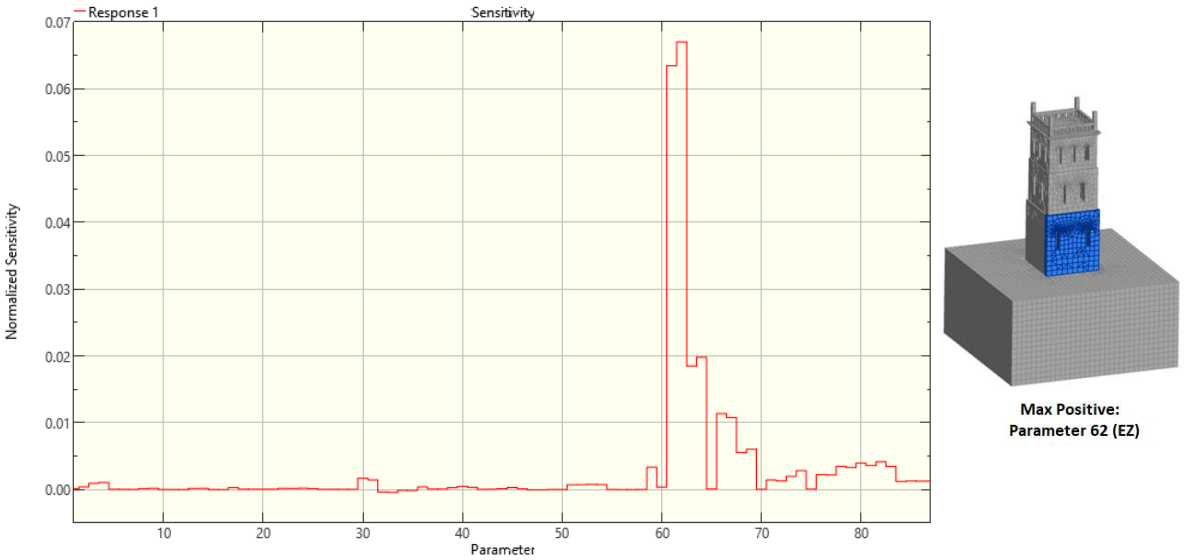

Figure 57 Sensitivity graph of the first frequency to a change in elasticity modulus / SB model

Figure 57 highlights that parameters 60 to 64 indicating the first-floor sets have shown the highest sensitivity to E_z change. Also, parameters 65 to 69, which are the second-floor sets, have shown the second highest sensitivity, and parameters 70 to 74 related to the third-floor sets are the next ones.

Figure 58 shows the sensitivity graph and values of the first mode shape to a change in elasticity modulus for defined parameters. Parameter 82 (E_z of Soil3) has the most positive effect on the fourth mode shape. Also, the highest negative sensitivity has been observed to a change in parameter 80 (E_z of Soil1). Comparison of sets revealed that the mode shapes are sensitive to a change in E_z of soil sets.

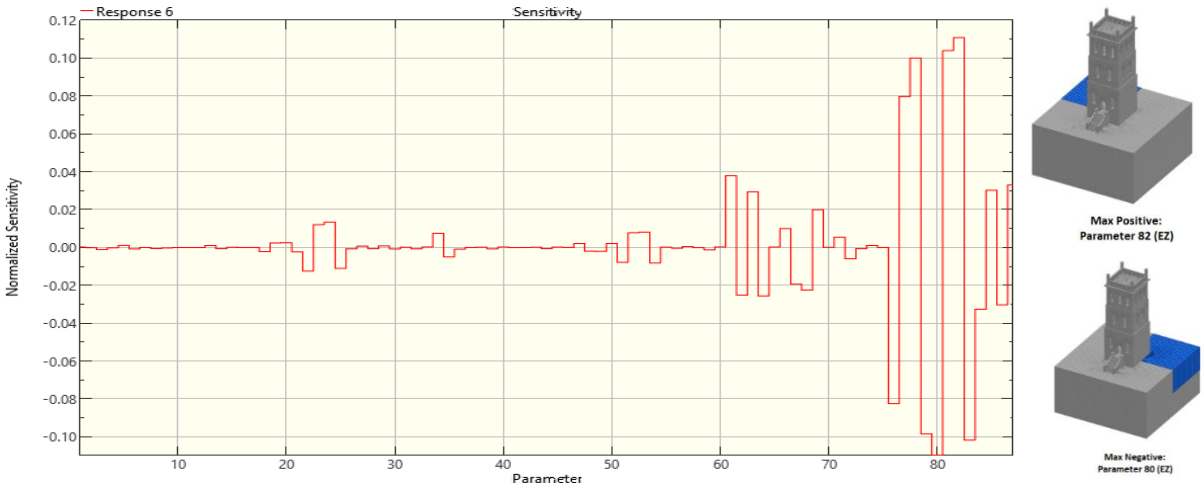

Figure 58 Sensitivity graph of the first mode shape to a change in elasticity modulus / SB model

The sensitivity graph related to the sum of the responses to a change in elasticity modulus has been shown in Figure 59. The most positive sensitivity is a change in parameter 61 (E_z of Wall1F), the first floor's front wall. The most negative sensitivity also belongs to parameter 80 (E_z of soil1).

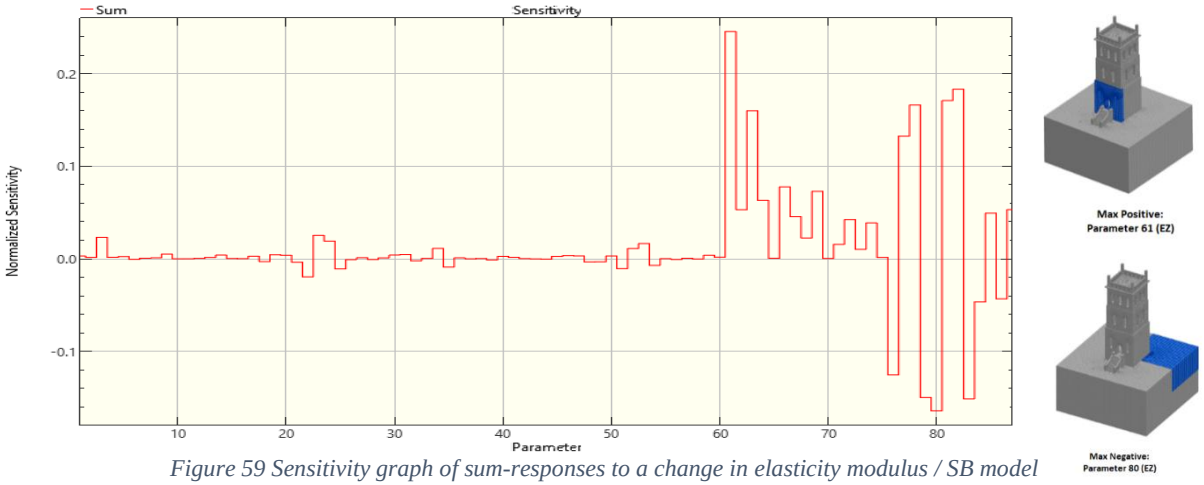

Figure 59 Sensitivity graph of sum-responses to a change in elasticity modulus / SB model

The sensitivity graph of all responses to a change in the sum of parameters has been presented in Figure 60. As can be seen, all responses have positive sensitivity to a change in the sum of parameters. The most sensitive response is the second frequency, with a normalized sensitivity of around 0.27. This value shows that a 1% change in the sum of elasticity modulus for different sets will result in a 0.27% change in the second frequency of the structure.

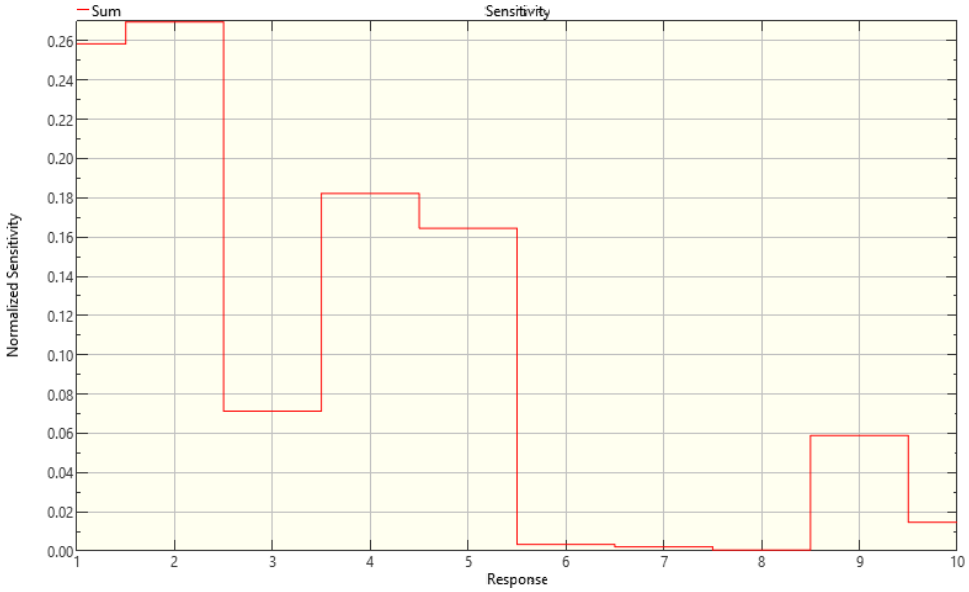

Figure 60 Sensitivity graph of all-responses to a change in elasticity modulus for sum-parameters / SB model

It should also be mentioned that higher sensitivity has been observed for the first-floor sets than sets of the second and third floors. The first, second, and third floors are normalized sensitivity values for the first, second, and third floors, which are 0.523, 0.219, and 0.108. The values show a 103% increase in the sensitivity values from the third floor to the second floor and a 139% increase from the second to the first one.

6.3.1.3 SS Model

Sensitivity graphs of the SS model to a change in elasticity modulus have been presented in this section.

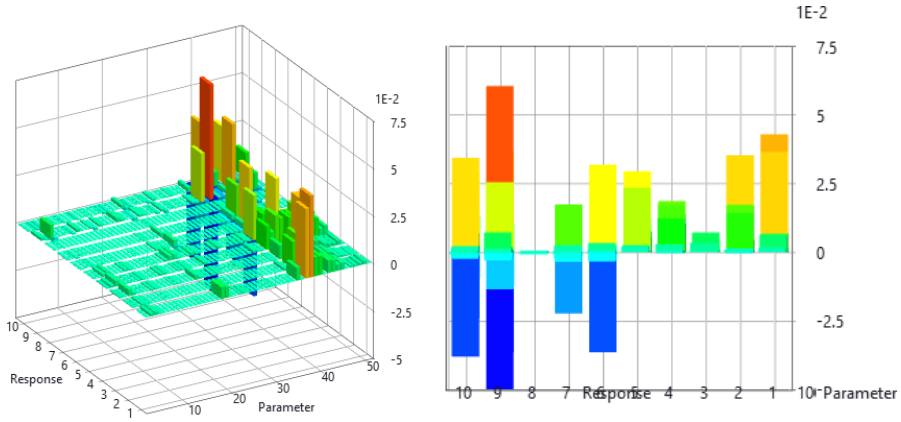

Parameters	
1-17	Ex
18-34	Ey
35-51	Ez

Responses	
1-5	Frequencies
6-10	Mode shapes

Figure 61 Sensitivity graph to a change in elasticity modulus / SS model

The sensitivity of the responses to a change in E_z is more than E_x and E_y. It means that changes in E_x and E_y values do not affect the frequencies and mode shapes significantly.

The fourth mode shape has shown both maximum negative and positive sensitivity to a change in elasticity modulus among the target responses. Frequencies have only positive sensitivity to a change in elasticity modulus with the maximum normalized sensitivity value for the first natural frequency.

Figure 62 shows the sensitivity graph related to the first response, which is the first frequency.

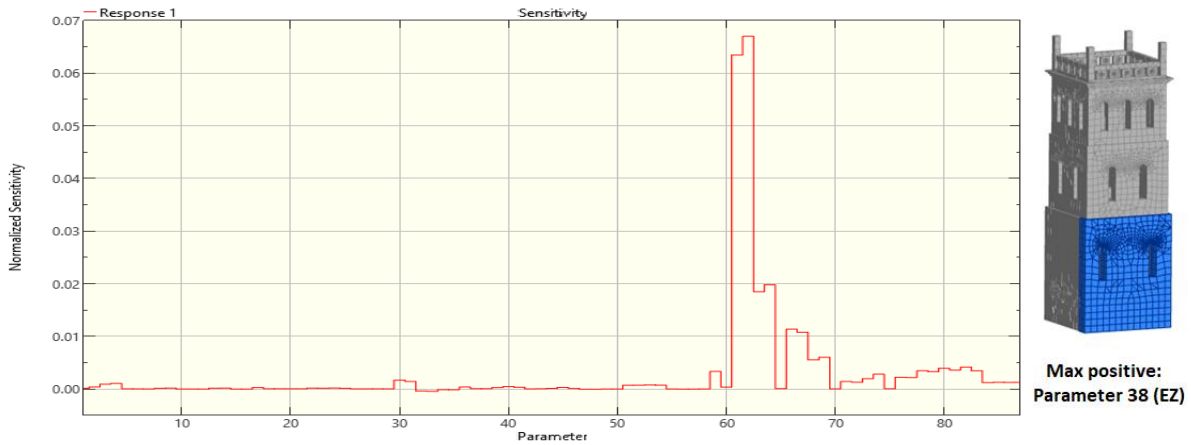

Figure 62 Sensitivity graph of the first frequency to a change in elasticity modulus / SS model

The first frequency has the most sensitivity to a change in parameter 38 (E_z of Wall1B), as shown in Figure 62.

The sensitivity graph of the first mode shape to a change in elasticity modulus has been shown in Figure 63.

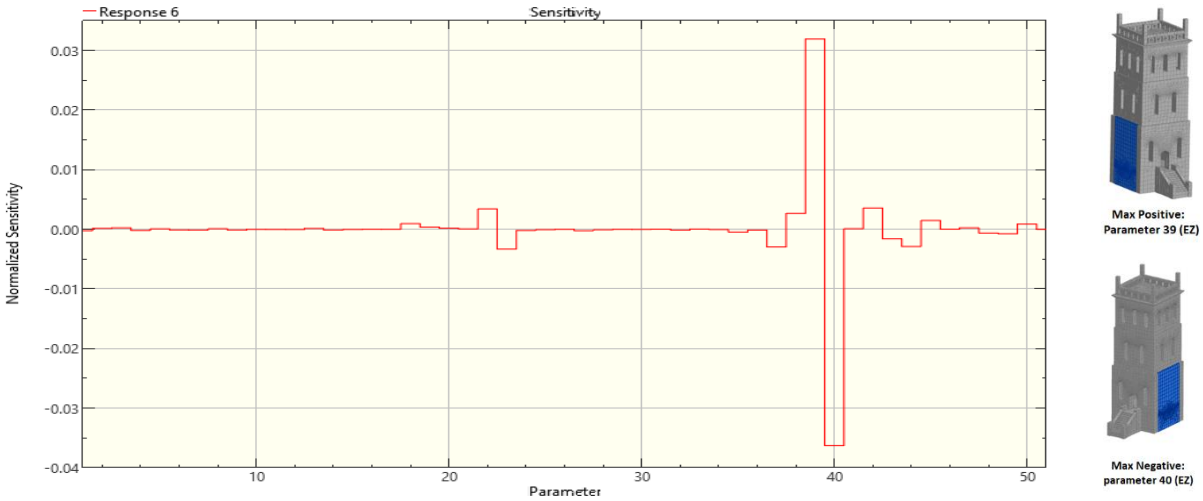

Figure 63 Sensitivity graph of the first mode shape to a change in elasticity modulus / SS model

It is shown that parameter 39 (E_z of Wall1L) and parameter 40 (E_z of Wall1R) have the most positive and negative effects on the first mode shape.

Resulting from Figure 64, which is the sensitivity graph related to the sum of responses to a change in elasticity modulus, parameter 39 (E_z of Wall1L) is the most effective.

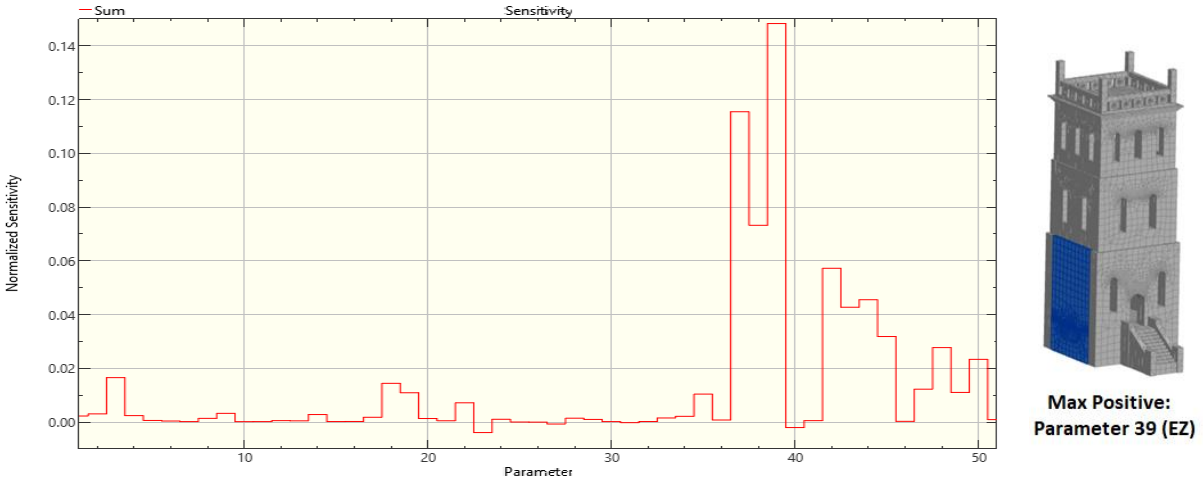

Figure 64 Sensitivity graph of sum-responses to a change in elasticity modulus / SS model

Also, the sensitivity graph to a change in elasticity modulus for parameters has been shown in Figure 65. The normalized sensitivity values of each response have been obtained for the summation of parameters. The graph reports that the fourth frequency is the most sensitive target response while comparing the E effects on different structure parts.

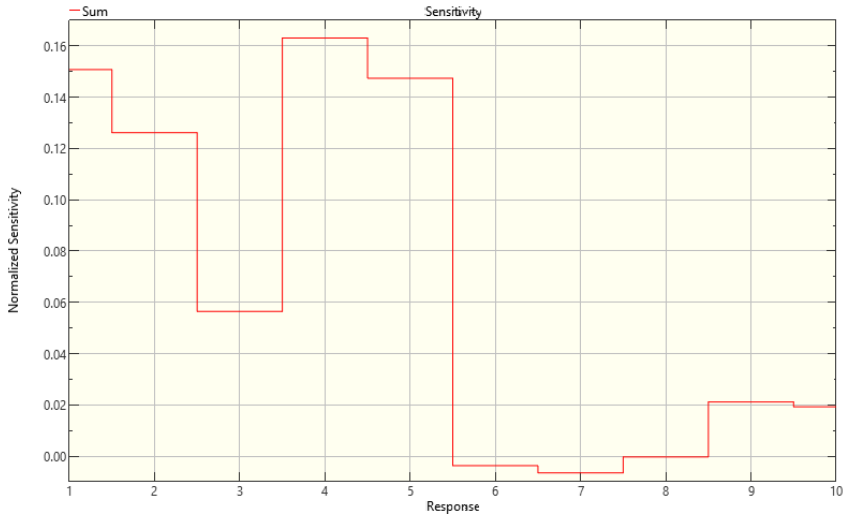

Figure 65 Sensitivity graph of all-responses to a change in elasticity modulus for sum-parameters / SS model

The sensitivity investigations to a change in elasticity modulus should be concluded by saying that the target responses are more sensitive to E_z changes than E_x and E_y. The sensitivity decreases as height increases. Investigating the sensitivity graphs of the SB model to a change in elasticity modulus reveals that the higher the height parameter set, the minor sensitivity. In this case, normalized sensitivity values for the first, second, and third floors are 0.718, 0.549,

and 0.240, respectively, which show a 30% increase from the second to the first one as well and a 128% increase from the third floor to the second floor.

It is noteworthy that the sensitivity values to a change in E_z for the FB model were higher than SB and SS models, as shown in Figure 66. Also, the SB model was more sensitive to a change in E_z compared to the SS model.

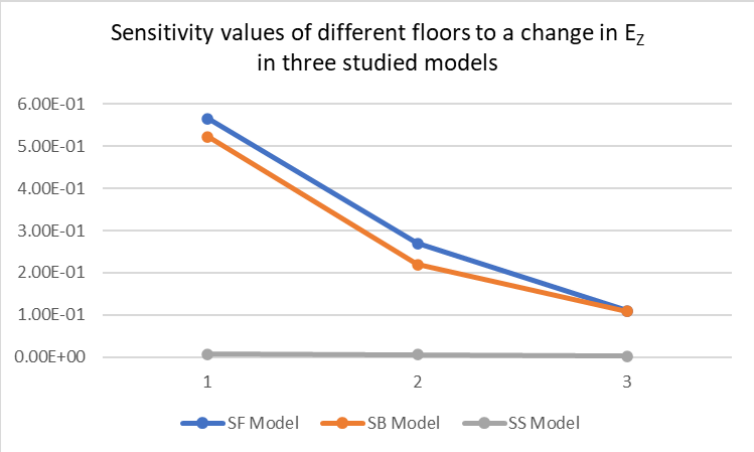

Figure 66 Sensitivity values of different floors to a change in Ez / all models

6.3.2 Sensitivity to a Change in Poisson's Ratio

In this section, sensitivity graphs of target responses, including five frequencies and five mode shapes to a change in the NU_{xy}, NU_{xz}, and NU_{yz}, have been presented and discussed.

6.3.2.1 FB Model

The number of sets in the FB model is 51 parameters as defined in the sensitivity module. Figure 67 demonstrates the sensitivity graph to a change in Poisson's ratio in the FB model.

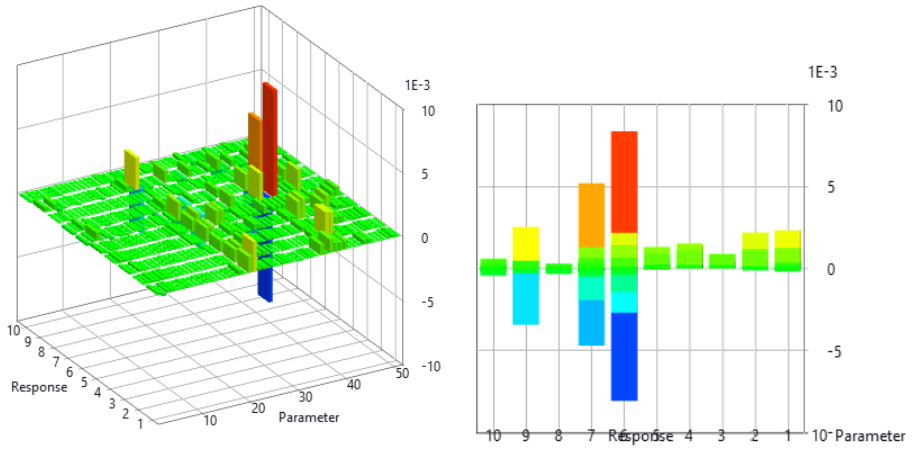

Parameters	
1-17	NUxy
18-34	NUxz
35-51	NUyz

Responses	
1-5	Frequencies
6-10	Mode shapes

Figure 67 Sensitivity graph to a change in Poisson's ratio / FB model

Although very small negative sensitivities have been observed based on the graph, the overall sensitivity of frequencies to a change in Poisson's ratio is positive. Nevertheless, the mode shape's sensitivity to a change in Poisson's ratio can be negative or positive with the maximum sensitivity values at the first mode shape.

The sensitivity graph to a change in Poisson's ratio for the first frequency and associated mode shape has been presented in Figure 68 and Figure 69. Parameter 21 (NU_{xy} of Wall1B) has been observed as the most influential parameter on the first frequency.

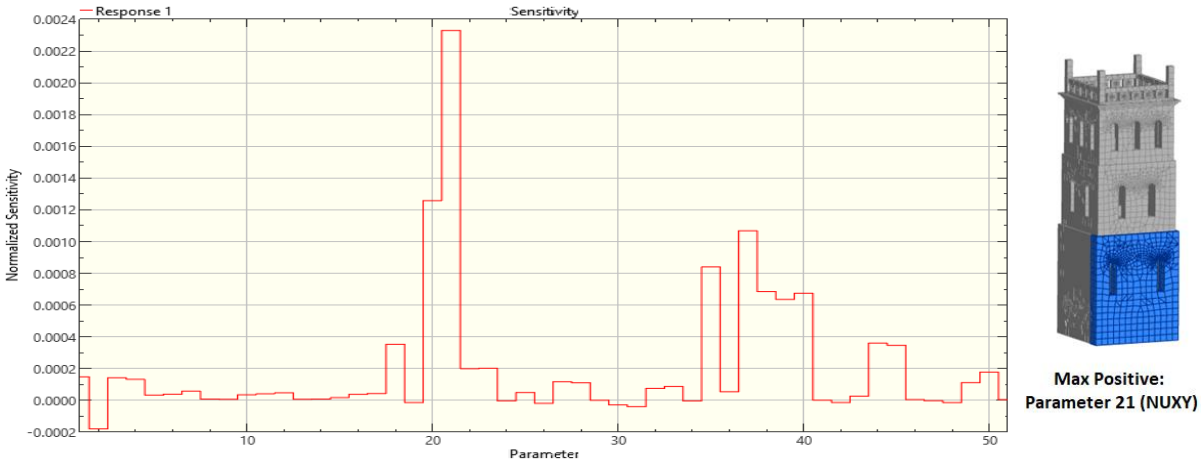

Figure 68 Sensitivity graph of the first frequency to a change in Poisson's ratio / FB model

Figure 69 illustrates that the sensitivity of the first mode shape to a change in Poisson's ratio has the highest positive value at parameter 40 (NU_{yz} of Wall1R) and the highest negative value at parameter 39 (NU_{yz} of Wall1L).

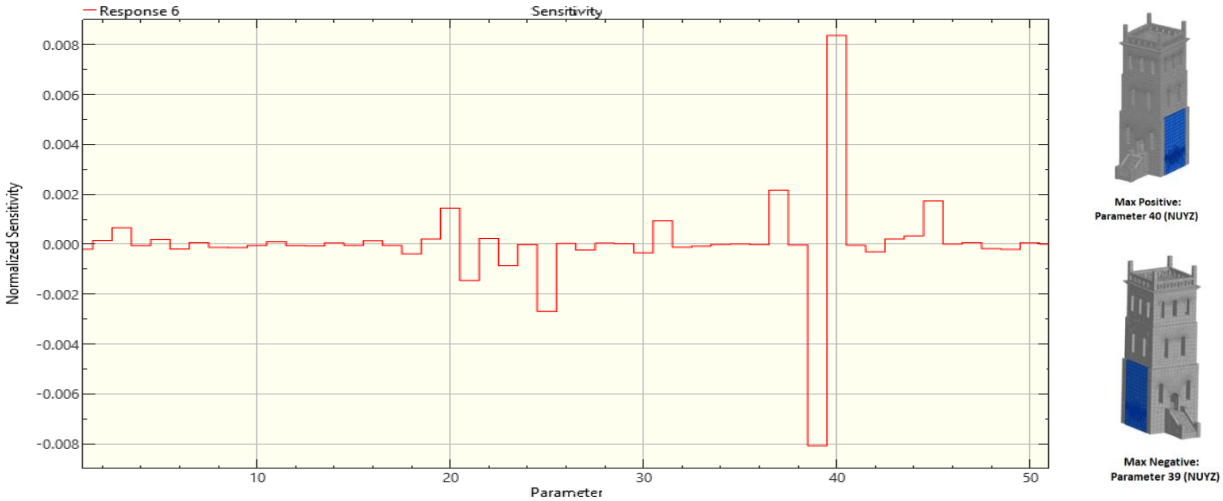

Figure 69 Sensitivity graph of the first mode shape to a change in Poisson's ratio / FB model

Figure 70 exhibits the sensitivity graph related to the sum of responses to a change in Poisson's ratio. The most positive effective parameter on the sum of responses is parameter 40 (NU_{yz} of

Wall1L), while the most negative is parameter 39 (NU_{yz} of Wall1R). It is shown that sensitivity values to a change in Poisson's ratio decrease as height increases.

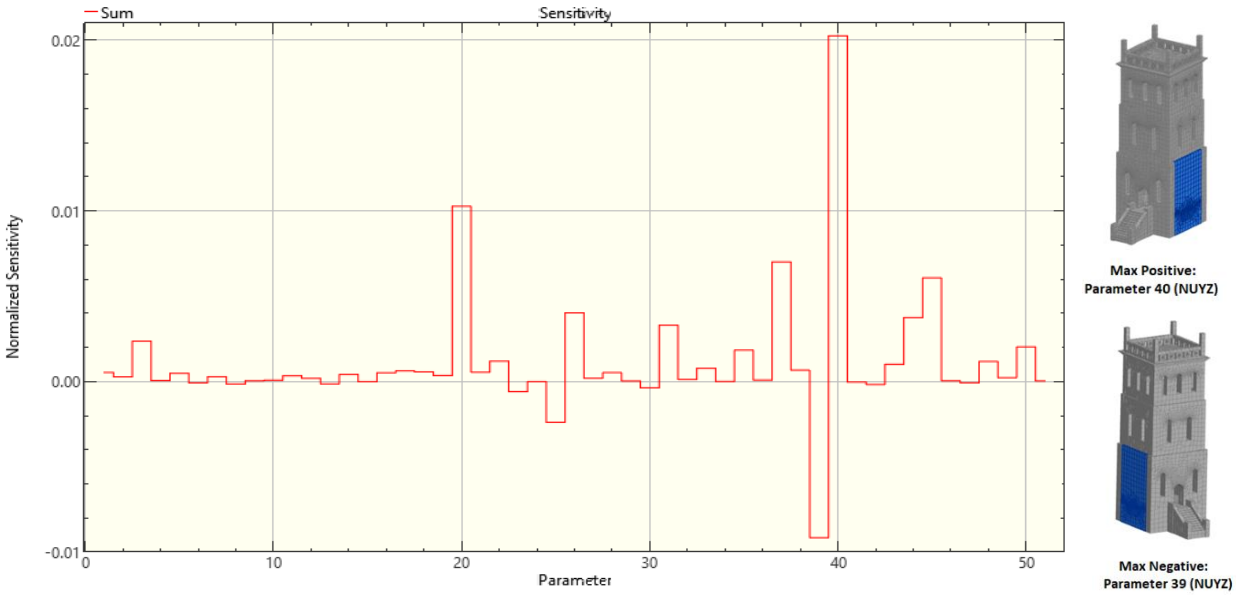

Figure 70 Sensitivity graph of sum-responses to a change in Poisson's ratio / FB model

The sensitivity graph to a change in Poisson's ratio for the sum of parameters has been presented in Figure 71. The figure represents the fourth frequency as the most sensitive response to a change in Poisson's ratio. Also, it is reported that all responses are positive to a change in the sum Poisson's ratio value of all parameters.

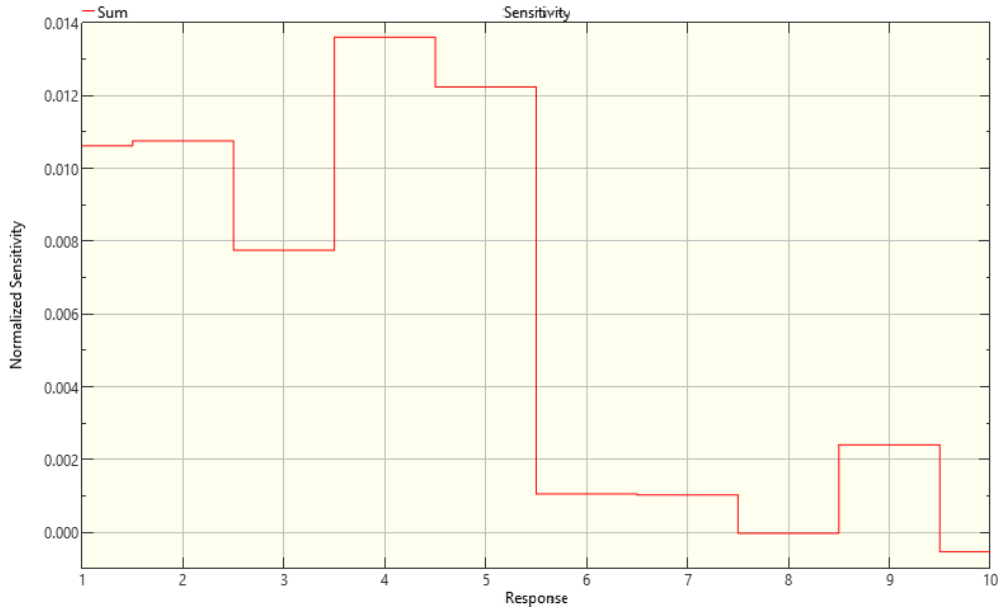

Figure 71 Sensitivity graph of all-responses to a change in Poisson's ratio for sum-parameters / FB model

6.3.2.2 SB Model

Sensitivity graphs to a change in Poisson's ratio for the SB model have been presented in Figure 72.

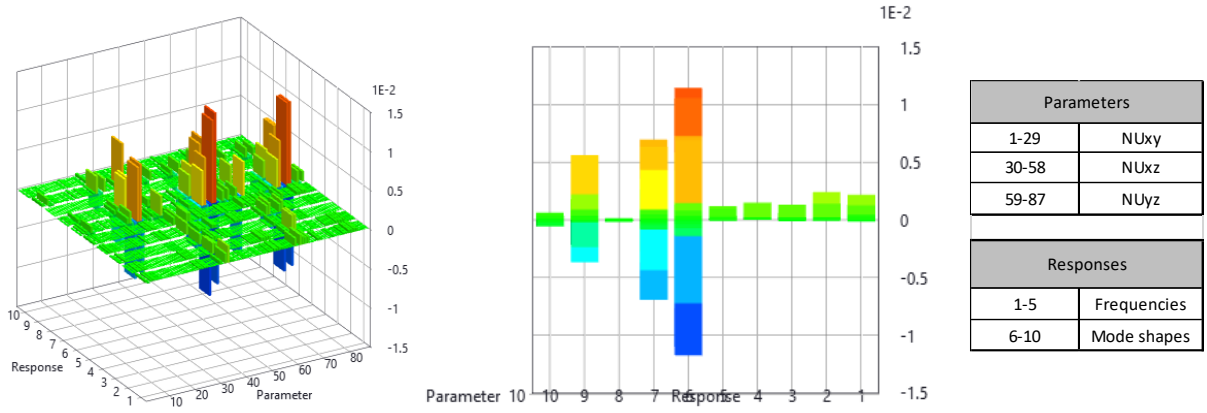

Figure 72 Sensitivity graph to a change in Poisson's ratio / SB model

From Figure 72, it is evident that the sensitivity of the frequencies is positive, while the mode shapes have shown both positive and negative sensitivities. The most positive and negative sensitivity has been observed for the first mode shape. It can be concluded that Poisson's ratio has more effect on the mode shapes rather than frequencies.

The sensitivity graph on the first frequency has been shown in Figure 73. Parameter 33 (NU_{xz} of Wall1B) is the most positive effective set on the first frequency. Also, it is highlighted that most of the effects are positive in this regard.

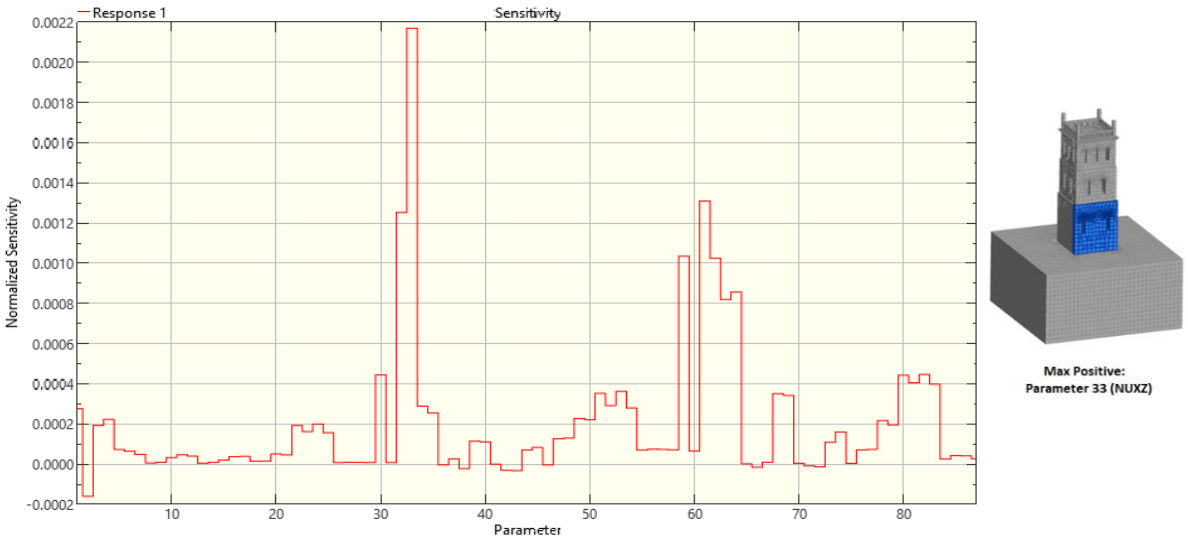

Figure 73 Sensitivity graph of the first frequency to a change in Poisson's ratio / SB model

The most positive sensitive set to a change in Poisson's ratio in the SB model is parameter 53 (NU_{xz} of Soil3), while the most negative sensitive one is parameter 51 (NU_{xz} of Soil1) as shown in Figure 74.

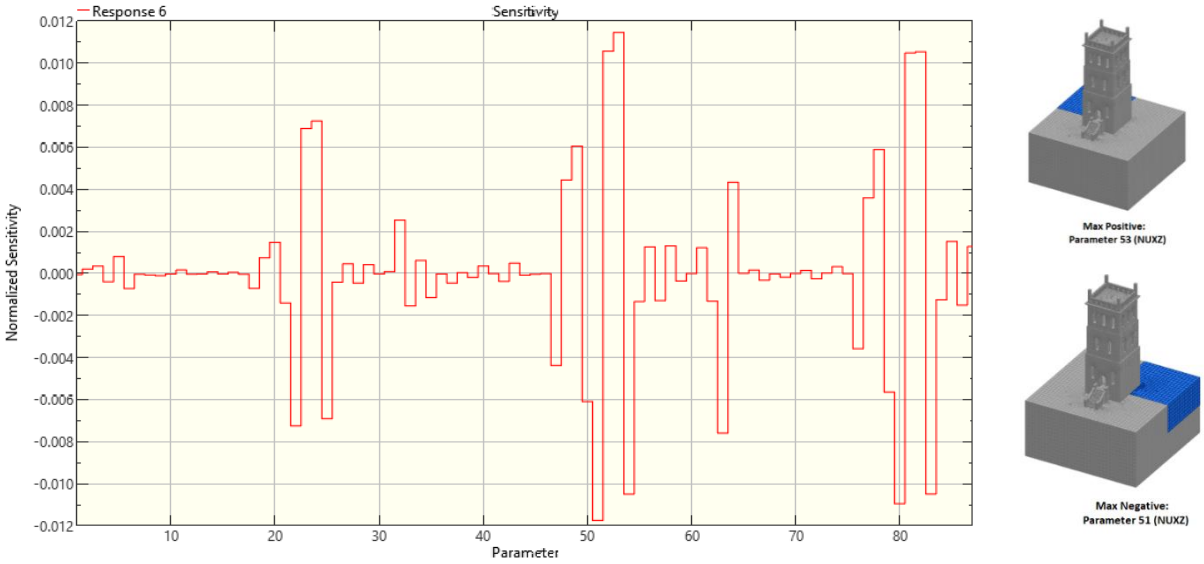

Figure 74 Sensitivity graph of the first mode shape to a change in Poisson's ratio / SB model

Figure 75 shows the sensitivity graph related to the sum of responses to a change in Poisson's ratio. Parameter 53 (NU_{xz} of Soil3) has shown the most positive sensitivity to a change in Poisson's ratio, while parameter 51 (NU_{xz} of soil1) takes the most negative one.

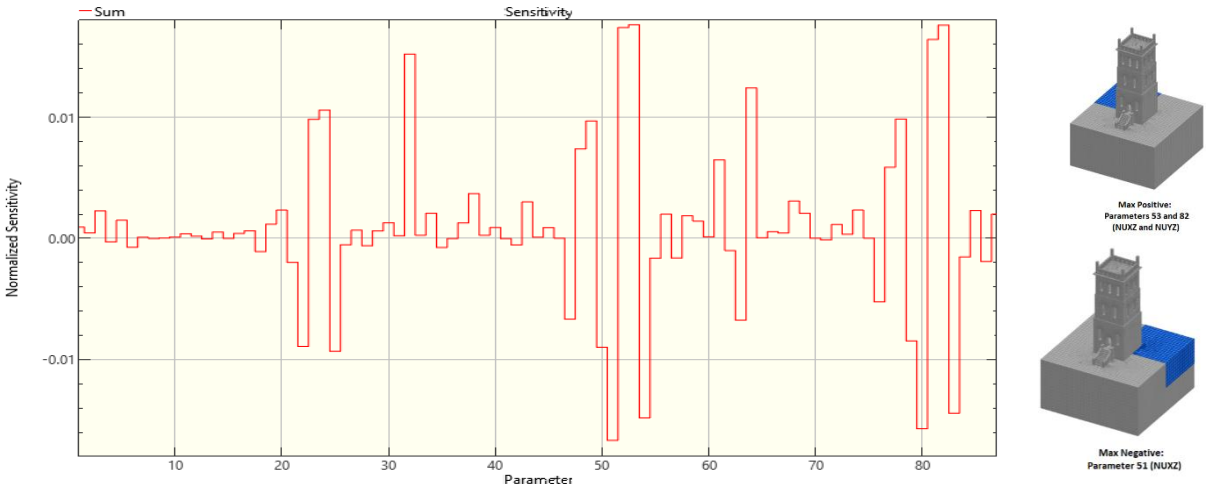

Figure 75 Sensitivity graph of sum-responses to a change in Poisson's ratio / SB model

It should be mentioned that sensitivity values to a change in Poisson's ratio decrease as height increases, as Figure 75 shows. Figure 76 highlights that the second frequency is the most sensitive response to a change in Poisson's ratio in the SB model.

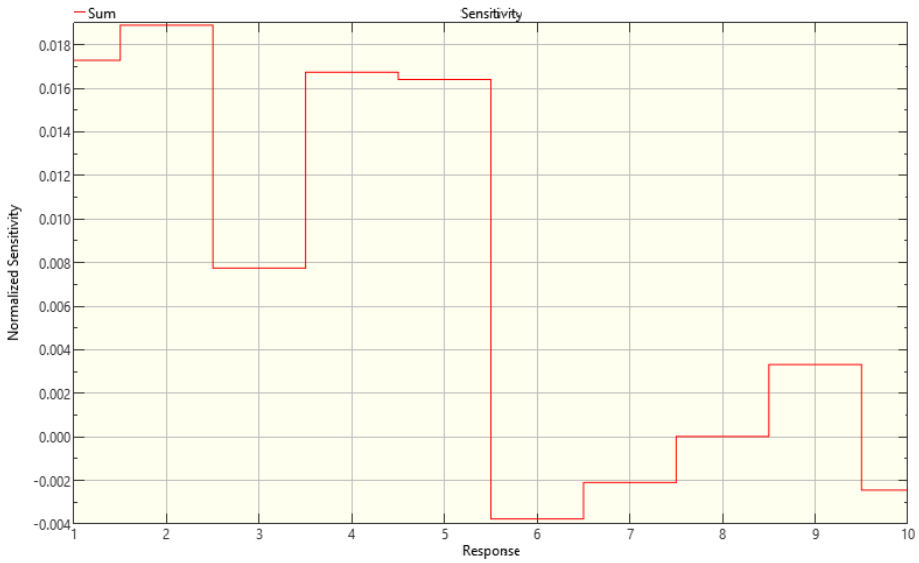

Figure 76 Sensitivity graph of all-responses to a change in Poisson's ratio for sum-parameters / SB model

6.3.2.3 SS Model

In Figure 77, the sensitivity graphs of the SS model to a change in Poisson's ratio have been presented.

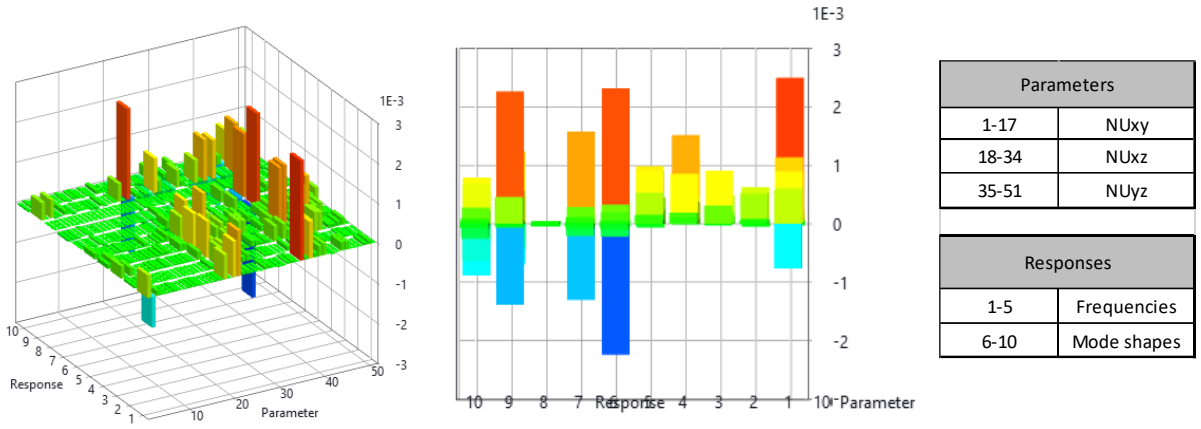

Figure 77 Sensitivity graph to a change in Poisson's ratio / SS model

Figure 77 reports that NU_{xy} has minor effects on the responses. The impacts of NU_{xz} and NU_{yz} on all responses have been observed as both positive and negative.

The sensitivity graph of the first response to a change in Poisson's ratio has been shown in Figure 78.

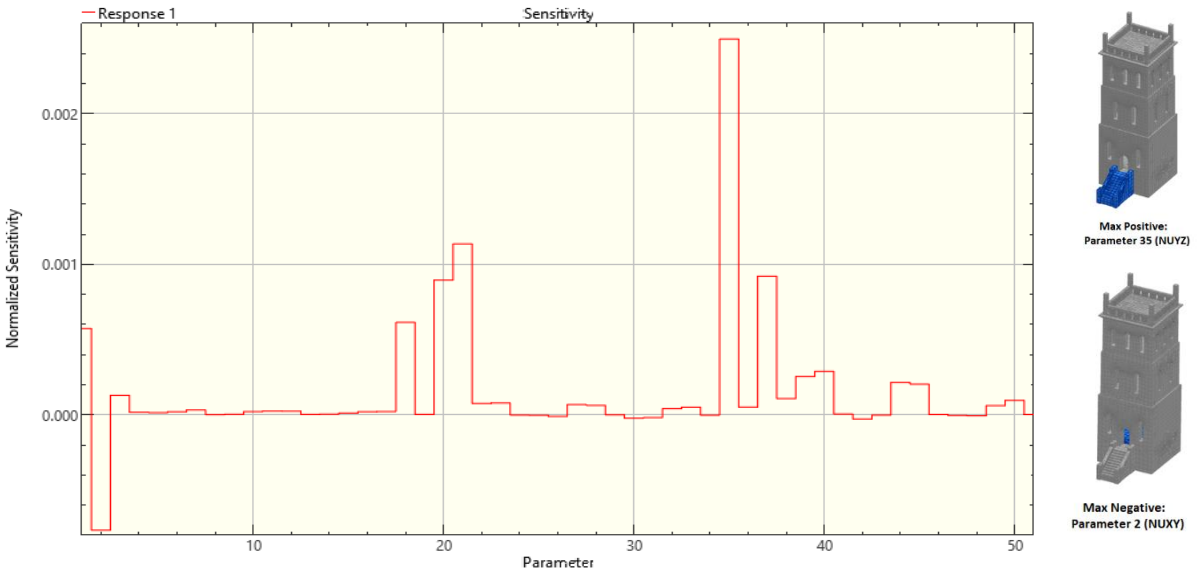

Figure 78 Sensitivity graph of the first frequency to a change in Poisson's ratio / SS model

The graph indicates that only for parameter 2 (NU_{xy} of Floor1) has negative sensitivity been recorded. The maximum positive sensitivity is for parameter 35 (NU_{xz} of Entrance).

The sensitivity graph to a change in Poisson's ratio for the first mode shape is shown in Figure 79. The most positive and negative sensitivities are parameter 40 (NU_{yz} of Wall1R) and parameter 39 (NU_{yz} of Wall1L).

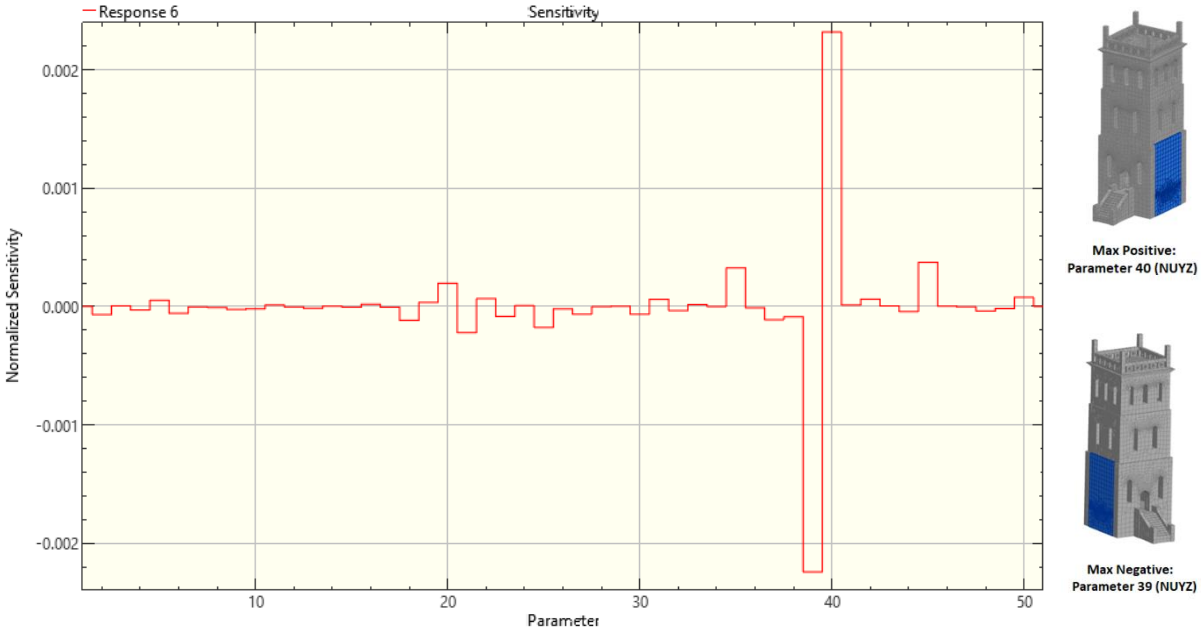

Figure 79 Sensitivity graph of the first mode shape to a change in Poisson's ratio / SS model

The sensitivity analysis graph to a change in the Poisson's ratio sum of parameters has been shown in Figure 80. The most positive sensitivity is parameter 40 (NUyz of Wall1R), while for parameter 2 (NU_{xy} of Floor1), maximum negative sensitivity has been obtained.

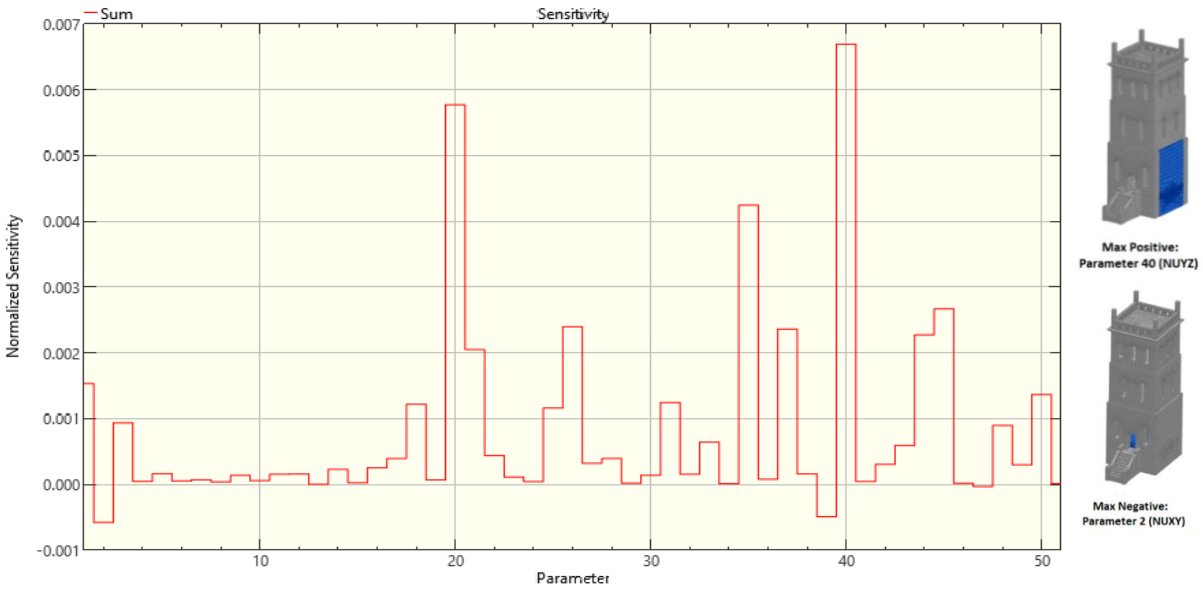

Figure 80 Sensitivity graph of sum-responses to a change in Poisson's ratio / SS model

Figure 81 shows the sensitivity graph of sum responses to a change in Poisson's ratio. The fourth frequency has the most sensitivity to a change in Poisson's ratio in the parameter sets.

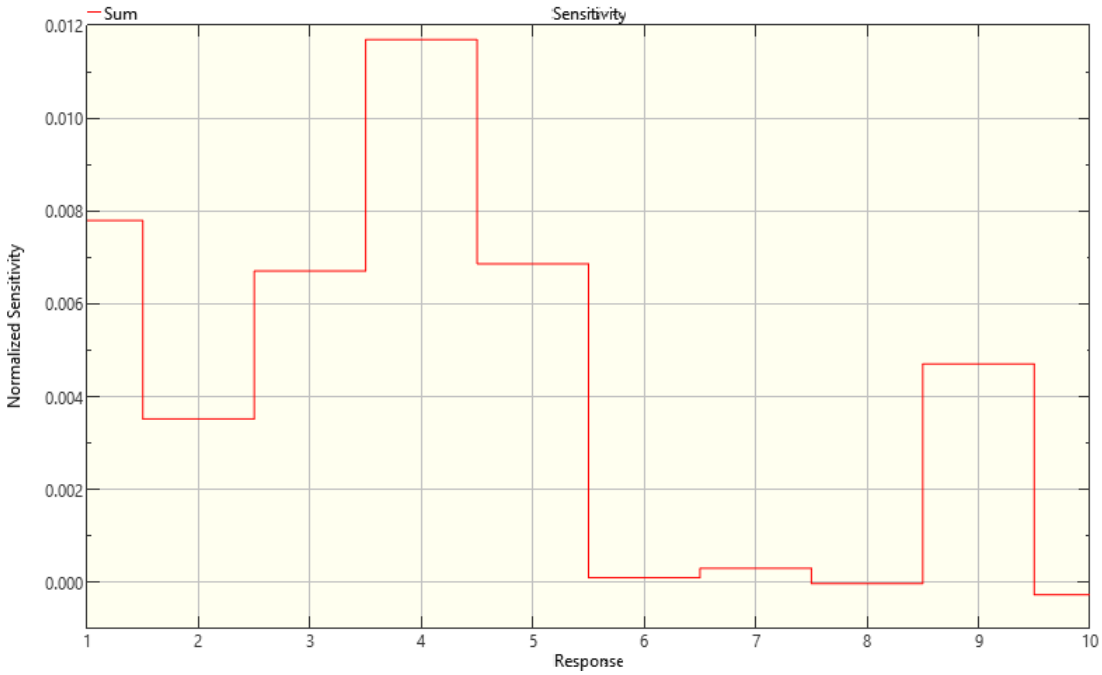

Figure 81 Sensitivity graph of sum-responses to a change in Poisson's ratio / SS model

6.3.3 Sensitivity to a Change in Density

Sensitivity analysis results to a change in density have been presented in this section.

6.3.3.1 FB Model

Based on Figure 82, which shows the sensitivity of the FB model to a change in density, the sensitivity of all frequencies is negative. It means that an increase in density will lead to a decrease in frequency. Both positive and negative sensitivities have been observed for mode shapes.

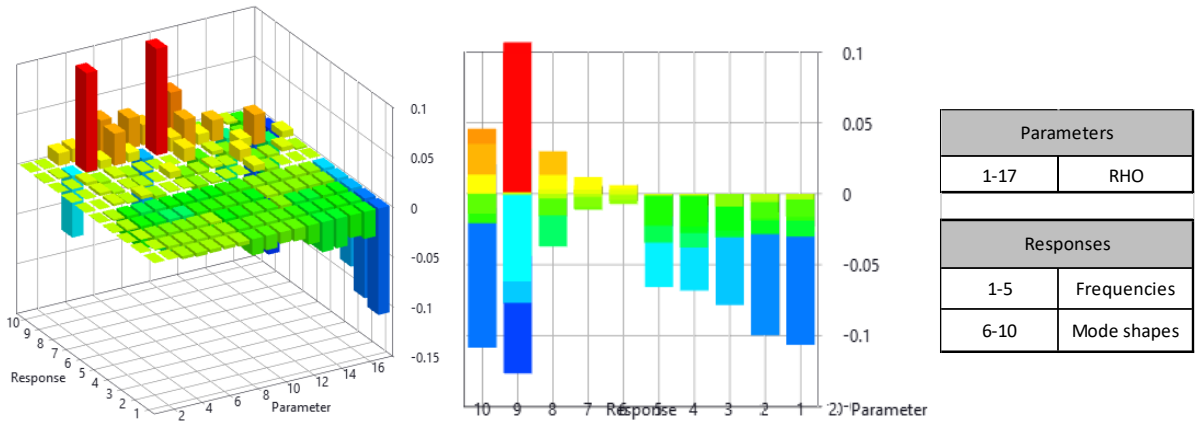

Figure 82 Sensitivity graph to a change in density / FB model

Figure 83 and Figure 84 will help investigate the sensitivity of different parameters of the FB model to a change in density for the first frequency and the first mode shape.

According to Figure 83, all the sensitivity values to a change in density for all parameters are negative. It is essential to underline that the normalized sensitivity values increase negatively for the higher sets. Therefore, parameter 17 (RHO of Roof) is the maximum negative effective parameter on the first frequency.

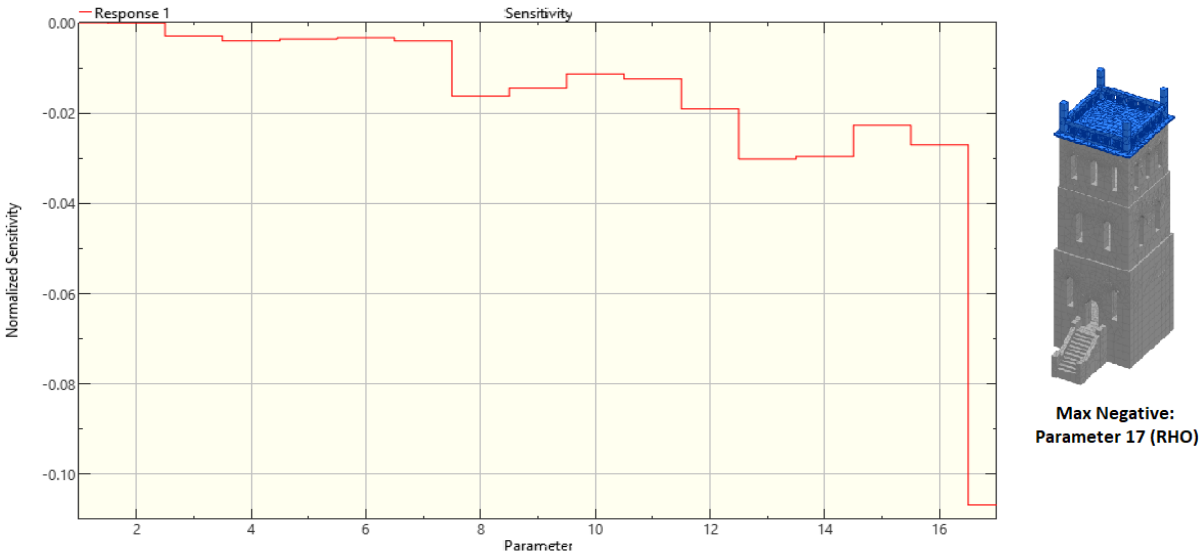

Figure 83 Sensitivity graph of the first frequency to a change in density / FB model

No significant trend was observed for the sensitivity of the first mode shape to a change in density. The maximum positive sensitivity has been reported for parameter 13 (RHO of Wall3F), while the maximum negative is parameter 9 (RHO of Wall2B).

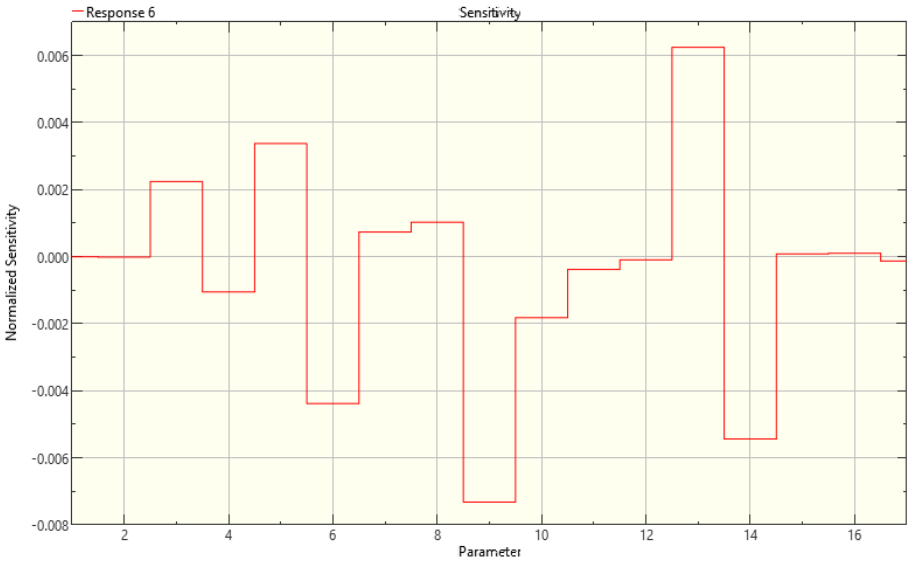

Figure 84 Sensitivity graph of the first mode shape to a change in density / FB model

Figure 85 shows the sensitivity graph of the sum of responses to a change in density. As already discussed, the graph points out that the maximum negative sensitivity is related to parameter 17 (RHO of Roof).

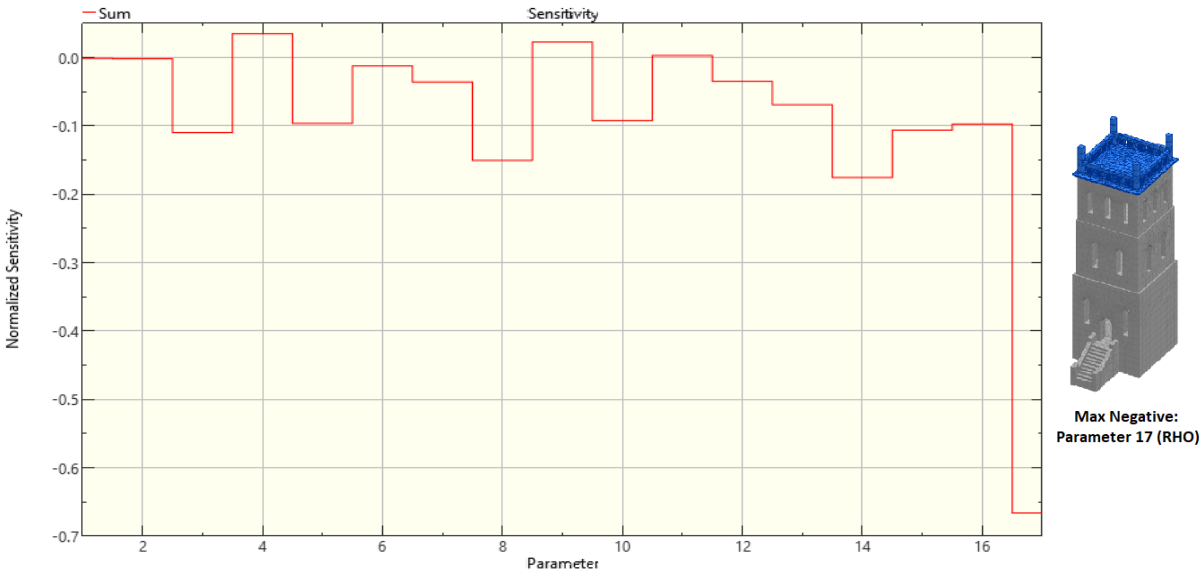

Figure 85 Sensitivity graph of sum-responses to a change in density / FB model

Also, the sensitivity graph to a change in density for the sum of parameters has been shown in Figure 86. It is shown that the overall sensitivity to a change in density of different structure

sets is negative for all frequencies and nearly zero for mode shapes. In conclusion, changes in the density of different sets do not significantly affect the mode shapes.

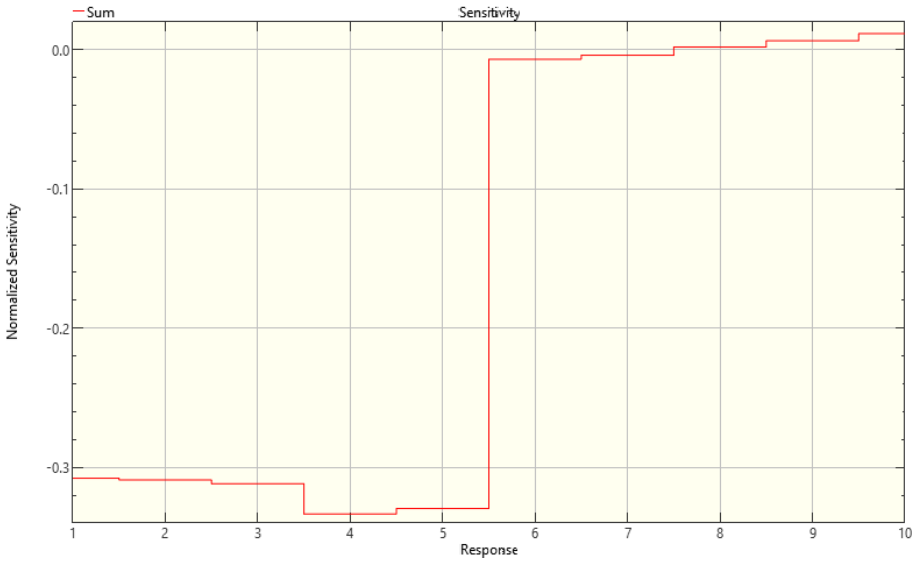

Figure 86 Sensitivity graph of responses to a change in density for sum-parameters / FB model

Normalized sensitivity values of the sum responses for the first, second, and third floors are -0.185, -0.252, and -0.482. The results show that the density variations have more effect on the response of the upper sets. The effect of density variations from the second to the third floor (91%) is much more significant than the first to the second floor (36%).

6.3.3.2 SB Model

Regarding the SB model, sensitivity graphs to a change in density for different parameters have been reported in this section.

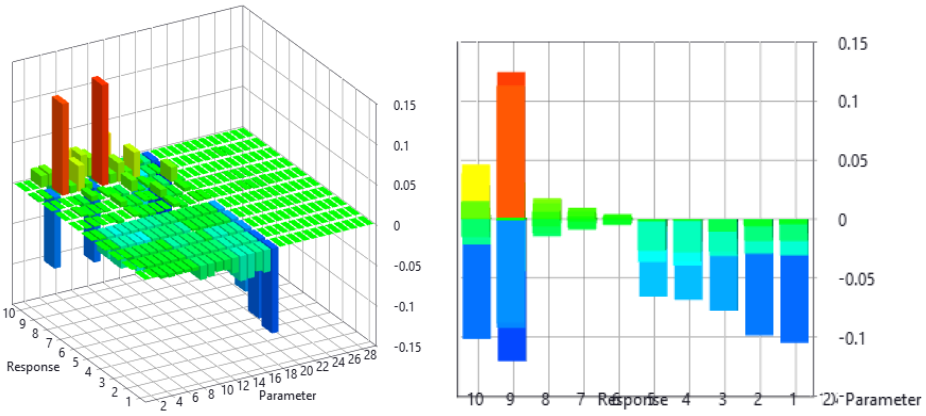

Parameters	
1-29	RHO

Responses	
1-5	Frequencies
6-10	Mode shapes

Figure 87 Sensitivity graph to a change in density / SB model

Figure 87 indicates that the target responses are not sensitive to a change in the density of soil and foundation sets. Also, it is shown that the frequencies' sensitivity to a change in density is negative, while for the mode shapes, the sensitivity can be positive or negative.

The sensitivity analysis to a change in density for the first frequency is shown in Figure 88. It is noteworthy to stress that in this model, the higher height sets have higher sensitivity values. Therefore, the maximum sensitivity to a change in density has been observed for parameter 17 (RHO of Roof).

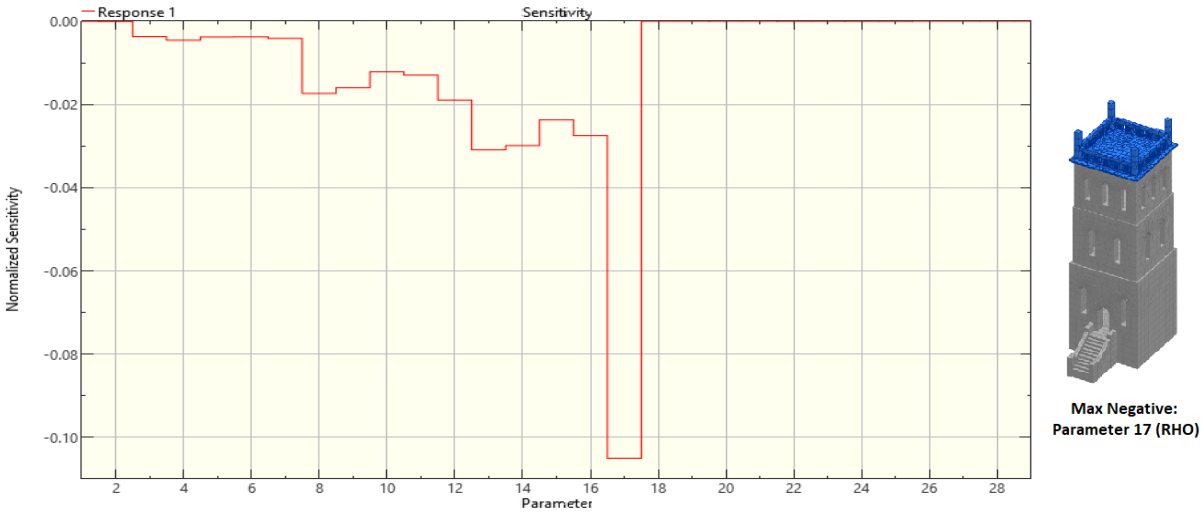

Figure 88 Sensitivity graph of the first frequency to a change in density / SB model

The sensitivity graph to a change in density for the first mode shape has been shown in Figure 89. The maximum positive and negative sensitivity is for parameter 13 (RHO of Wall3F) and parameter 9 (RHO of Wall2R).

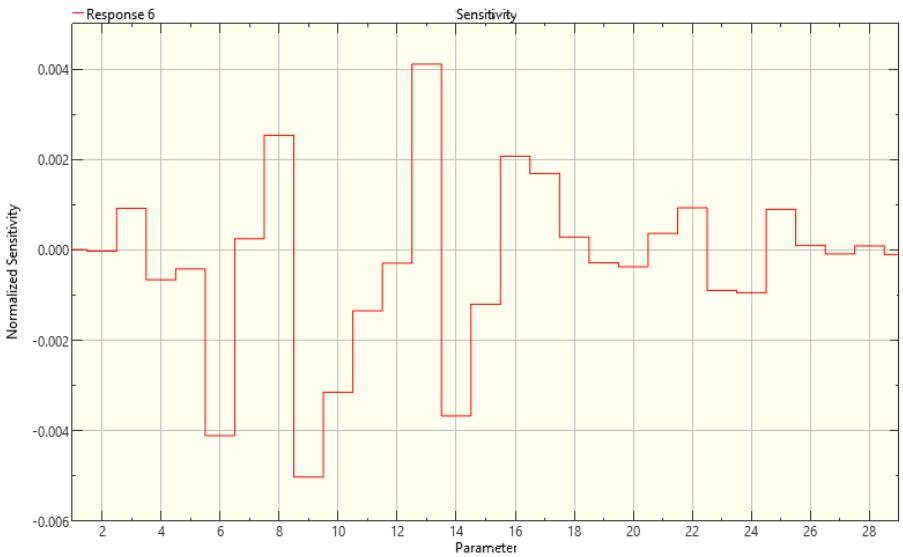

Figure 89 Sensitivity graph of the first mode shape to a change in density / SB model

The sensitivity analysis graph regarding the sum of the responses to a change in density has been shown in Figure 90. The graph depicts that the most effective set of the structure to a change in the density is parameter 17 (RHO of Roof), which is in the highest height.

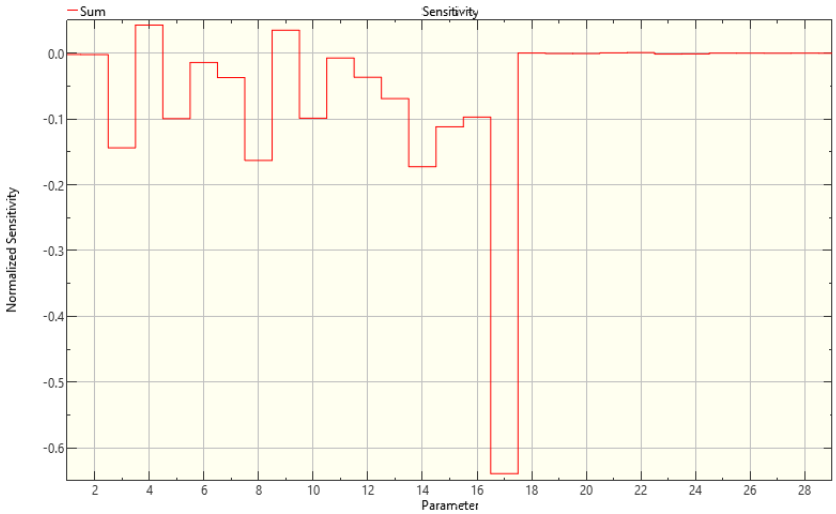

Figure 90 Sensitivity graph of sum-responses to a change in density / SB model

It is interesting to state that based on Figure 91, which shows the sensitivity graph to a change in density for the sum of the parameters, the mode shapes do not have a significant overall effect. The graph also confirms that the sensitivity of frequencies to a change in density is negative.

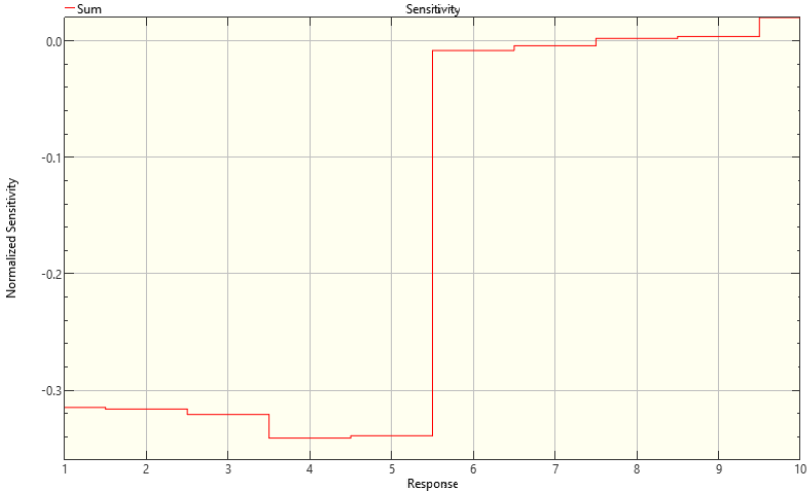

Figure 91 Sensitivity graph of all-responses to a change in density for sum-parameters / SB model

In the SB model, normalized sensitivity values of the sum-responses for the first, second, and third floors are -0.217, -0.271, and -0.487, respectively. These values show an 80% increase in sensitivity values from the second floor to the third, while the growth is around 25% from the first floor to the second one.

6.3.3.3 SS Model

The sensitivity graphs of the SS model to a change in density for all responses have been shown in Figure 92.

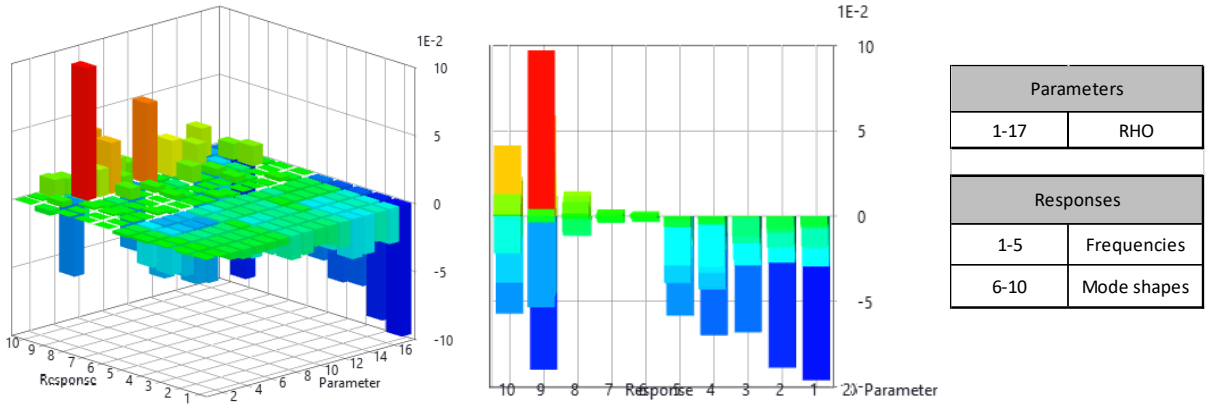

Figure 92 Sensitivity graph to a change in density / SS model

The sensitivity to a change in density for all frequencies is negative, while both positive and negative sensitivities have been observed for the mode shapes. The maximum positive sensitivity has been reported in the fourth mode shape. Also, the most negative sensitivity is for the first frequency.

The sensitivity graphs to a change in the density for the first frequency and associated mode shape have been shown in Figure 93 and Figure 94, respectively.

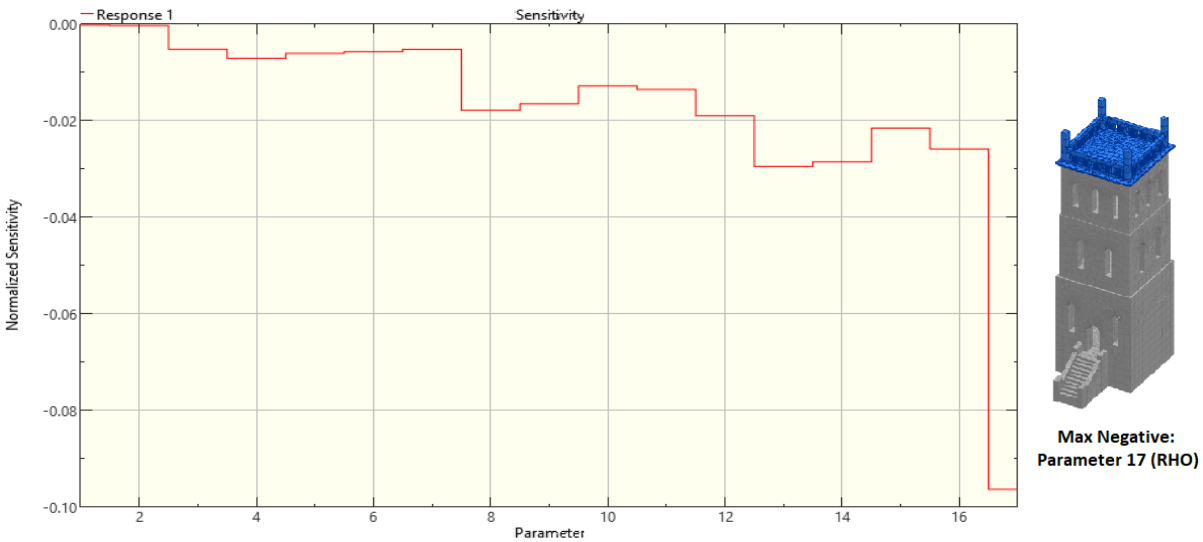

Figure 93 Sensitivity graph of the first frequency to a change in density / SS model

Regarding the first frequency, all the sensitivity values to a change in density are negative with the maximum effect at parameter 17 (RHO of Roof).

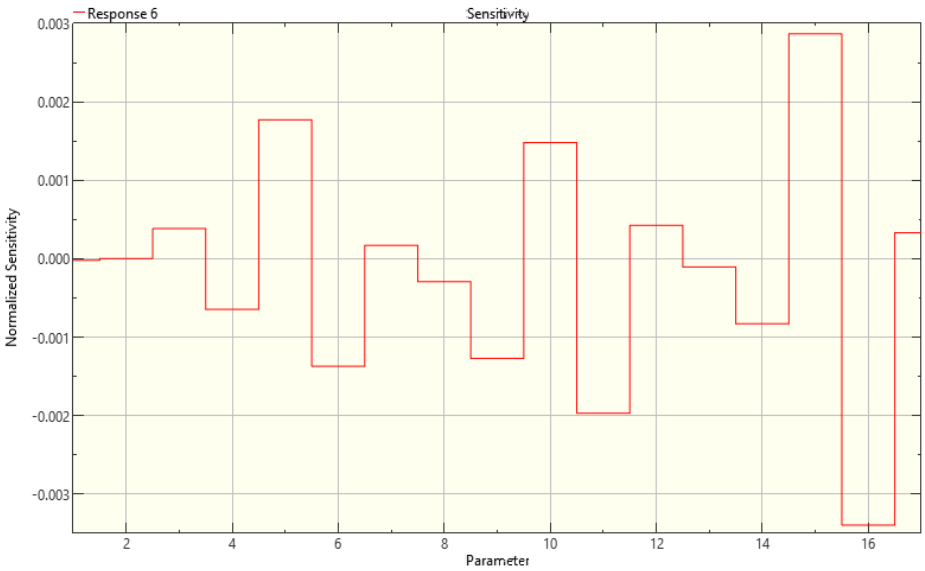

Figure 94 Sensitivity graph of the first mode shape to a change in density / SS model

In Figure 94, which contains the sensitivity values related to the first mode shape, the most positive sensitivity has been gained at parameter 15 (RHO of Wall3L), while the most negative one is at parameter 16, which is the density of the right wall of the third floor (RHO of Wall3R).

Figure 95 shows the sensitivity graph to a change in density for the sum of responses. As expected, the sensitivity is negative with the maximum value at parameter 17 (RHO of Roof).

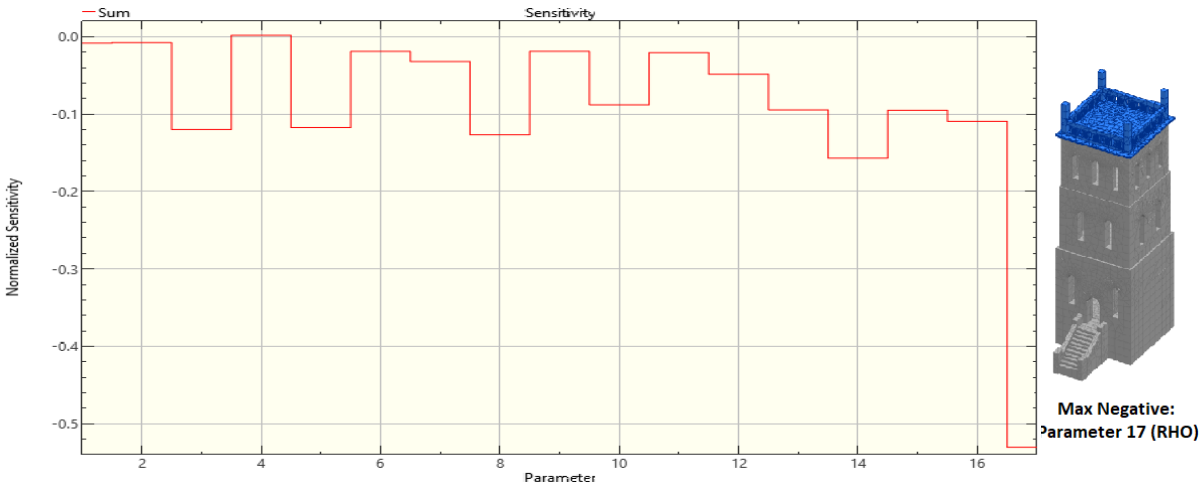

Figure 95 Sensitivity graph of sum-responses to a change in density / SS model

From Figure 96, it can be concluded that only frequencies are sensitive to a change in the density of the structure's sets.

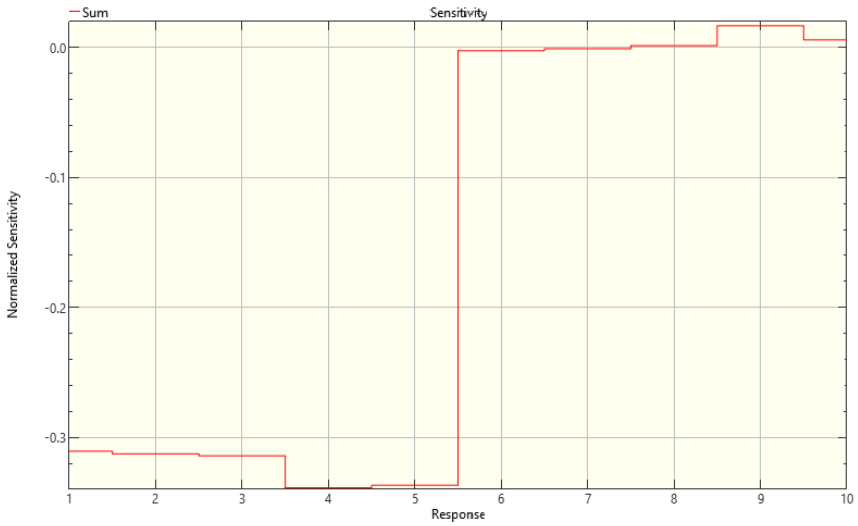

Figure 96 Sensitivity graph of sum-responses to a change in density / SS model

In the SB model, normalized sensitivity values of the sum-responses for the first, second, and third floors are -0.262, -0.287, and -0.505, respectively. These values show a 76% increase in sensitivity values from the second floor to the floor, while the growth is around 10% from the first floor to the second one.

It should also be noted that comparing sensitivity values of three studies models concluded that the sensitivity of the SS model to a change in density is more than two other models (Figure 97). Also, the SB model is more sensitive to a change in density than the FB model.

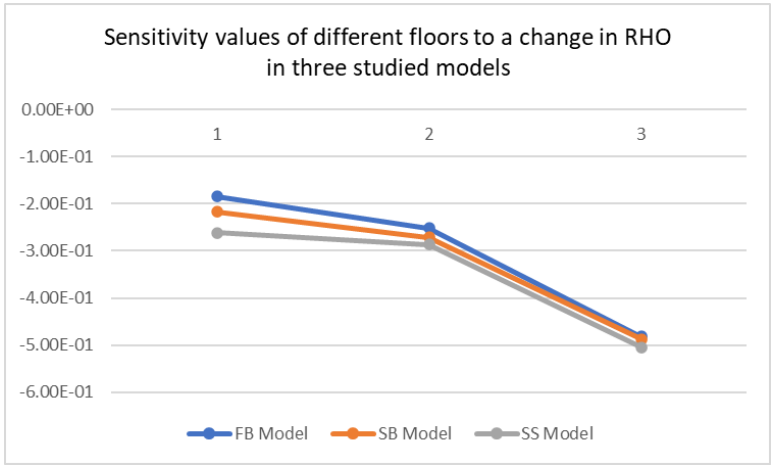

Figure 97 Sensitivity values of different floors to a change in density / all models

6.3.4 Sensitivity to a Change in Shear Modulus

6.3.4.1 FB Model

Sensitivity analysis results of shear modulus variations have been presented in Figure 98.

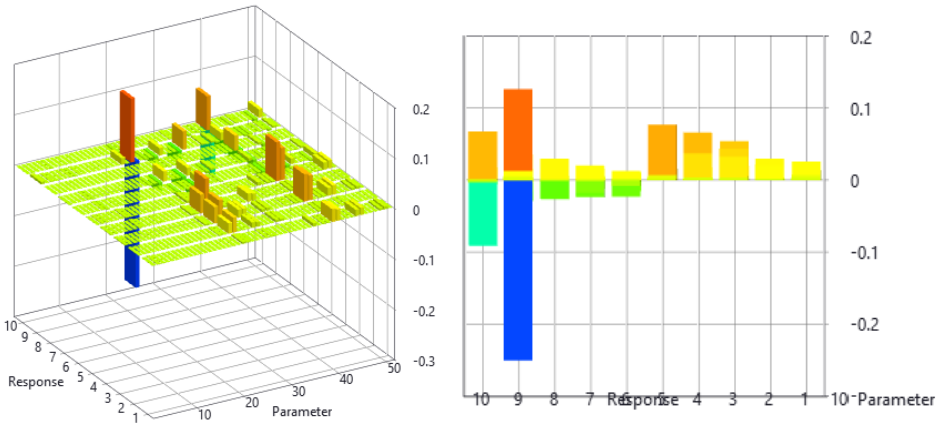

Parameters	
1-17	Gxy
18-34	Gxz
35-51	Gyz

Responses	
1-5	Frequencies
6-10	Mode shapes

Figure 98 Sensitivity graph to a change in shear modulus / FB model

The sensitivity of responses to a change in G_{xy} takes small values. The graph also indicates that shear modulus changes on the frequency variations are positive while the mode shapes are both positive and negative. Also, it should be noted that the most negative and positive effects have been recorded for the fourth mode shape.

The sensitivity analysis graph to a change in shear modulus for the first frequency as the target response has been illustrated in Figure 99.

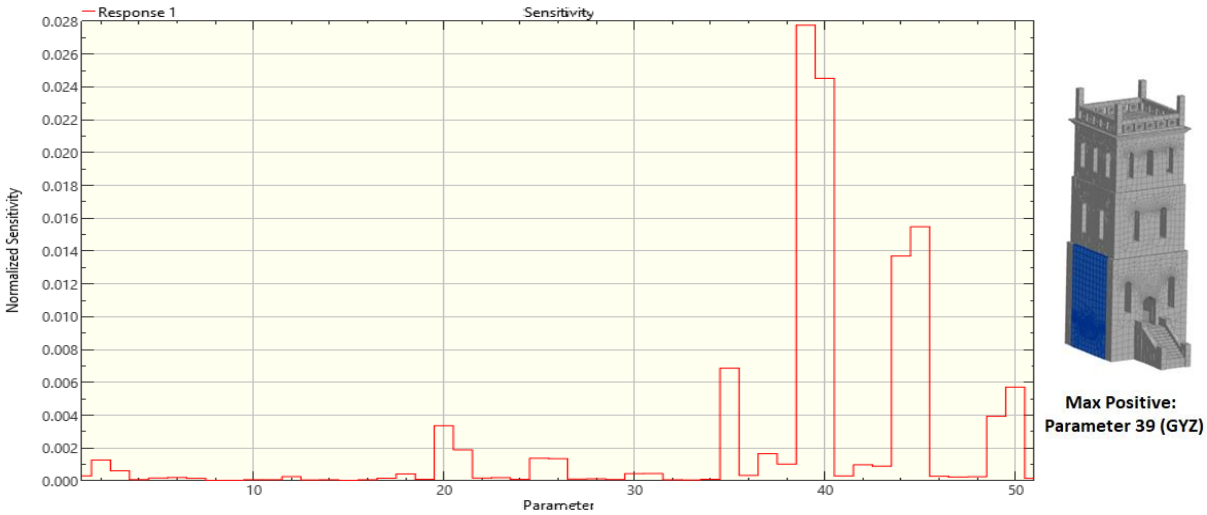

Figure 99 Sensitivity graph of the first frequency to a change in shear modulus / FB model

All the normalized sensitivity values are over zero, showing that the sensitivity of the first frequency to a change in all the parameters is positive. The maximum sensitivity has been recorded for parameter 39 (G_{yz} of Wall1L).

As shown in Figure 100, the maximum positive and negative sensitivity to a change in the density for the first mode shape occurred at parameter 36 (G_{yz} of Floor1) and parameter 35 (G_{yz} of Entrance), respectively.

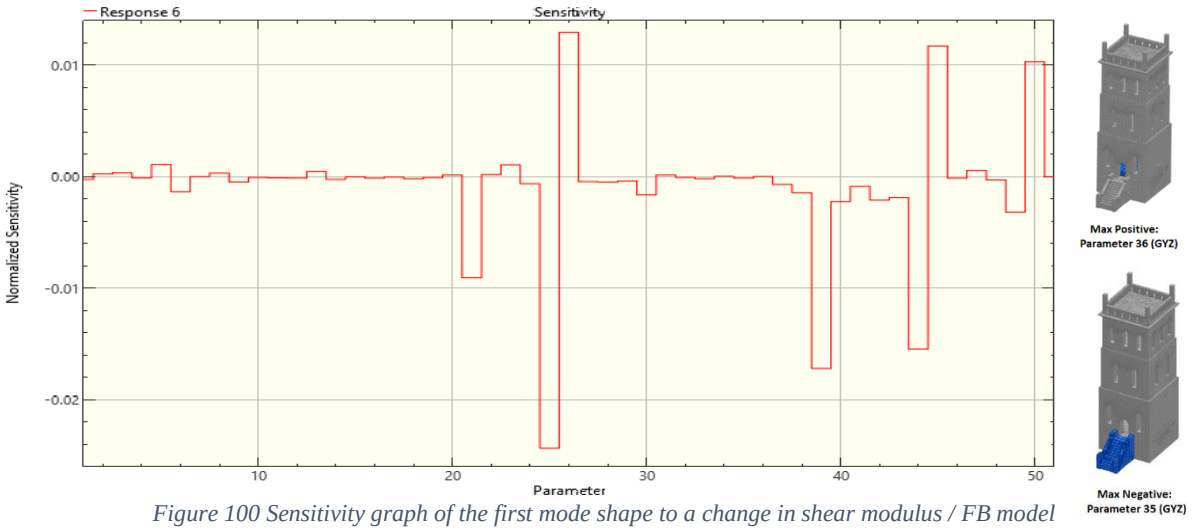

Figure 100 Sensitivity graph of the first mode shape to a change in shear modulus / FB model

The sensitivity graph to a change in shear modulus related to the summary of responses has been shown in Figure 101. The maximum positive effect is parameter 39 (G_{yz} of Wall1L), the first floor's left wall. Also, the maximum negative sensitivity has been registered for parameter 21 (Wall1B).

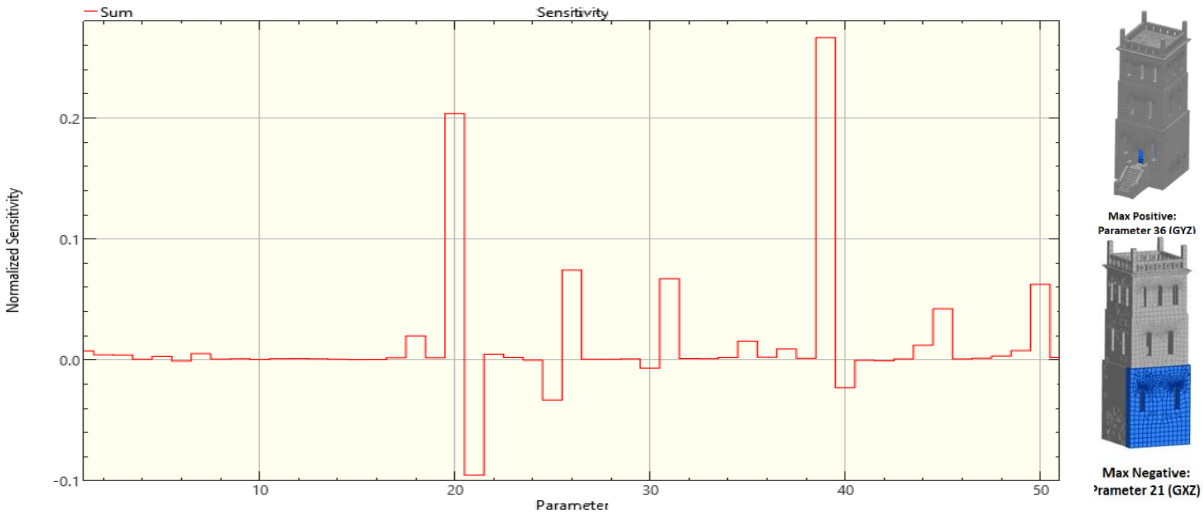

Figure 101 Sensitivity graph of sum-responses to a change in shear modulus / FB model

The sensitivity graph for the sum of the parameters has been shown in Figure 102. The most sensitive response to a change in shear modulus values is the third frequency affected positively. Also, the maximum negative sensitivity among the target responses has been registered for the fourth mode shape.

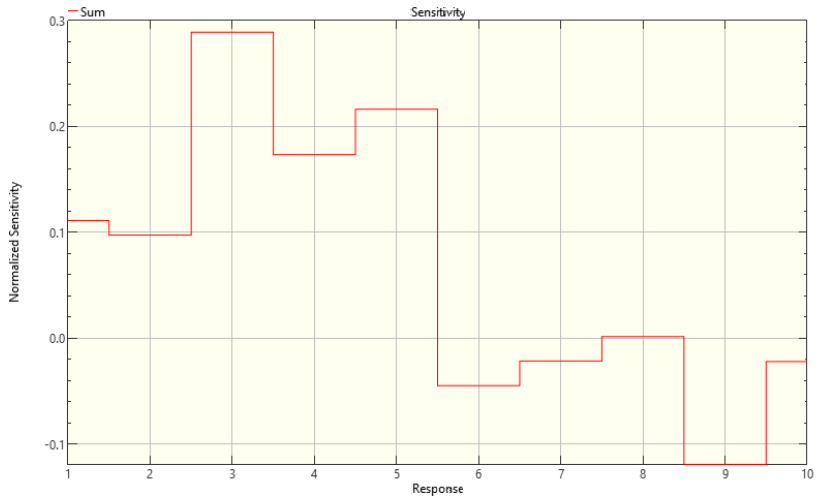

Figure 102 Sensitivity graph of all-responses to a change in shear modulus for sum-parameters / FB model

The sensitivity investigations to a change in shear modulus for the FB model showed that responses are more sensitive to G_{yz} among shear modulus parameters. Sensitivity values to a change in G_{yz} were highest for the first-floor sets and lowest for the third-floor sets. In this case, normalized sensitivity values for the first, second, and third floors are 0.256, 0.0883, and 0.0758, respectively.

6.3.4.2 SB Model

The sensitivity graph to a change in shear modulus of different parameters is shown in Figure 103.

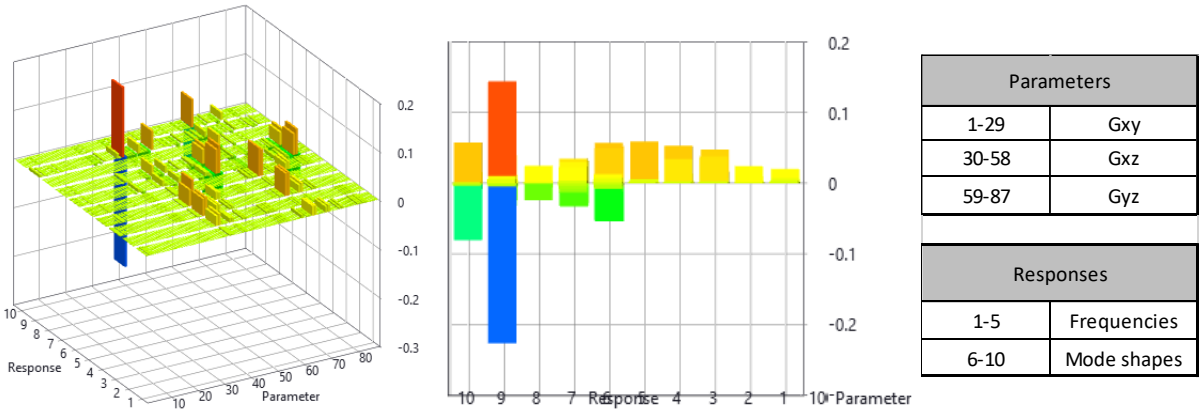

Parameters	
1-29	Gxy
30-58	Gxz
59-87	Gyz

Responses	
1-5	Frequencies
6-10	Mode shapes

Figure 103 Sensitivity graph to a change in shear modulus / SB model

The figure clearly states that only G_{xz} and G_{yz} affect both frequencies and mode shapes. The effect on the frequencies is positive, while on the mode shapes, both negative and positive

sensitivities have been observed. The most positive and negative effects have been observed on the fourth mode shape.

The sensitivity analysis to investigate the effect of changing shear modulus on the first frequency is shown in Figure 104. Knowing that the sensitivities are all positive, the highest sensitivity is related to parameter 63 (G_{yz} of Wall1L).

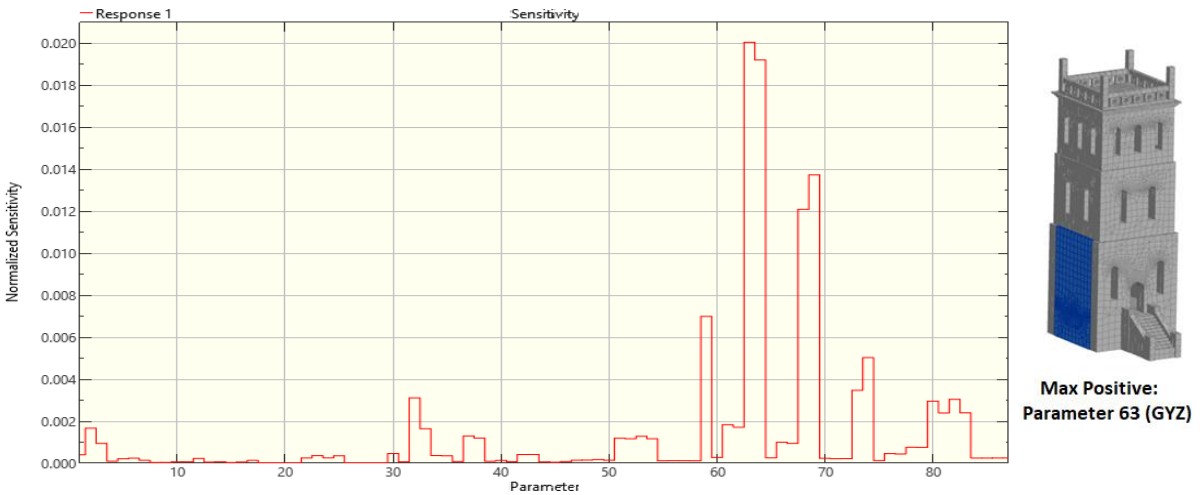

Figure 104 Sensitivity graph of the first frequency to a change in shear modulus / SB model

Figure 105 is related to the sensitivity graph to a change in shear modulus for the first mode shape.

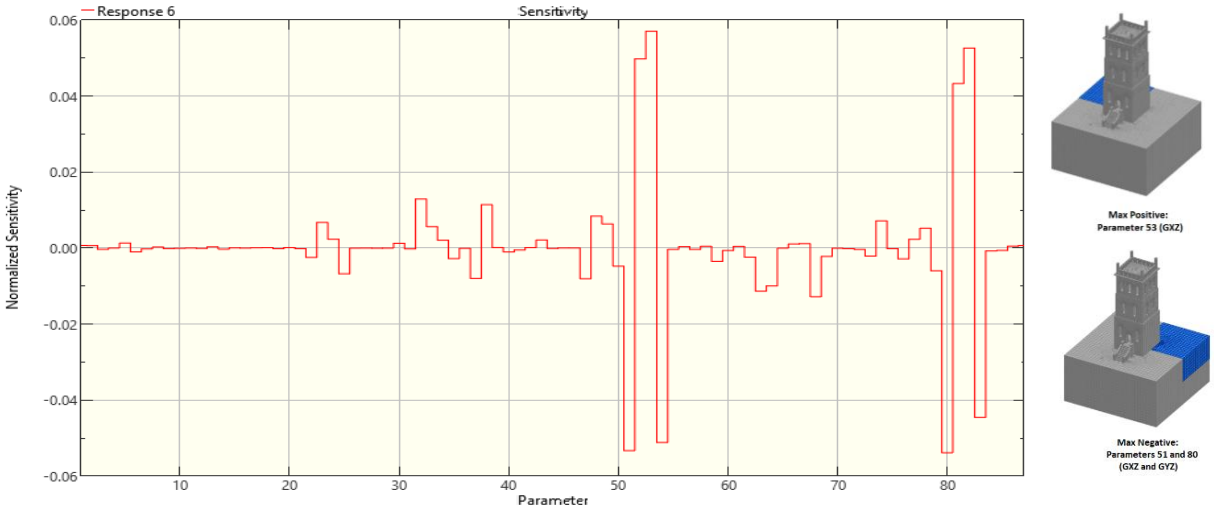

Figure 105 Sensitivity graph of the first mode shape to a change in shear modulus / SB model

In Figure 105, the most positive sensitivity is for parameter 53 (G_{xz} of soil3), and the most negative sensitivity is for parameter 80 (G_{yz} of soil1).

The sensitivity analysis for the sum of the responses to a change in shear modulus is shown in Figure 106. The maximum positive sensitivity is for parameter 32 (G_{xz} of Wall1F), while the maximum negative is parameter 33 (G_{xz} of Wall1B).

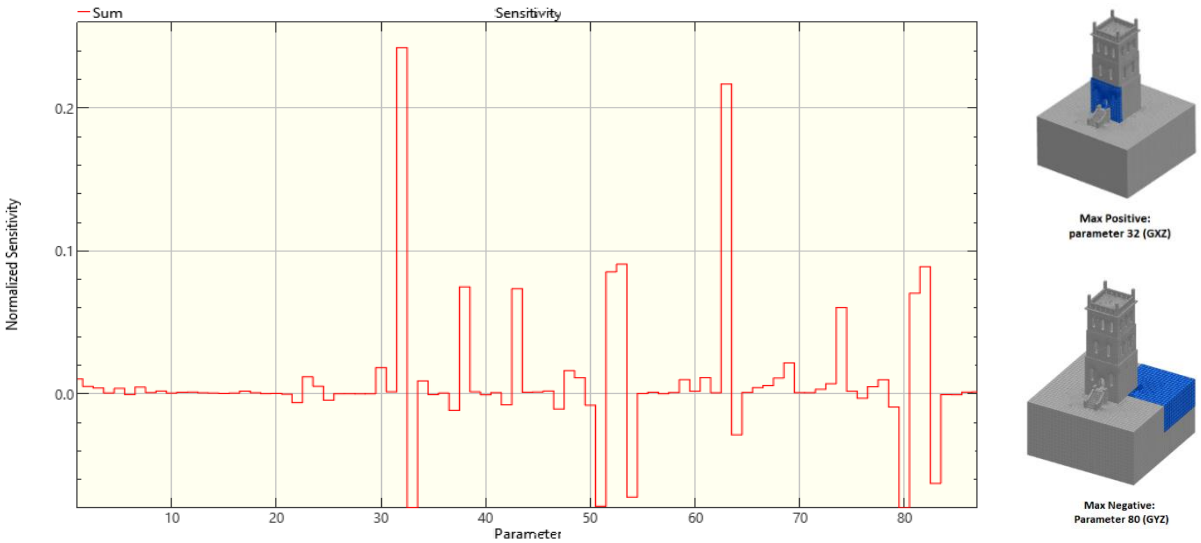

Figure 106 Sensitivity graph of sum-responses to a change in shear modulus / SB model

Figure 107 shows the sensitivity graph to a change in shear modulus for the sum of the parameters. The third frequency has shown the most positive sensitivity, and the fourth mode shape has the maximum negative sensitivity to a change in shear modulus in the SB model.

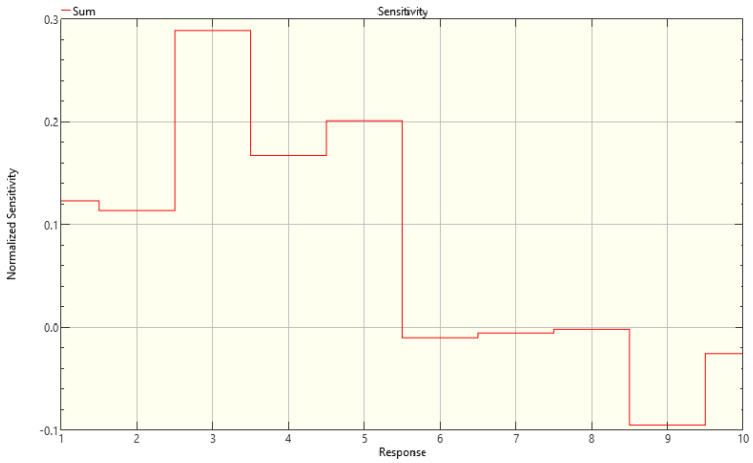

Figure 107 Sensitivity graph of all-responses to a change in shear modulus for sum-parameters / SB model

In the SB model, the responses are more sensitive to G_{xz} and G_{yz} parameters. Like the FB model, the higher the floor height, the lower sensitivity values to a change in G_{xz} and G_{yz}. The normalized sensitivity values to a change in G_{yz} for the first, second, and third floors are 0.202,

0.0821, and 0.0721, respectively. Also, the sensitivity values to a change in G_{xz} are 0.173, 0.0710, and 0.0690 for the first, second, and third floors, respectively.

6.3.4.3 SS Model

Figure 108 includes the sensitivity graphs of the SS model to a change in shear modulus.

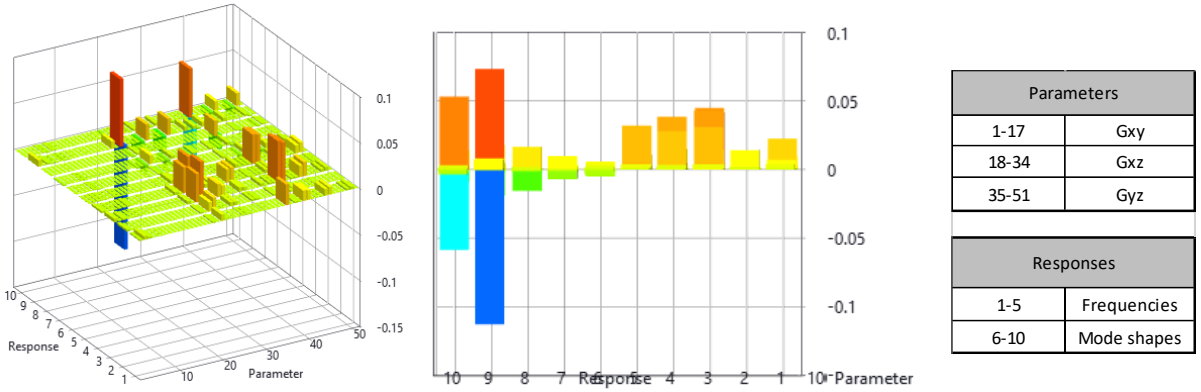

Figure 108 Sensitivity graph to a change in shear modulus / SS model

The effect of parameters on the frequencies is positive, while the impact on the mode shapes is both positive and negative. The most positive and negative responses are in the fourth mode shape.

The sensitivity graphs to a change in shear modulus for the first frequency have been presented in Figure 109. All the sensitivities, in this case, are positive, with the maximum value for parameter 35 (G_{yz} of Entrance).

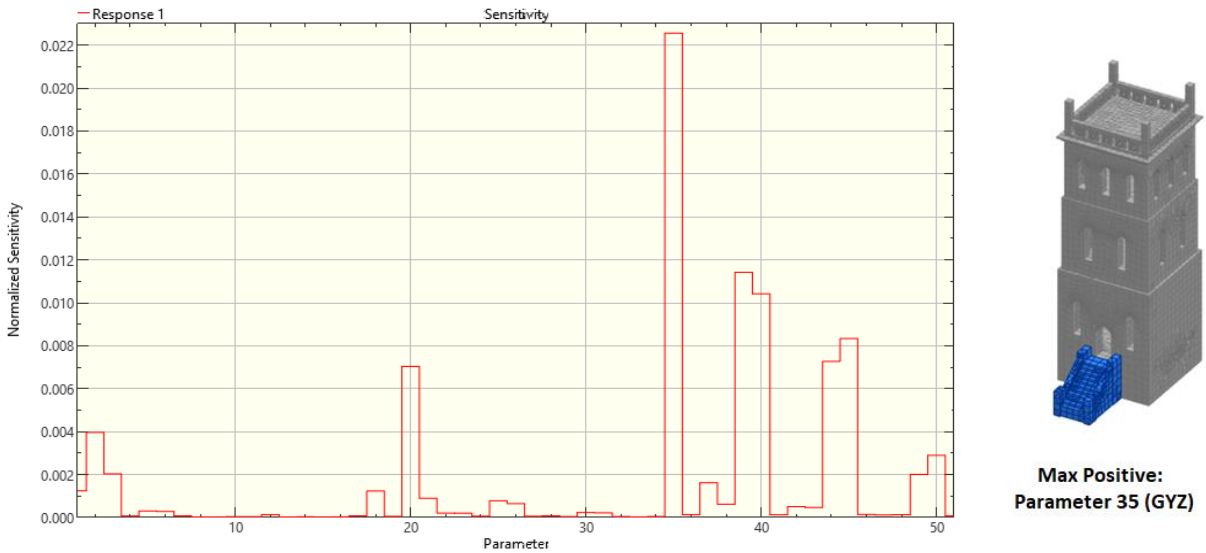

Figure 109 Sensitivity graph of the first frequency to a change in shear modulus / SS model

Looking at Figure 110, one can see that the maximum positive and negative sensitivities are for parameters 45 and 44, respectively. Parameter 45 is (G_{yz} of Wall2R), and parameter 44 is the roof set in this case (G_{xz} of Roof).

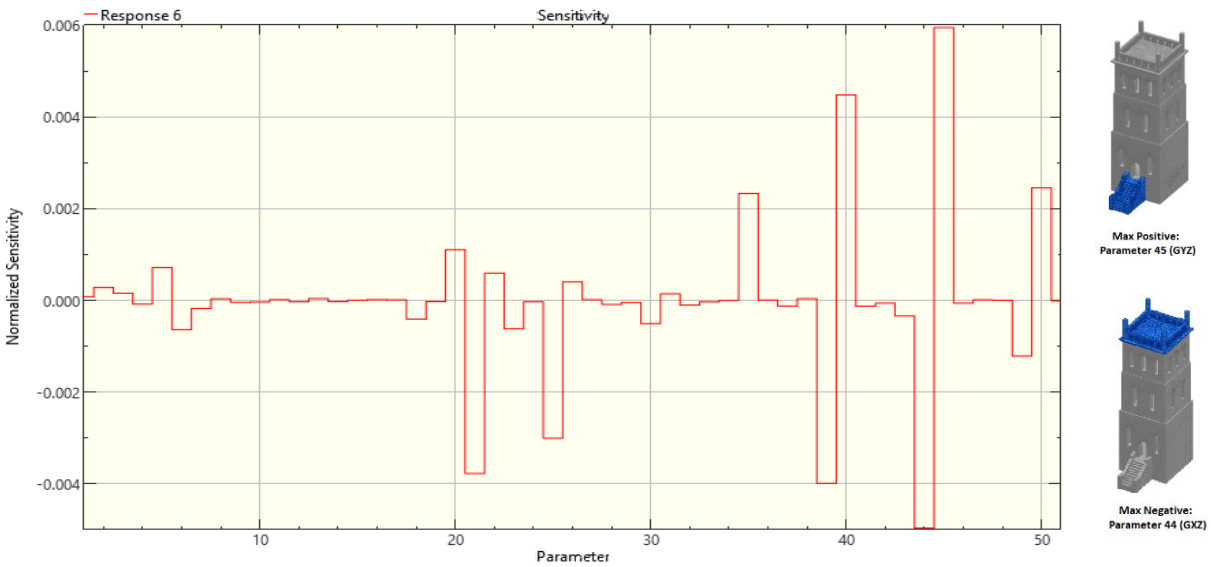

Figure 110 Sensitivity graph of the first mode shape to a change in shear modulus / SS model

Figure 111 shows the sensitivity analysis graph of the shear modulus changing effects on the sum of the responses. Parameter 39 (G_{yz} Wall1L) is the most influential parameter on the sum of responses.

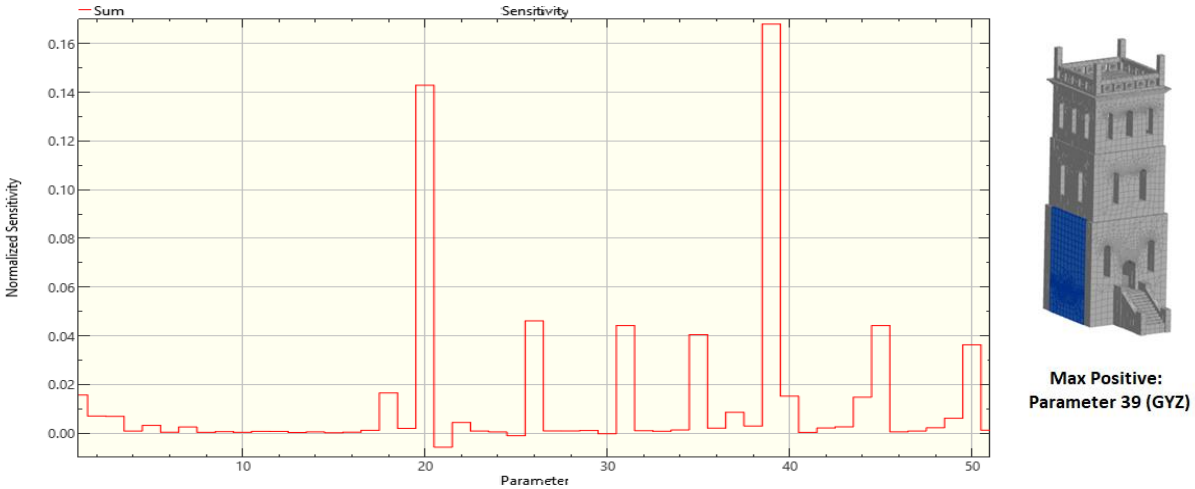

Figure 111 Sensitivity graph of sum-responses to a change in shear modulus / SS model

Figure 112 is related to the sensitivity graph to a change in shear modulus for the sum of the parameters. It is shown that the third frequency is the most sensitive response to a change in shear modulus of different sets in the SS model.

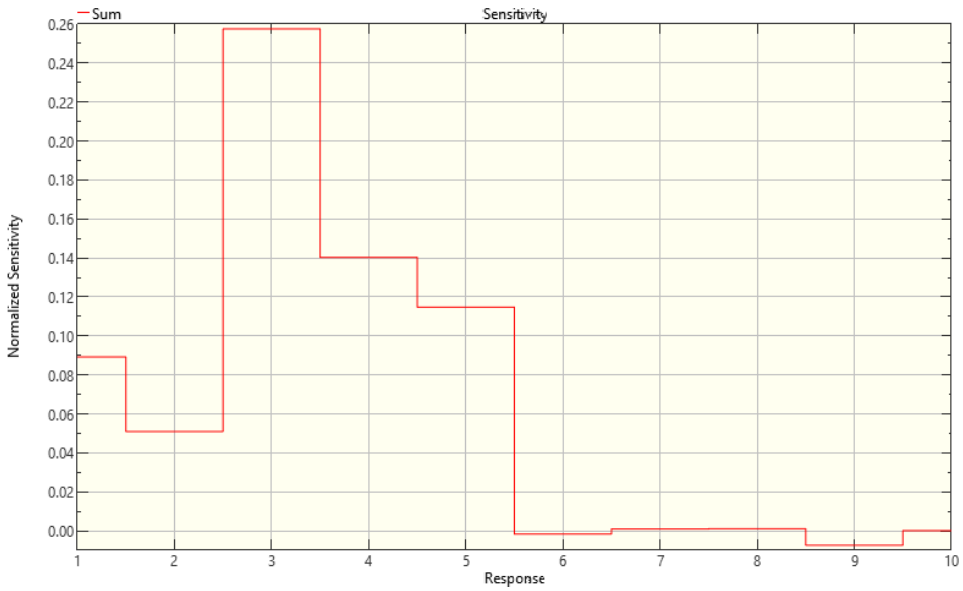

Figure 112 Sensitivity graph of sum-parameters to a change in shear modulus / SS model

The sensitivity investigations to a change in shear modulus for the SS model revealed that among shear modulus parameters, responses are more sensitive to G_{xz} and G_{yz}. Also, the sensitivity decreases as height increases. Sensitivity values to a change in G_{yz} were highest for the first-floor sets and lowest for the third-floor sets. The normalized sensitivity values to a change in G_{yz} for the first, second, and third floors are 0.197, 0.0539, and 0.0449, respectively. Also, the sensitivity values to a change in G_{xz} are 0.144, 0.0473, and 0.0467 for the first, second, and third floors, respectively.

Analyzing the obtained sensitivity values to a change in G_{yz}, in all three models, it is interesting to note that the FB model was more sensitive to a change in the G_{yz} parameter than the other two models. Also, the SB model took more sensitivity than the SS model, as shown in Figure 113.

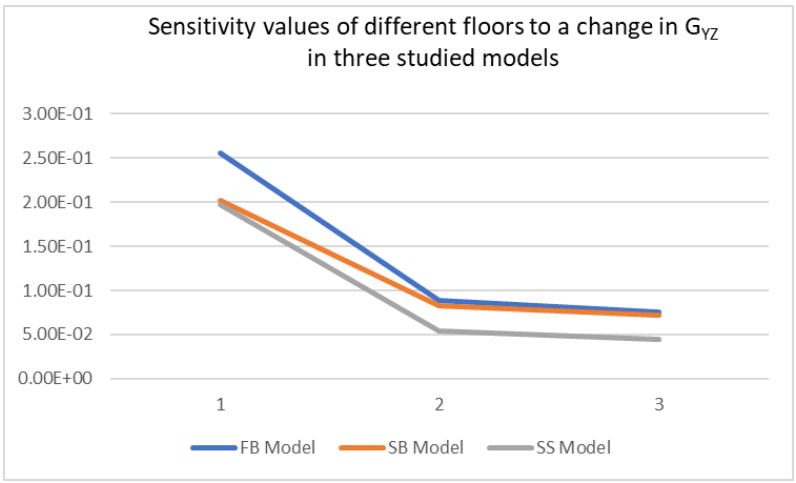

Figure 113 Sensitivity values to a change in G_{yz} of different floors / all models

6.3.5 Sensitivity to a Change in Spring Stiffness

In this section, the model's sensitivity to a change in the spring stiffness would be investigated. There are springs only for the SS model, so only the third model would be discussed.

Since orthotropic has been considered material properties for both structure and soil sets, there would be three spring stiffness in x, y, and z directions. More in detail, three parameters should be checked during sensitivity analysis to a change in spring stiffness. Like previous sensitivity simulations, there are ten responses, including five frequencies with five associated mode shapes in the study.

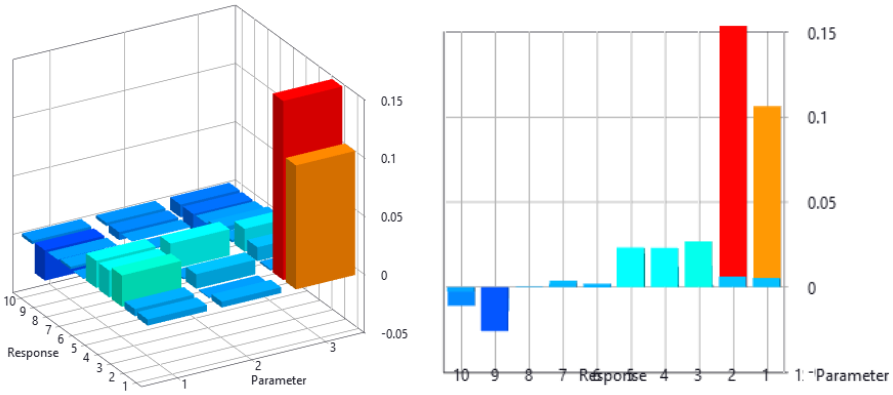

Figure 114 Sensitivity graph to a change in spring stiffness / SS model

As Figure 114 shows, the conducted analysis has shown only positive sensitivity for the frequencies while both positive and negative sensitivity for mode shapes have been observed. Positive sensitivity regarding the frequency represents the same variation between spring stiffness and the structure's natural frequency. In other words, increasing/decreasing the springs' stiffness would increase/reduce the frequencies as target responses.

The most positive sensitivities have been observed for parameter 1 (K_x) and parameter 2 (K_y) in order. Also, the sensitivity of the fourth and fifth mode shapes to a change in the spring stiffness has been recorded as negative. The highest of these two values is for the fourth mode shape.

The sensitivity to a change in the spring stiffness for the first frequency and the first mode shape as the most dynamic parameters of the structure has been shown in Figure 115 and Figure 116.

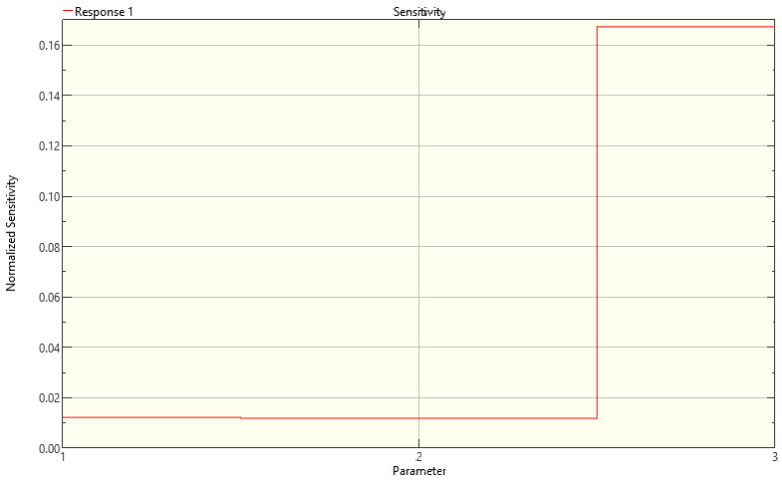

Figure 115 Sensitivity graph of the first frequency to a change in spring stiffness / SS model

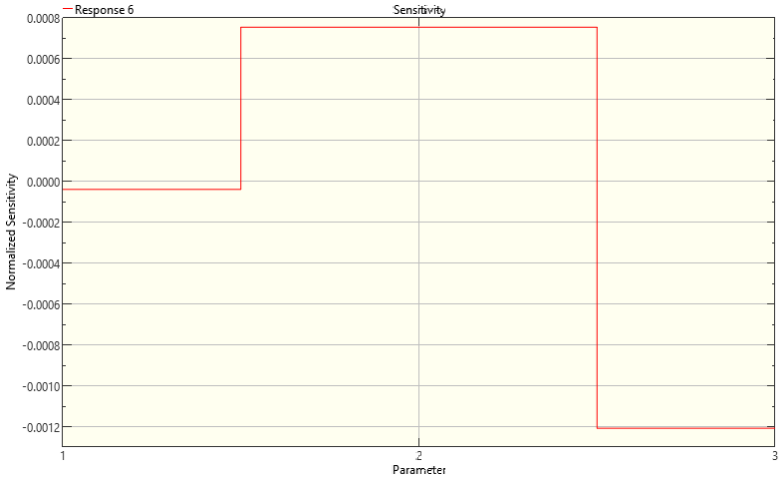

Figure 116 Sensitivity graph of the first mode shape to a change in spring stiffness / SS model

The sensitivity graphs for three parameters for the sum of responses have shown in Figure 117. The graph shows that the most influential parameter on the target responses, in this case, is the third parameter (K_z).

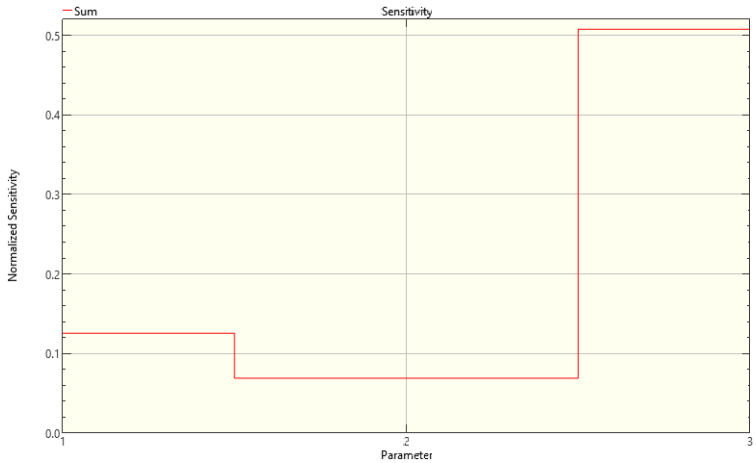

Figure 117 Sensitivity graph of sum-responses to a change in spring stiffness / SS model

The sensitivity graph of the sum of responses to a change in spring stiffnesses for the sum of parameters has been shown in Figure 118.

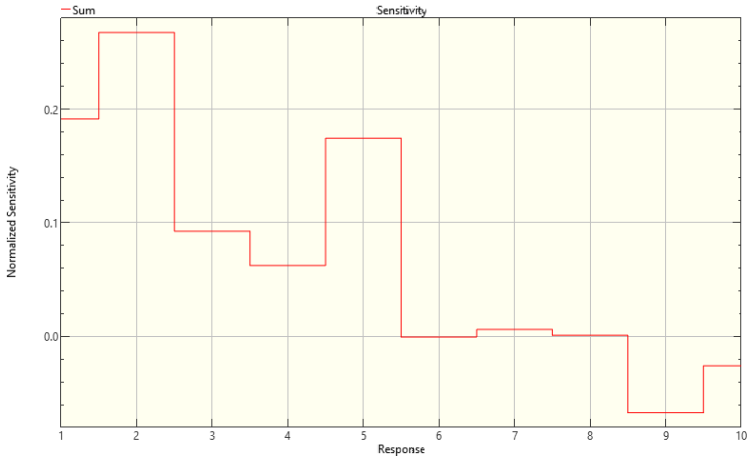

Figure 118 Sensitivity graph of sum-responses to a change in spring stiffness / SS model

From Figure 118, it is concluded that the spring stiffness has more effect on the second frequency and then on the fifth frequency. Spring stiffness variations impact on the target mode shapes are not significant.

6.3.6 Selecting Parameters for Updating the Finite Element Model

To provide the most accurate numerical model, uncertain parameters of the finite element model should be found first, and then optimal values should be assigned to them. This can be done with sensitivity analysis and model updating simulations based on the results obtained from the OMA or EMA techniques. The level of uncertainty has been lowered by using a 3D laser scanner for surveying the tower structure. Hence, there would be uncertainty only among the finite element model's material properties and boundary conditions.

Investigating the ineffective parameters through sensitivity analysis should be done before doing the model updating. In the model updating procedure, these parameters should be excluded from the simulations. Using the optimal values resulted from the updating processes will provide a more accurate finite element model for further studies on the desired structure.

In this section, the results of a sensitivity analysis done on all the involved parameters have been presented and discussed. This analysis helps to find the parameters which do not have significant effects on the target responses.

6.3.6.1 FB Model

In this section, a complete sensitivity analysis of the FB model, including all involved parameters, has been done. 170 parameters have been selected as follows:

Table 7 Selected materials for complete sensitivity analysis / FB model

Property	Number	Property	Number	Property	Number	Property	Number
RHO	1-17	E_x	18-34	G_{xy}	69-85	NU_{xy}	120-136
		E_y	35-51	G_{xz}	86-102	NU_{xz}	137-153
		E_z	52-68	G_{yz}	103-119	NU_{yz}	154-170

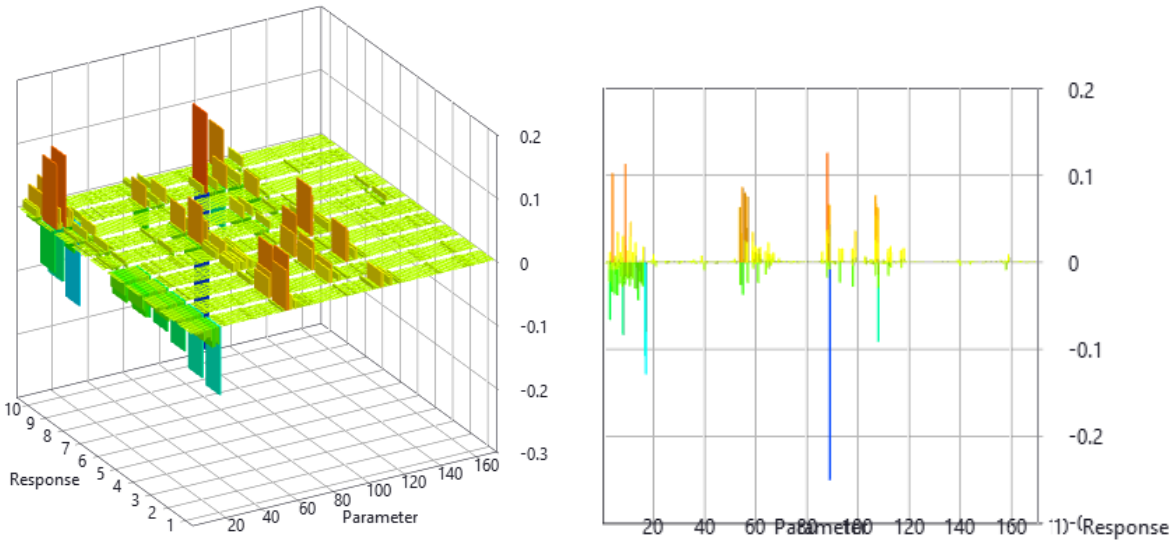

Figure 119 Sensitivity graph to a change in all parameters / FB model

The sensitivity analysis graph has been shown in Figure 119. Based on the information obtained from this figure, parameters numbered between 120-170 do not have a significant effect on the selected responses. More specifically, Poisson's ratio variations in different structure sets show a minor impact on the target responses among the selected parameters. Therefore, they have been excluded from the updating simulations of the FB model.

6.3.6.2 SB Model

A complete sensitivity analysis of the SB model, including 290 parameters (as reported in Table 8), has been done in this section.

Table 8 Selected materials for complete sensitivity analysis / SB model

Property	Number	Property	Number	Property	Number	Property	Number
RHO	1-29	E_x	30-58	G_{xy}	117-145	NU_{xy}	204-232
		E_y	59-87	G_{xz}	146-174	NU_{xz}	233-261
		E_z	88-116	G_{yz}	175-203	NU_{yz}	262-290

Figure 120 shows the result of sensitivity analysis implemented on the SB model including all involved parameters.

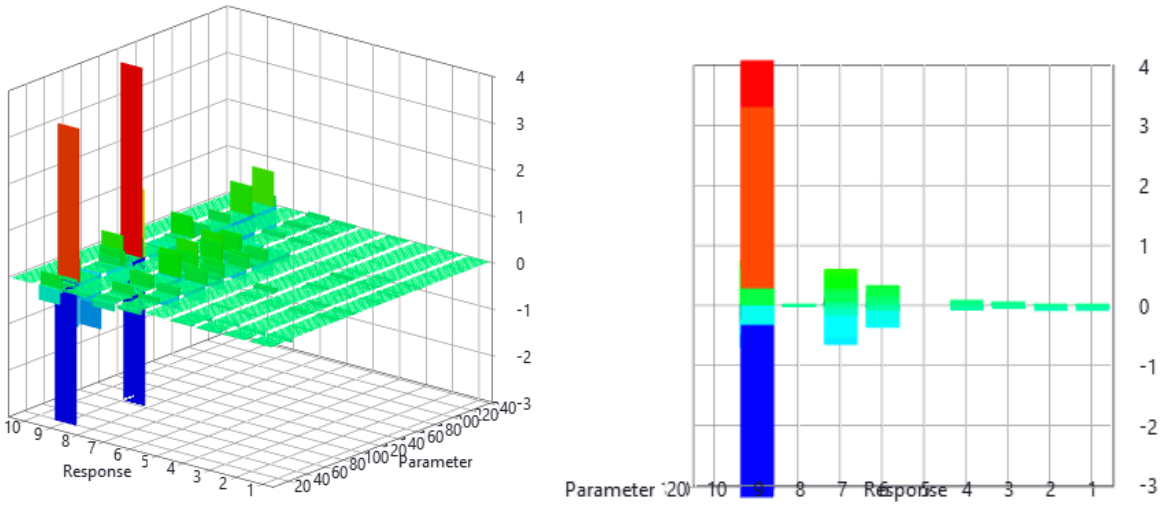

Figure 120 Sensitivity graph to a change in all parameters / SB model

As shown in Figure 120, all parameters affect the target responses, so all will be considered in the model updating simulations.

6.3.6.3 SS Model

A sensitivity analysis has been carried out on the SS model, which with 173 included parameters, as presented in Table 9.

Table 9 Selected materials for complete sensitivity analysis / SS model

Property	Number	Property	Number	Property	Number	Property	Number
K_x	1	E_x	21-37	G_{xy}	72-88	NU_{xy}	123-139
K_y	2	E_y	38-54	G_{xz}	89-105	NU_{xz}	140-156
K_z	3	E_z	55-71	G_{yz}	106-122	NU_{yz}	157-173
RHO	4-20						

The sensitivity analysis on the SS model, including all involved parameters, has been presented in Figure 121.

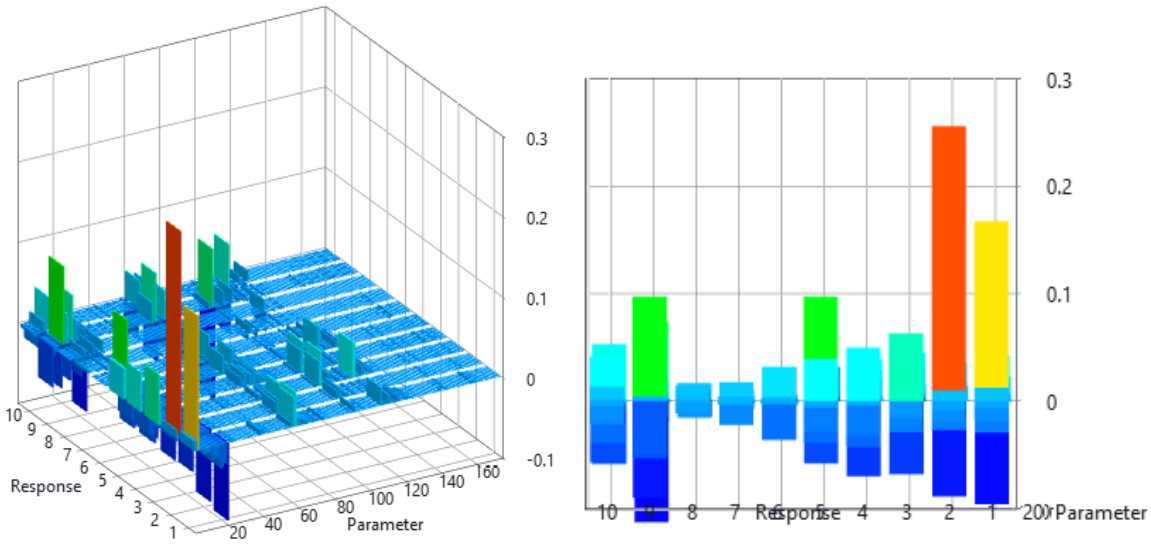

Figure 121 Sensitivity graph to a change in all parameters / SS model

The target responses are weakly affected by Poisson's parameters numbered between 123-173. Therefore, only spring stiffness, density, and elasticity modulus parameters have been selected as updating parameters.

Chapter 7: Model Updating

7.1 Overview

In this chapter, the model updating procedure and results have been presented and discussed. The model updating flow chart has been shown in Figure 122.

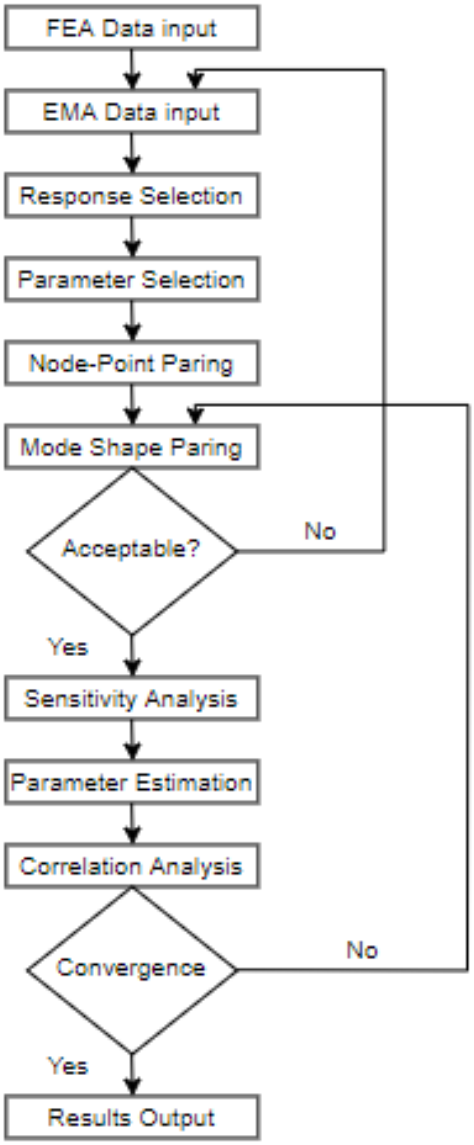

Figure 122 Model updating flow chart

Based on the findings mentioned in section 6.3.6, ineffective parameters are excluded from the model updating simulations. After doing many model updating simulations and consulting with the FEMtools technical support team, it was concluded that two main actions must be taken for a successful updating of the Slottsfjell tower finite element model.

The first action concerns the type of material for both structure and soil parameters. As the first updating scenario, isotropic behavior was assumed, and the finite element model was updated. Simulations did not work for any of the three models used in this study, and none of them can be successfully updated using the isotropic material property. As a result, in the subsequent simulations, the orthotropic property was chosen for the material.

The second action is related to the necessity of dividing the structure into different sets. It has been concluded that successful model updating, and convergence would be possible if more parameter sets the model. This is also mentioned in the FEMtools model updating manual [7]. Therefore, the finite element model of the tower has been divided into seventeenth, eighteenth, and twenty-ninth sets for the FB, the SS, and the SB models, respectively. Every story has four wall sets in addition to the floor set. There would also be an entrance and roof for all three models. It should be mentioned that the SB model has four foundation sets plus eight soil sets. The number of soil sets has been regarded based on model updating simulations in the SB model.

To summarize, a successful model updating of the masonry Slottsfjell tower needs two prerequisites. They were assuming orthotropic material property and dividing the structure into many parts. Therefore, geometry sets for all three models have been considered in Figure 50. Also, Table 4 has been used for material properties.

After the model updating each model, optimal values for each set named actual values have been reported in the related section. Using the optimal values resulted from the updating procedures will provide a more accurate finite element model for further studies on the desired structure.

7.2. Model Updating Results

According to model updating simulations done on three models considering two prerequisites mentioned in section 7.1, it was observed that only the SB model and the SS model could be updated, which will be further discussed in more detail. It is essential to underline that the SB model and the SS model can be updated even with stiffer material properties rather than those mentioned in Table 4. Given that taking the assumed values provides better agreement with the test results, the model updating simulations proceeded using supposed Table 4 values.

7.2.1 FB Model

The FB model that does not consider soil-structure interaction effects cannot be updated using the assumed material properties. Doing more updating model simulations on this model concluded that it could be updated with material values equal to or less than values mentioned in Table 10.

Table 10 Material properties used for updating the FB model

Property	Sign	Value
Mass density	RHO	2700 Kg/m3
Elasticity modulus in direction X	E_x	28 Gpa
Elasticity modulus in direction Y	E_y	28 Gpa
Elasticity modulus in direction Z	E_z	28 Gpa
Shear modulus in plane XY	G_{xy}	9.33 Gpa
Shear modulus in plane XZ	G_{xz}	9.33 Gpa
Shear modulus in plane YZ	G_{yz}	9.33 Gpa
Poisson's ratio in plane XY	NU_{xy}	0.2
Poisson's ratio in plane XZ	NU_{xz}	0.2
Poisson's ratio in plane YZ	NU_{yz}	0.2

This indicates that models that do not accurately model the soil-structure condition (FB models) cannot reflect the masonry tower's accurate structural characteristics.

7.2.1.1 Comparison of Test Data and Finite Element Model Results

In Table 11, Initial FE frequencies, EMA frequencies, and differences have been shown. The average difference in frequencies is around 3.52 Hz. Although it is normal to have differences between the FE and test results which depend on the structure dimensions and boundary conditions, the differences, in this case, are relatively high and show the necessity of doing model updating.

To minimize the differences between test and numeric models, model updating should be done to update the finite element model based on the measure test data.

Table 11 Initial FE frequencies, EMA frequencies, and differences / FB model

FEA Mode in FB model	Frequency (Hz)	EMA Mode	Frequency (Hz)	Difference (%)
1	7.19	1	5.78	1.41
2	7.50	2	6.06	1.44
3	15.48	3	13.43	2.05
4	21.50	4	15.75	5.75
5	23.36	5	16.4	6.96
				Average= 3.52 %

7.2.1.2 MAC Before and After Model Updating

MAC graphs before and after model updating have been shown in Figure 123.

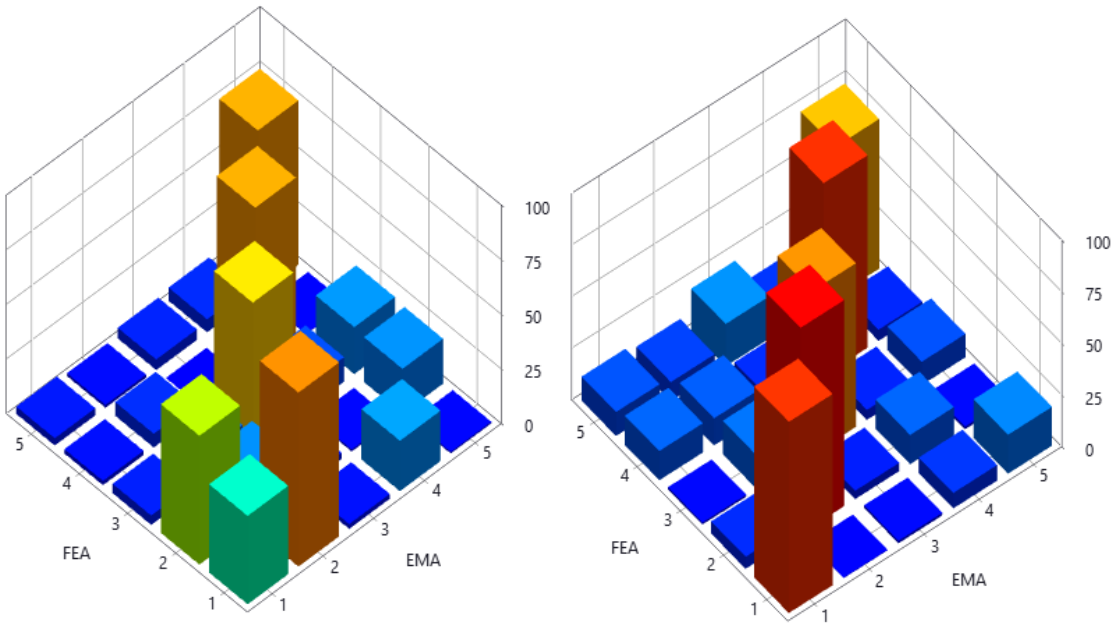

a) *b)*

Figure 123 MAC graphs a) before and b) after model updating / FB model

MAC criterion has been defined to investigate the differences between numeric and test mode shapes. MAC values before and after model updating have been shown in Table 12. Diagonal values of Figure 123 and Table 12 illustrate the correlation between the finite element and test models.

Table 12 MAC values a) before and b) after model updating / FB model

FE \ EMA	1	2	3	4	5
1	40.4	79.6	2.2	23	0.7
2	58.9	20.2	2.9	0.8	20.5
3	4.3	14.7	67.2	11.2	21.4
4	2	6.3	0.1	75.2	0.2
5	3.3	1.3	4.8	6	75.1

a) Before

FE \ EMA	1	2	3	4	5
1	92.6	0.2	1.2	7.5	18.8
2	5.9	99.8	4.0	14.1	1.2
3	0.9	16.2	79.3	4.8	11.3
4	14.2	13.1	6.2	93.2	5.4
5	11.6	9.2	20.5	7.4	72.5

b) After

Updated MAC values show a high correlation between the first, second, and fourth mode shapes. Also, a good correlation has been observed between the third and fifth mode shapes.

7.2.1.3 Updated Paired Mode Shapes

After doing model updating mode shapes paring have been done as Figure 124:

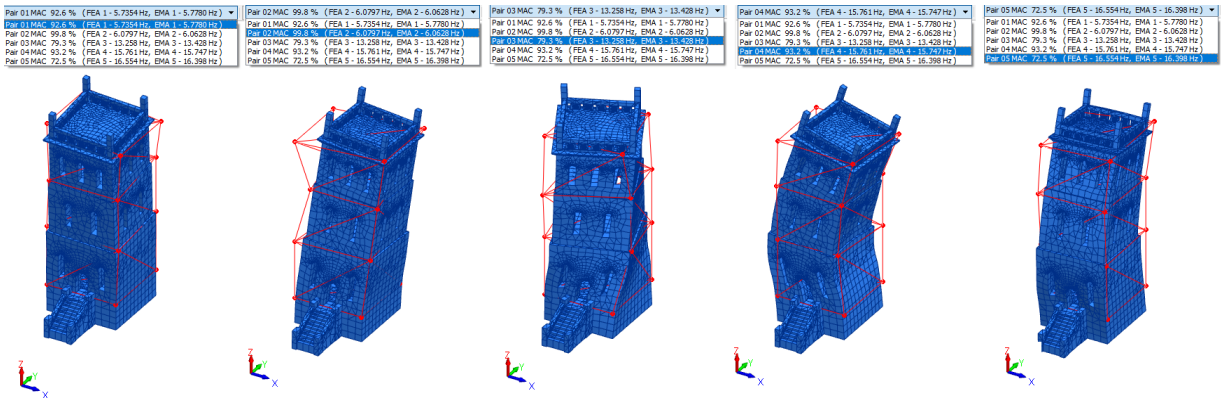

Figure 124 Updated paired mode shapes / FB model

7.2.1.4 Parameter Values After Updating of Finite Element Model

The updated material properties for different sets have been presented in Figure 125. The element numbering has been counted from the entrance and first floor sets to the third-floor sets and roof.

41	GLOBAL	EY	7	2.80E+10	2.71E+10	-3.16E+00
42	GLOBAL	EY	8	2.80E+10	2.79E+10	-2.15E-01
43	GLOBAL	EY	9	2.80E+10	2.77E+10	-1.24E+00
44	GLOBAL	EY	10	2.80E+10	2.83E+10	9.11E-01
45	GLOBAL	EY	11	2.80E+10	2.73E+10	-2.52E+00
46	GLOBAL	EY	12	2.80E+10	2.72E+10	-2.95E+00
47	GLOBAL	EY	13	2.80E+10	2.84E+10	1.27E+00
48	GLOBAL	EY	14	2.80E+10	2.77E+10	-1.18E+00
49	GLOBAL	EY	15	2.80E+10	2.77E+10	-9.16E-01
50	GLOBAL	EY	16	2.80E+10	2.69E+10	-3.79E+00
51	GLOBAL	EY	17	2.80E+10	2.62E+10	-6.42E+00
52	GLOBAL	EZ	1	2.80E+10	2.74E+10	-2.01E+00
53	GLOBAL	EZ	2	2.80E+10	2.75E+10	-1.87E+00
54	GLOBAL	EZ	3	2.80E+10	1.09E+10	-6.09E+01
55	GLOBAL	EZ	4	2.80E+10	1.41E+09	-9.50E+01
56	GLOBAL	EZ	5	2.80E+10	7.73E+09	-7.24E+01
57	GLOBAL	EZ	6	2.80E+10	1.53E+10	-4.55E+01
58	GLOBAL	EZ	7	2.80E+10	2.79E+10	-4.28E-01
59	GLOBAL	EZ	8	2.80E+10	1.07E+10	-6.20E+01
60	GLOBAL	EZ	9	2.80E+10	1.06E+10	-6.20E+01
61	GLOBAL	EZ	10	2.80E+10	1.29E+10	-5.40E+01
62	GLOBAL	EZ	11	2.80E+10	1.43E+10	-4.89E+01
63	GLOBAL	EZ	12	2.80E+10	2.78E+10	-6.78E-01
64	GLOBAL	EZ	13	2.80E+10	1.77E+10	-3.66E+01
65	GLOBAL	EZ	14	2.80E+10	1.64E+10	-4.13E+01
66	GLOBAL	EZ	15	2.80E+10	1.92E+10	-3.14E+01
67	GLOBAL	EZ	16	2.80E+10	1.91E+10	-3.19E+01
68	GLOBAL	EZ	17	2.80E+10	2.72E+10	-2.79E+00
69	GLOBAL	GXY	1	9.33E+09	9.43E+09	1.11E+00
70	GLOBAL	GXY	2	9.33E+09	8.72E+09	-6.57E+00
71	GLOBAL	GXY	3	9.33E+09	9.06E+09	-2.94E+00
72	GLOBAL	GXY	4	9.33E+09	9.11E+09	-2.41E+00
73	GLOBAL	GXY	5	9.33E+09	9.40E+09	7.09E-01
74	GLOBAL	GXY	6	9.33E+09	8.97E+09	-3.85E+00
75	GLOBAL	GXY	7	9.33E+09	8.72E+09	-6.50E+00
76	GLOBAL	GXY	8	9.33E+09	9.20E+09	-1.42E+00
77	GLOBAL	GXY	9	9.33E+09	9.09E+09	-2.54E+00
78	GLOBAL	GXY	10	9.33E+09	9.27E+09	-6.39E-01
79	GLOBAL	GXY	11	9.33E+09	9.21E+09	-1.29E+00
80	GLOBAL	GXY	12	9.33E+09	9.16E+09	-1.80E+00

#	Level	Type	Elem/Set	Old	Actual	Difference (%)
1	GLOBAL	RHO	1	2.70E+03	2.71E+03	5.14E-01
2	GLOBAL	RHO	2	2.70E+03	2.84E+03	5.15E+00
3	GLOBAL	RHO	3	2.70E+03	7.39E+03	1.74E+02
4	GLOBAL	RHO	4	2.70E+03	1.05E+04	2.90E+02
5	GLOBAL	RHO	5	2.70E+03	1.36E+04	4.05E+02
6	GLOBAL	RHO	6	2.70E+03	1.41E+04	4.21E+02
7	GLOBAL	RHO	7	2.70E+03	8.46E+03	2.13E+02
8	GLOBAL	RHO	8	2.70E+03	5.64E+03	1.09E+02
9	GLOBAL	RHO	9	2.70E+03	4.50E+03	6.66E+01
10	GLOBAL	RHO	10	2.70E+03	4.38E+03	6.23E+01
11	GLOBAL	RHO	11	2.70E+03	6.34E+03	1.35E+02
12	GLOBAL	RHO	12	2.70E+03	3.15E+03	1.68E+01
13	GLOBAL	RHO	13	2.70E+03	2.35E+03	-1.30E+01
14	GLOBAL	RHO	14	2.70E+03	2.36E+03	-1.25E+01
15	GLOBAL	RHO	15	2.70E+03	2.52E+03	-6.74E+00
16	GLOBAL	RHO	16	2.70E+03	2.46E+03	-8.77E+00
17	GLOBAL	RHO	17	2.70E+03	5.15E+03	9.06E+01
18	GLOBAL	EX	1	2.80E+10	2.81E+10	4.98E-01
19	GLOBAL	EX	2	2.80E+10	2.62E+10	-6.33E+00
20	GLOBAL	EX	3	2.80E+10	2.57E+10	-8.04E+00
21	GLOBAL	EX	4	2.80E+10	2.63E+10	-6.09E+00
22	GLOBAL	EX	5	2.80E+10	2.79E+10	-1.96E-01
23	GLOBAL	EX	6	2.80E+10	2.77E+10	-9.46E-01
24	GLOBAL	EX	7	2.80E+10	2.78E+10	-7.45E-01
25	GLOBAL	EX	8	2.80E+10	2.67E+10	-4.57E+00
26	GLOBAL	EX	9	2.80E+10	2.64E+10	-5.64E+00
27	GLOBAL	EX	10	2.80E+10	2.80E+10	-1.13E-01
28	GLOBAL	EX	11	2.80E+10	2.82E+10	5.95E-01
29	GLOBAL	EX	12	2.80E+10	2.78E+10	-8.15E-01
30	GLOBAL	EX	13	2.80E+10	2.78E+10	-6.94E-01
31	GLOBAL	EX	14	2.80E+10	2.70E+10	-3.70E+00
32	GLOBAL	EX	15	2.80E+10	2.80E+10	7.48E-02
33	GLOBAL	EX	16	2.80E+10	2.71E+10	-3.11E+00
34	GLOBAL	EX	17	2.80E+10	2.65E+10	-5.19E+00
35	GLOBAL	EY	1	2.80E+10	2.68E+10	-4.24E+00
36	GLOBAL	EY	2	2.80E+10	2.42E+10	-1.36E+01
37	GLOBAL	EY	3	2.80E+10	2.72E+10	-2.85E+00
38	GLOBAL	EY	4	2.80E+10	2.79E+10	-3.56E-01
39	GLOBAL	EY	5	2.80E+10	2.92E+10	4.12E+00
40	GLOBAL	EY	6	2.80E+10	2.51E+10	-1.03E+01

81	GLOBAL	GXY	13	9.33E+09	9.44E+09	1.18E+00
82	GLOBAL	GXY	14	9.33E+09	9.18E+09	-1.65E+00
83	GLOBAL	GXY	15	9.33E+09	9.36E+09	2.90E-01
84	GLOBAL	GXY	16	9.33E+09	9.03E+09	-3.24E+00
85	GLOBAL	GXY	17	9.33E+09	8.91E+09	-4.49E+00
86	GLOBAL	GXZ	1	9.33E+09	8.98E+09	-3.73E+00
87	GLOBAL	GXZ	2	9.33E+09	8.90E+09	-4.61E+00
88	GLOBAL	GXZ	3	9.33E+09	4.33E+09	-5.36E+01
89	GLOBAL	GXZ	4	9.33E+09	4.37E+09	-5.31E+01
90	GLOBAL	GXZ	5	9.33E+09	9.00E+09	-3.48E+00
91	GLOBAL	GXZ	6	9.33E+09	8.84E+09	-5.23E+00
92	GLOBAL	GXZ	7	9.33E+09	9.30E+09	-3.30E-01
93	GLOBAL	GXZ	8	9.33E+09	1.07E+10	1.44E+01
94	GLOBAL	GXZ	9	9.33E+09	1.08E+10	1.55E+01
95	GLOBAL	GXZ	10	9.33E+09	9.24E+09	-9.93E-01
96	GLOBAL	GXZ	11	9.33E+09	9.32E+09	-8.95E-02
97	GLOBAL	GXZ	12	9.33E+09	9.15E+09	-1.92E+00
98	GLOBAL	GXZ	13	9.33E+09	7.10E+09	-2.39E+01
99	GLOBAL	GXZ	14	9.33E+09	6.16E+09	-3.40E+01
100	GLOBAL	GXZ	15	9.33E+09	9.22E+09	-1.22E+00
101	GLOBAL	GXZ	16	9.33E+09	8.93E+09	-4.32E+00
102	GLOBAL	GXZ	17	9.33E+09	9.02E+09	-3.33E+00
103	GLOBAL	GYZ	1	9.33E+09	7.44E+09	-2.03E+01
104	GLOBAL	GYZ	2	9.33E+09	8.88E+09	-4.84E+00
105	GLOBAL	GYZ	3	9.33E+09	8.58E+09	-8.04E+00
106	GLOBAL	GYZ	4	9.33E+09	8.84E+09	-5.30E+00
107	GLOBAL	GYZ	5	9.33E+09	3.69E+09	-6.04E+01
108	GLOBAL	GYZ	6	9.33E+09	2.25E+09	-7.59E+01
109	GLOBAL	GYZ	7	9.33E+09	9.31E+09	-1.98E-01
110	GLOBAL	GYZ	8	9.33E+09	9.48E+09	1.65E+00
111	GLOBAL	GYZ	9	9.33E+09	9.35E+09	1.69E-01
112	GLOBAL	GYZ	10	9.33E+09	9.96E+09	6.72E+00
113	GLOBAL	GYZ	11	9.33E+09	1.12E+10	1.96E+01
114	GLOBAL	GYZ	12	9.33E+09	9.18E+09	-1.63E+00
115	GLOBAL	GYZ	13	9.33E+09	9.27E+09	-6.62E-01
116	GLOBAL	GYZ	14	9.33E+09	8.94E+09	-4.23E+00
117	GLOBAL	GYZ	15	9.33E+09	6.31E+09	-3.23E+01
118	GLOBAL	GYZ	16	9.33E+09	6.87E+09	-2.63E+01
119	GLOBAL	GYZ	17	9.33E+09	9.00E+09	-3.51E+00

Figure 125 Updated values after model updating / FB model

The average initial and updated values related to the different material properties of the FB model have been summarized in Table 13.

Table 13 Average updated values of material properties / FB model

Material	Phase \ Property	RHO	EX	EY	EZ	GXY	GXZ	GYZ	NUXY	NUXZ	NUYZ
Masonry	Initial	2.70E+03	2.80E+10	2.80E+10	2.80E+10	9.30E+09	9.33E+09	9.33E+09	0.20	0.20	0.20
	Updated	5.79E+03	2.73E+10	2.72E+10	1.73E+10	9.13E+09	8.43E+09	8.15E+09	0.20	0.20	0.20
	Change Percentage	114.44%	-2.50%	-2.86%	-38.21%	-1.83%	-9.65%	-12.65%	0.00%	0.00%	0.00%

7.2.1.5 Comparison of Test Data and Updated Finite Element Model Results

Table 14 shows the updated finite element model frequencies with related MAC for the FB model.

Table 14 Updated finite element model frequencies with related MAC / FB model

#	FEA	Hz	EMA	Hz	Diff. (%)	MAC (%)
1	1	5.7354	1	5.7780	-0.74	92.6
2	2	6.0797	2	6.0628	0.28	99.8
3	3	13.258	3	13.428	-1.27	79.3
4	4	15.761	4	15.747	0.09	93.2
5	5	16.554	5	16.398	0.95	72.5

Based on Table 14, the differences between the first FE and the first EMA frequencies are less than 0.75%. Also, the maximum difference for other frequencies is less than 1.3 % which shows a very good correlation between all frequencies.

7.2.2 SB Model

As described in section 7.2, the SB model can be updated based on the assumed material properties mentioned in Table 4 of section 4.2.4.

7.2.2.1 Comparison of Test Data and Finite Element Model Results

Initial FE frequencies, EMA frequencies, and differences for the SB model have been presented in Table 15. The average difference in frequencies is 1.94 Hz, around 45% less than the FB model. It clearly shows that the accuracy of the finite element model will higher in the case of considering the soil-structure interaction.

Table 15 Initial FE frequencies, EMA frequencies, and differences / SB model

FEA Mode in SB model	Frequency (Hz)	EMA Mode	Frequency (Hz)	Difference (%)
1	5.84	1	5.78	0.06
2	6.24	2	6.06	0.18
3	14.83	3	13.43	1.40
4	19.79	4	15.75	4.04
5	20.4	5	16.4	4.00
				Average= 1.94 %

7.2.2.2 MAC Before and After Model Updating

MAC graphs before and after model updating have been shown in Figure 126.

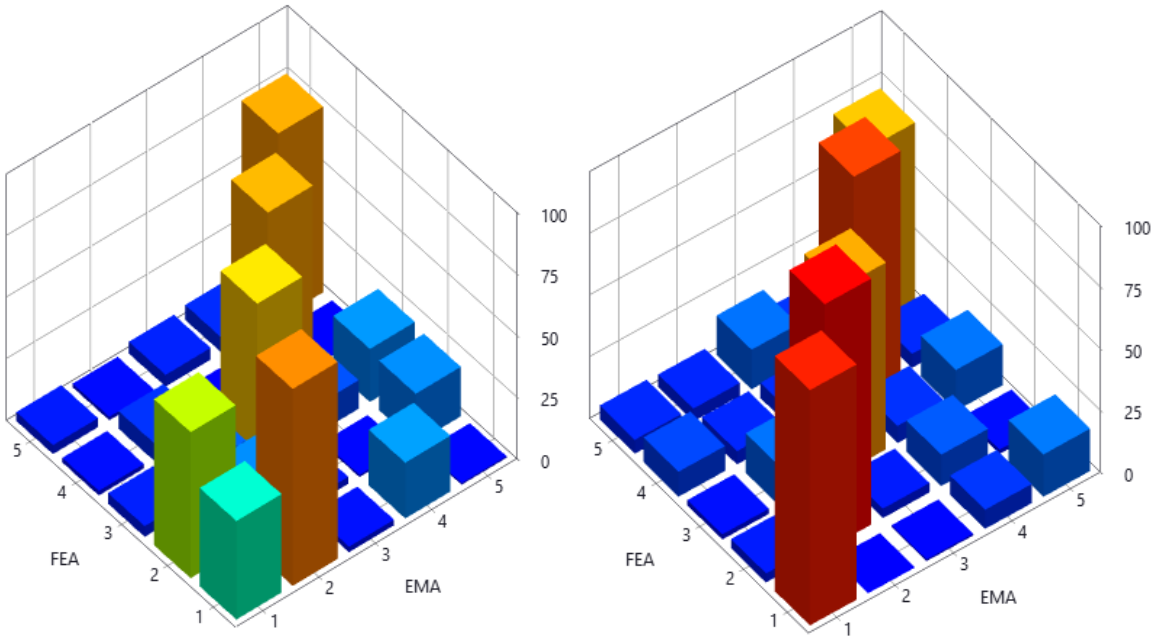

a) *b)*

Figure 126 MAC graphs a) before and b) after model updating / SB model

Also, before and after model updating of the SB model, MAC values have been shown in Table 16. Diagonal values of Figure 126 and Table 16 illustrate the correlation between the finite element and test models.

Table 16 MAC values a) before and b) after model updating / SB model

FE \ EMA	1	2	3	4	5
1	40.0	80.0	2.2	22.6	0.6
2	59.3	20.0	2.8	0.8	20.1
3	4.3	14.5	67.3	11.6	21.5
4	1.8	7.1	0.0	73.8	0.1
5	3.6	1.4	4.8	6.1	75.4

a) Before

FE \ EMA	1	2	3	4	5
1	95.3	0.0	0.7	7.7	17.1
2	3.7	99.7	3.8	12.7	1.7
3	2.1	16.2	75.7	6.9	16.5
4	10.1	5.4	6.1	90.5	5.7
5	5.6	5.2	16.0	7.6	71.6

b) After

The same as the FB model, updated MAC values show a high correlation between the first, second, and fourth mode shapes.

7.2.3.3 Updated Paired Mode Shapes

After doing model updating mode shapes paring have been done as Figure 127:

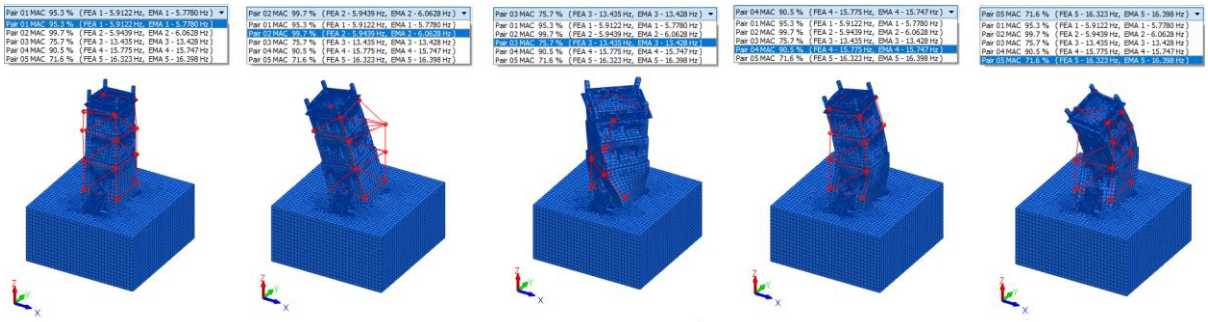

Figure 127 Updated paired mode shapes / SB model

7.2.2.4 Parameter Values After Updating of Finite Element Model

The updated material properties for different sets starting from structural sets, followed by foundations sets and ending with soil sets, have been presented in six continuous pictures. Figure 128 includes the type of parameter, set number, initial assumed value, and updated value named actual, and the difference between the old and actual value in percentage.

	Level	Type	Set ID	Old	Actual	Difference (%)
1	GLOBAL	RHO	101	2.70E+03	2.76E+03	2.32E+00
2	GLOBAL	RHO	102	2.70E+03	2.79E+03	3.40E+00
3	GLOBAL	RHO	103	2.70E+03	4.84E+03	7.91E+01
4	GLOBAL	RHO	104	2.70E+03	6.10E+03	1.26E+02
5	GLOBAL	RHO	105	2.70E+03	7.19E+03	1.66E+02
6	GLOBAL	RHO	106	2.70E+03	8.79E+03	2.26E+02
7	GLOBAL	RHO	107	2.70E+03	3.26E+03	2.08E+01
8	GLOBAL	RHO	108	2.70E+03	4.13E+03	5.29E+01
9	GLOBAL	RHO	109	2.70E+03	3.65E+03	3.52E+01
10	GLOBAL	RHO	110	2.70E+03	3.45E+03	2.76E+01
11	GLOBAL	RHO	111	2.70E+03	3.84E+03	4.22E+01
12	GLOBAL	RHO	112	2.70E+03	3.05E+03	1.31E+01
13	GLOBAL	RHO	113	2.70E+03	3.96E+03	4.67E+01
14	GLOBAL	RHO	114	2.70E+03	3.52E+03	3.05E+01
15	GLOBAL	RHO	115	2.70E+03	3.34E+03	2.38E+01
16	GLOBAL	RHO	116	2.70E+03	3.84E+03	4.21E+01
17	GLOBAL	RHO	117	2.70E+03	1.38E+04	4.13E+02
18	GLOBAL	RHO	118	2.70E+03	2.73E+03	9.52E-01
19	GLOBAL	RHO	119	2.70E+03	2.72E+03	7.91E-01
20	GLOBAL	RHO	120	2.70E+03	2.73E+03	1.12E+00
21	GLOBAL	RHO	121	2.70E+03	2.74E+03	1.32E+00
22	GLOBAL	RHO	122	2.70E+03	2.84E+03	5.17E+00
23	GLOBAL	RHO	123	2.70E+03	2.90E+03	7.38E+00
24	GLOBAL	RHO	124	2.70E+03	2.78E+03	2.95E+00
25	GLOBAL	RHO	125	2.70E+03	2.87E+03	6.35E+00
26	GLOBAL	RHO	126	2.70E+03	2.72E+03	6.32E-01
27	GLOBAL	RHO	127	2.70E+03	2.71E+03	5.36E-01
28	GLOBAL	RHO	128	2.70E+03	2.71E+03	5.43E-01
29	GLOBAL	RHO	129	2.70E+03	2.71E+03	4.32E-01
30	GLOBAL	EX	101	4.00E+10	3.96E+10	-9.09E-01
31	GLOBAL	EX	102	4.00E+10	3.88E+10	-2.92E+00
32	GLOBAL	EX	103	4.00E+10	3.70E+10	-7.50E+00
33	GLOBAL	EX	104	4.00E+10	3.84E+10	-3.97E+00
34	GLOBAL	EX	105	4.00E+10	4.00E+10	-2.16E-02
35	GLOBAL	EX	106	4.00E+10	3.97E+10	-7.19E-01
36	GLOBAL	EX	107	4.00E+10	3.99E+10	-1.43E-01
37	GLOBAL	EX	108	4.00E+10	3.94E+10	-1.62E+00
38	GLOBAL	EX	109	4.00E+10	3.96E+10	-1.01E+00
39	GLOBAL	EX	110	4.00E+10	4.01E+10	1.59E-01
40	GLOBAL	EX	111	4.00E+10	3.99E+10	-2.71E-01
41	GLOBAL	EX	112	4.00E+10	4.00E+10	-9.63E-02
42	GLOBAL	EX	113	4.00E+10	3.95E+10	-1.34E+00
43	GLOBAL	EX	114	4.00E+10	3.96E+10	-1.05E+00
44	GLOBAL	EX	115	4.00E+10	4.00E+10	-2.27E-02
45	GLOBAL	EX	116	4.00E+10	4.00E+10	-1.24E-01
46	GLOBAL	EX	117	4.00E+10	3.96E+10	-1.06E+00
47	GLOBAL	EX	118	4.00E+10	4.00E+10	8.15E-02
48	GLOBAL	EX	119	4.00E+10	4.00E+10	1.00E-01
49	GLOBAL	EX	120	4.00E+10	4.00E+10	-6.55E-02
50	GLOBAL	EX	121	4.00E+10	4.00E+10	-1.05E-01

151	GLOBAL	GXZ	106	1.33E+10	1.29E+10	-3.27E+00
152	GLOBAL	GXZ	107	1.33E+10	1.33E+10	-2.41E-01
153	GLOBAL	GXZ	108	1.33E+10	1.13E+10	-1.51E+01
154	GLOBAL	GXZ	109	1.33E+10	1.14E+10	-1.43E+01
155	GLOBAL	GXZ	110	1.33E+10	1.33E+10	-2.03E-01
156	GLOBAL	GXZ	111	1.33E+10	1.32E+10	-8.74E-01
157	GLOBAL	GXZ	112	1.33E+10	1.32E+10	-6.00E-01
158	GLOBAL	GXZ	113	1.33E+10	1.17E+10	-1.19E+01
159	GLOBAL	GXZ	114	1.33E+10	1.15E+10	-1.33E+01
160	GLOBAL	GXZ	115	1.33E+10	1.33E+10	-3.73E-01
161	GLOBAL	GXZ	116	1.33E+10	1.32E+10	-4.86E-01
162	GLOBAL	GXZ	117	1.33E+10	1.32E+10	-1.07E+00
163	GLOBAL	GXZ	118	1.33E+10	1.33E+10	-3.21E-01
164	GLOBAL	GXZ	119	1.33E+10	1.32E+10	-8.61E-01
165	GLOBAL	GXZ	120	1.33E+10	1.30E+10	-1.95E+00
166	GLOBAL	GXZ	121	1.33E+10	1.31E+10	-1.29E+00
167	GLOBAL	GXZ	122	2.00E+09	2.06E+09	2.87E+00
168	GLOBAL	GXZ	123	2.00E+09	2.00E+09	-2.18E-01
169	GLOBAL	GXZ	124	2.00E+09	1.97E+09	-1.40E+00
170	GLOBAL	GXZ	125	2.00E+09	2.04E+09	2.13E+00
171	GLOBAL	GXZ	126	2.00E+09	2.00E+09	-1.45E-01
172	GLOBAL	GXZ	127	2.00E+09	2.00E+09	-2.21E-01
173	GLOBAL	GXZ	128	2.00E+09	2.00E+09	-2.17E-01
174	GLOBAL	GXZ	129	2.00E+09	2.00E+09	-1.63E-01
175	GLOBAL	GYZ	101	1.33E+10	1.09E+10	-1.81E+01
176	GLOBAL	GYZ	102	1.33E+10	1.31E+10	-1.47E+00
177	GLOBAL	GYZ	103	1.33E+10	1.23E+10	-7.37E+00
178	GLOBAL	GYZ	104	1.33E+10	1.28E+10	-4.13E+00
179	GLOBAL	GYZ	105	1.33E+10	4.55E+09	-6.58E+01
180	GLOBAL	GYZ	106	1.33E+10	5.42E+09	-5.93E+01
181	GLOBAL	GYZ	107	1.33E+10	1.32E+10	-6.75E-01
182	GLOBAL	GYZ	108	1.33E+10	1.30E+10	-2.58E+00
183	GLOBAL	GYZ	109	1.33E+10	1.30E+10	-2.29E+00
184	GLOBAL	GYZ	110	1.33E+10	1.02E+10	-2.33E+01
185	GLOBAL	GYZ	111	1.33E+10	9.63E+09	-2.76E+01
186	GLOBAL	GYZ	112	1.33E+10	1.32E+10	-5.54E-01
187	GLOBAL	GYZ	113	1.33E+10	1.31E+10	-1.21E+00
188	GLOBAL	GYZ	114	1.33E+10	1.32E+10	-9.13E-01
189	GLOBAL	GYZ	115	1.33E+10	1.21E+10	-8.67E+00
190	GLOBAL	GYZ	116	1.33E+10	1.16E+10	-1.25E+01
191	GLOBAL	GYZ	117	1.33E+10	1.32E+10	-5.65E-01
192	GLOBAL	GYZ	118	1.33E+10	1.31E+10	-1.49E+00
193	GLOBAL	GYZ	119	1.33E+10	1.32E+10	-1.09E+00
194	GLOBAL	GYZ	120	1.33E+10	1.30E+10	-2.10E+00
195	GLOBAL	GYZ	121	1.33E+10	1.30E+10	-2.07E+00
196	GLOBAL	GYZ	122	2.00E+09	1.76E+09	-1.22E+01
197	GLOBAL	GYZ	123	2.00E+09	1.77E+09	-1.17E+01
198	GLOBAL	GYZ	124	2.00E+09	1.73E+09	-1.37E+01
199	GLOBAL	GYZ	125	2.00E+09	1.80E+09	-1.01E+01
200	GLOBAL	GYZ	126	2.00E+09	1.97E+09	-1.56E+00

101	GLOBAL	EZ	114	4.00E+10	3.61E+10	-9.87E+00
102	GLOBAL	EZ	115	4.00E+10	3.73E+10	-6.87E+00
103	GLOBAL	EZ	116	4.00E+10	3.63E+10	-9.14E+00
104	GLOBAL	EZ	117	4.00E+10	3.98E+10	-5.66E-01
105	GLOBAL	EZ	118	4.00E+10	4.03E+10	8.15E-01
106	GLOBAL	EZ	119	4.00E+10	3.95E+10	-1.21E+00
107	GLOBAL	EZ	120	4.00E+10	3.83E+10	-4.28E+00
108	GLOBAL	EZ	121	4.00E+10	3.94E+10	-1.38E+00
109	GLOBAL	EZ	122	6.00E+09	5.65E+09	-5.87E+00
110	GLOBAL	EZ	123	6.00E+09	5.49E+09	-8.49E+00
111	GLOBAL	EZ	124	6.00E+09	5.45E+09	-9.16E+00
112	GLOBAL	EZ	125	6.00E+09	5.66E+09	-5.70E+00
113	GLOBAL	EZ	126	6.00E+09	5.66E+09	-5.69E+00
114	GLOBAL	EZ	127	6.00E+09	5.57E+09	-7.16E+00
115	GLOBAL	EZ	128	6.00E+09	5.65E+09	-5.86E+00
116	GLOBAL	EZ	129	6.00E+09	5.57E+09	-7.11E+00
117	GLOBAL	GXY	101	1.33E+10	1.29E+10	-3.36E+00
118	GLOBAL	GXY	102	1.33E+10	1.27E+10	-4.52E+00
119	GLOBAL	GXY	103	1.33E+10	1.26E+10	-5.07E+00
120	GLOBAL	GXY	104	1.33E+10	1.32E+10	-7.34E-01
121	GLOBAL	GXY	105	1.33E+10	1.32E+10	-1.08E+00
122	GLOBAL	GXY	106	1.33E+10	1.30E+10	-1.92E+00
123	GLOBAL	GXY	107	1.33E+10	1.32E+10	-9.95E-01
124	GLOBAL	GXY	108	1.33E+10	1.32E+10	-7.05E-01
125	GLOBAL	GXY	109	1.33E+10	1.33E+10	-2.22E-01
126	GLOBAL	GXY	110	1.33E+10	1.33E+10	-7.13E-02
127	GLOBAL	GXY	111	1.33E+10	1.32E+10	-8.01E-01
128	GLOBAL	GXY	112	1.33E+10	1.33E+10	-2.77E-01
129	GLOBAL	GXY	113	1.33E+10	1.32E+10	-4.36E-01
130	GLOBAL	GXY	114	1.33E+10	1.33E+10	-1.93E-01
131	GLOBAL	GXY	115	1.33E+10	1.33E+10	-4.01E-02
132	GLOBAL	GXY	116	1.33E+10	1.33E+10	-2.57E-01
133	GLOBAL	GXY	117	1.33E+10	1.32E+10	-1.05E+00
134	GLOBAL	GXY	118	1.33E+10	1.32E+10	-5.06E-01
135	GLOBAL	GXY	119	1.33E+10	1.32E+10	-4.62E-01
136	GLOBAL	GXY	120	1.33E+10	1.32E+10	-4.55E-01
137	GLOBAL	GXY	121	1.33E+10	1.32E+10	-4.01E-01
138	GLOBAL	GXY	122	2.00E+09	1.88E+09	-5.85E+00
139	GLOBAL	GXY	123	2.00E+09	1.87E+09	-6.57E+00
140	GLOBAL	GXY	124	2.00E+09	1.86E+09	-6.97E+00
141	GLOBAL	GXY	125	2.00E+09	1.89E+09	-5.48E+00
142	GLOBAL	GXY	126	2.00E+09	2.00E+09	-6.69E-02
143	GLOBAL	GXY	127	2.00E+09	2.00E+09	-1.26E-01
144	GLOBAL	GXY	128	2.00E+09	2.00E+09	-1.09E-01
145	GLOBAL	GXY	129	2.00E+09	2.00E+09	-2.45E-02
146	GLOBAL	GXZ	101	1.33E+10	1.24E+10	-6.80E+00
147	GLOBAL	GXZ	102	1.33E+10	1.31E+10	-1.59E+00
148	GLOBAL	GXZ	103	1.33E+10	7.10E+09	-4.66E+01
149	GLOBAL	GXZ	104	1.33E+10	6.34E+09	-5.23E+01
150	GLOBAL	GXZ	105	1.33E+10	1.29E+10	-2.65E+00

51	GLOBAL	EX	122	6.00E+09	5.80E+09	-3.36E+00
52	GLOBAL	EX	123	6.00E+09	5.70E+09	-4.95E+00
53	GLOBAL	EX	124	6.00E+09	5.70E+09	-4.99E+00
54	GLOBAL	EX	125	6.00E+09	5.76E+09	-4.05E+00
55	GLOBAL	EX	126	6.00E+09	5.95E+09	-8.57E-01
56	GLOBAL	EX	127	6.00E+09	5.94E+09	-1.06E+00
57	GLOBAL	EX	128	6.00E+09	5.94E+09	-9.71E-01
58	GLOBAL	EX	129	6.00E+09	5.95E+09	-8.68E-01
59	GLOBAL	EY	101	4.00E+10	3.71E+10	-7.15E+00
60	GLOBAL	EY	102	4.00E+10	3.80E+10	-5.02E+00
61	GLOBAL	EY	103	4.00E+10	3.94E+10	-1.54E+00
62	GLOBAL	EY	104	4.00E+10	4.00E+10	-5.97E-02
63	GLOBAL	EY	105	4.00E+10	3.95E+10	-1.28E+00
64	GLOBAL	EY	106	4.00E+10	3.86E+10	-3.56E+00
65	GLOBAL	EY	107	4.00E+10	3.96E+10	-8.81E-01
66	GLOBAL	EY	108	4.00E+10	3.98E+10	-4.93E-01
67	GLOBAL	EY	109	4.00E+10	4.00E+10	4.44E-03
68	GLOBAL	EY	110	4.00E+10	4.00E+10	7.87E-02
69	GLOBAL	EY	111	4.00E+10	3.93E+10	-1.65E+00
70	GLOBAL	EY	112	4.00E+10	3.98E+10	-4.88E-01
71	GLOBAL	EY	113	4.00E+10	3.99E+10	-2.85E-01
72	GLOBAL	EY	114	4.00E+10	4.00E+10	7.15E-02
73	GLOBAL	EY	115	4.00E+10	3.99E+10	-1.87E-01
74	GLOBAL	EY	116	4.00E+10	3.97E+10	-7.52E-01
75	GLOBAL	EY	117	4.00E+10	3.96E+10	-9.74E-01
76	GLOBAL	EY	118	4.00E+10	3.98E+10	-3.97E-01
77	GLOBAL	EY	119	4.00E+10	3.98E+10	-5.03E-01
78	GLOBAL	EY	120	4.00E+10	3.97E+10	-7.15E-01
79	GLOBAL	EY	121	4.00E+10	3.97E+10	-6.56E-01
80	GLOBAL	EY	122	6.00E+09	5.44E+09	-9.27E+00
81	GLOBAL	EY	123	6.00E+09	5.37E+09	-1.06E+01
82	GLOBAL	EY	124	6.00E+09	5.45E+09	-9.24E+00
83	GLOBAL	EY	125	6.00E+09	5.43E+09	-9.55E+00
84	GLOBAL	EY	126	6.00E+09	5.98E+09	-2.76E-01
85	GLOBAL	EY	127	6.00E+09	6.00E+09	3.73E-02
86	GLOBAL	EY	128	6.00E+09	6.00E+09	1.75E-02
87	GLOBAL	EY	129	6.00E+09	5.99E+09	-2.39E-01
88	GLOBAL	EZ	101	4.00E+10	3.75E+10	-6.24E+00
89	GLOBAL	EZ	102	4.00E+10	3.96E+10	-8.98E-01
90	GLOBAL	EZ	103	4.00E+10	1.22E+10	-6.96E+01
91	GLOBAL	EZ	104	4.00E+10	1.43E+10	-6.42E+01
92	GLOBAL	EZ	105	4.00E+10	3.71E+10	-7.28E+00
93	GLOBAL	EZ	106	4.00E+10	3.41E+10	-1.47E+01
94	GLOBAL	EZ	107	4.00E+10	3.98E+10	-5.13E-01
95	GLOBAL	EZ	108	4.00E+10	2.99E+10	-2.52E+01
96	GLOBAL	EZ	109	4.00E+10	2.95E+10	-2.64E+01
97	GLOBAL	EZ	110	4.00E+10	3.30E+10	-1.76E+01
98	GLOBAL	EZ	111	4.00E+10	3.20E+10	-2.01E+01
99	GLOBAL	EZ	112	4.00E+10	3.99E+10	-2.11E-01
100	GLOBAL	EZ	113	4.00E+10	3.61E+10	-9.77E+00

201	GLOBAL	GYZ	127	2.00E+09	1.97E+09	-1.71E+00
202	GLOBAL	GYZ	128	2.00E+09	1.96E+09	-1.80E+00
203	GLOBAL	GYZ	129	2.00E+09	1.97E+09	-1.70E+00
204	GLOBAL	NUXY	101	2.00E-01	1.99E-01	-6.06E-01
205	GLOBAL	NUXY	102	2.00E-01	2.01E-01	4.38E-01
206	GLOBAL	NUXY	103	2.00E-01	1.98E-01	-1.11E+00
207	GLOBAL	NUXY	104	2.00E-01	2.00E-01	-9.02E-02
208	GLOBAL	NUXY	105	2.00E-01	2.00E-01	7.46E-02
209	GLOBAL	NUXY	106	2.00E-01	2.00E-01	-1.48E-01
210	GLOBAL	NUXY	107	2.00E-01	2.00E-01	-7.48E-02
211	GLOBAL	NUXY	108	2.00E-01	1.99E-01	-3.57E-01
212	GLOBAL	NUXY	109	2.00E-01	2.00E-01	1.98E-01
213	GLOBAL	NUXY	110	2.00E-01	2.00E-01	1.95E-01
214	GLOBAL	NUXY	111	2.00E-01	2.00E-01	-2.05E-01
215	GLOBAL	NUXY	112	2.00E-01	2.00E-01	-5.48E-02
216	GLOBAL	NUXY	113	2.00E-01	1.99E-01	-2.97E-01
217	GLOBAL	NUXY	114	2.00E-01	2.00E-01	2.96E-02
218	GLOBAL	NUXY	115	2.00E-01	2.00E-01	7.12E-02
219	GLOBAL	NUXY	116	2.00E-01	2.00E-01	-1.15E-01
220	GLOBAL	NUXY	117	2.00E-01	2.00E-01	-1.53E-01
221	GLOBAL	NUXY	118	2.00E-01	2.00E-01	1.27E-02
222	GLOBAL	NUXY	119	2.00E-01	2.00E-01	7.11E-03
223	GLOBAL	NUXY	120	2.00E-01	2.00E-01	-6.41E-02
224	GLOBAL	NUXY	121	2.00E-01	2.00E-01	-1.92E-02
225	GLOBAL	NUXY	122	2.50E-01	2.49E-01	-5.54E-01
226	GLOBAL	NUXY	123	2.50E-01	2.47E-01	-1.31E+00
227	GLOBAL	NUXY	124	2.50E-01	2.47E-01	-1.09E+00
228	GLOBAL	NUXY	125	2.50E-01	2.49E-01	-5.32E-01
229	GLOBAL	NUXY	126	2.50E-01	2.49E-01	-2.28E-01
230	GLOBAL	NUXY	127	2.50E-01	2.49E-01	-3.86E-01
231	GLOBAL	NUXY	128	2.50E-01	2.49E-01	-2.51E-01
232	GLOBAL	NUXY	129	2.50E-01	2.49E-01	-2.37E-01
233	GLOBAL	NUXZ	101	2.00E-01	1.98E-01	-9.21E-01
234	GLOBAL	NUXZ	102	2.00E-01	2.00E-01	4.92E-02
235	GLOBAL	NUXZ	103	2.00E-01	1.92E-01	-4.20E+00
236	GLOBAL	NUXZ	104	2.00E-01	1.93E-01	-3.73E+00
237	GLOBAL	NUXZ	105	2.00E-01	2.00E-01	-1.48E-02
238	GLOBAL	NUXZ	106	2.00E-01	1.99E-01	-3.56E-01
239	GLOBAL	NUXZ	107	2.00E-01	2.00E-01	-2.99E-02
240	GLOBAL	NUXZ	108	2.00E-01	1.98E-01	-9.63E-01
241	GLOBAL	NUXZ	109	2.00E-01	2.00E-01	-2.30E-01
242	GLOBAL	NUXZ	110	2.00E-01	2.00E-01	-9.03E-02
243	GLOBAL	NUXZ	111	2.00E-01	1.99E-01	-4.78E-01
244	GLOBAL	NUXZ	112	2.00E-01	2.00E-01	-1.56E-03
245	GLOBAL	NUXZ	113	2.00E-01	1.99E-01	-5.88E-01
246	GLOBAL	NUXZ	114	2.00E-01	1.99E-01	-2.53E-01
247	GLOBAL	NUXZ	115	2.00E-01	2.00E-01	-6.30E-03
248	GLOBAL	NUXZ	116	2.00E-01	2.00E-01	-2.21E-01
249	GLOBAL	NUXZ	117	2.00E-01	2.00E-01	-2.34E-02
250	GLOBAL	NUXZ	118	2.00E-01	2.00E-01	6.84E-02
251	GLOBAL	NUXZ	119	2.00E-01	2.00E-01	4.35E-02
252	GLOBAL	NUXZ	120	2.00E-01	2.00E-01	-4.28E-02
253	GLOBAL	NUXZ	121	2.00E-01	2.00E-01	3.74E-02
254	GLOBAL	NUXZ	122	2.50E-01	2.48E-01	-9.20E-01
255	GLOBAL	NUXZ	123	2.50E-01	2.46E-01	-1.70E+00
256	GLOBAL	NUXZ	124	2.50E-01	2.46E-01	-1.67E+00
257	GLOBAL	NUXZ	125	2.50E-01	2.48E-01	-9.39E-01
258	GLOBAL	NUXZ	126	2.50E-01	2.47E-01	-1.21E+00
259	GLOBAL	NUXZ	127	2.50E-01	2.46E-01	-1.58E+00
260	GLOBAL	NUXZ	128	2.50E-01	2.47E-01	-1.33E+00
261	GLOBAL	NUXZ	129	2.50E-01	2.47E-01	-1.32E+00
262	GLOBAL	NUYZ	101	2.00E-01	1.95E-01	-2.46E+00
263	GLOBAL	NUYZ	102	2.00E-01	2.00E-01	-8.62E-02
264	GLOBAL	NUYZ	103	2.00E-01	1.95E-01	-2.58E+00
265	GLOBAL	NUYZ	104	2.00E-01	1.99E-01	-6.78E-01
266	GLOBAL	NUYZ	105	2.00E-01	1.97E-01	-1.63E+00
267	GLOBAL	NUYZ	106	2.00E-01	1.92E-01	-3.87E+00
268	GLOBAL	NUYZ	107	2.00E-01	2.00E-01	-9.66E-03
269	GLOBAL	NUYZ	108	2.00E-01	1.99E-01	-4.34E-01
270	GLOBAL	NUYZ	109	2.00E-01	2.00E-01	1.52E-01
271	GLOBAL	NUYZ	110	2.00E-01	1.98E-01	-1.10E+00
272	GLOBAL	NUYZ	111	2.00E-01	1.96E-01	-2.00E+00
273	GLOBAL	NUYZ	112	2.00E-01	2.00E-01	3.06E-03
274	GLOBAL	NUYZ	113	2.00E-01	1.99E-01	-4.13E-01
275	GLOBAL	NUYZ	114	2.00E-01	2.00E-01	-1.13E-01
276	GLOBAL	NUYZ	115	2.00E-01	2.00E-01	-1.94E-01
277	GLOBAL	NUYZ	116	2.00E-01	1.99E-01	-5.38E-01
278	GLOBAL	NUYZ	117	2.00E-01	2.00E-01	-1.47E-02
279	GLOBAL	NUYZ	118	2.00E-01	2.00E-01	2.33E-02
280	GLOBAL	NUYZ	119	2.00E-01	2.00E-01	7.37E-02
281	GLOBAL	NUYZ	120	2.00E-01	1.99E-01	-4.46E-01
282	GLOBAL	NUYZ	121	2.00E-01	1.99E-01	-2.89E-01
283	GLOBAL	NUYZ	122	2.50E-01	2.46E-01	-1.80E+00
284	GLOBAL	NUYZ	123	2.50E-01	2.43E-01	-2.92E+00
285	GLOBAL	NUYZ	124	2.50E-01	2.44E-01	-2.42E+00
286	GLOBAL	NUYZ	125	2.50E-01	2.45E-01	-1.85E+00
287	GLOBAL	NUYZ	126	2.50E-01	2.49E-01	-5.50E-01
288	GLOBAL	NUYZ	127	2.50E-01	2.48E-01	-9.66E-01
289	GLOBAL	NUYZ	128	2.50E-01	2.48E-01	-6.79E-01
290	GLOBAL	NUYZ	129	2.50E-01	2.49E-01	-5.68E-01

Figure 128 Updated values after model updating / SB model

The average initial and updated values related to the different material properties of the SB model have been summarized in Table 17.

Table 17 Average updated values of material properties / SB model

Material	Phase \ Property	RHO	EX	EY	EZ	GXY	GXZ	GYZ	NUXY	NUXZ	NUYZ
Masonry	Initial	2.70E+03	4.00E+10	4.00E+10	4.00E+10	1.33E+11	1.33E+11	1.33E+11	2.000E-01	2.000E-01	2.000E-01
	Updated	4.80E+03	3.95E+10	3.94E+10	3.32E+10	1.31E+11	1.20E+11	1.15E+11	1.997E-01	1.986E-01	1.980E-01
	Change Percentage	77.78%	-1.25%	-1.50%	-17.00%	-1.28%	-10.08%	-13.91%	-0.15%	-0.70%	-1.00%
Foundation	Initial	2.70E+03	4.00E+10	4.00E+10	4.00E+10	1.33E+11	1.33E+11	1.33E+11	2.000E-01	2.000E-01	2.000E-01
	Updated	2.73E+03	4.00E+10	3.98E+10	3.94E+10	1.32E+01	1.32E+11	1.31E+11	2.600E-01	2.000E-01	1.990E-01
	Change Percentage	1.11%	0.00%	-0.50%	-1.50%	-100.00%	-1.13%	-1.65%	30.00%	0.00%	-0.50%
Soil	Initial	2.70E+03	6.00E+09	6.00E+09	6.00E+09	2.00E+09	2.00E+09	2.00E+09	2.500E-01	2.500E-01	2.500E-01
	Updated	2.78E+03	5.84E+09	5.71E+10	5.59E+10	1.94E+09	2.01E+09	1.86E+09	2.480E-01	2.470E-01	2.460E-01
	Change Percentage	2.96%	-2.67%	851.67%	831.67%	-3.00%	0.35%	-7.00%	-0.80%	-1.20%	-1.60%

7.2.2.5 Comparison of Test Data and Updated Finite Element Model Results

The updated finite element model frequencies, EMA frequencies, and the differences associated with related MAC for the SB model have been presented in Table 18.

Table 18 Updated finite element model frequencies with related MAC / SB model

#	FEA	Hz	EMA	Hz	Diff. (%)	MAC (%)
1	1	5.9122	1	5.7780	2.32	95.3
2	2	5.9439	2	6.0628	-1.96	99.7
3	3	13.435	3	13.428	0.06	75.7
4	4	15.775	4	15.747	0.18	90.5
5	5	16.323	5	16.398	-0.46	71.6

Table 18 shows the differences between the first FE and the first EMA frequencies are less than 2.32%, which shows a good correlation between all frequencies.

7.2.3 SS Model

Like the SB model, the SS model can also be updated based on assumed material properties mentioned in Table 4 of section 4.2.4.

7.2.3.1 Comparison of Test Data and Finite Element Model Results

Initial FE frequencies, EMA frequencies, and differences for the SS model have been presented in Table 19. The average difference in frequencies is 10.26 Hz which is more than five times the SB model. It can be concluded that the SB model simulates the soil-structure interaction more accurately. The differences are more than the FB model because numerical modal

analysis for this model has been done based on higher values of material properties rather than the FB model.

Table 19 Initial FE frequencies, EMA frequencies, and differences / SS model

FEA Mode in SS model	Frequency (Hz)	EMA Mode	Frequency (Hz)	Difference (%)
1	8.01	1	5.78	2.23
2	9.36	2	6.06	3.30
3	24.34	3	13.43	10.91
4	32.64	4	15.75	16.89
5	34.35	5	16.4	17.95
				Average= 10.26%

7.2.3.2 MAC Before and After Model Updating

MAC graphs before and after model updating have been shown in Figure 129.

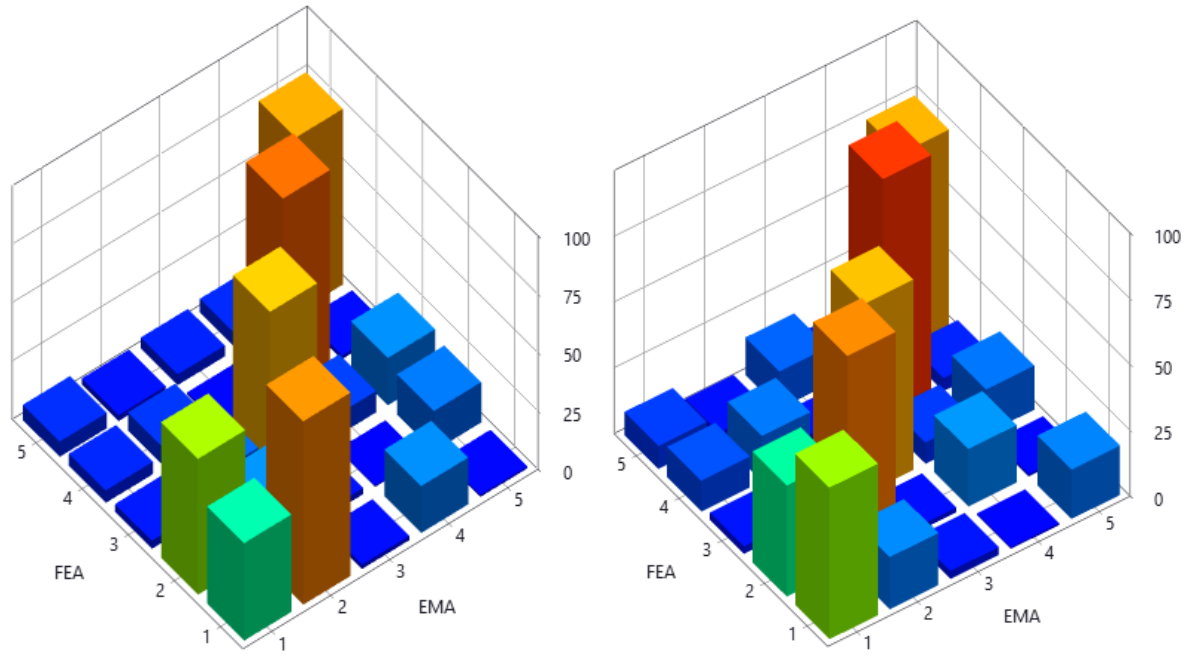

a) *b)*

Figure 129 MAC graphs a) before and b) after model updating / SS model

Also, before and after model updating of the SB model, MAC values have been shown in Table 20. Diagonal values of Figure 129 and Table 20 illustrate the correlation between the finite element and test models.

Table 20 MAC values a) before and b) after model updating / SS model

FE \ EMA	1	2	3	4	5
1	41.8	78.5	1.8	20.0	0.8
2	58.2	21.0	2.7	0.6	17.2
3	3.5	15.6	70.7	9.1	20.3
4	5.3	7.8	0.8	84.1	1.5
5	6.6	2.6	4.6	5.8	75.2

a)

FE \ EMA	1	2	3	4	5
1	57.6	19.8	3.0	0.6	18.7
2	42.2	80.0	1.9	21.7	0.8
3	2.8	0.0	72.3	8.1	16.8
4	11.7	17.2	2.7	92.0	4.9
5	8.7	2.3	14.2	5.6	74.1

b)

The same as the FB model, updated MAC values show a high correlation between the first, second, and fourth mode shapes.

7.2.3.3 Updated Paired Mode Shapes

After doing model updating mode shapes paring have been done as Figure 130:

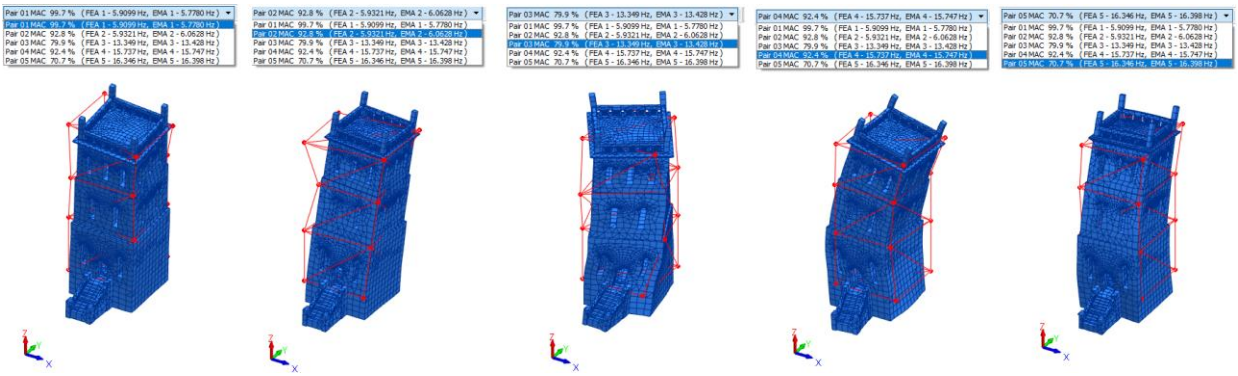

Figure 130 Updated paired mode shapes / SS model

7.2.3.4 Parameter Values After Updating the Finite Element Model

The updated material properties for different sets have been presented in Figure 131, consisting of three continuous pictures. The figure includes the type of parameter, set number, initial assumed value, and updated value named actual, and the difference between the old and actual value in percentage. Like the FB model, the element numbering has been counted from the entrance and the first-floor sets to the third-floor sets and roof.

121	GLOBAL	GYZ	16	1.33E+10	9.91E+09	-2.55E+01
122	GLOBAL	GYZ	17	1.33E+10	1.30E+10	-2.20E+00
123	GLOBAL	NUXY	1	2.00E-01	1.98E-01	-1.04E+00
124	GLOBAL	NUXY	2	2.00E-01	2.03E-01	1.41E+00
125	GLOBAL	NUXY	3	2.00E-01	2.00E-01	-1.56E-01
126	GLOBAL	NUXY	4	2.00E-01	2.00E-01	-1.20E-01
127	GLOBAL	NUXY	5	2.00E-01	2.00E-01	-2.39E-01
128	GLOBAL	NUXY	6	2.00E-01	2.00E-01	-2.01E-01
129	GLOBAL	NUXY	7	2.00E-01	2.00E-01	-1.35E-01
130	GLOBAL	NUXY	8	2.00E-01	2.00E-01	-1.87E-02
131	GLOBAL	NUXY	9	2.00E-01	2.00E-01	-6.48E-02
132	GLOBAL	NUXY	10	2.00E-01	2.00E-01	-1.20E-01
133	GLOBAL	NUXY	11	2.00E-01	2.00E-01	-1.13E-01
134	GLOBAL	NUXY	12	2.00E-01	1.99E-01	-2.73E-01
135	GLOBAL	NUXY	13	2.00E-01	2.00E-01	-6.22E-02
136	GLOBAL	NUXY	14	2.00E-01	2.00E-01	-1.49E-01
137	GLOBAL	NUXY	15	2.00E-01	2.00E-01	-1.32E-01
138	GLOBAL	NUXY	16	2.00E-01	2.00E-01	-1.88E-01
139	GLOBAL	NUXY	17	2.00E-01	1.98E-01	-8.28E-01
140	GLOBAL	NUXZ	1	2.00E-01	1.97E-01	-1.56E+00
141	GLOBAL	NUXZ	2	2.00E-01	2.00E-01	-3.58E-03
142	GLOBAL	NUXZ	3	2.00E-01	1.92E-01	-4.17E+00
143	GLOBAL	NUXZ	4	2.00E-01	1.88E-01	-5.91E+00
144	GLOBAL	NUXZ	5	2.00E-01	1.99E-01	-5.89E-01
145	GLOBAL	NUXZ	6	2.00E-01	1.99E-01	-6.01E-01
146	GLOBAL	NUXZ	7	2.00E-01	2.00E-01	-3.68E-02
147	GLOBAL	NUXZ	8	2.00E-01	1.96E-01	-2.18E+00
148	GLOBAL	NUXZ	9	2.00E-01	1.96E-01	-1.90E+00
149	GLOBAL	NUXZ	10	2.00E-01	1.99E-01	-6.79E-01
150	GLOBAL	NUXZ	11	2.00E-01	1.99E-01	-6.66E-01
151	GLOBAL	NUXZ	12	2.00E-01	2.00E-01	-2.59E-02
152	GLOBAL	NUXZ	13	2.00E-01	1.99E-01	-5.56E-01
153	GLOBAL	NUXZ	14	2.00E-01	1.98E-01	-8.14E-01
154	GLOBAL	NUXZ	15	2.00E-01	1.99E-01	-5.67E-01
155	GLOBAL	NUXZ	16	2.00E-01	1.99E-01	-6.10E-01
156	GLOBAL	NUXZ	17	2.00E-01	2.00E-01	1.07E-02
157	GLOBAL	NUYZ	1	2.00E-01	1.85E-01	-7.33E+00
158	GLOBAL	NUYZ	2	2.00E-01	2.00E-01	-1.34E-01
159	GLOBAL	NUYZ	3	2.00E-01	1.97E-01	-1.33E+00
160	GLOBAL	NUYZ	4	2.00E-01	1.99E-01	-3.19E-01
161	GLOBAL	NUYZ	5	2.00E-01	1.88E-01	-6.04E+00
162	GLOBAL	NUYZ	6	2.00E-01	1.94E-01	-2.79E+00
163	GLOBAL	NUYZ	7	2.00E-01	2.00E-01	-3.99E-02
164	GLOBAL	NUYZ	8	2.00E-01	2.00E-01	1.07E-01
165	GLOBAL	NUYZ	9	2.00E-01	2.00E-01	4.80E-02
166	GLOBAL	NUYZ	10	2.00E-01	1.96E-01	-2.13E+00
167	GLOBAL	NUYZ	11	2.00E-01	1.94E-01	-2.95E+00
168	GLOBAL	NUYZ	12	2.00E-01	2.00E-01	-2.73E-02
169	GLOBAL	NUYZ	13	2.00E-01	2.00E-01	-2.21E-01
170	GLOBAL	NUYZ	14	2.00E-01	1.99E-01	-4.92E-01

61	GLOBAL	EZ	7	4.00E+10	3.98E+10	-4.02E-01
62	GLOBAL	EZ	8	4.00E+10	1.36E+10	-6.60E+01
63	GLOBAL	EZ	9	4.00E+10	2.02E+10	-4.95E+01
64	GLOBAL	EZ	10	4.00E+10	2.25E+10	-4.37E+01
65	GLOBAL	EZ	11	4.00E+10	2.35E+10	-4.13E+01
66	GLOBAL	EZ	12	4.00E+10	3.98E+10	-3.98E-01
67	GLOBAL	EZ	13	4.00E+10	2.95E+10	-2.63E+01
68	GLOBAL	EZ	14	4.00E+10	2.97E+10	-2.58E+01
69	GLOBAL	EZ	15	4.00E+10	3.15E+10	-2.13E+01
70	GLOBAL	EZ	16	4.00E+10	3.02E+10	-2.46E+01
71	GLOBAL	EZ	17	4.00E+10	3.93E+10	-1.86E+00
72	GLOBAL	GXY	1	1.33E+10	1.40E+10	4.90E+00
73	GLOBAL	GXY	2	1.33E+10	1.20E+10	-1.00E+01
74	GLOBAL	GXY	3	1.33E+10	1.28E+10	-3.44E+00
75	GLOBAL	GXY	4	1.33E+10	1.31E+10	-1.43E+00
76	GLOBAL	GXY	5	1.33E+10	1.31E+10	-1.73E+00
77	GLOBAL	GXY	6	1.33E+10	1.29E+10	-3.17E+00
78	GLOBAL	GXY	7	1.33E+10	1.27E+10	-4.14E+00
79	GLOBAL	GXY	8	1.33E+10	1.32E+10	-4.67E-01
80	GLOBAL	GXY	9	1.33E+10	1.32E+10	-4.70E-01
81	GLOBAL	GXY	10	1.33E+10	1.33E+10	-3.45E-01
82	GLOBAL	GXY	11	1.33E+10	1.32E+10	-1.03E+00
83	GLOBAL	GXY	12	1.33E+10	1.32E+10	-6.42E-01
84	GLOBAL	GXY	13	1.33E+10	1.33E+10	-2.09E-01
85	GLOBAL	GXY	14	1.33E+10	1.32E+10	-4.59E-01
86	GLOBAL	GXY	15	1.33E+10	1.33E+10	-2.47E-01
87	GLOBAL	GXY	16	1.33E+10	1.33E+10	-2.79E-01
88	GLOBAL	GXY	17	1.33E+10	1.31E+10	-1.83E+00
89	GLOBAL	GXZ	1	1.33E+10	1.31E+10	-1.65E+00
90	GLOBAL	GXZ	2	1.33E+10	1.29E+10	-2.81E+00
91	GLOBAL	GXZ	3	1.33E+10	9.73E+09	-2.69E+01
92	GLOBAL	GXZ	4	1.33E+10	1.97E+10	4.81E+01
93	GLOBAL	GXZ	5	1.33E+10	1.30E+10	-2.08E+00
94	GLOBAL	GXZ	6	1.33E+10	1.30E+10	-2.18E+00
95	GLOBAL	GXZ	7	1.33E+10	1.33E+10	3.62E-01
96	GLOBAL	GXZ	8	1.33E+10	1.56E+10	1.73E+01
97	GLOBAL	GXZ	9	1.33E+10	1.30E+10	-1.96E+00
98	GLOBAL	GXZ	10	1.33E+10	1.33E+10	-3.62E-01
99	GLOBAL	GXZ	11	1.33E+10	1.32E+10	-7.93E-01
100	GLOBAL	GXZ	12	1.33E+10	1.32E+10	-1.05E+00
101	GLOBAL	GXZ	13	1.33E+10	1.18E+10	-1.15E+01
102	GLOBAL	GXZ	14	1.33E+10	9.83E+09	-2.61E+01
103	GLOBAL	GXZ	15	1.33E+10	1.31E+10	-1.35E+00
104	GLOBAL	GXZ	16	1.33E+10	1.32E+10	-8.95E-01
105	GLOBAL	GXZ	17	1.33E+10	1.30E+10	-2.13E+00
106	GLOBAL	GYZ	1	1.33E+10	4.83E+09	-6.37E+01
107	GLOBAL	GYZ	2	1.33E+10	1.29E+10	-3.16E+00
108	GLOBAL	GYZ	3	1.33E+10	1.24E+10	-6.95E+00
109	GLOBAL	GYZ	4	1.33E+10	1.30E+10	-2.02E+00
110	GLOBAL	GYZ	5	1.33E+10	6.46E+09	-5.14E+01
111	GLOBAL	GYZ	6	1.33E+10	6.06E+09	-5.44E+01
112	GLOBAL	GYZ	7	1.33E+10	1.33E+10	-3.05E-01
113	GLOBAL	GYZ	8	1.33E+10	1.33E+10	-4.18E-02
114	GLOBAL	GYZ	9	1.33E+10	1.32E+10	-8.22E-01
115	GLOBAL	GYZ	10	1.33E+10	1.12E+10	-1.59E+01
116	GLOBAL	GYZ	11	1.33E+10	1.16E+10	-1.27E+01
117	GLOBAL	GYZ	12	1.33E+10	1.31E+10	-1.39E+00
118	GLOBAL	GYZ	13	1.33E+10	1.31E+10	-1.27E+00
119	GLOBAL	GYZ	14	1.33E+10	1.30E+10	-2.06E+00
120	GLOBAL	GYZ	15	1.33E+10	1.04E+10	-2.20E+01

#	Level	Type	Elem/Set	Old	Actual	Difference (%)
1	GLOBAL	KX	102	8.00E+08	1.89E+08	-7.64E+01
2	GLOBAL	KY	103	8.00E+08	2.52E+08	-6.86E+01
3	GLOBAL	KZ	104	8.00E+08	1.36E+09	6.99E+01
4	GLOBAL	RHO	1	2.70E+03	3.27E+03	2.10E+01
5	GLOBAL	RHO	2	2.70E+03	3.66E+03	3.54E+01
6	GLOBAL	RHO	3	2.70E+03	1.32E+04	3.89E+02
7	GLOBAL	RHO	4	2.70E+03	6.35E+03	1.35E+02
8	GLOBAL	RHO	5	2.70E+03	1.29E+04	3.77E+02
9	GLOBAL	RHO	6	2.70E+03	1.84E+04	5.83E+02
10	GLOBAL	RHO	7	2.70E+03	5.37E+03	9.90E+01
11	GLOBAL	RHO	8	2.70E+03	4.56E+03	6.89E+01
12	GLOBAL	RHO	9	2.70E+03	2.76E+03	2.07E+00
13	GLOBAL	RHO	10	2.70E+03	3.38E+03	2.50E+01
14	GLOBAL	RHO	11	2.70E+03	3.79E+03	4.03E+01
15	GLOBAL	RHO	12	2.70E+03	2.90E+03	7.42E+00
16	GLOBAL	RHO	13	2.70E+03	2.85E+03	5.38E+00
17	GLOBAL	RHO	14	2.70E+03	2.62E+03	-2.84E+00
18	GLOBAL	RHO	15	2.70E+03	2.77E+03	2.70E+00
19	GLOBAL	RHO	16	2.70E+03	2.65E+03	-1.94E+00
20	GLOBAL	RHO	17	2.70E+03	1.09E+04	3.03E+02
21	GLOBAL	EX	1	4.00E+10	4.01E+10	2.42E-01
22	GLOBAL	EX	2	4.00E+10	3.69E+10	-7.65E+00
23	GLOBAL	EX	3	4.00E+10	3.69E+10	-7.85E+00
24	GLOBAL	EX	4	4.00E+10	3.77E+10	-5.82E+00
25	GLOBAL	EX	5	4.00E+10	3.99E+10	-1.51E-01
26	GLOBAL	EX	6	4.00E+10	3.98E+10	-4.18E-01
27	GLOBAL	EX	7	4.00E+10	3.98E+10	-5.12E-01
28	GLOBAL	EX	8	4.00E+10	3.95E+10	-1.16E+00
29	GLOBAL	EX	9	4.00E+10	3.91E+10	-2.15E+00
30	GLOBAL	EX	10	4.00E+10	4.00E+10	-8.85E-02
31	GLOBAL	EX	11	4.00E+10	3.99E+10	-1.90E-01
32	GLOBAL	EX	12	4.00E+10	3.98E+10	-4.25E-01
33	GLOBAL	EX	13	4.00E+10	3.96E+10	-1.07E+00
34	GLOBAL	EX	14	4.00E+10	3.91E+10	-2.25E+00
35	GLOBAL	EX	15	4.00E+10	3.99E+10	-3.45E-01
36	GLOBAL	EX	16	4.00E+10	3.99E+10	-2.28E-01
37	GLOBAL	EX	17	4.00E+10	3.86E+10	-3.45E+00
38	GLOBAL	EY	1	4.00E+10	3.65E+10	-8.72E+00
39	GLOBAL	EY	2	4.00E+10	3.17E+10	-2.07E+01
40	GLOBAL	EY	3	4.00E+10	3.96E+10	-1.11E+00
41	GLOBAL	EY	4	4.00E+10	3.99E+10	-2.43E-01
42	GLOBAL	EY	5	4.00E+10	3.90E+10	-2.44E+00
43	GLOBAL	EY	6	4.00E+10	3.63E+10	-9.34E+00
44	GLOBAL	EY	7	4.00E+10	3.90E+10	-2.56E+00
45	GLOBAL	EY	8	4.00E+10	3.98E+10	-5.16E-01
46	GLOBAL	EY	9	4.00E+10	3.99E+10	-2.79E-01
47	GLOBAL	EY	10	4.00E+10	4.01E+10	2.51E-01
48	GLOBAL	EY	11	4.00E+10	3.95E+10	-1.19E+00
49	GLOBAL	EY	12	4.00E+10	3.91E+10	-2.36E+00
50	GLOBAL	EY	13	4.00E+10	3.99E+10	-1.36E-01
51	GLOBAL	EY	14	4.00E+10	4.00E+10	-4.20E-02
52	GLOBAL	EY	15	4.00E+10	3.97E+10	-8.64E-01
53	GLOBAL	EY	16	4.00E+10	3.95E+10	-1.19E+00
54	GLOBAL	EY	17	4.00E+10	3.84E+10	-4.05E+00
55	GLOBAL	EZ	1	4.00E+10	3.19E+10	-2.04E+01
56	GLOBAL	EZ	2	4.00E+10	3.98E+10	-5.82E-01
57	GLOBAL	EZ	3	4.00E+10	7.27E+09	-8.18E+01
58	GLOBAL	EZ	4	4.00E+10	8.01E+09	-8.00E+01
59	GLOBAL	EZ	5	4.00E+10	3.36E+10	-1.61E+01
60	GLOBAL	EZ	6	4.00E+10	4.48E+10	1.21E+01

Figure 131 Updated values after model updating / SS model

The average initial and updated values related to the different material properties of the SS model have been summarized in Table 21.

Table 21 Average updated values of material properties / SS model

Material	State \ Property	RHO	EX	EY	EZ	GXY	GXZ	GYZ	NUXY	NUXZ	NUYZ	KX	KY	KZ
Masonry	Initial	2.70E+03	4.00E+10	4.00E+10	4.00E+10	1.33E+11	1.33E+11	1.33E+11	0.2	0.2	0.2	8.00E+08	8.00E+08	8.00E+08
	Updated	6.02E+03	3.92E+10	3.87E+10	2.87E+10	1.31E+11	1.32E+11	1.12E+11	0.210	0.197	0.160	1.89E+08	2.52E+08	1.36E+09
	Change Percentage	122.96%	-2.00%	-3.25%	-28.25%	-1.50%	-0.90%	-15.64%	5.00%	-1.50%	-20.00%	-76.38%	-68.50%	69.88%

7.2.3.5 Comparison of Test Data and Updated Finite Element Model Results

The updated finite element model frequencies, EMA frequencies, and the differences associated with related MAC for the SB model have been presented in Table 22.

Table 22 Updated finite element model frequencies with related MAC / SS model

#	FEA	Hz	EMA	Hz	Diff. (%)	MAC (%)
1	1	5.7558	1	5.7780	-0.38	57.6
2	2	6.0350	2	6.0628	-0.46	80.0
3	3	13.317	3	13.428	-0.82	72.3
4	4	15.815	4	15.747	0.43	92.0
5	5	16.312	5	16.398	-0.52	74.1

Table 22 shows the differences between the first FE and the first EMA frequencies are less than 0.82 %, which shows a perfect correlation between all frequencies.

7.3. Model Updating Discussions

The percentage of changes in every parameter for different models has been shown in Figure 132. The most positive variations have been observed for the density with around 115%, 80%, and 122% increased values for FB, SB, and SS models, respectively. Also, the most negative changes have been recorded for the elasticity modulus in the z-direction. The decrease values are around 38% for the FB model, 17% for the SB model, and 29% for the SS model.

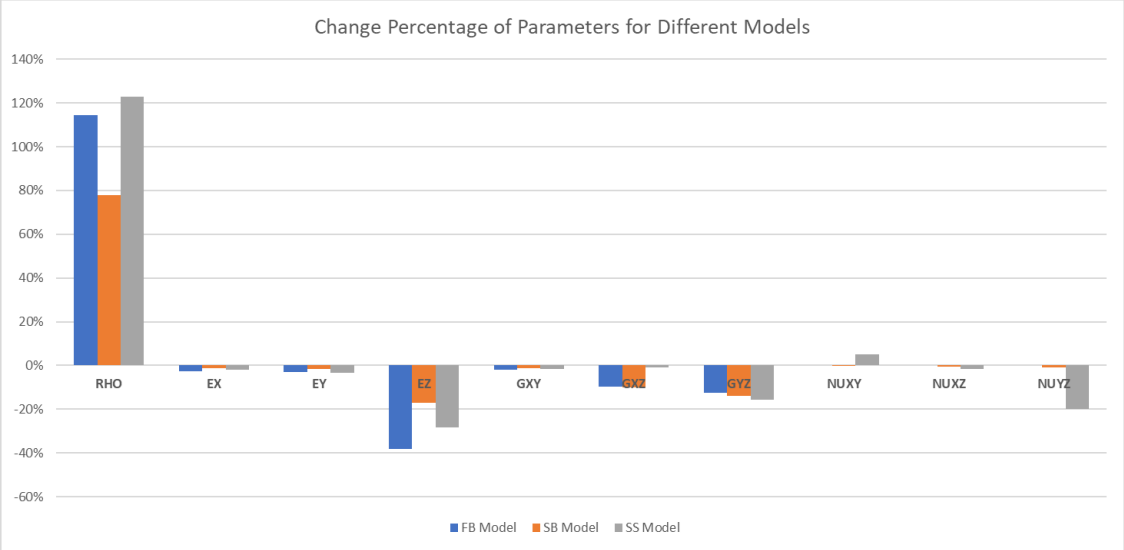

Figure 132 Change percentage of parameters / all models

The figure also depicts that Poisson's ratio does not significantly change the SB and SS models. The variations for other parameters (all the shear modulus and elasticity modulus in x and y directions) have been gained negative.

Also, the mac values of different model updating have been shown in Figure 133. It is evident that the FB and SB models have shown the best correlation for the natural frequencies.

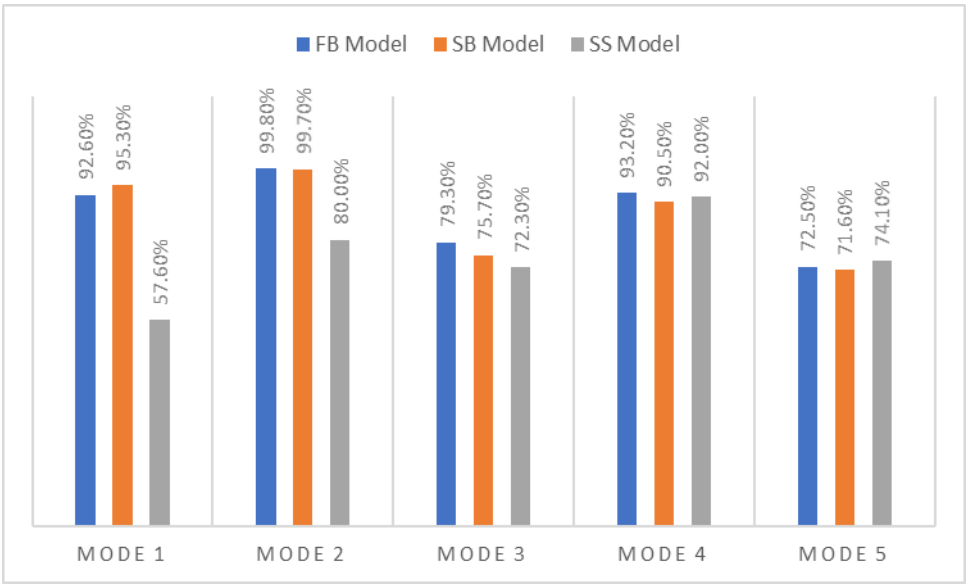

Figure 133 MAC values after model updating / all models

Chapter 8: Conclusion and Future Works

8.1 Conclusion

The operational modal analysis (OMA) has been used in this thesis to extract the modal parameters of a historic masonry tower, "Slottsfjelltårnet," located in Tønsberg, Norway. The modal parameters identification has been carried out using ambient vibration test (AVT) data of some sensors installed on the tower. A sensitivity analysis has been carried out to investigate the most sensitive parameters of the structure. Moreover, the finite element model of the Slottsfjell tower has been updated with and without considering the soil-structure interaction effects to find the optimized values for material properties of the structure. The following conclusions can be drawn from this research.

- The obtained modal analysis results revealed a remarkable difference between the natural frequencies of models with and without soil-structure interaction effects. The frequencies of SB and SS models which consider soil-structure interaction effects are smaller than the frequencies of the FB model without soil-structure interaction effects. The results are consistent with previous studies and confirms the impacts of considering soil-structure interaction on the numerical modeling of structures.

- Regarding the sensitivity of responses to a change in the elasticity modulus, it has been concluded that the frequencies and the mode shapes are more sensitive to E_z changes than E_x and E_y. The sensitivity graphs show that the frequencies have positive sensitivity while the mode shapes have both positive and negative sensitivity to a change in elasticity modulus. Also, the sensitivity graphs reveal that the highest sensitivity to a change in elasticity modulus has been observed for the first-floor sets. Therefore, the higher the height of the parameter set, the minor sensitivity. Also, it has been concluded that sensitivity values to a change in E_z for the FB model were higher than SB and SS models.

- Based on the sensitivity graphs to change in Poisson’s ratio, it is illustrated that sensitivity of frequencies to a change in Poisson's ratio is positive in most cases, while the mode shape's sensitivity can be negative or positive. It has been concluded that sensitivity values to a change in Poisson's ratio decrease as height increases.

- Considering the sensitivity graphs to a change in density, only negative sensitivity has been observed for the frequencies, which shows that an increase in the density of structure’s sets leads to a decrease in frequency. In contrast, both positive and negative sensitivities have been

observed for the mode shapes. It is shown that the overall changes in the density of different sets do not significantly affect the mode shapes. Also, the graphs report that the sensitivity values increase negatively for the higher parameter sets, which shows that density variations have more effect on the upper sets' response. It should also be noted that comparing sensitivity values of three models concluded that the maximum and minimum sensitivity model to a change in density is for the SS model and the FB model, respectively.

- Reviewing the sensitivity graphs to a change in shear modulus indicates that the shear modulus changes on the frequency variations are positive while the mode shapes are positive and negative. The graphs showed that responses are more sensitive to G_{yz} among shear modulus parameters. Sensitivity values to a change in G_{xz} and G_{yz} were highest for the first-floor sets and lowest for the third-floor sets. Also, it is concluded that the FB model and the SS model have the maximum and minimum sensitivity to a change in shear modulus, respectively.

- Summarizing the sensitivity graphs to a change in different parameters illustrated that the trend of elasticity modulus, Poisson’s ratio, and shear modulus are similar, showing a decrease as the height of the sets increases. In contrast, the trend for density is different due to an increase in sensitivity values in the higher floors.

- Investigating the sensitivity graphs to a change in spring stiffness in the SS model shows only positive sensitivity for the frequencies. In contrast, both positive and negative sensitivity have been observed for the mode shapes. It is also concluded that the most influential parameter on the target responses is the spring stiffness in the z-direction.

- The FB model that does not consider soil-structure interaction effects cannot be updated using the assumed material properties, indicating such models can not reflect the masonry tower's accurate structural characteristics. It can be a confirmation of the importance of considering soil-structure interaction in the modeling of structures. It should be noted that the elasticity modulus results from the SB model and the SS model provide better agreement with the masonry stone results than the FB model.

- The average difference in frequencies in the SS model is five times more than the SB model's values, indicating that in this research, a direct method simulates the soil-structure interaction more accurately than the substructure method.

- Comparing the percentage of the change of parameters after model updating in different models shows that the most positive variations have been observed for density. In contrast, the most negative variations have been recorded for elasticity modulus in the z-direction.

- Due to the good correlation between the numerical and experimental models, the SB model seems to be more reliable than the other two models to predict the actual situation of the Slottsfjell tower for future structural analysis.

8.2 Recommendation for Future Works

- Regarding the ambient vibration test (AVT) work, it is recommended to do the experimental testing once more with optimum sensor locations obtained from modal pretest analysis of FEMTools.

- Other OMA techniques for identifying the modal parameters can be applied to AVT data compared to the current results.

- Future studies can address more numerical modeling methods to consider the soil-structure interaction effects on the modal parameters of the structure.

References

[1] A. Ademi, "Finite element model updating of a stone masonry tower using 3D laser scanner and accelerometers (Master's Thesis)," Oslo Metropolitan University, Oslo, 2020.

[2] M. Romero, P. Pachon, V. Compan and M. Camara, "Operational Modal Analysis: A Tool for Assessing Changes on Structural Health State of Historical Constructions after Consolidation and Reinforcement Workshop Jura Chapel (Jerez de la Frontera, Spain)," *Structural Health Monitoring through Vibration-Based Approaches,* 2018.

[3] A. Shabani, M. Kioumarsi and M. Zucconi, "State of the art of simplified analytical methods for seismic vulnerability assessment of unreinforced masonry buildings," *Engineering structures,* vol. 239, 2021.

[4] O. Zienkiewicz, O.C. and R. Taylor, The finite element method, Butterworth Heinemann, 2000.

[5] R. Cook, R.D., D. Malkus and M. Plesha, Concepts and Applications of Finite Element Analysis, New York: Wiley, 1989.

[6] J. K. Sinha, A. Rama Rao and R. Moorthy, "Significance of analytical modelling for complete interpretation of experimental modal analysis: a case study," *Nuclear Engineering and Design,* vol. 220, pp. 91-97, 2003.

[7] D. D. S. N. (DDS), "FEMTools Model Updating TUser's Guide Version 4.1," Dynamic Design Solutions Company, Leuven, 2020.

[8] G. Liu, G.-R. and S. Quek, The finite element method: a practical course, Butterworth-Heinemann, 2013.

[9] L. Wang, W. Ping, C. Zhao , J. Zhen and Y. Zhao, "In situ evaluation of dynamic characteristics of prefabricated ballastless track slab using EMA and OMA techniques," *Measurement,* vol. 160, 2020.

[10] M. Ghalishooyan and A. Shooshtari, "Operational modal analysis techniques and their theoretical and practical aspects: A comprehensive review and introduction," in *6th International Operational Modal Analysis Conference,* Gijón, Spain, 2015.

[11] M. Damgaard, "An Introduction to Operational Modal Identification of Offshore Wind Turbine Structures," Aalborg universitet, Aalborg , 2011.

[12] M. Anuar, L. Roslan and A. Azlan, "Dynamic Parameter Identification Using Ambient Response Analysis and Ibrahim Time Domain Approach: A Case Study On A Steel Plate Structure," *Applied Mechanics and Materials,* Vols. 110-116, pp. 2395-2399, 2012.

[13] M. Diaferio , D. Foti , M. Mongelli and N. Giannoccaro, "Operational Modal Analysis of a Historic Tower in Bari," in *Civil Engineering Topics,* 2011.

[14] R. Brincker, L. Zhang and P. Andersen, "Modal Identification from Ambient Responses using Frequency Domain Decomposition," in *International Modal Analysis Conference (IMAC 18),* San Antonio, 2000.

[15] R. Brincker, C. Ventura and P. Andersen, "Damping Estimation by Frequency Domain Decomposition," in *Conference on Structural Dynamics (IMAC 19),* Hyatt Orlando, 2001.

[16] M. Masjedian and M. Keshmiri, "A Review on Operational Modal Analysis Researches: Classification of Methods and Applications," in *3rd International Operational Modal Analysis Conference (IOMAC'09),* Portonovo, 2009.

[17] B. Jaishi, W.-X. Ren, Z.-H. Zong and P. N. Maskey, "Dynamic and seismic performance of old multi-tiered temples in Nepal," *Engineering Structures,* vol. 25, no. 14, pp. 1827-1839, 2003.

[18] L. F. Ramos , R. Aguilar, P. B. Lourenço and S. T. Moreira, "Dynamic structural health monitoring of Saint Torcato church," *Mechanical Systems and Signal Processing,* vol. 35, no. 1-2, pp. 1-15, 2013.

[19] K.-W. Min, J. Kim, S.-A. Park and C.-S. Park, "Ambient Vibration Testing for Story Stiffness Estimation of a Heritage Timber Building," *Health Monitoring of Civil Infrastructure and Materials,* 2013.

[20] V. Compan, P. Pachon and M. Camara, "Ambient vibration testing and dynamic identification of a historical building. Basilica of the Fourteen Holy Helpers (Germany)," in *X International Conference on Structural Dynamics, EURODYN 2017*, Rome, 2017.

[21] G. Cimellaro, S. Piantà and A. De Stefano, "Output-only modal identification of ancient L'Aquila city hall and civic tower," *Structural Engineering,* vol. 138, pp. 481-491, 2011.

[22] H. A. Awlla, N. R. Taher and Y. I. Mawlood, "Effect of Fixed Based and Soil Structure Interaction on the Dynamic Responses of Steel Structures," *International Journal of Emerging Trends in Engineering Research,* vol. 8, 2020.

[23] M. Choinière, P. Paultre and P. Léger, "Influence of soil-structure interaction on seismic demands in shear wall building gravity load frames," *Engineering Structures 198 (2019) 109259,* vol. 198, 2019.

[24] V. Anand and S. S. Kumar, "Seismic Soil-structure interaction: A State-of-the-Art Review," *Structures,* vol. 16, pp. 317-326, 2018.

[25] G. Lacanna, M. Ripepe, E. Marchet, M. Coli and C. A. Garzonio , "Dynamic response of the Baptistery of San Giovanni in Florence, Italy, based on ambient vibration test," *Journal of Cultural Heritage,* vol. 20, pp. 632-640, 2016.

[26] V. Shimpi, M. V. Sivasubramanian and S. Singh, "System Identification of Heritage Structures Through AVT and OMA: A Review," *Structural Durability and Health Monitoring Journal,* vol. 13, 2019.

[27] R. A. Votsis, N. Kyriakides, C. Z. Chrysostomou, E. Tantele and T. Dem, "Ambient vibration testing of two masonry monuments in Cyprus," *Soil Dynamics and Earthquake Engineering,* vol. 43, p. 58–68, 2012.

[28] D. Foti, M. Diaferio, N. I. Giannocc and M. Mongelli , "Ambient vibration testing, dynamic identification and model updating of a historic tower," *NDT & E International*, vol. 47, pp. 88-95, 2012.

[29] L. F. Ramos, R. Aguilar, p. B. Lourenco and S. Moreira, "Dynamic structural health monitoring of Saint Torcato church," *Mechanical systems and Signal Processing*, vol. 35, pp. 1-15, 2013.

[30] B. Conde, L. F. Ramo, D. V. Oliveira, B. Riveiro and M. Solla, "Structural assessment of masonry arch bridges by combination of non-destructive testing techniques and three-dimensional numerical modelling: Application to Vilanova bridge," *Engineering Structures*, vol. 148, pp. 621-638, 2017.

[31] "Tønsberg," [Online]. Available: https://en.wikipedia.org/wiki/T%C3%B8nsberg.

[32] SLOTTSFJELLSMUSEET, "Slottsfjellstårnet," [Online]. Available: https://vestfoldmuseene.no/slottsfjellsmuseet/besok/slottsfjellstarnet/.

[33] C. Gentile, A. Saisi and A. Cabboi, "Structural Identification of a Masonry Tower Based on Operational Modal Analysis," *International Journal of Architectural Heritage*, vol. 9, pp. 98-110, 2015.

[34] A. Shabani, M. Kioumarsi, V. Plevris and H. Stamatopoulos, "Structural Vulnerability Assessment of Heritage Timber Buildings: A Methodological Proposal," *Forests*, vol. 11, no. 8, 2020.

[35] P. Debney and N. Rees, "Making Good Structural Analysis Models – Best Practices, Validation, and Reducing Errors (Webinar)," 2018.

[36] I. Felix, "Compressive strength and modulus of elasticity of masonry prisms," Carleton University, Carleton, 1999.

[37] R. Zavalis, B. Jonaitis and P. Lourenco, "Analysis of bed joint influence on masonry modulus of elasticity," in *9th International Masonry Conference*, Guimarães , 2014.

[38] M. Choinièrea, P. Paultrea and P. Légerb, "Influence of soil-structure interaction on seismic demands in shear wall building gravity load frames," *Engineering structures*, vol. 198, 2019.

[39] H. A. Awlla, N. R. Taher and Y. I. Mawlood, "Effect of Fixed-Base and Soil Structure Interaction on the Dynamic Responses of Steel Structures," *International Journal of Emerging Trends in Engineering Research*, vol. Volume 8. No. 9, 2020.

[40] A. Vesic, "Beams on elastic subgrade and Winkler's hypothesis," in *Fifth International Conference on Soil Mechanics and Foundation Engineering*, Paris, 1961.

[41] S. a. S. P. C. C. Engineers, "Unquake product," [Online]. Available: https://www.unquake.co/en/products.

Appendix 1 (FFT Results of Unquake)

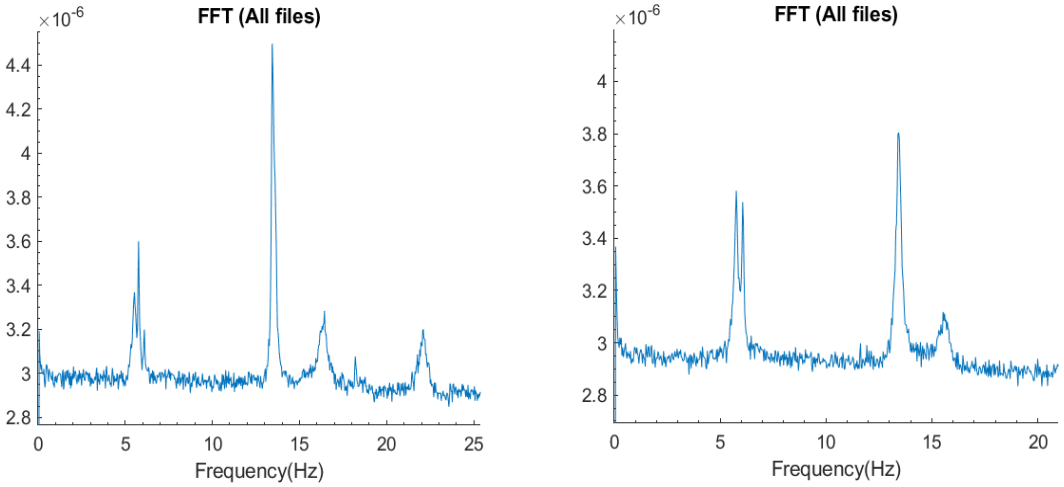

a) *b)*

Figure 134 FFT plot of Sensor 2, a) in the x-direction, b) in the y-direction

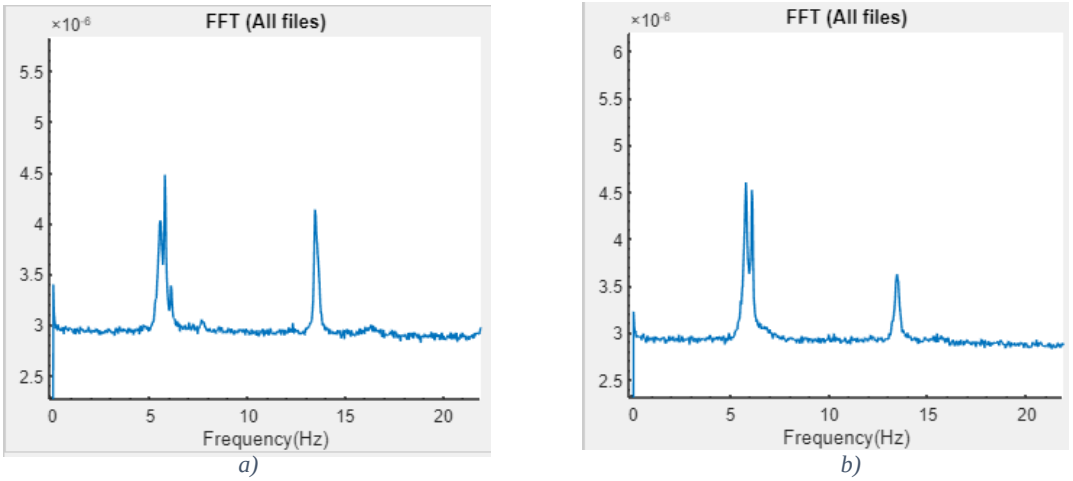

a) *b)*

Figure 135 FFT plot of Sensor 3, a) in the x-direction, b) in the y-direction

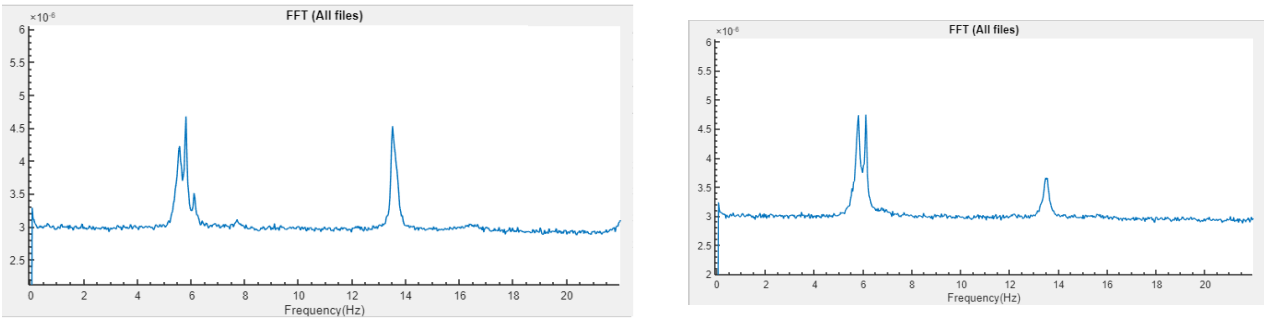

a) *b)*

Figure 136 FFT plot of Sensor 4, a) in the x-direction, b) in the y-direction

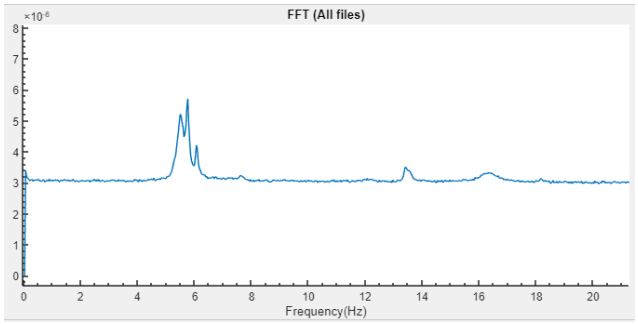

No Data

a) *b)*

Figure 137 FFT plot of Sensor 5, a) in the x-direction, b) in the y-direction

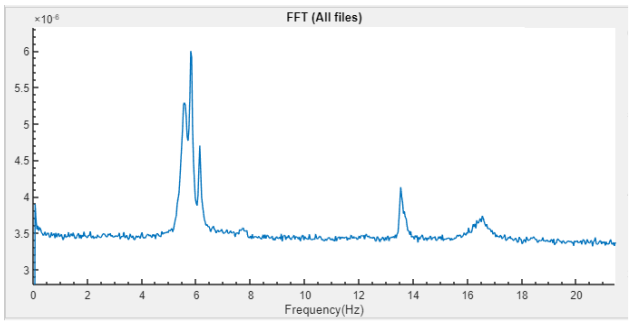

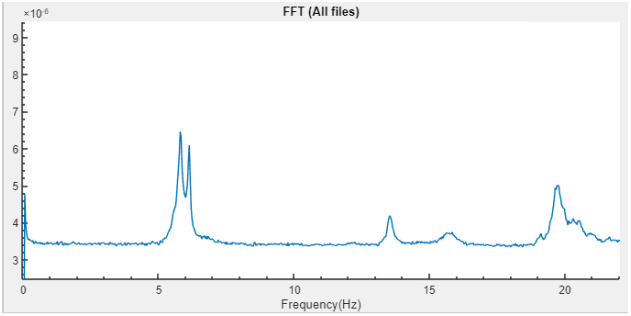

a) *b)*

Figure 138 FFT plot of Sensor 3, a) in the x-direction, b) in the y-direction

Appendix 2 (Time Histories)

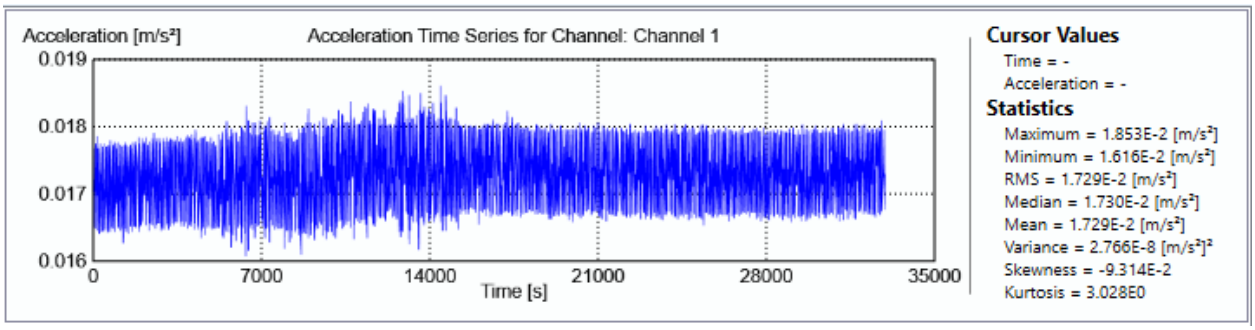

Figure 139 Time history plot of sensor 1 in the x-direction

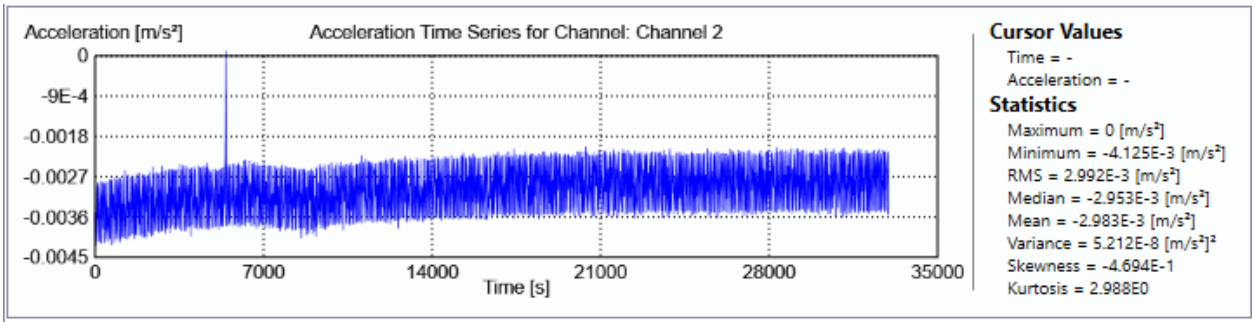

Figure 140 Time history plot of sensor 1 in the y-direction

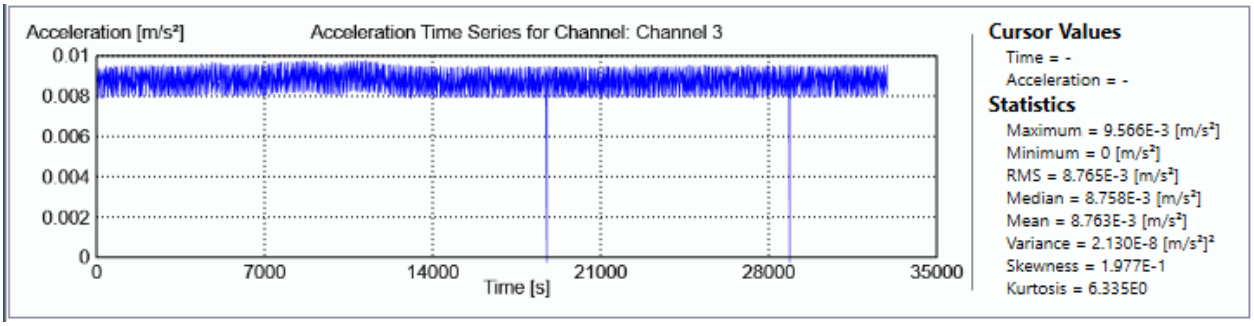

Figure 141 Time history plot of sensor 2 in the x-direction

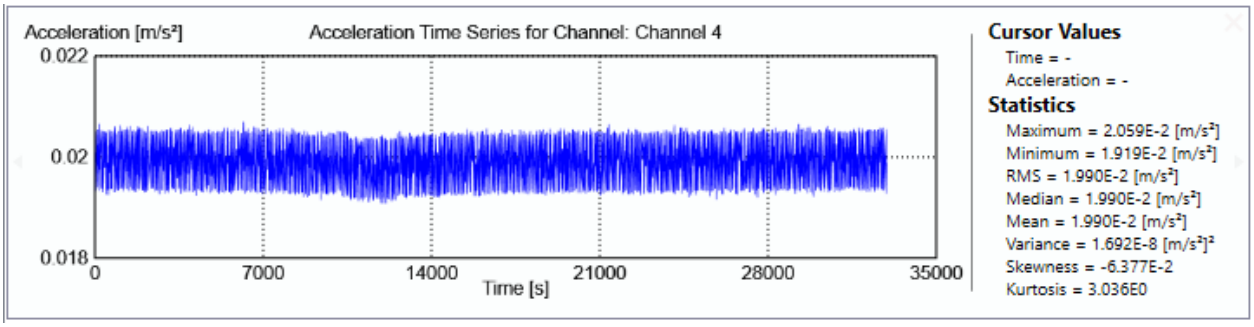

Figure 142 Time history plot of sensor 2 in the y-direction

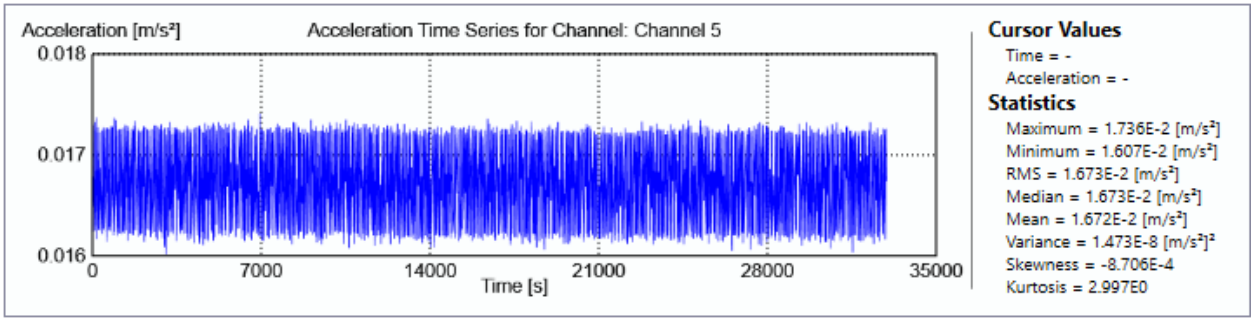

Figure 143 Time history plot of sensor 3 in the x-direction

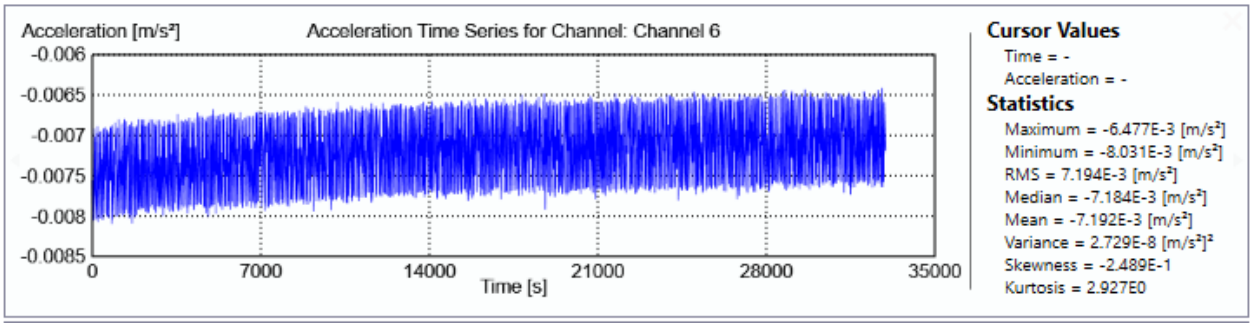

Figure 144 Time history plot of sensor 3 in the y-direction

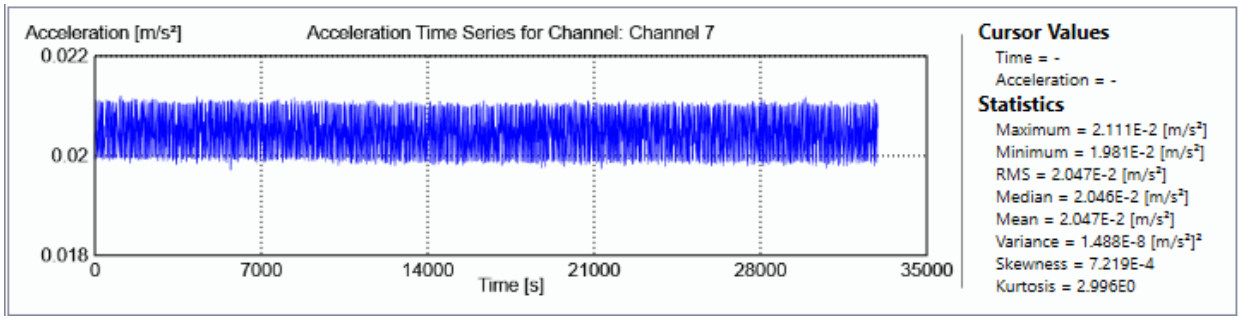

Figure 145 Time history plot of sensor 4 in the x-direction

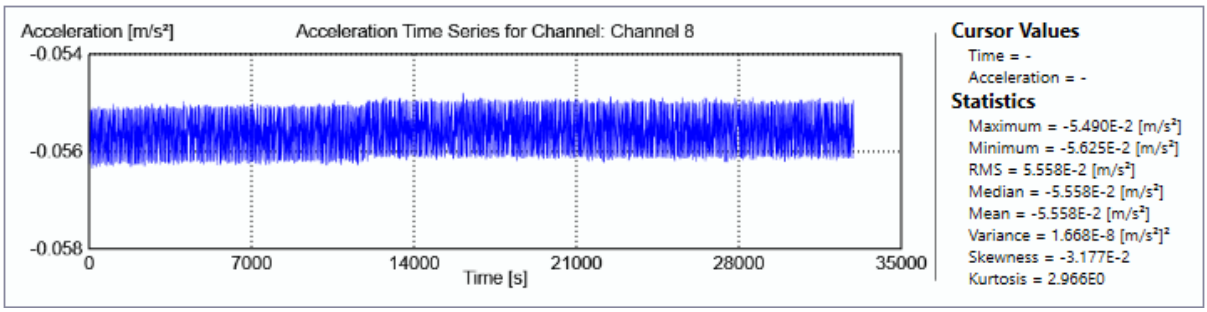

Figure 146 Time history plot of sensor 4 in the y-direction

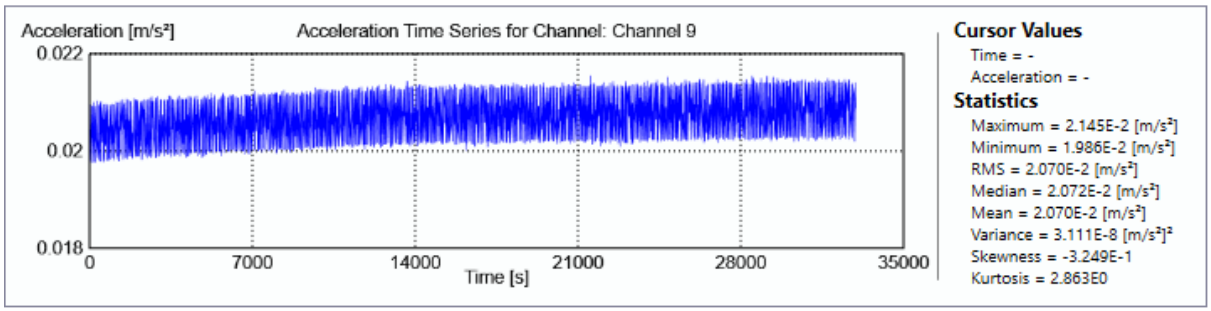

Figure 147 Time history plot of sensor 5 in the x-direction

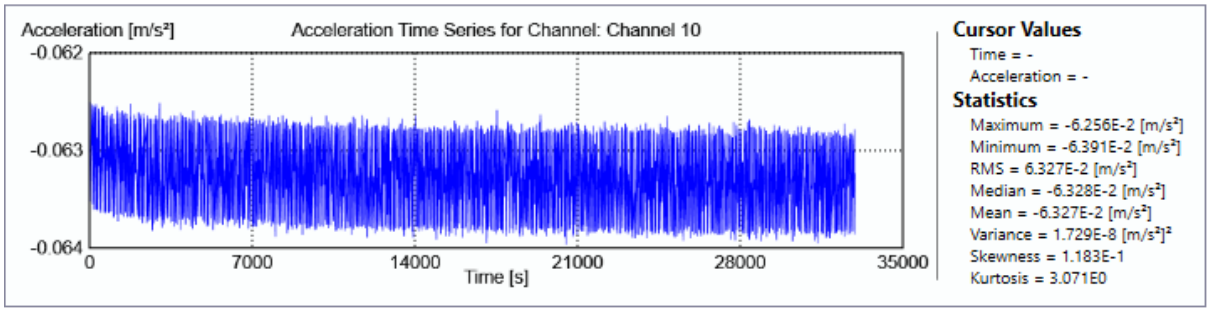

Figure 148 Time history plot of sensor 5 in the y-direction

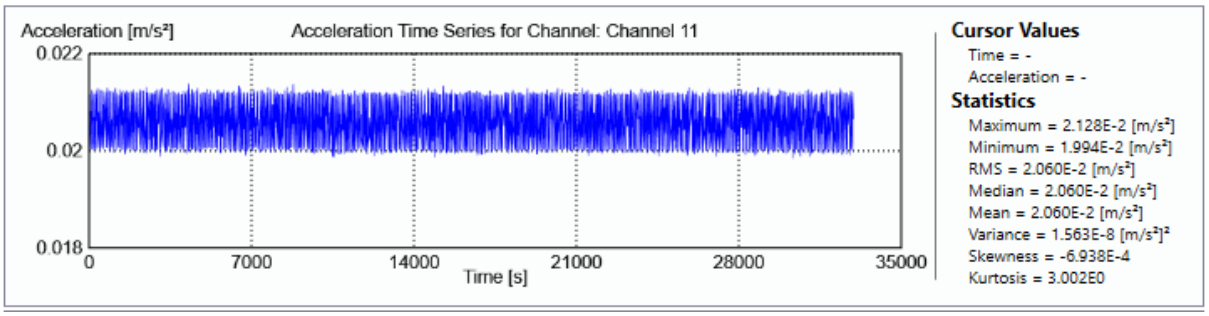

Figure 149 Time history plot of sensor 6 in the x-direction

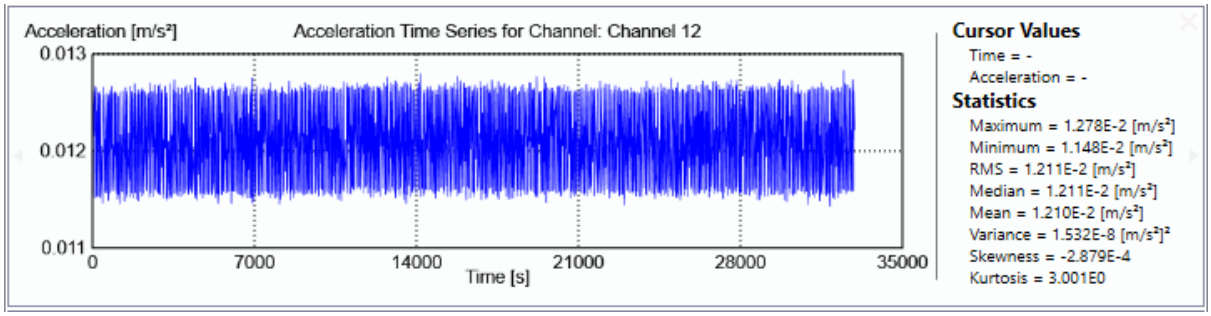

Figure 150 Time history plot of sensor 6 in the y-direction

Appendix 3 (Sensitivity Graphs to a Change in Different Parameters)

- To a change in elasticity modulus

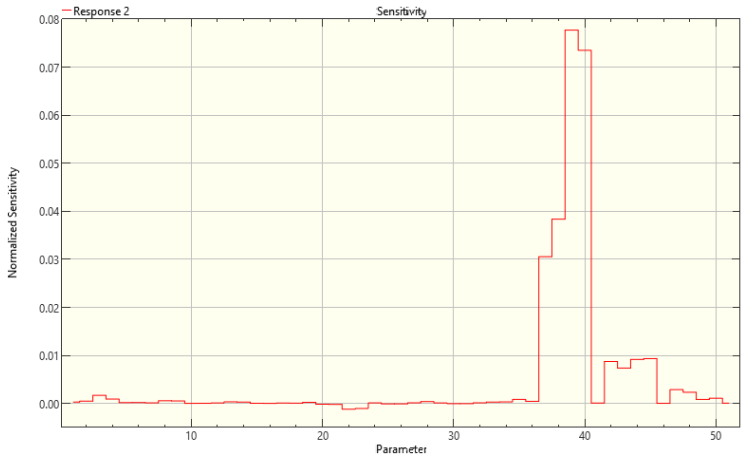

Figure 151 Sensitivity graph of the second frequency to a change in elasticity modulus / FB model

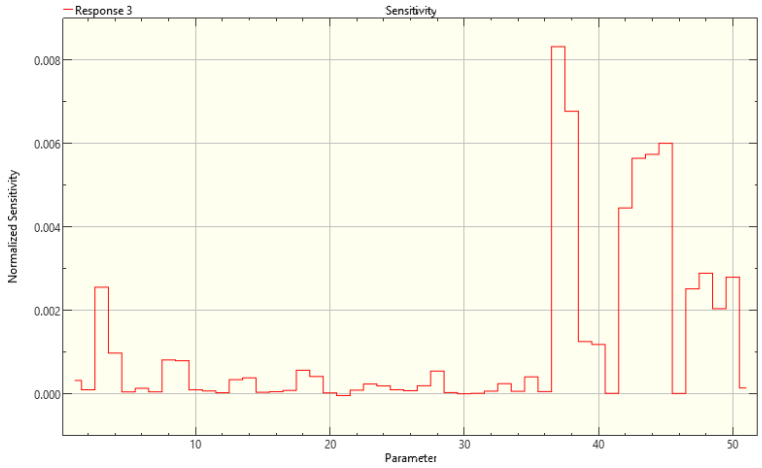

Figure 152 Sensitivity graph of the third frequency to a change in elasticity modulus / FB model

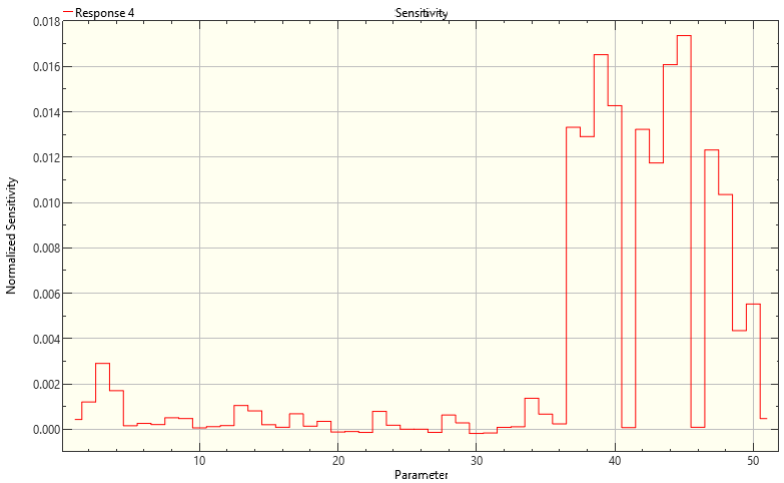

Figure 153 Sensitivity graph of the fourth frequency to a change in elasticity modulus / FB model

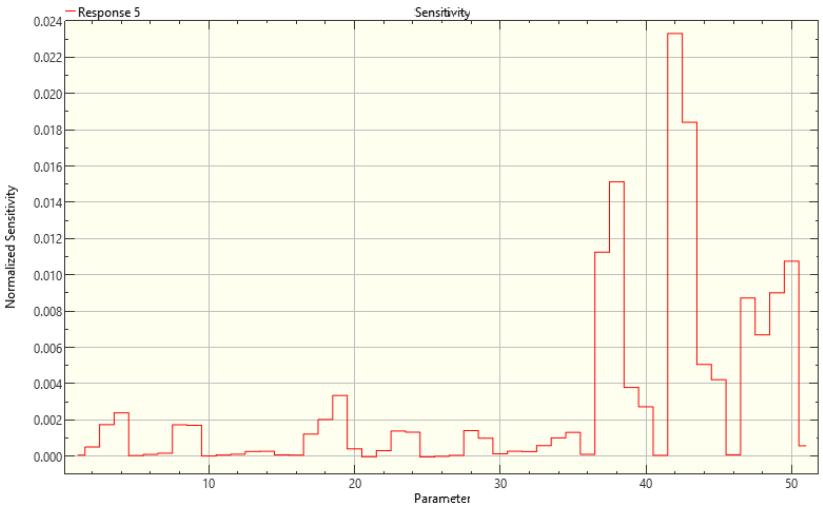

Figure 154 Sensitivity graph of the fifth frequency to a change in elasticity modulus / FB model

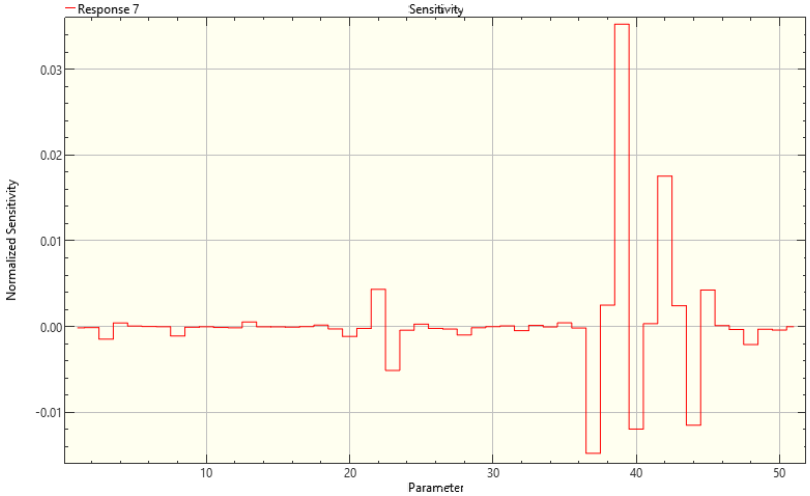

Figure 155 Sensitivity graph of the second mode shape to a change in elasticity modulus / FB model

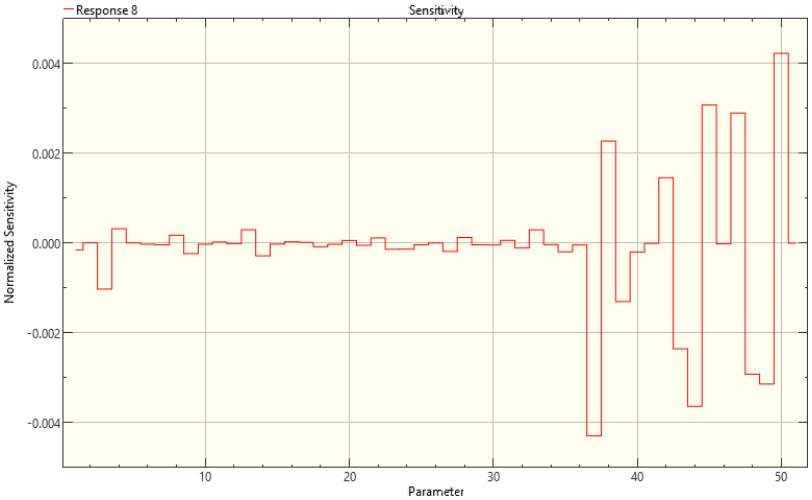

Figure 156 Sensitivity graph of the third mode shape to a change in elasticity modulus / FB model

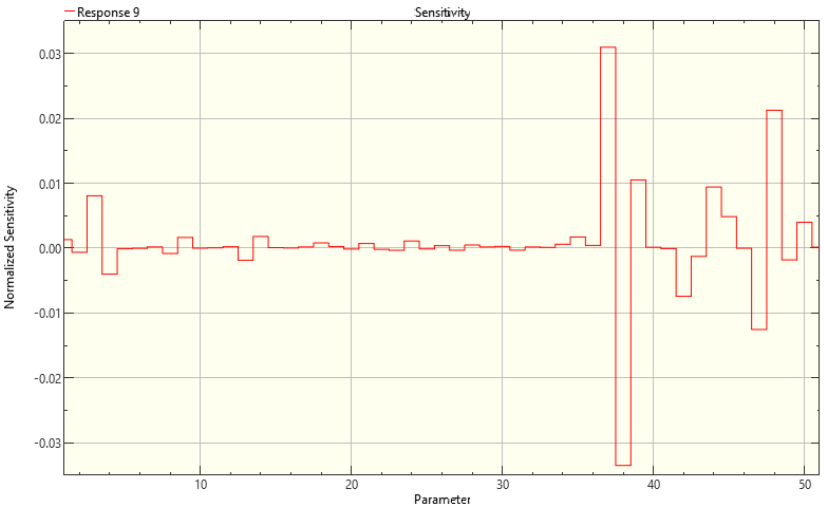

Figure 157 Sensitivity graph of the fourth mode shape to a change in elasticity modulus / FB model

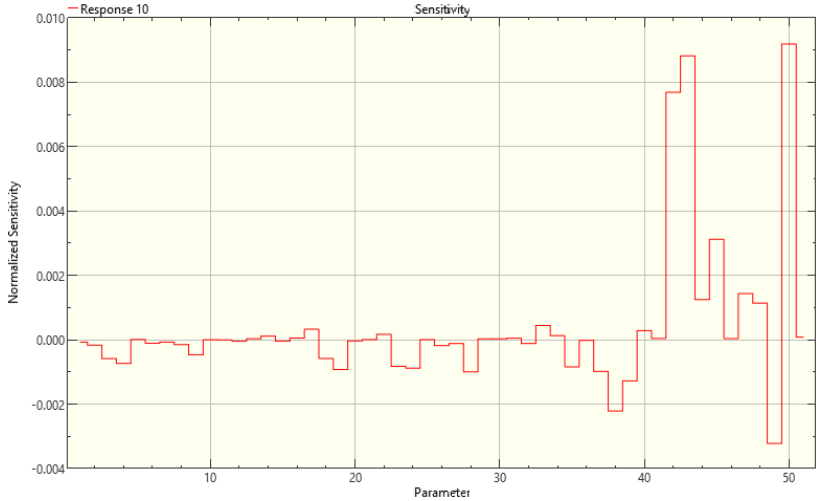

Figure 158 Sensitivity graph of the fifth mode shape to a change in elasticity modulus / FB model

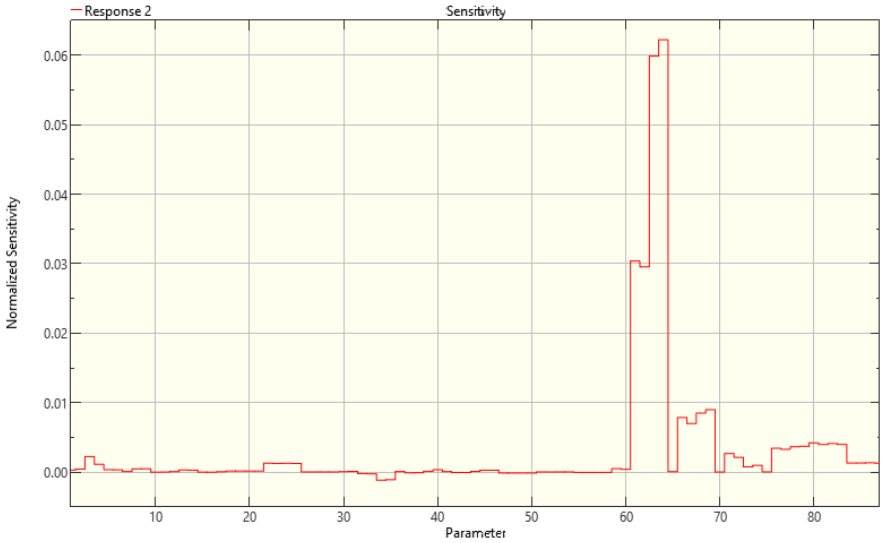

Figure 159 Sensitivity graph of the Second frequency to a change in elasticity modulus / SB model

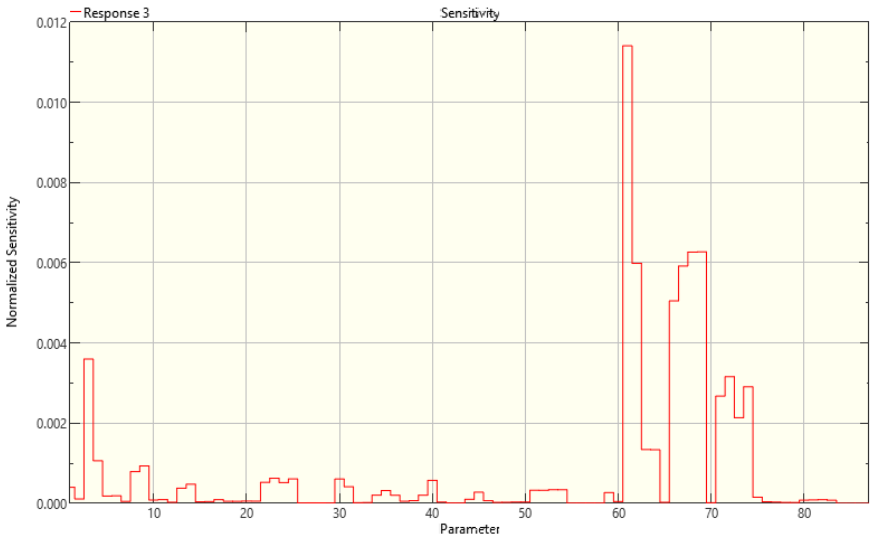

Figure 160 Sensitivity graph of the third frequency to a change in elasticity modulus / SB model

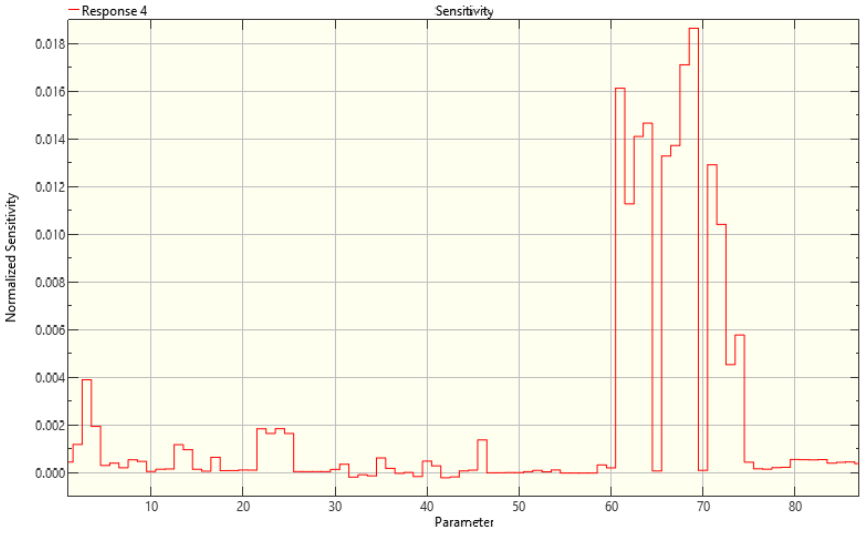

Figure 161 Sensitivity graph of the fourth frequency to a change in elasticity modulus / SB model

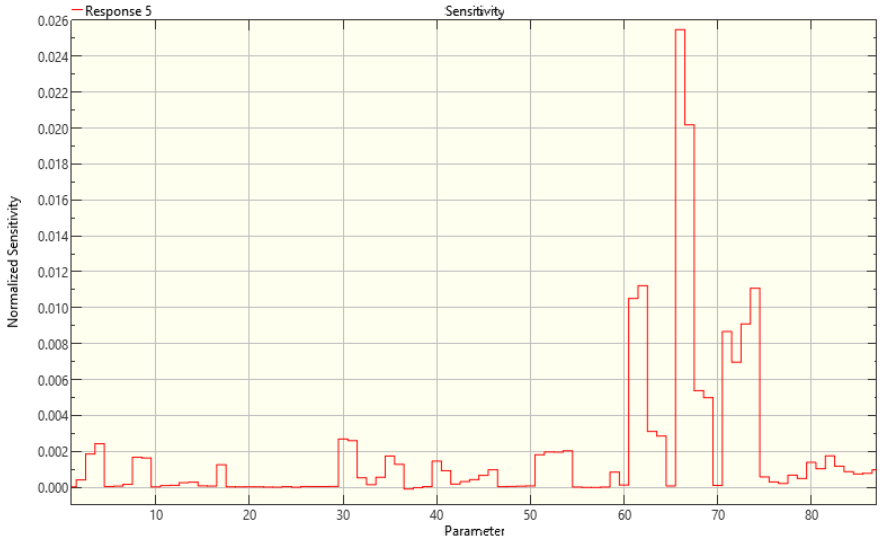

Figure 162 Sensitivity graph of the fifth frequency to a change in elasticity modulus / SB model

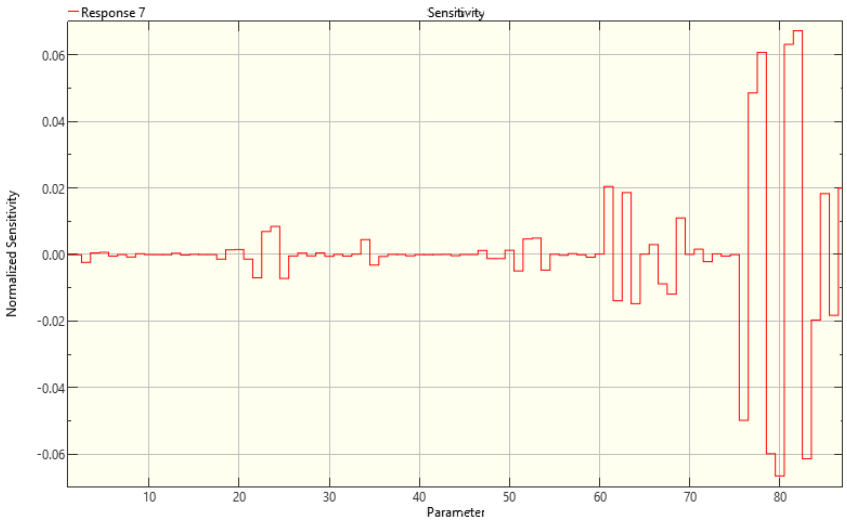

Figure 163 Sensitivity graph of the second mode shape to a change in elasticity modulus / SB model

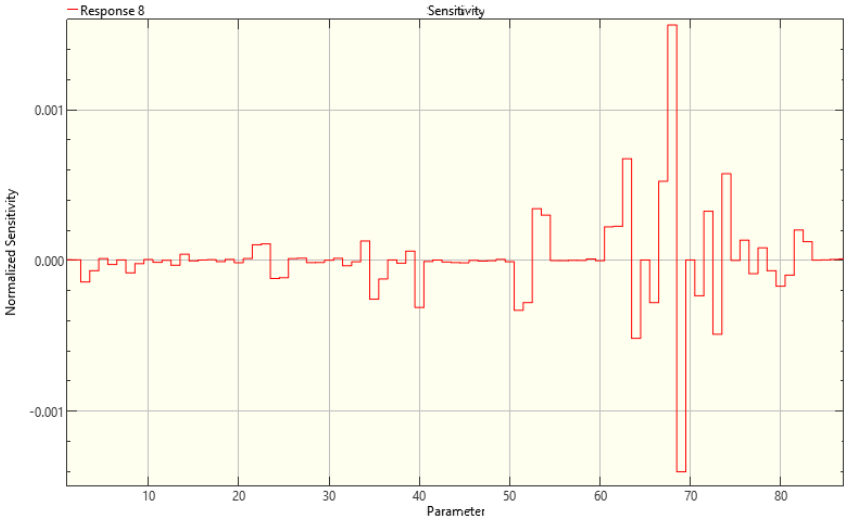

Figure 164 Sensitivity graph of the third mode shape to a change in elasticity modulus / SB model

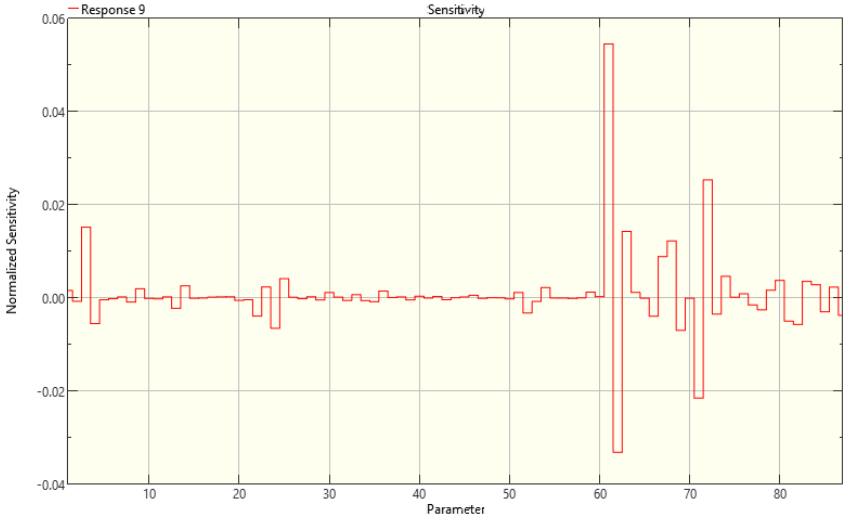

Figure 165 Sensitivity graph of the fourth mode shape to a change in elasticity modulus / SB model

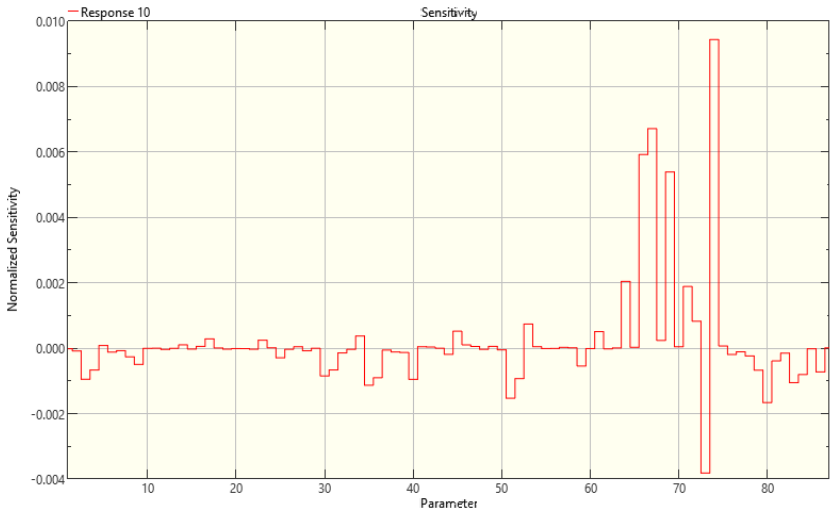

Figure 166 Sensitivity graph of the fifth mode shape to a change in elasticity modulus / SB model

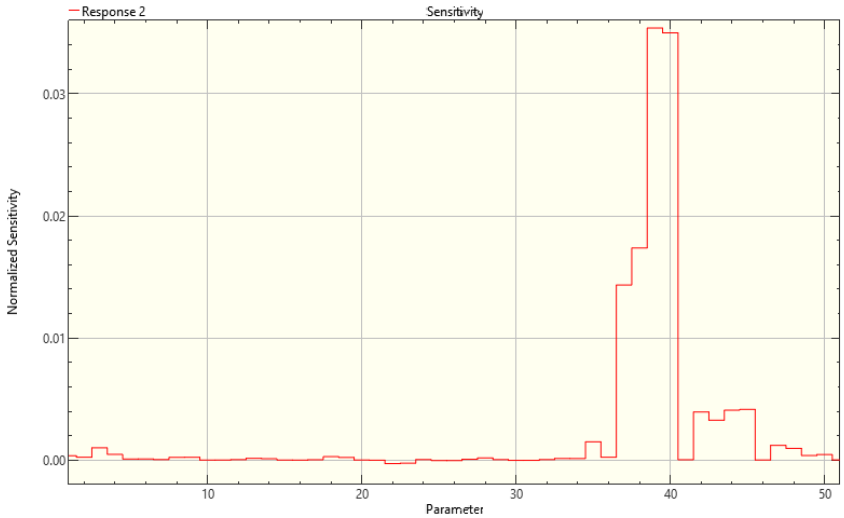

Figure 167 Sensitivity graph of the second frequency to a change in elasticity modulus / SS model

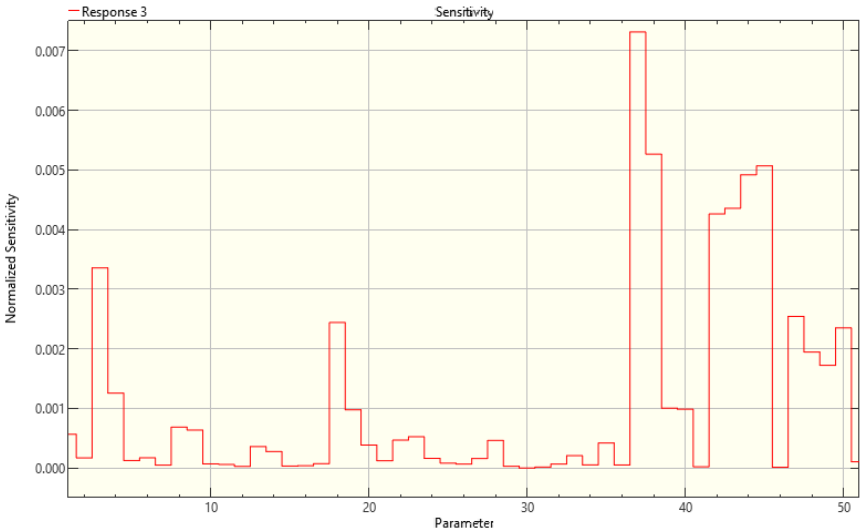

Figure 168 Sensitivity graph of the third frequency to a change in elasticity modulus / SS model

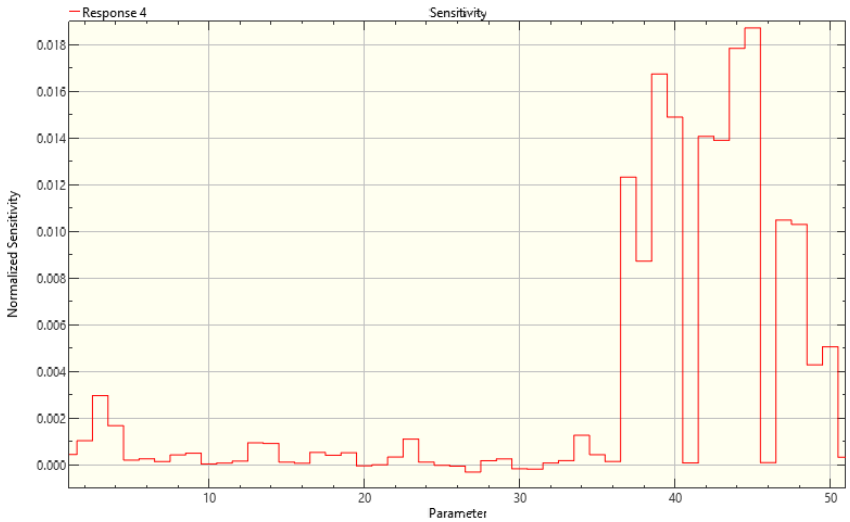

Figure 169 Sensitivity graph of the fourth frequency to a change in elasticity modulus / SS model

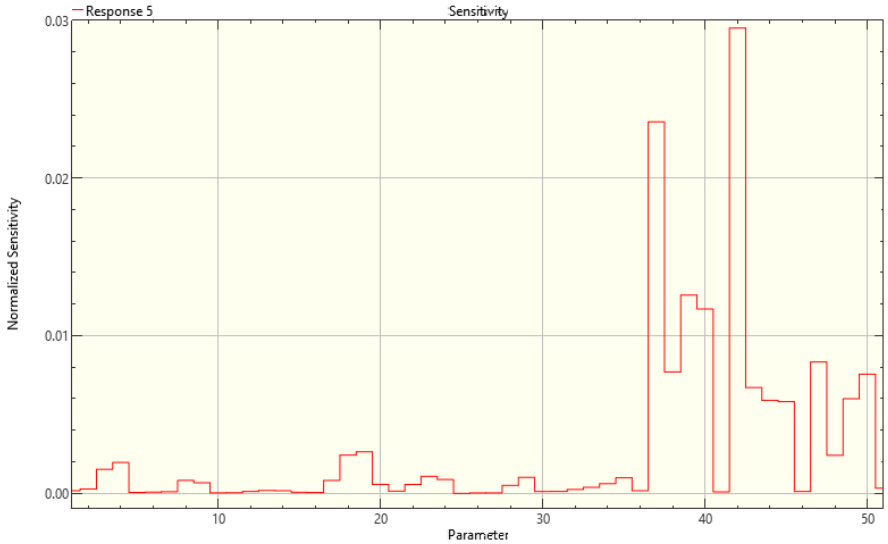

Figure 170 Sensitivity graph of the fifth frequency to a change in elasticity modulus / SS model

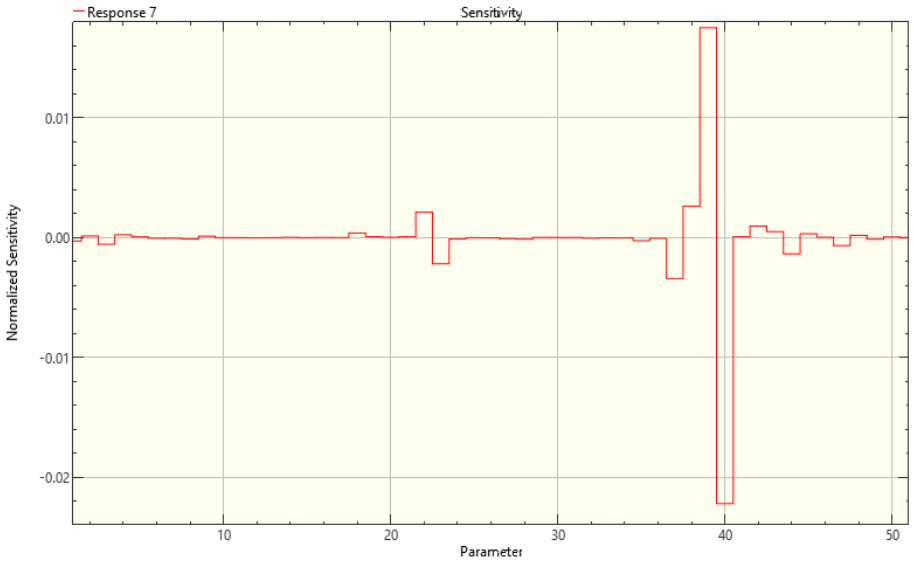

Figure 171 Sensitivity graph of the second mode shape to a change in elasticity modulus / SS model

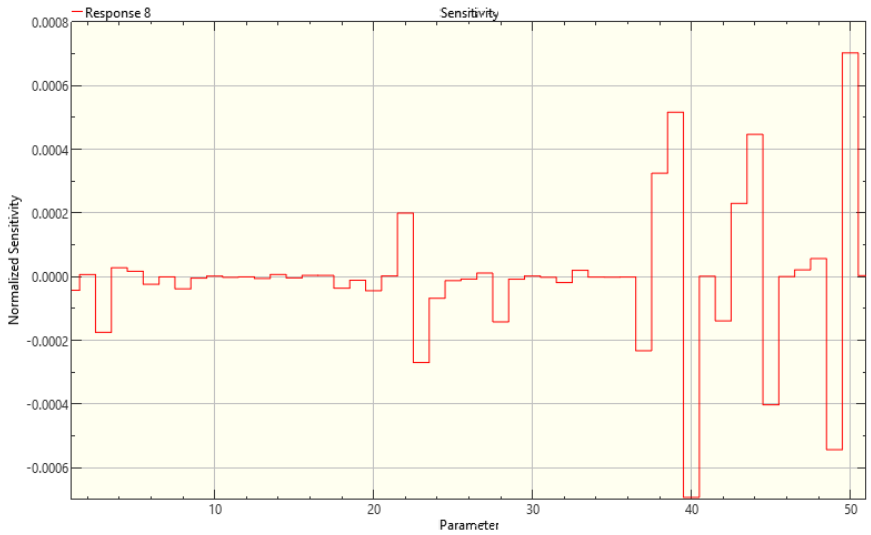

Figure 172 Sensitivity graph of the third mode shape to a change in elasticity modulus / SS model

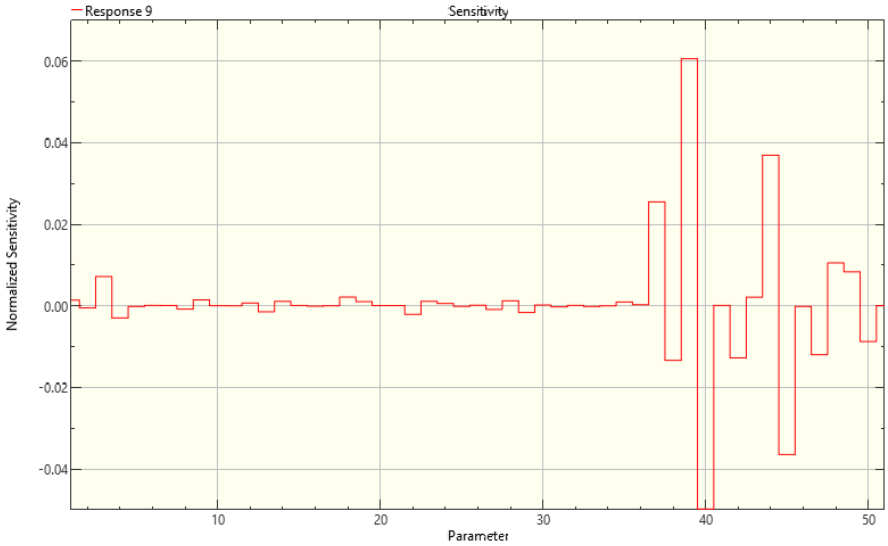

Figure 173 Sensitivity graph of the fourth mode shape to a change in elasticity modulus / SS model

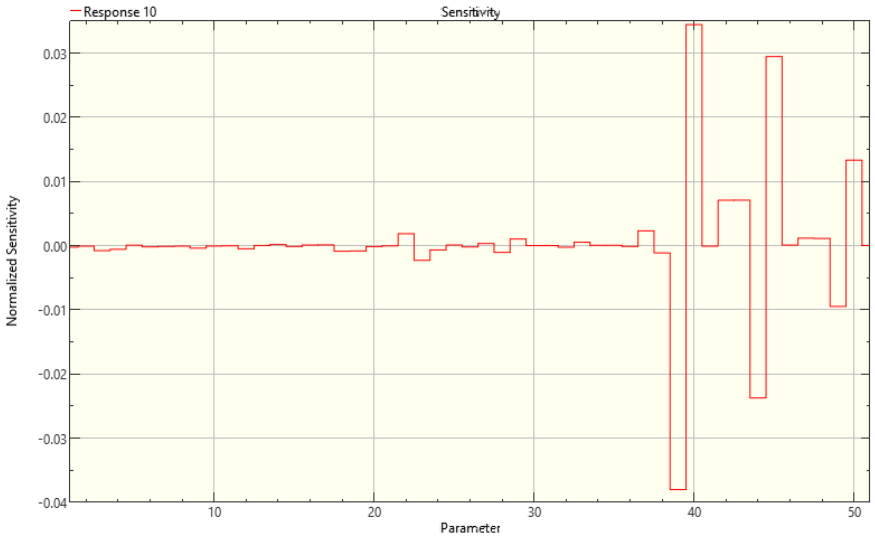

Figure 174 Sensitivity graph of the fifth mode shape to a change in elasticity modulus / SS model

- To a change in Poisson’s ratio

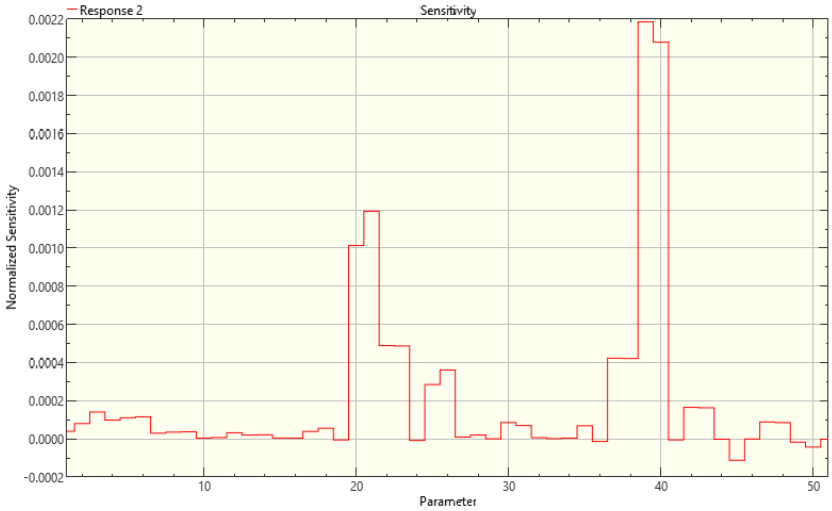

Figure 175 Sensitivity graph of the second frequency to a change in Poisson's ratio / FB model

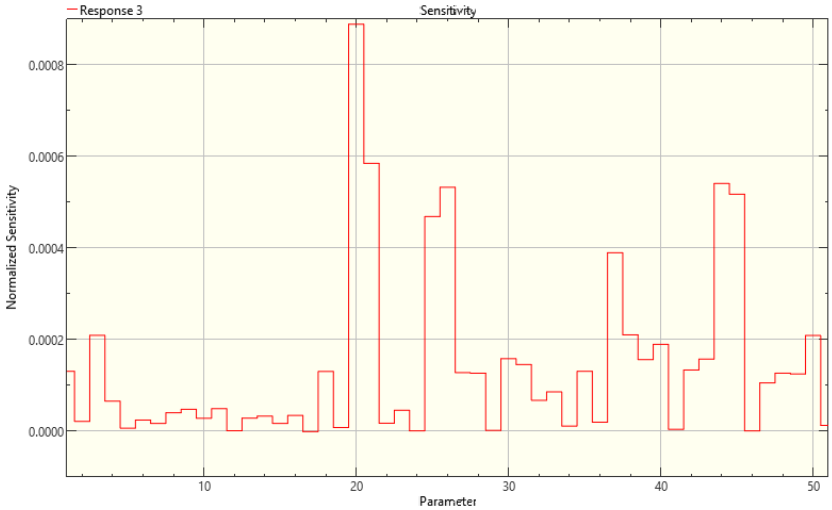

Figure 176 Sensitivity graph of the third frequency to a change in Poisson's ratio / FB model

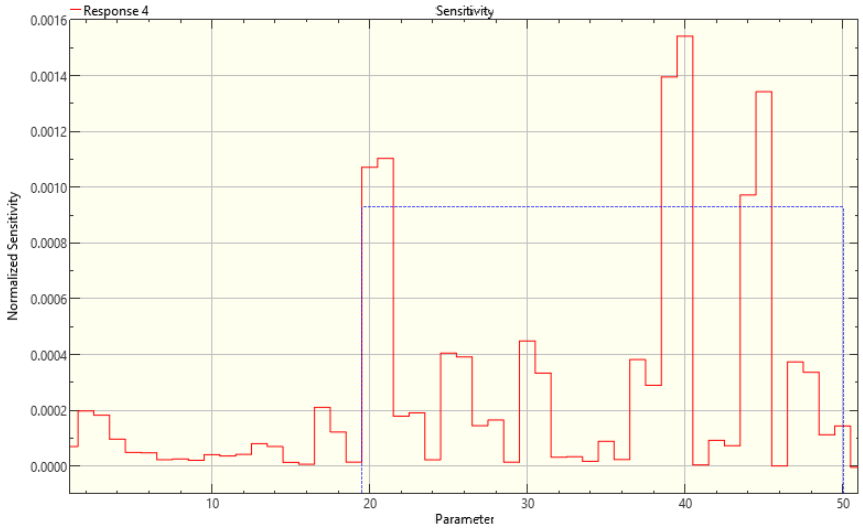

Figure 177 Sensitivity graph of the fourth frequency to a change in Poisson's ratio / FB model

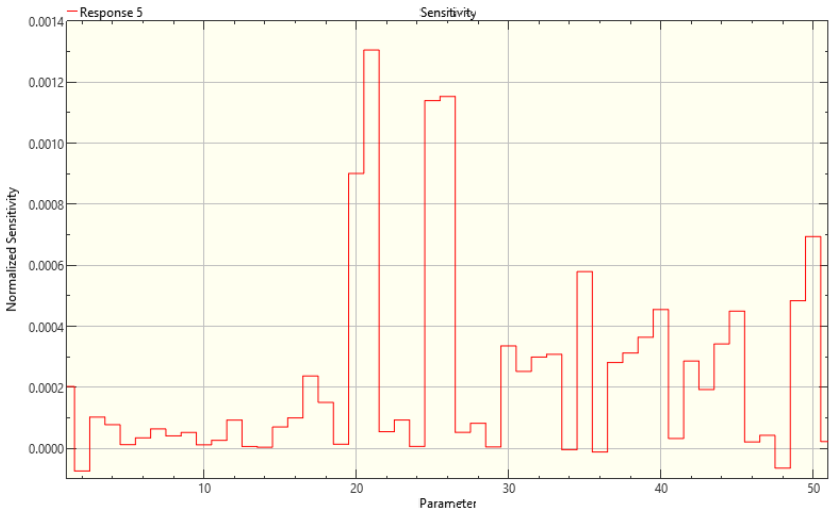

Figure 178 Sensitivity graph of the fifth frequency to a change in Poisson's ratio / FB model

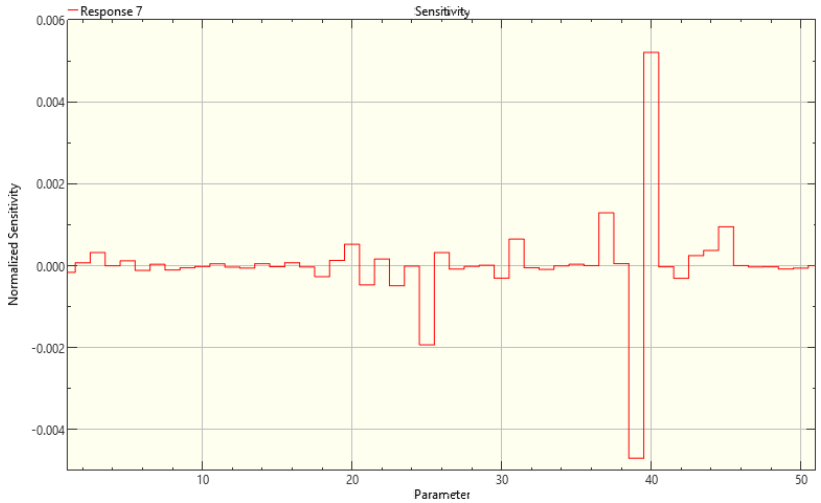

Figure 179 Sensitivity graph of the second mode shape to a change in Poisson's ratio / FB model

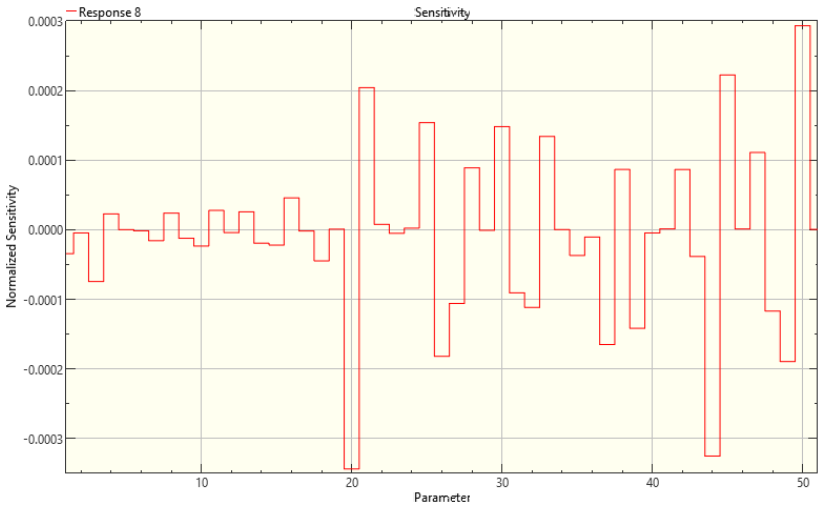

Figure 180 Sensitivity graph of the third mode shape to a change in Poisson's ratio / FB model

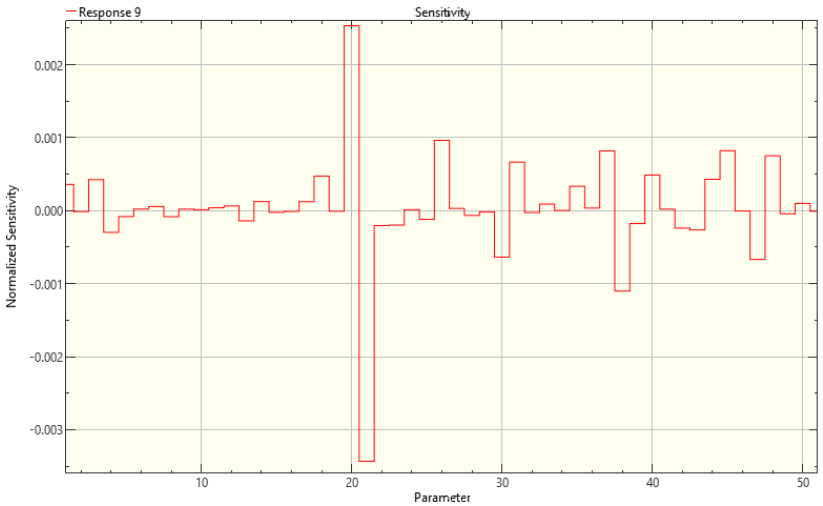

Figure 181 Sensitivity graph of the fourth mode shape to a change in Poisson's ratio / FB model

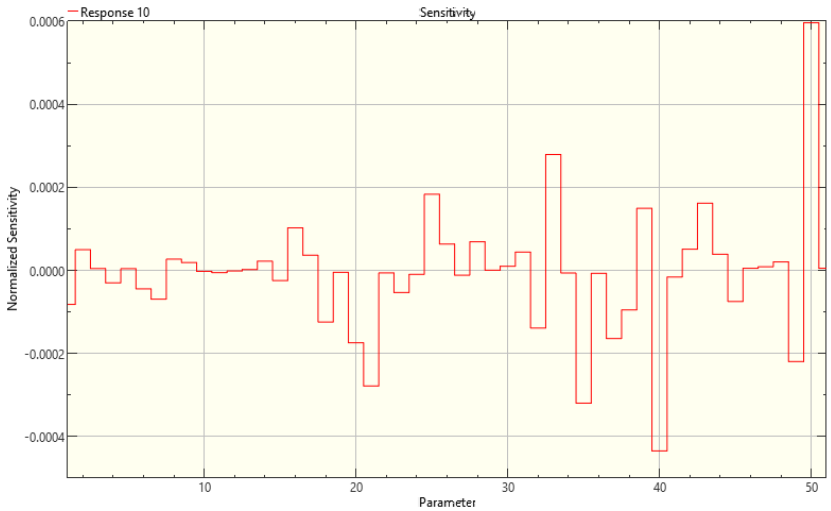

Figure 182 Sensitivity graph of the fifth mode shape to a change in Poisson's ratio / FB model

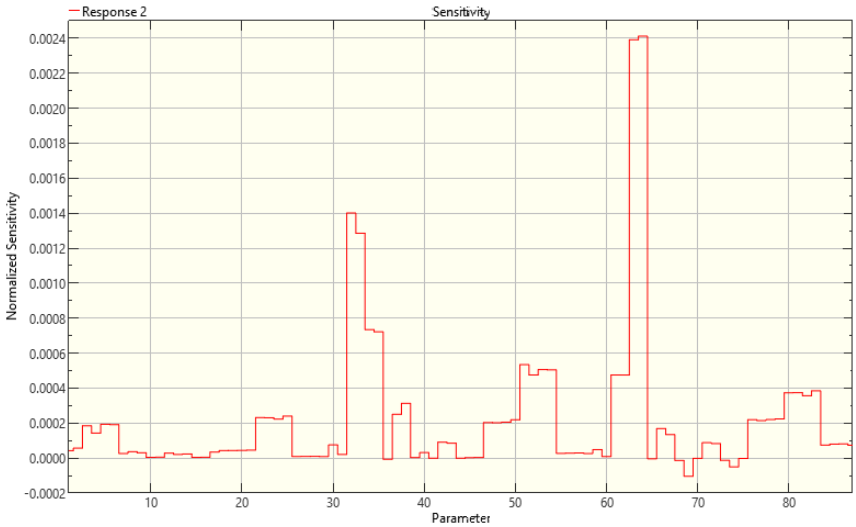

Figure 183 Sensitivity graph of the second frequency to a change in Poisson's ratio / SB model

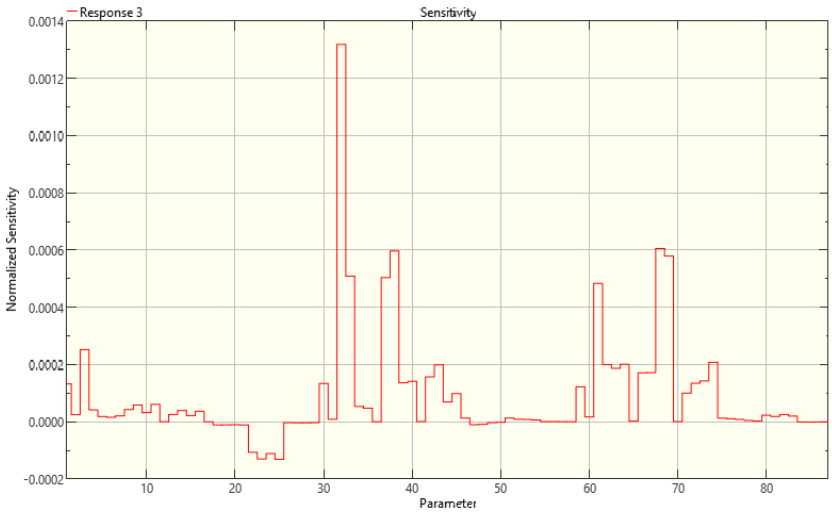

Figure 184 Sensitivity graph of the third frequency to a change in Poisson's ratio / SB model

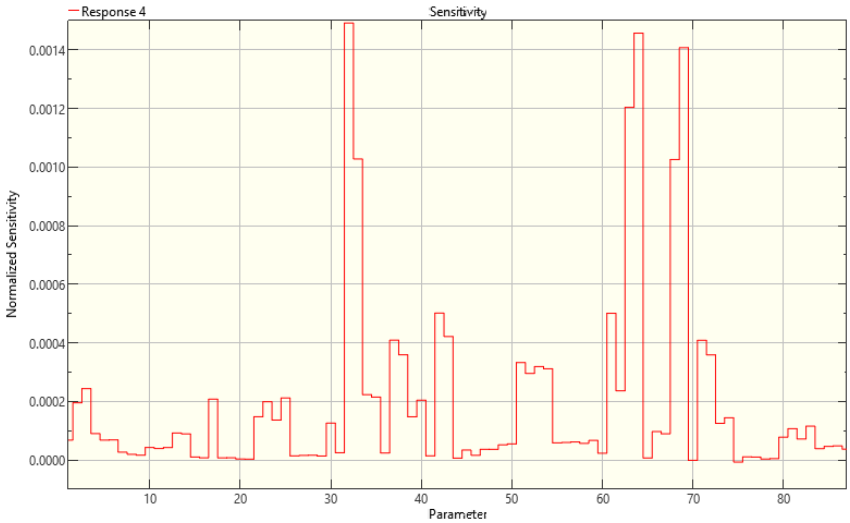

Figure 185 Sensitivity graph of the fourth frequency to a change in Poisson's ratio / SB model

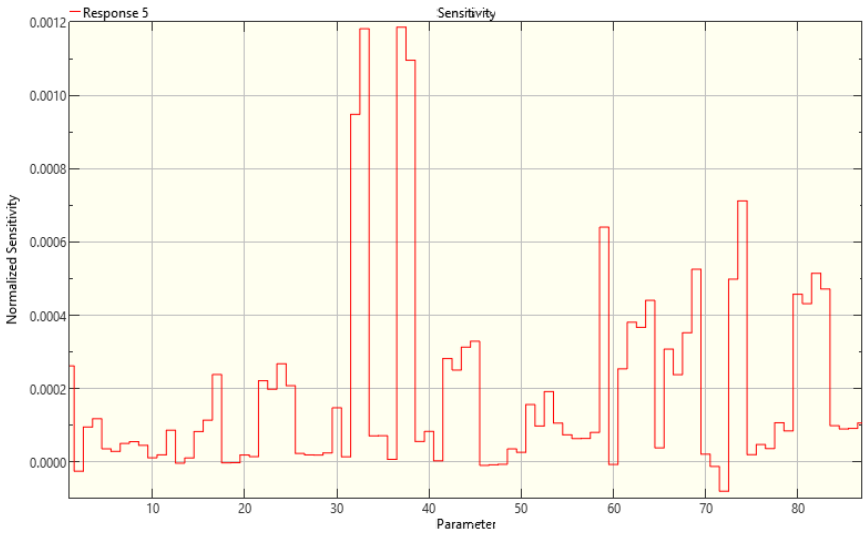

Figure 186 Sensitivity graph of the fifth frequency to a change in Poisson's ratio / SB model

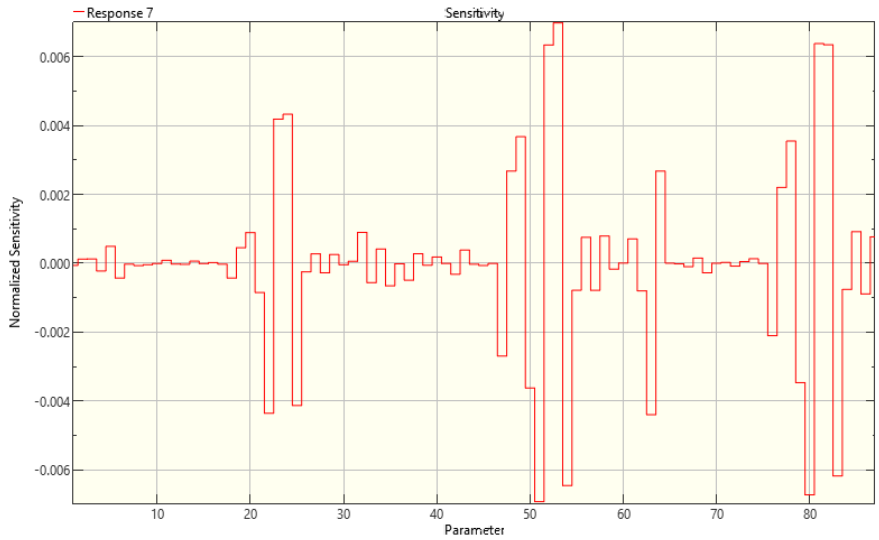

Figure 187 Sensitivity graph of the second mode shape to a change in Poisson's ratio / SB model

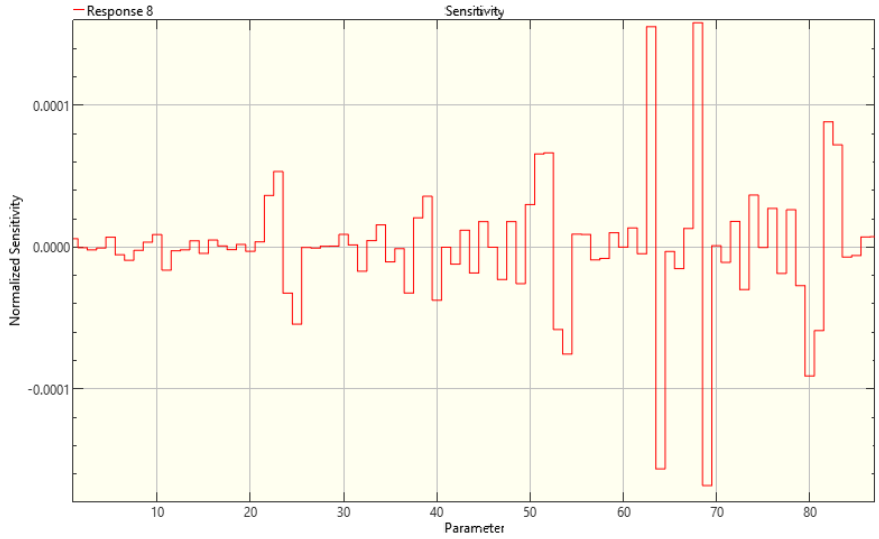

Figure 188 Sensitivity graph of the third mode shape to a change in Poisson's ratio / SB model

Figure 189 Sensitivity graph of the fourth mode shape to a change in Poisson's ratio / SB model

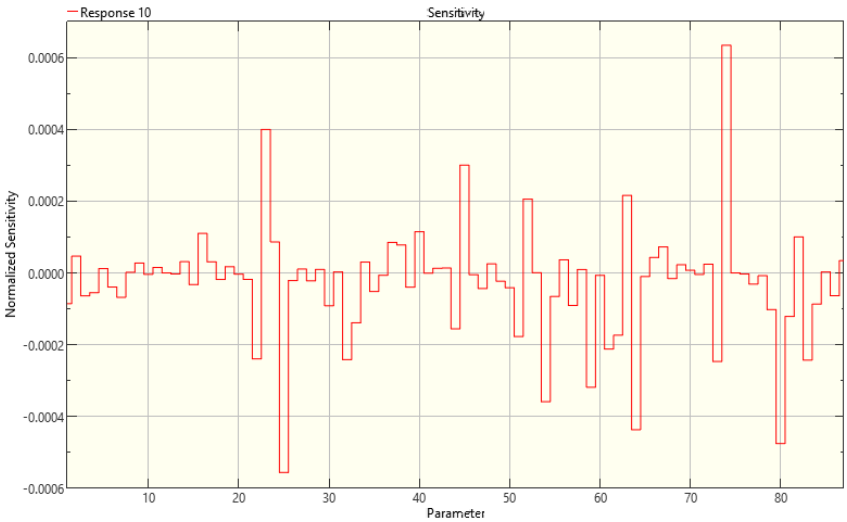

Figure 190 Sensitivity graph of the fifth mode shape to a change in Poisson's ratio / SB model

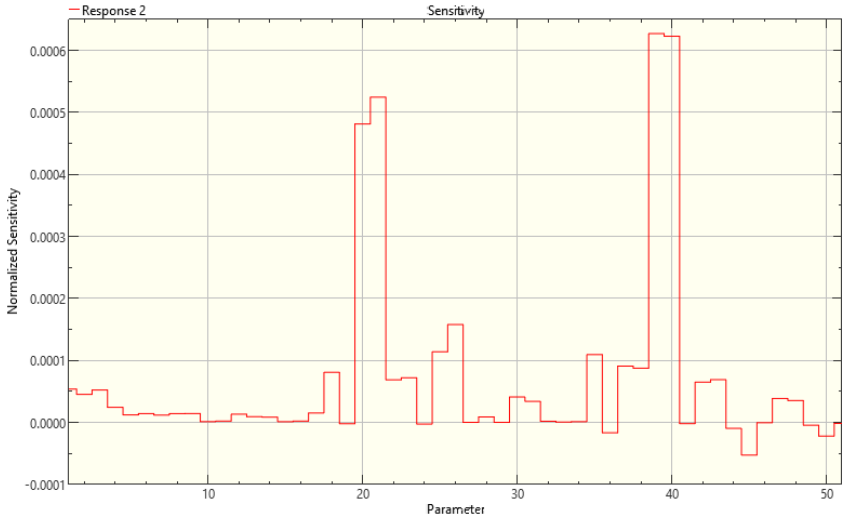

Figure 191 Sensitivity graph of the second frequency to a change in Poisson's ratio / SS model

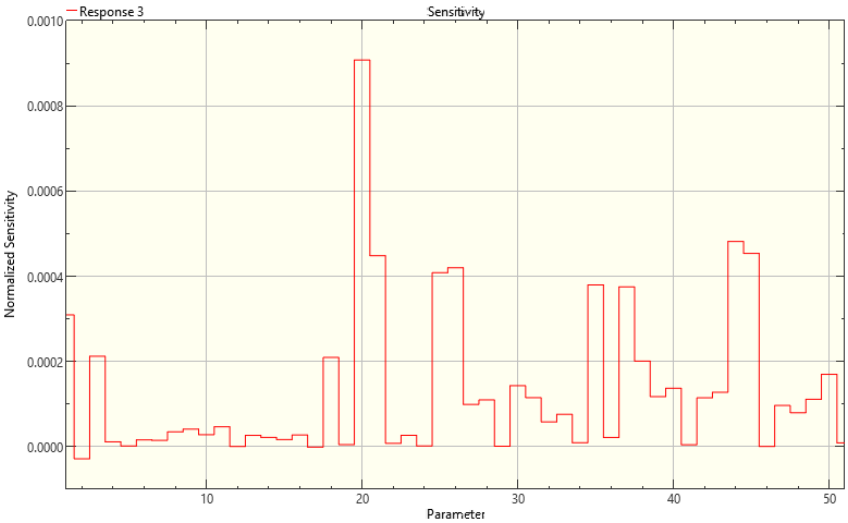

Figure 192 Sensitivity graph of the third frequency to a change in Poisson's ratio / SS model

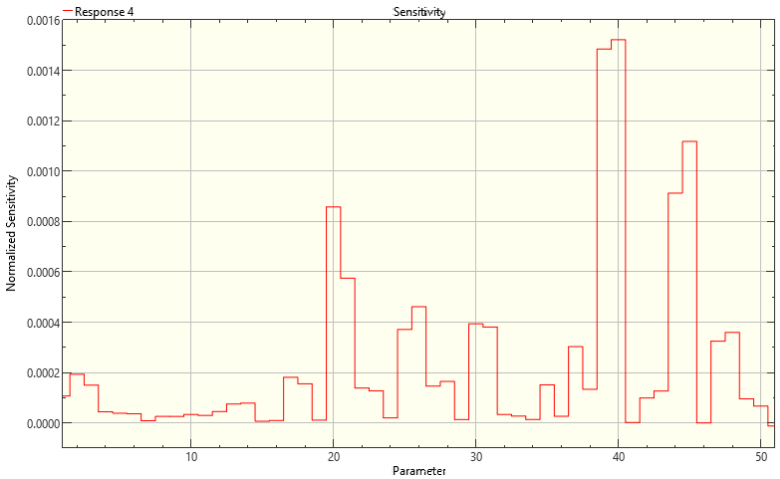

Figure 193 Sensitivity graph of the fourth frequency to a change in Poisson's ratio / SS model

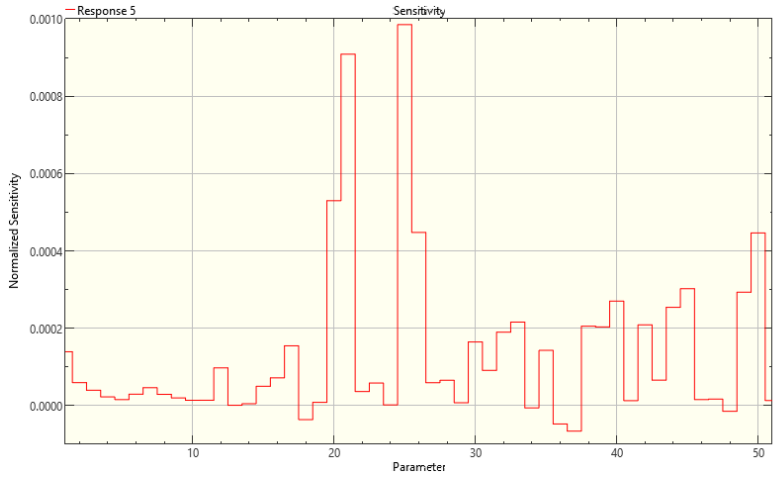

Figure 194 Sensitivity graph of the fifth frequency to a change in Poisson's ratio / SS model

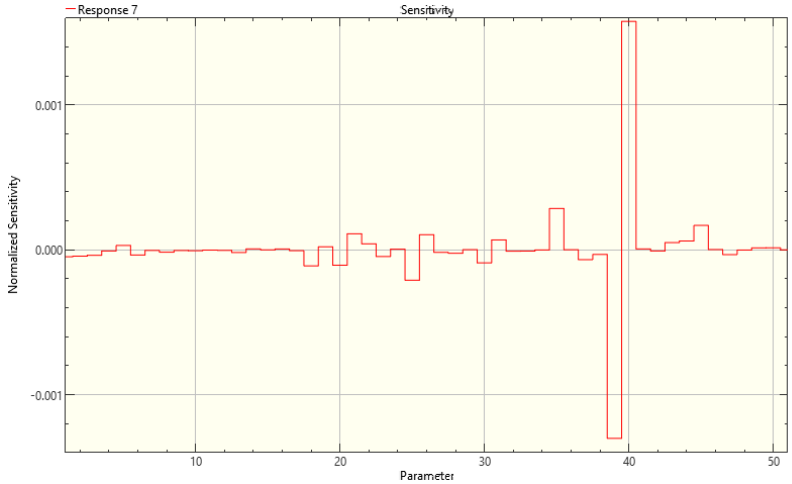

Figure 195 Sensitivity graph of the second mode shape to a change in Poisson's ratio / SS model

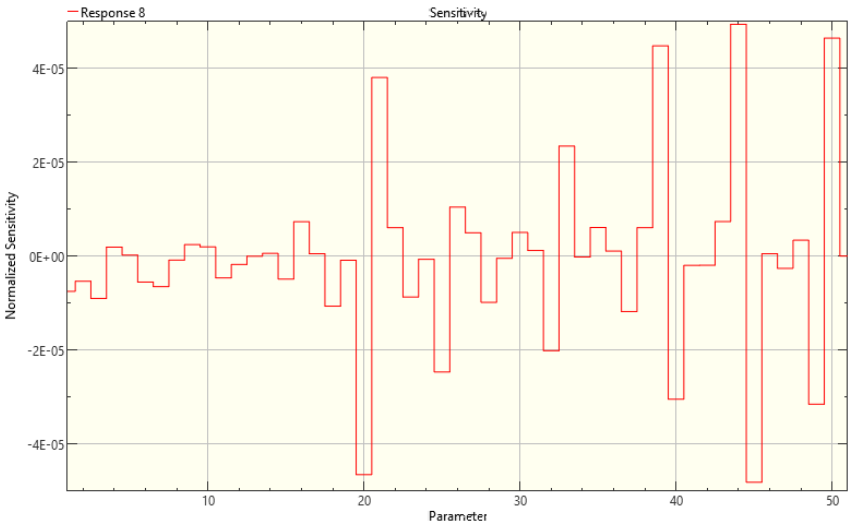

Figure 196 Sensitivity graph of the third mode shape to a change in Poisson's ratio / SS model

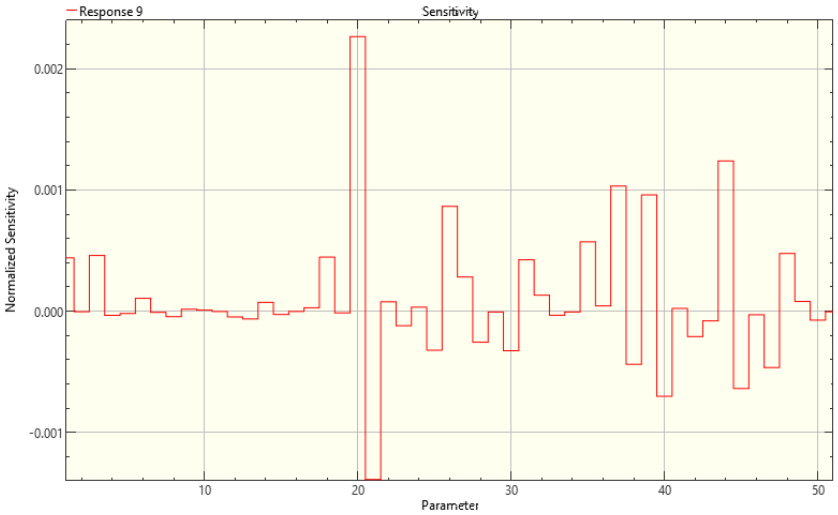

Figure 197 Sensitivity graph of the fourth mode shape to a change in Poisson's ratio / SS model

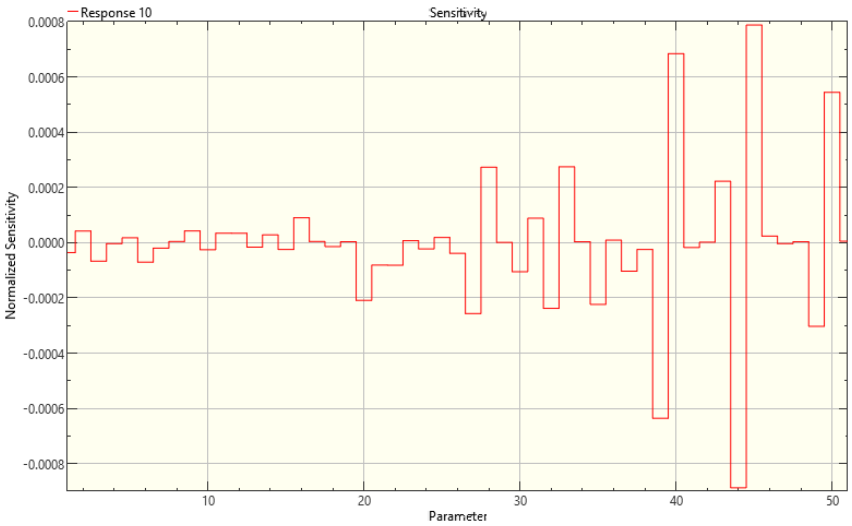

Figure 198 Sensitivity graph of the fifth mode shape to a change in Poisson's ratio / SS model

- To a change in density

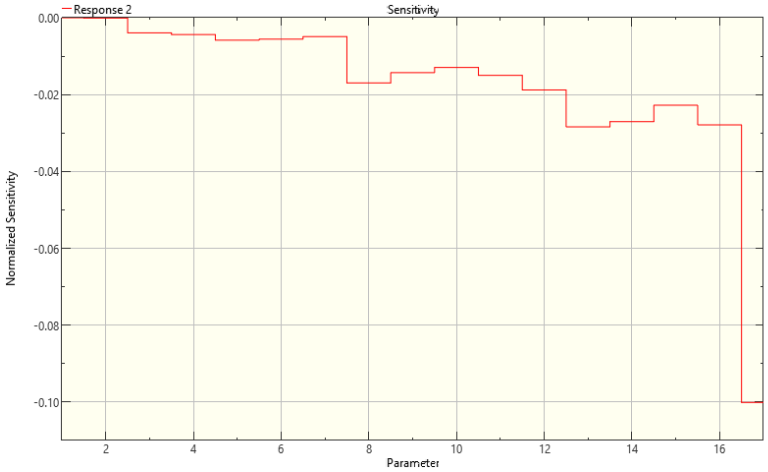

Figure 199 Sensitivity graph of the second frequency to a change in density / FB model

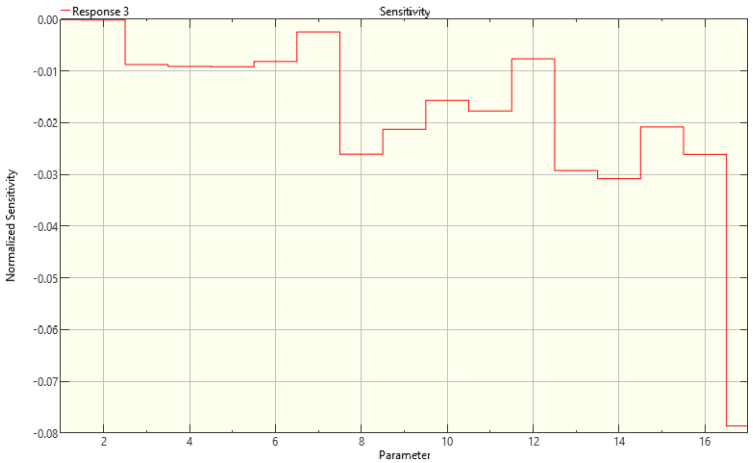

Figure 200 Sensitivity graph of the third frequency to a change in density / FB model

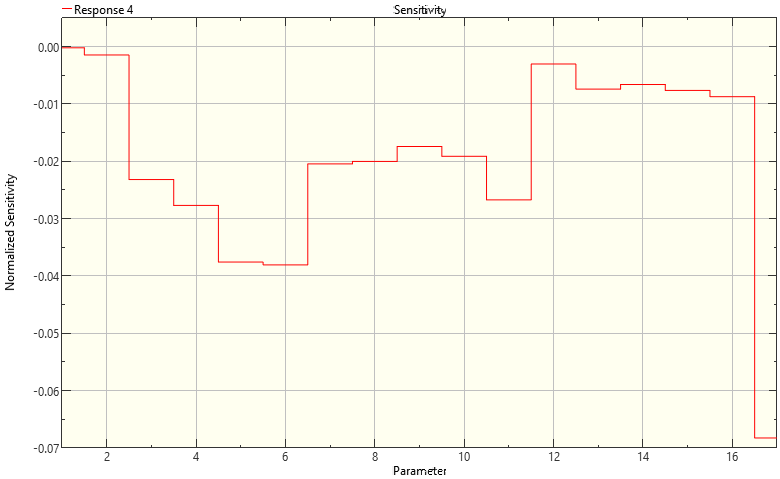

Figure 201 Sensitivity graph of the fourth frequency to a change in density / FB model

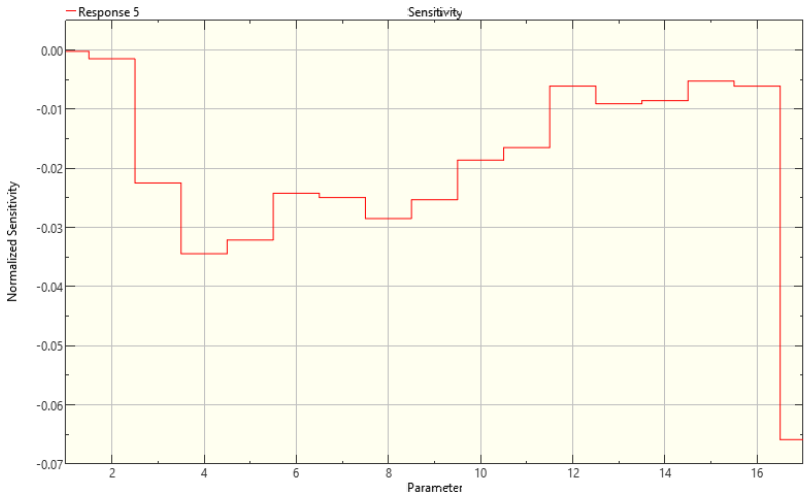

Figure 202 Sensitivity graph of the fifth frequency to a change in density / FB model

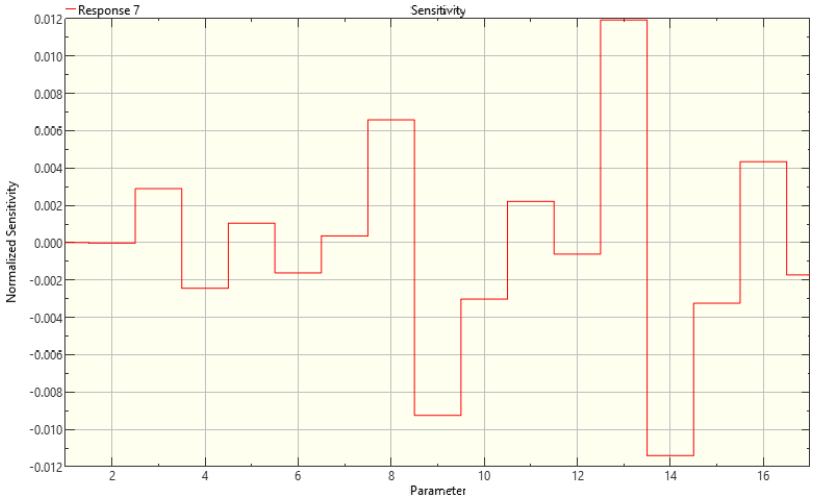

Figure 203 Sensitivity graph of the second mode shape to a change in density / FB model

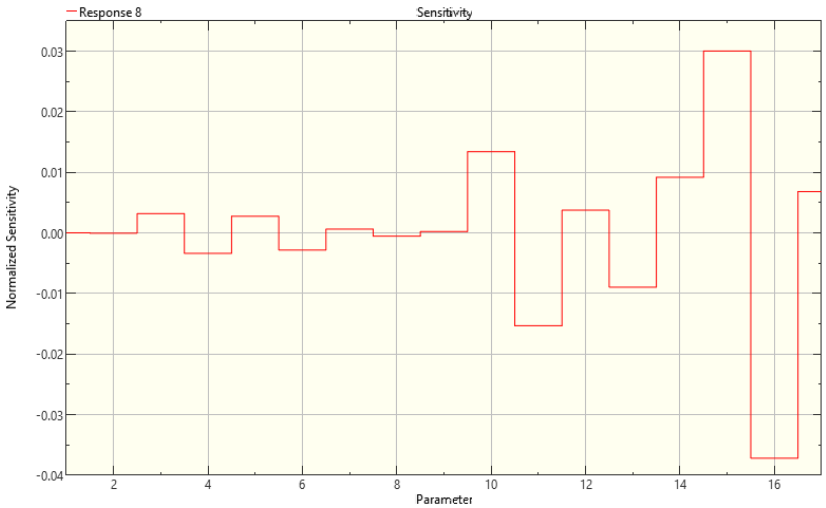

Figure 204 Sensitivity graph of the third mode shape to a change in density / FB model

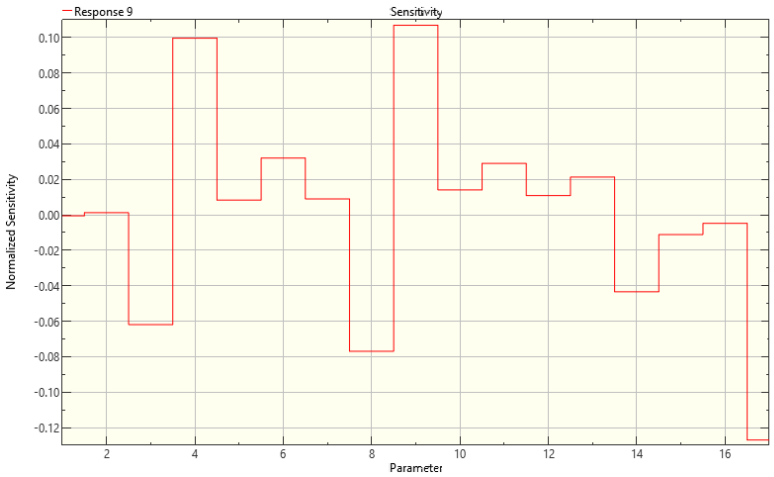

Figure 205 Sensitivity graph of the fourth mode shape to a change in density / FB model

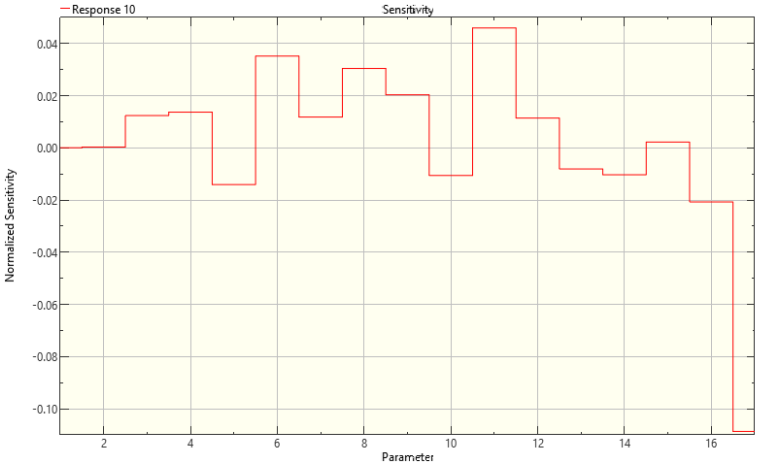

Figure 206 Sensitivity graph of the fifth mode shape to a change in density / FB model

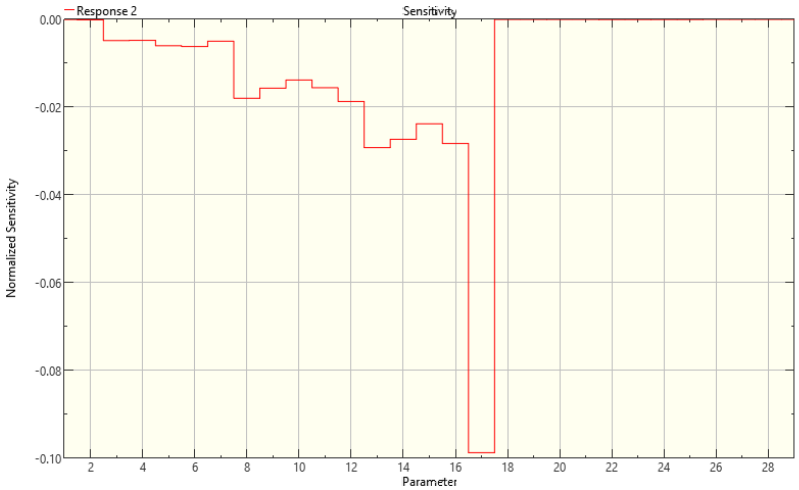

Figure 207 Sensitivity graph of the second frequency to a change in density / SB model

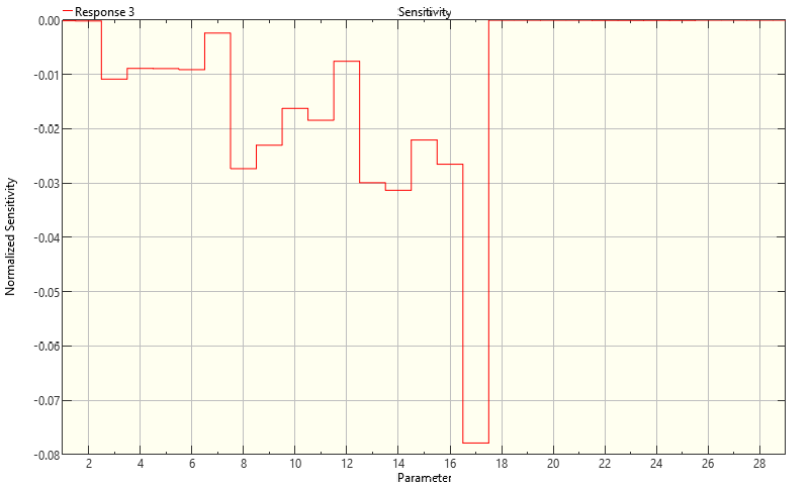

Figure 208 Sensitivity graph of the third frequency to a change in density / SB model

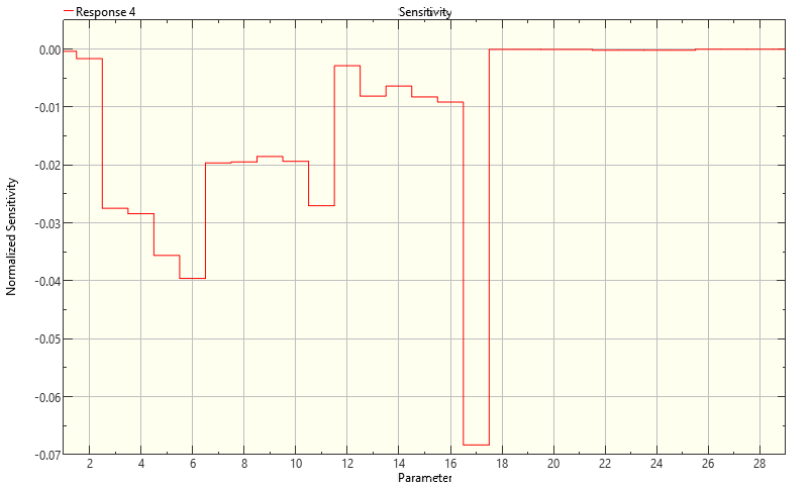

Figure 209 Sensitivity graph of the fourth frequency to a change in density / SB model

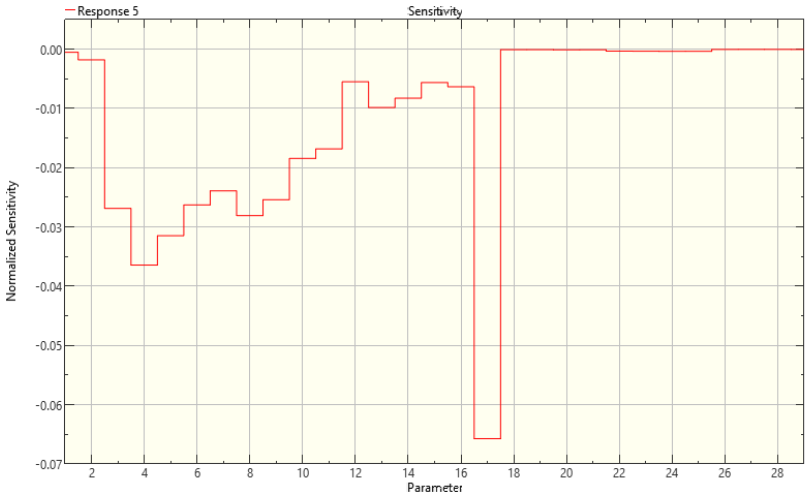

Figure 210 Sensitivity graph of the fifth frequency to a change in density / SB model

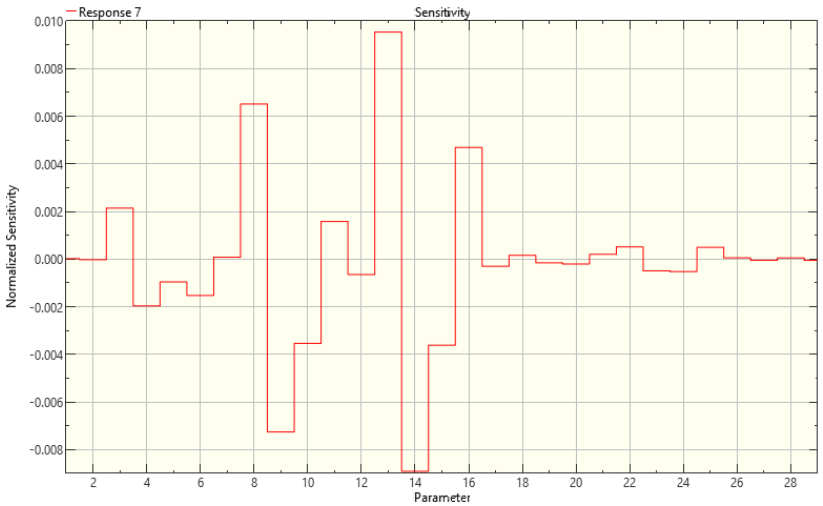

Figure 211 Sensitivity graph of the second mode shape to a change in density / SB model

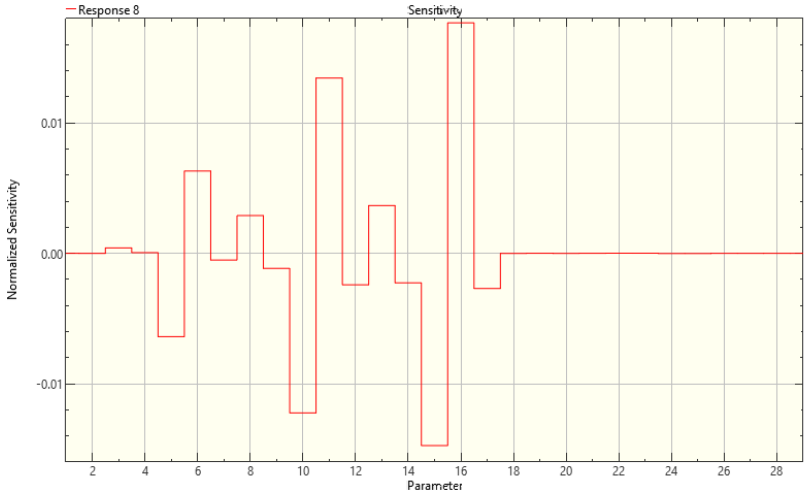

Figure 212 Sensitivity graph of the third mode shape to a change in density / SB model

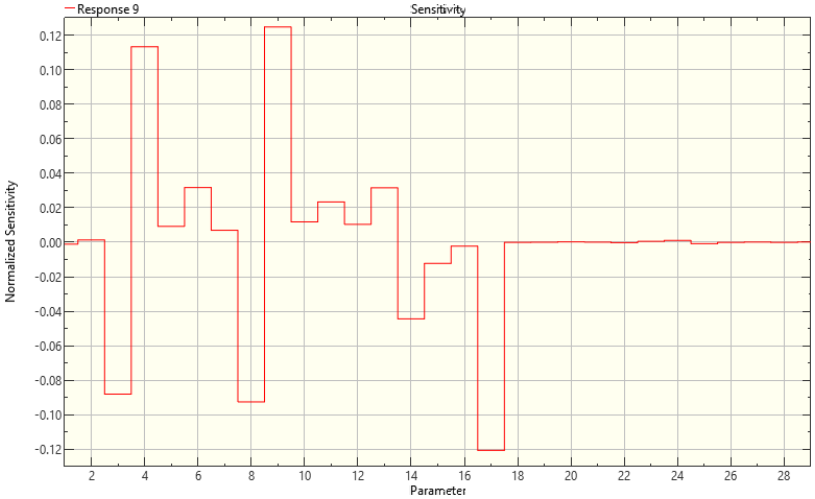

Figure 213 Sensitivity graph of the fourth mode shape to a change in density / SB model

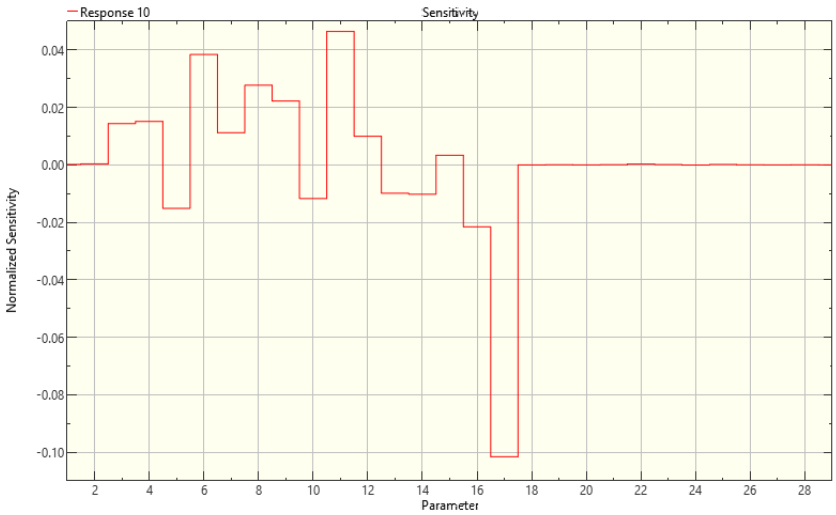

Figure 214 Sensitivity graph of the fifth mode shape to a change in density / SB model

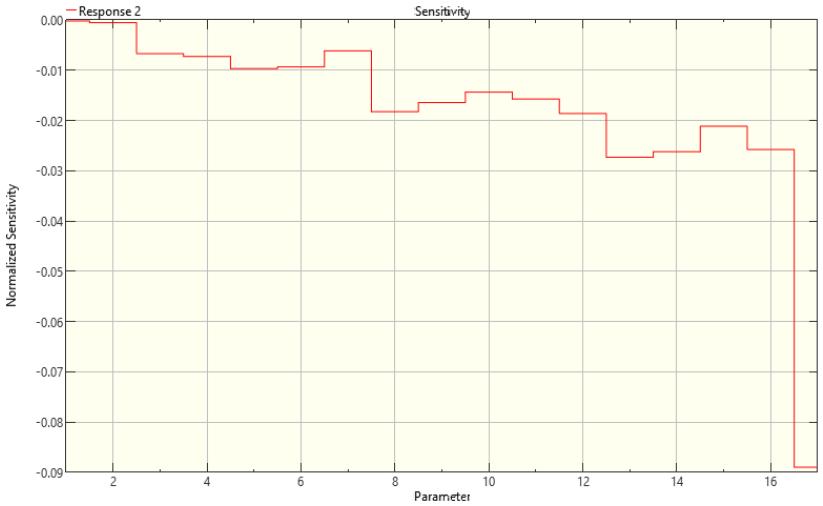

Figure 215 Sensitivity graph of the 2second frequency to a change in density / SS model

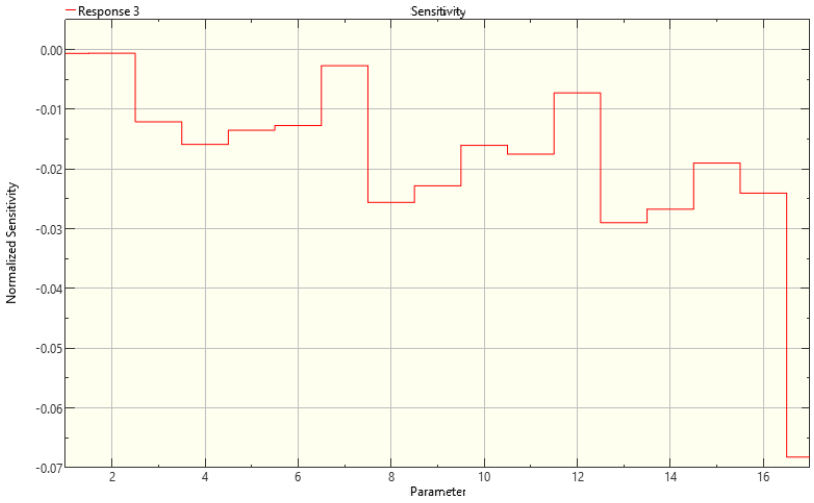

Figure 216 Sensitivity graph of the third frequency to a change in density / SS model

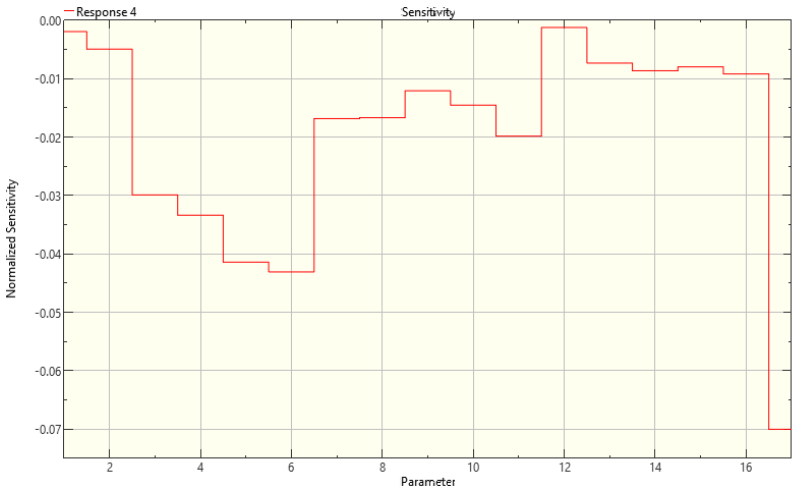

Figure 217 Sensitivity graph of the fourth frequency to a change in density / SS model

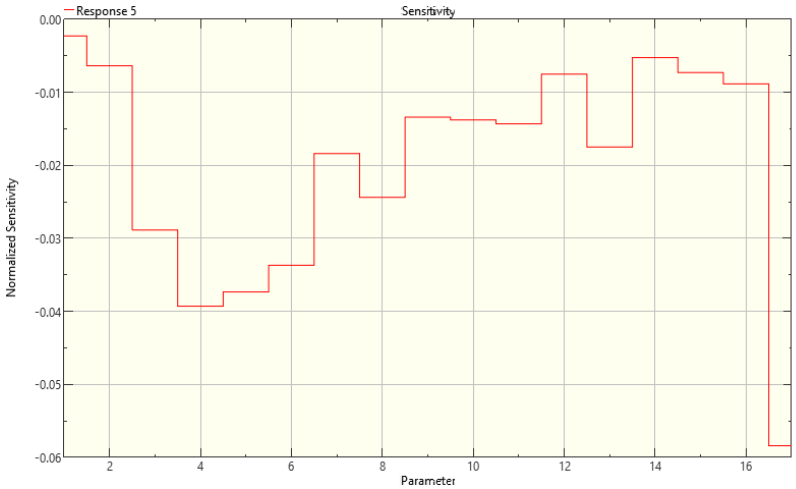

Figure 218 Sensitivity graph of the fifth frequency to a change in density / SS model

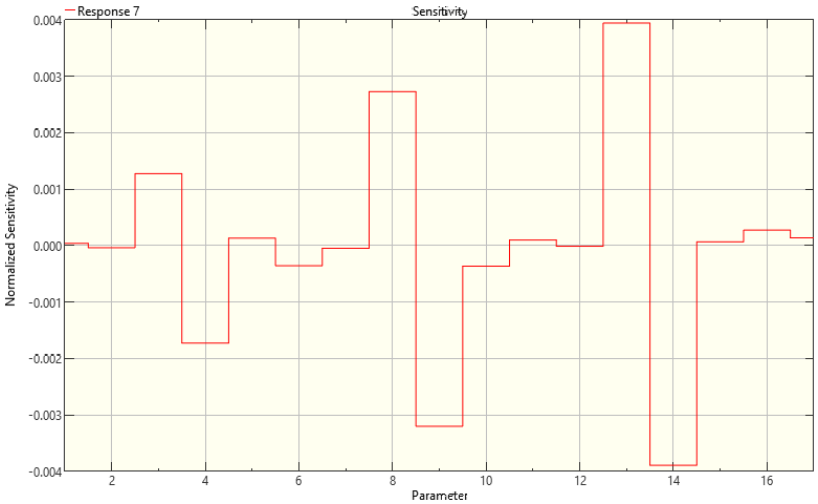

Figure 219 Sensitivity graph of the second mode shape to a change in density / SS model

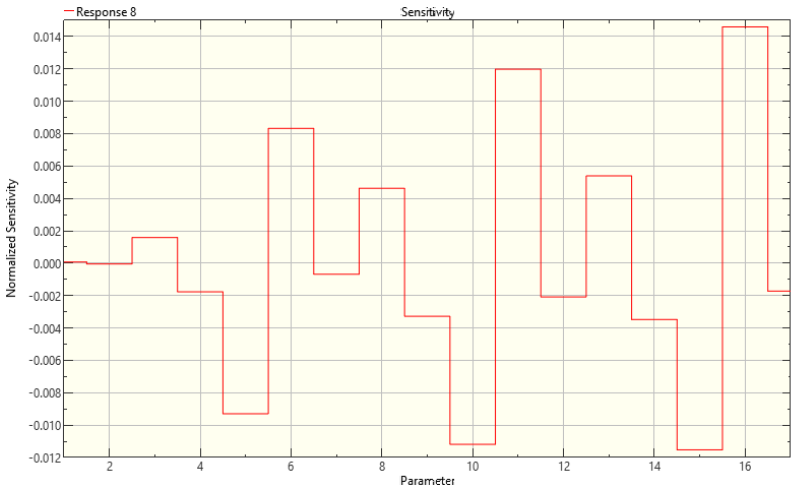

Figure 220 Sensitivity graph of the third mode shape to a change in density / SS model

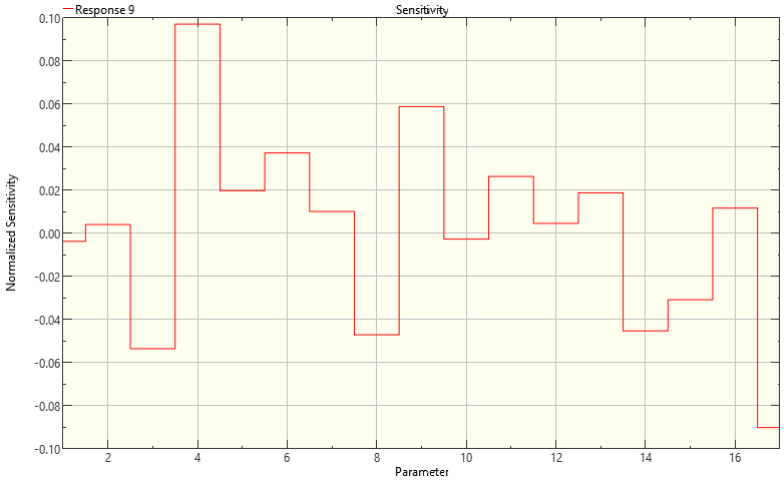

Figure 221 Sensitivity graph of the fourth mode shape to a change in density / SS model

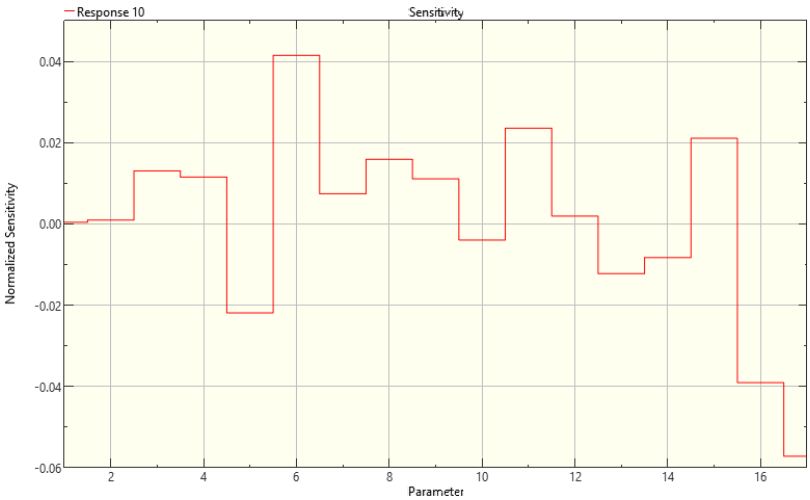

Figure 222 Sensitivity graph of the fifth mode shape to a change in density / SS model

- To a change in shear modulus

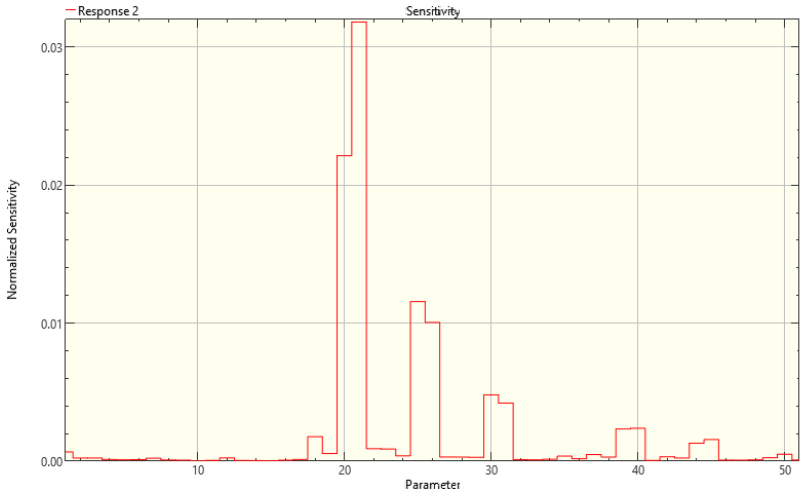

Figure 223 Sensitivity graph of the second frequency to a change in shear modulus / FB model

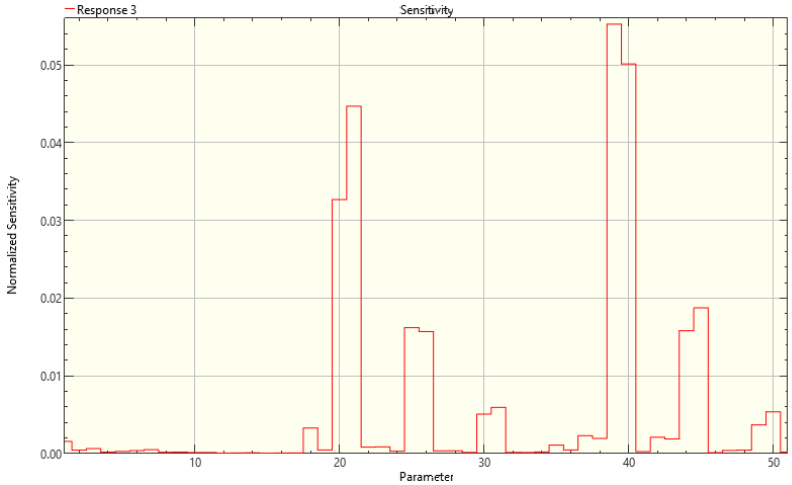

Figure 224 Sensitivity graph of the third frequency to a change in shear modulus / FB model

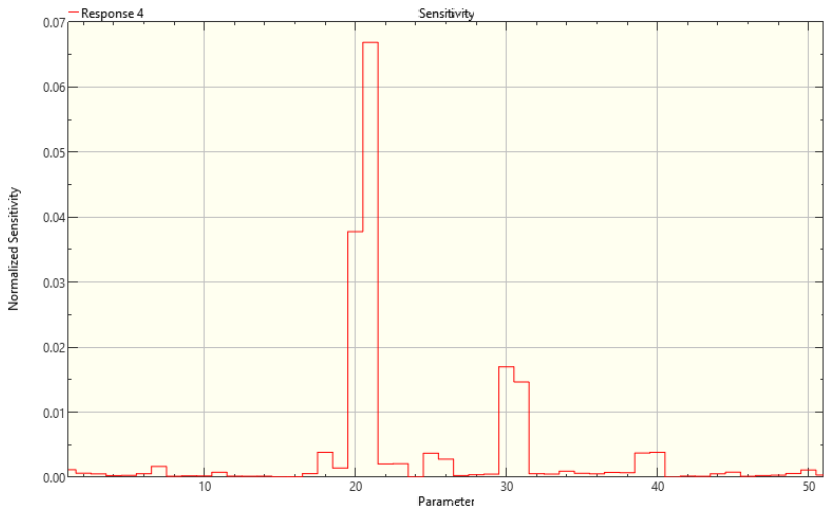

Figure 225 Sensitivity graph of the fourth frequency to a change in shear modulus / FB model

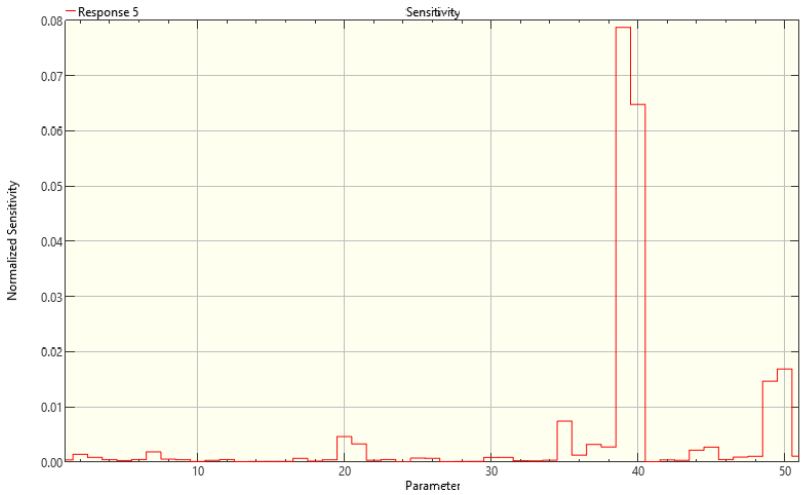

Figure 226 Sensitivity graph of the fifth frequency to a change in shear modulus / FB model

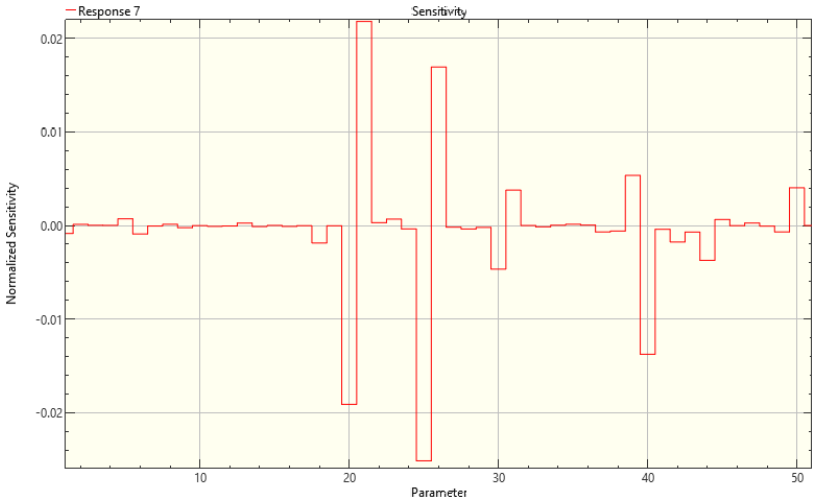

Figure 227 Sensitivity graph of the second mode shape to a change in shear modulus / FB model

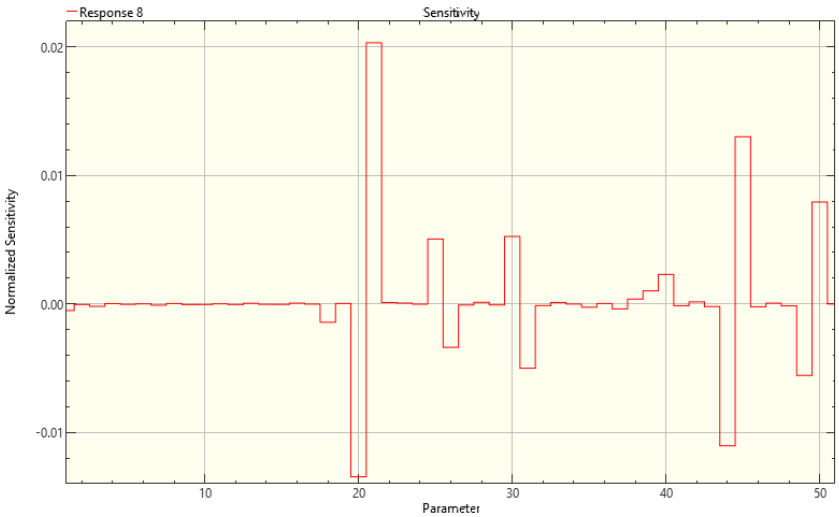

Figure 228 Sensitivity graph of the third mode shape to a change in shear modulus / FB model

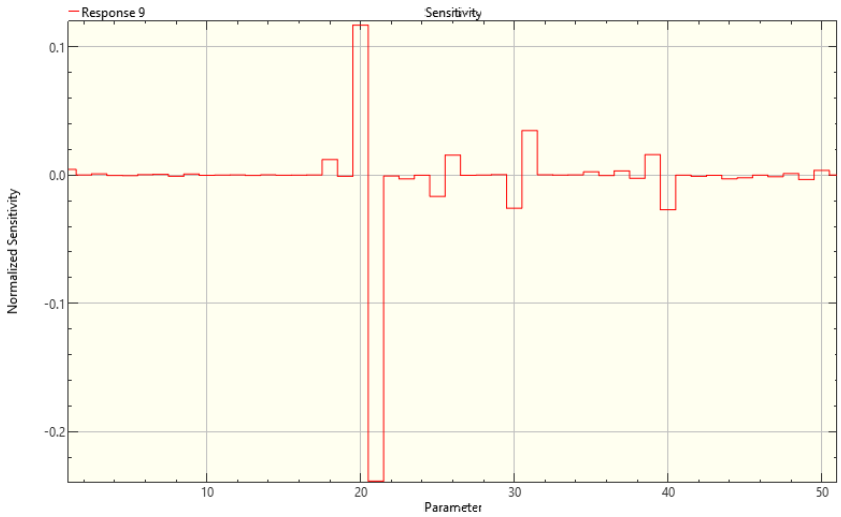

Figure 229 Sensitivity graph of the fourth mode shape to a change in shear modulus / FB model

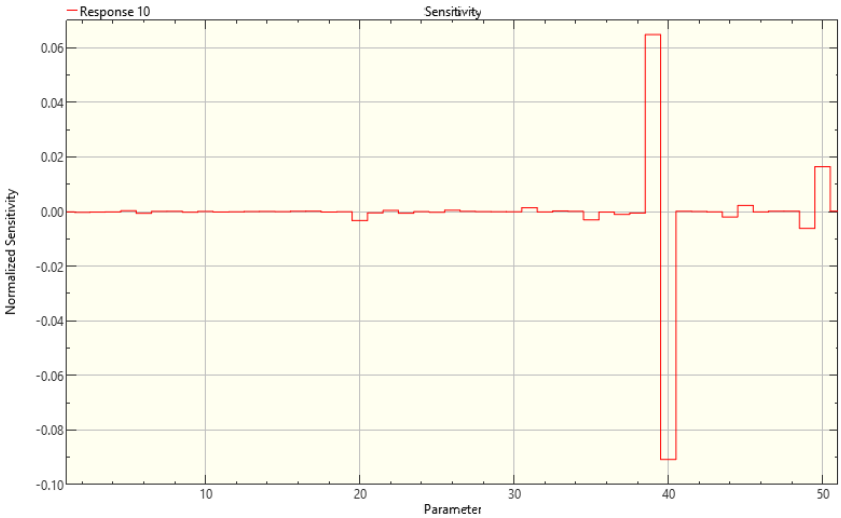

Figure 230 Sensitivity graph of the fifth mode shape to a change in shear modulus / FB model

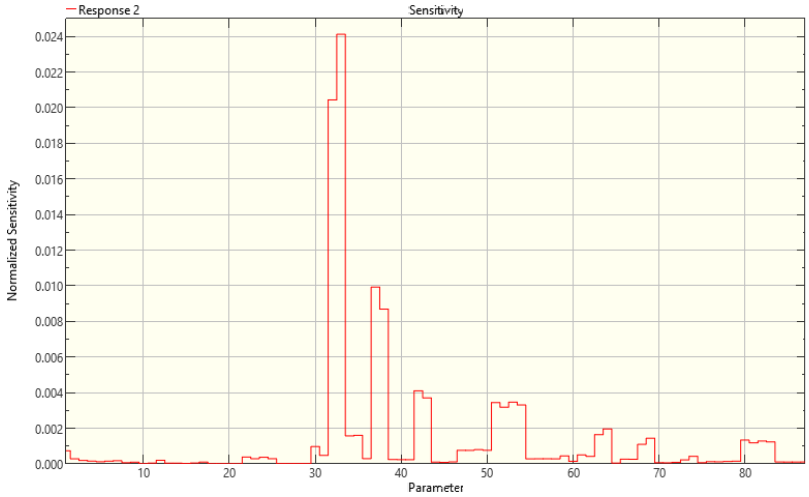

Figure 231 Sensitivity graph of the second frequency to a change in shear modulus / SB model

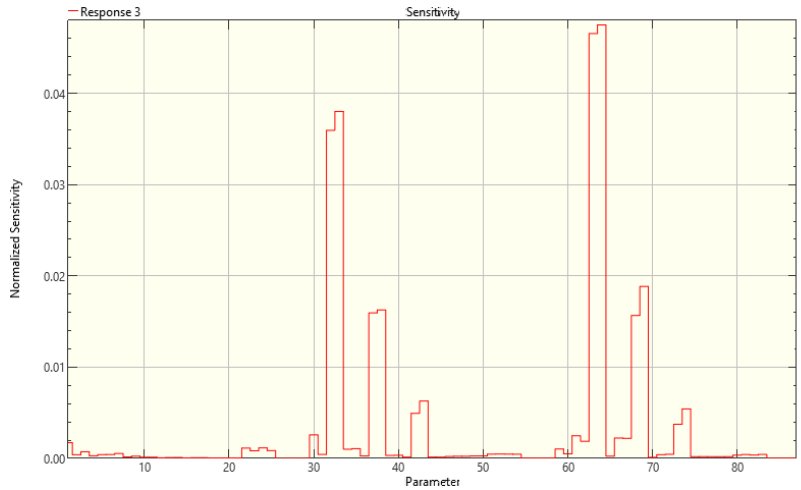

Figure 232 Sensitivity graph of the third frequency to a change in shear modulus / SB model

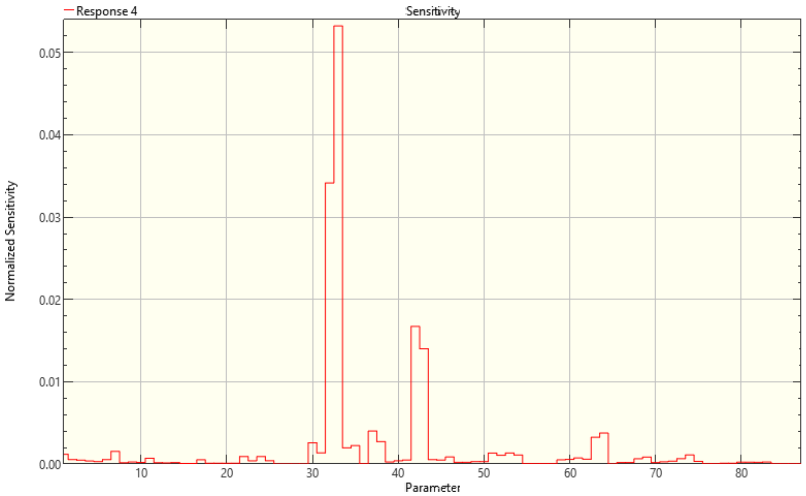

Figure 233 Sensitivity graph of the fourth frequency to a change in shear modulus / SB model

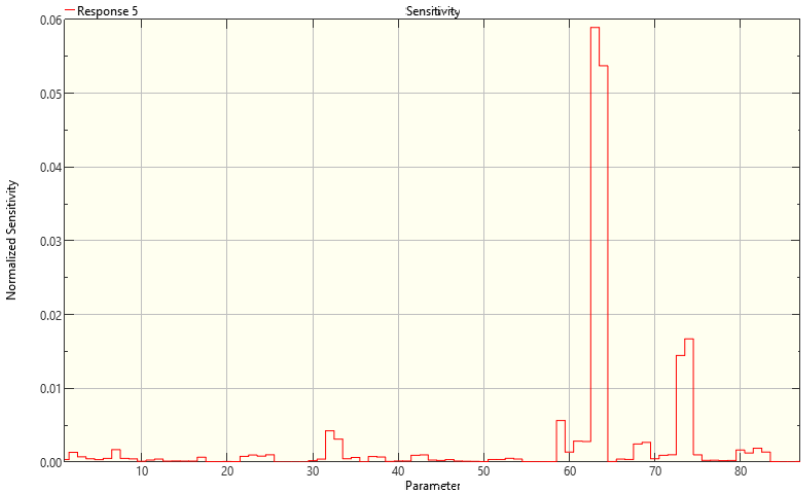

Figure 234 Sensitivity graph of the fifth frequency to a change in shear modulus / SB model

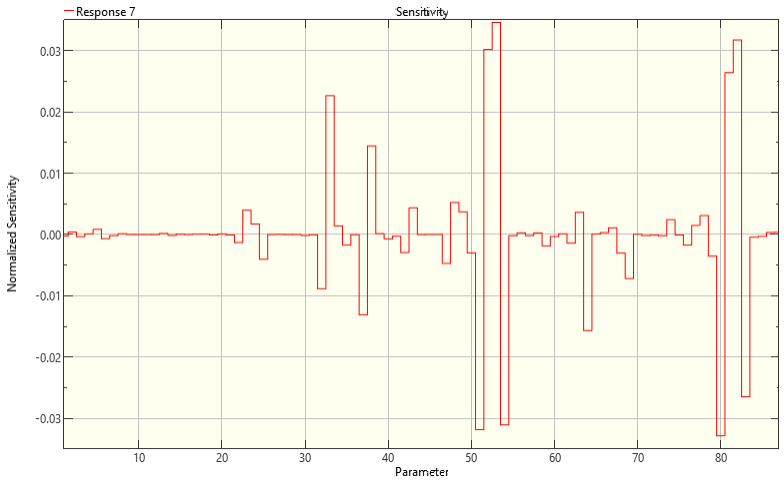

Figure 235 Sensitivity graph of the second mode shape to a change in shear modulus / SB model

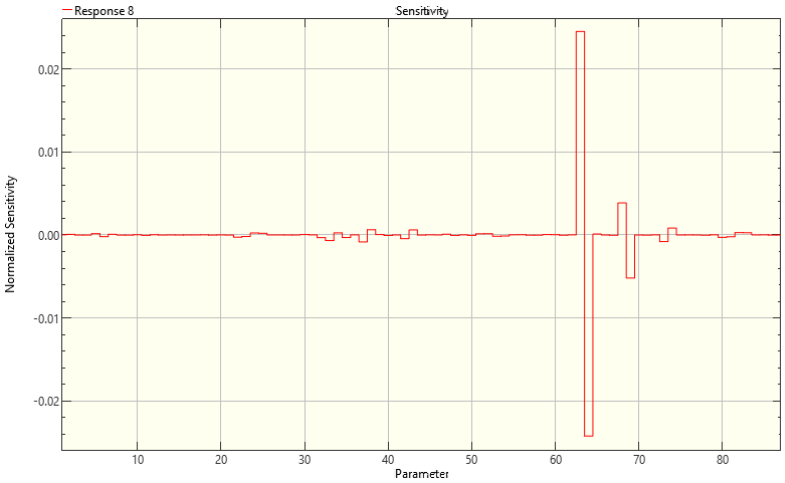

Figure 236 Sensitivity graph of the third mode shape to a change in shear modulus / SB model

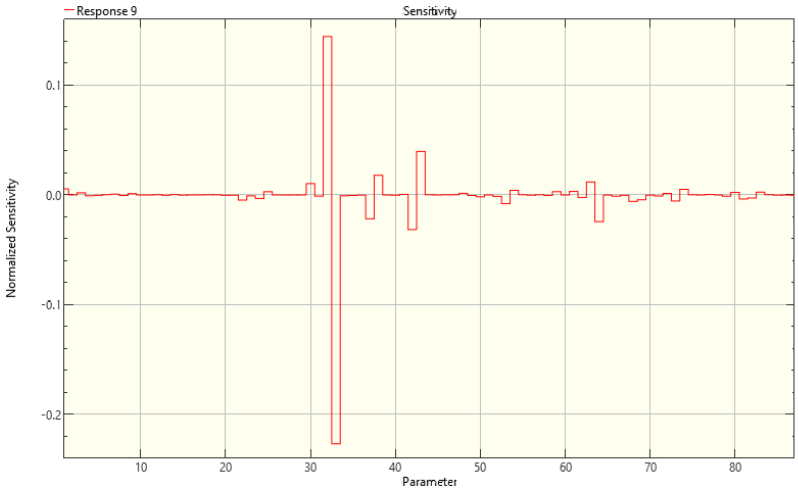

Figure 237 Sensitivity graph of the fourth mode shape to a change in shear modulus / SB model

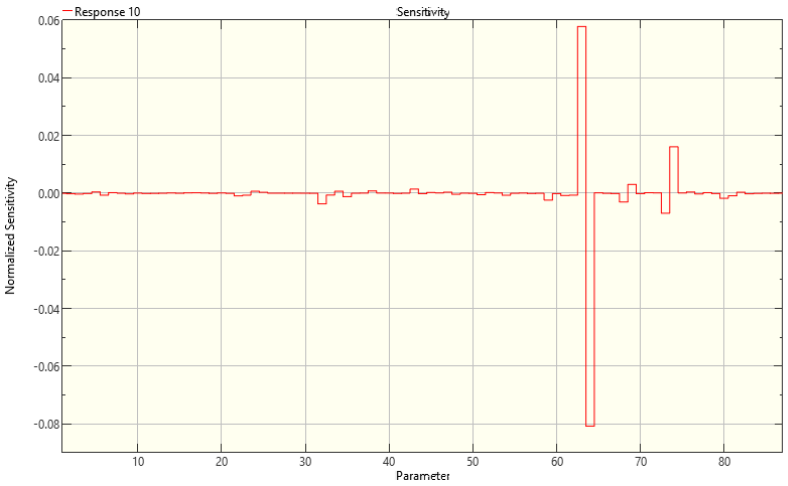

Figure 238 Sensitivity graph of the fifth mode shape to a change in shear modulus / SB model

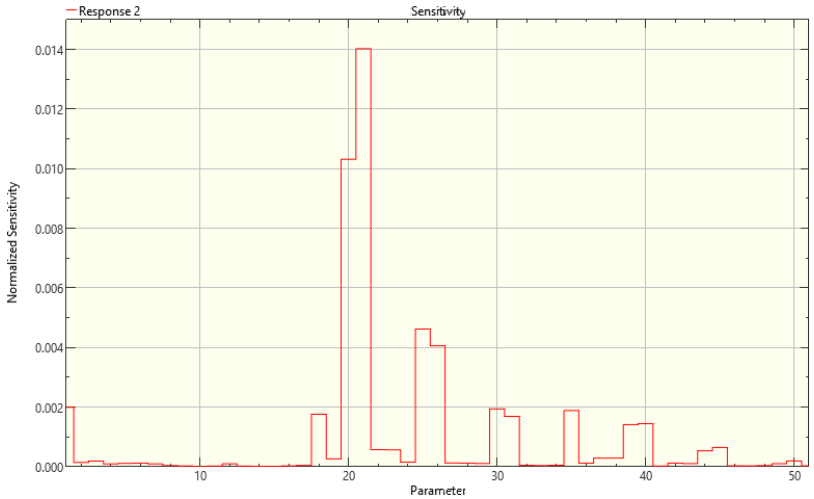

Figure 239 Sensitivity graph of the second frequency to a change in shear modulus / SS model

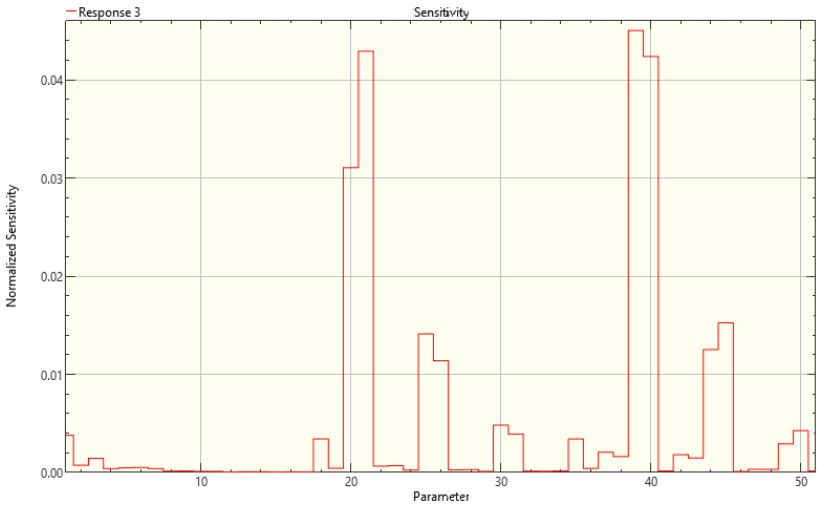

Figure 240 Sensitivity graph of the third frequency to a change in shear modulus / SS model

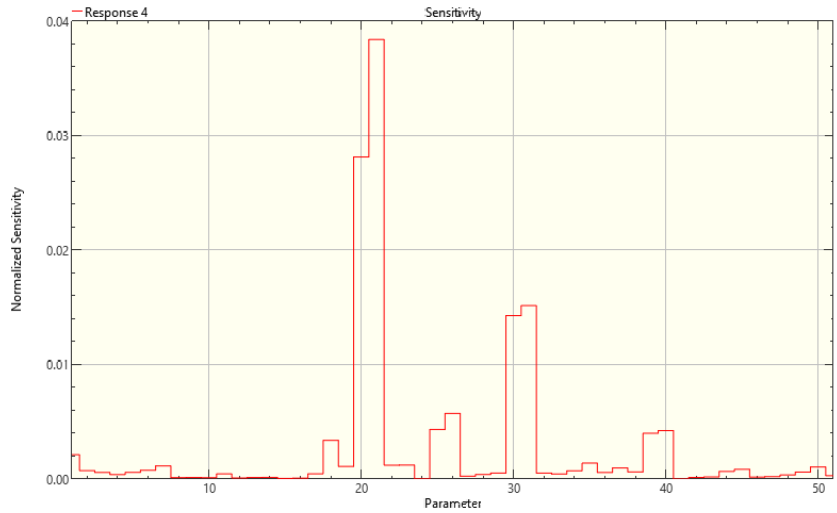

Figure 241 Sensitivity graph of the fourth frequency to a change in shear modulus / SS model

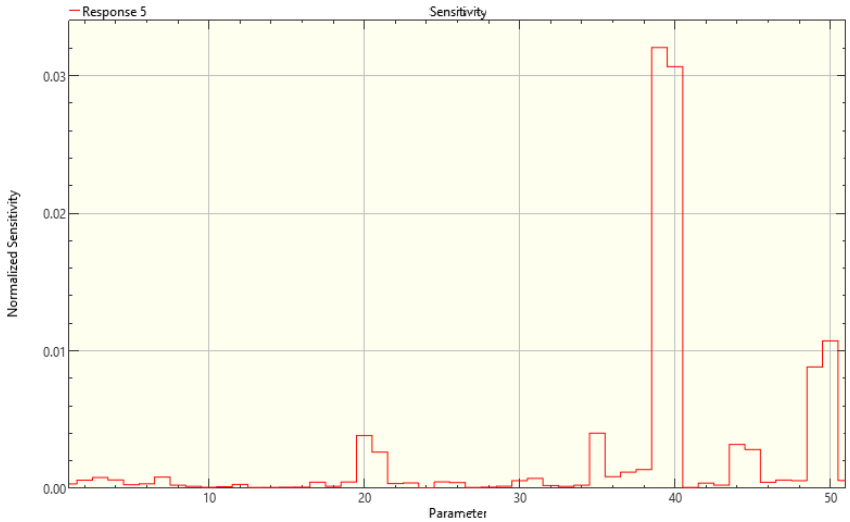

Figure 242 Sensitivity graph of the fifth frequency to a change in shear modulus / SS model

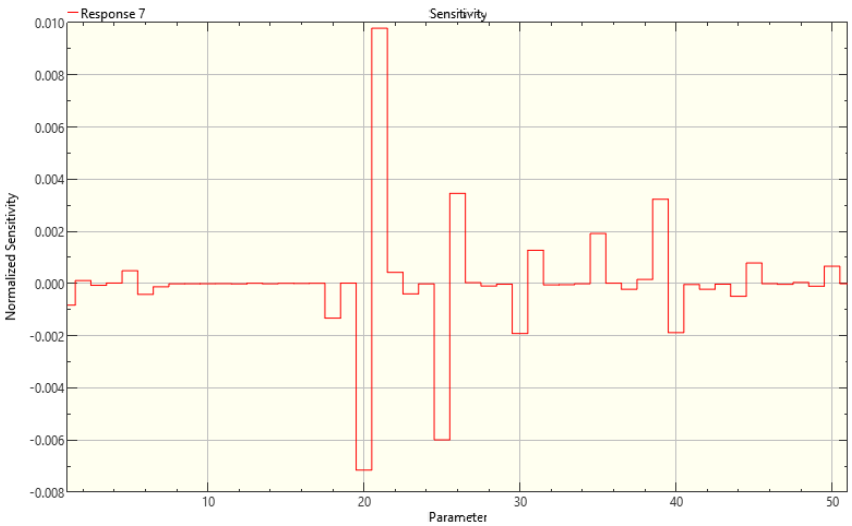

Figure 243 Sensitivity graph of the second mode shape to a change in shear modulus / SS model

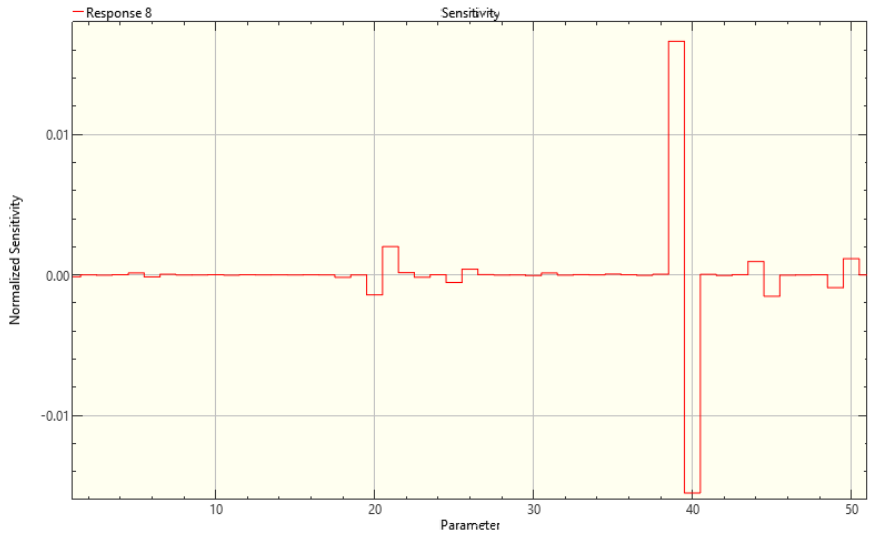

Figure 244 Sensitivity graph of the third mode shape to a change in shear modulus / SS model

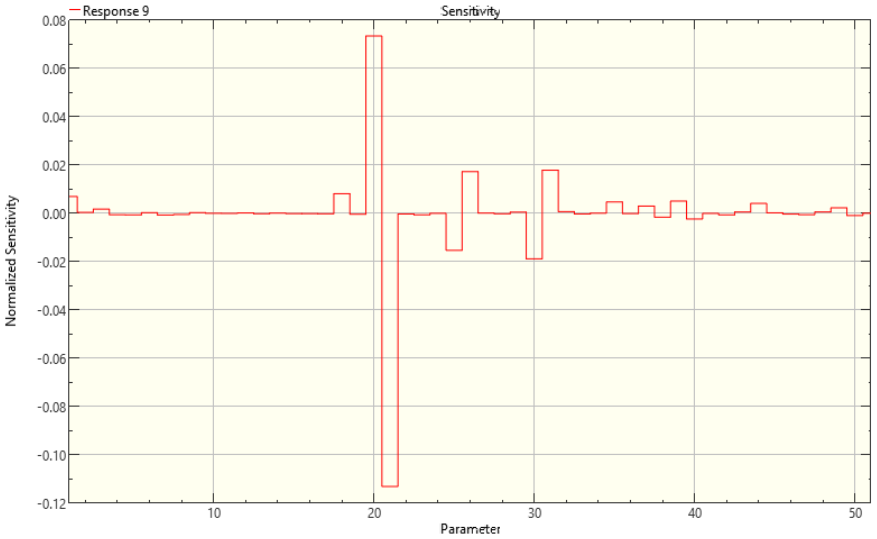

Figure 245 Sensitivity graph of the fourth mode shape to a change in shear modulus / SS model

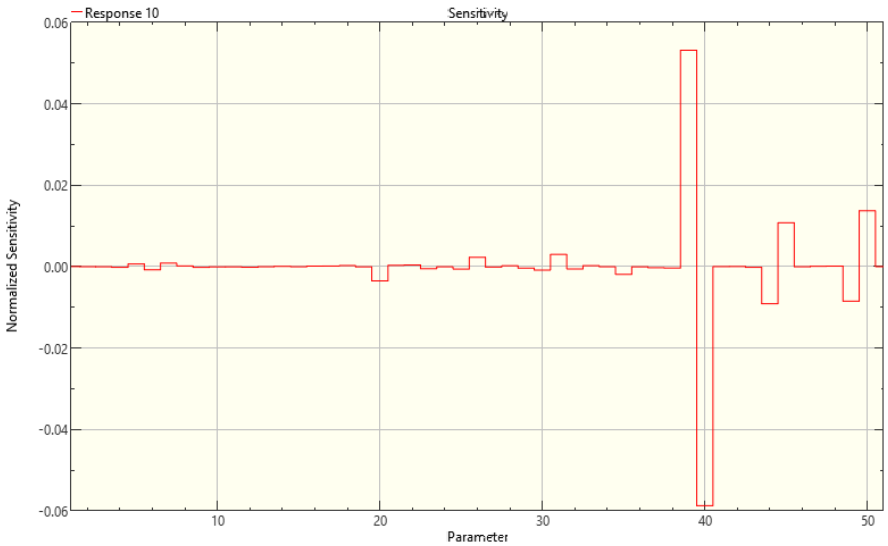

Figure 246 Sensitivity graph of the fifth mode shape to a change in shear modulus / SS model

- To a change in spring stiffness

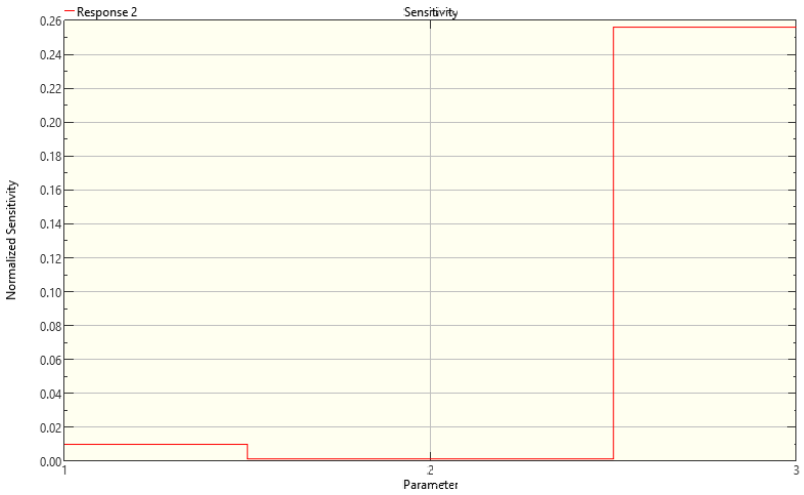

Figure 247 Sensitivity graph of the second frequency to a change in spring stiffness / SS model

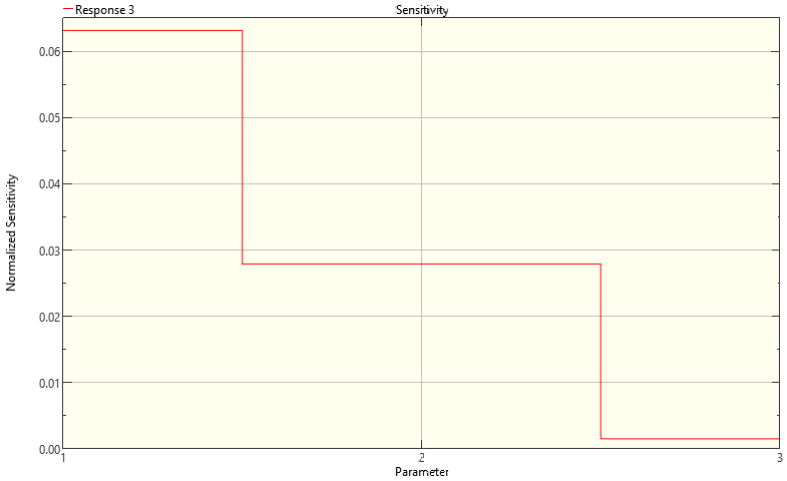

Figure 248 Sensitivity graph of the third frequency to a change in spring stiffness / SS model

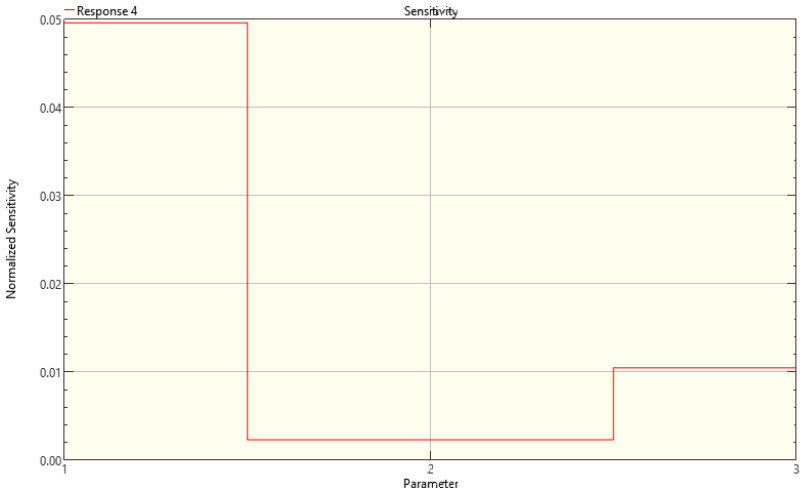

Figure 249 Sensitivity graph of the fourth frequency to a change in spring stiffness / SS model

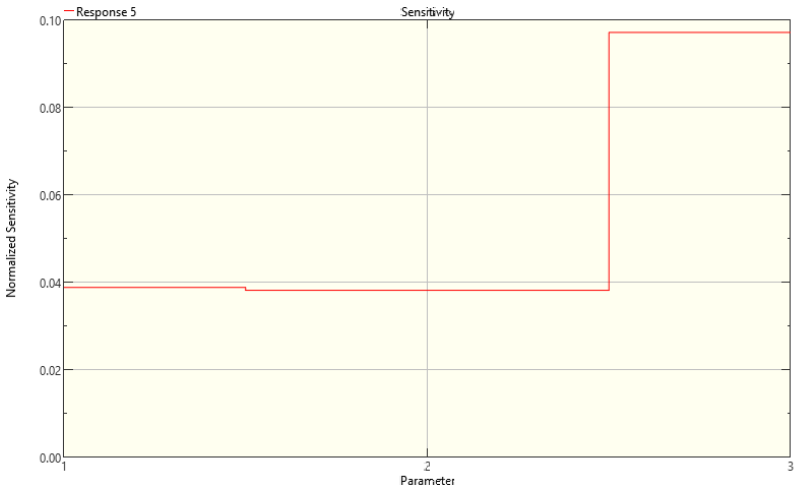

Figure 250 Sensitivity graph of the fifth frequency to a change in spring stiffness / SS model

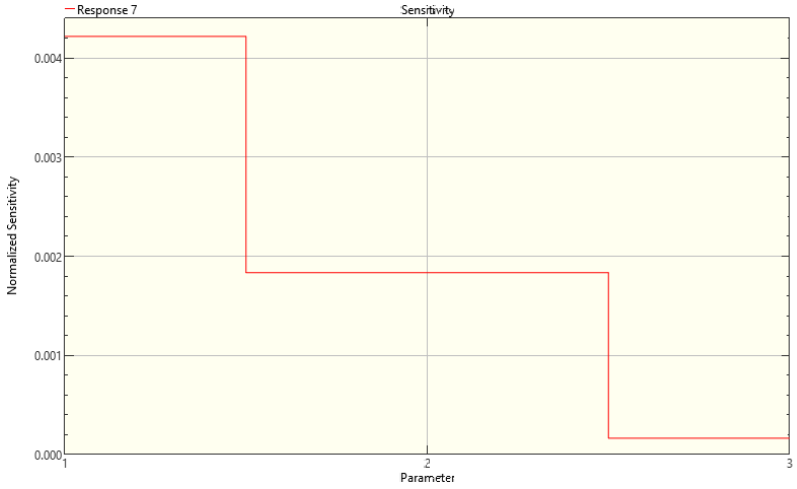

Figure 251 Sensitivity graph of the second mode shape to a change in spring stiffness / SS model

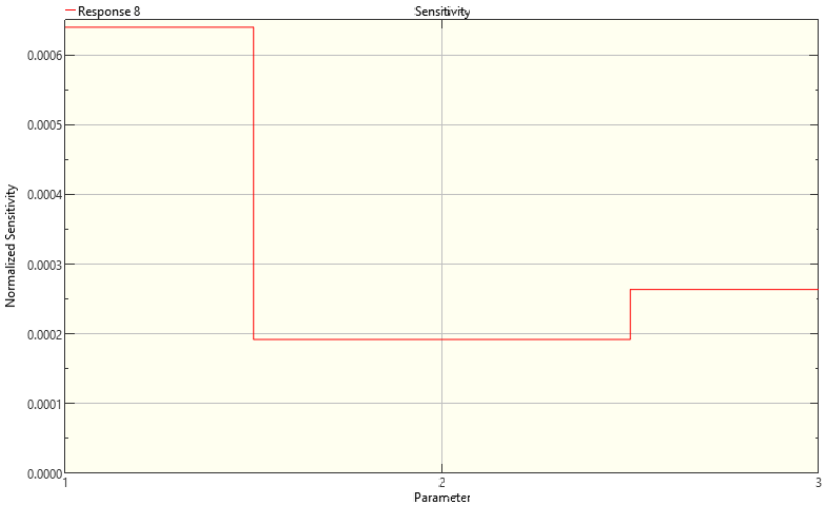

Figure 252 Sensitivity graph of the third mode shape to a change in spring stiffness / SS model

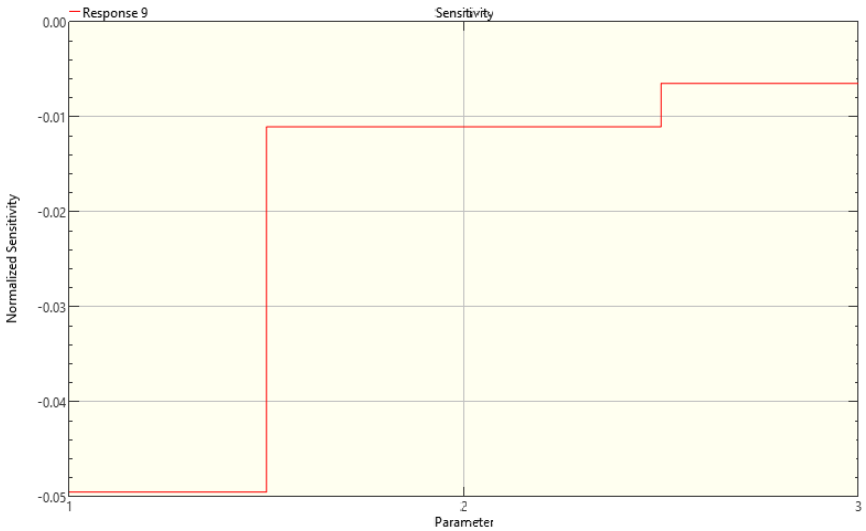

Figure 253 Sensitivity graph of the fourth mode shape to a change in spring stiffness / SS model

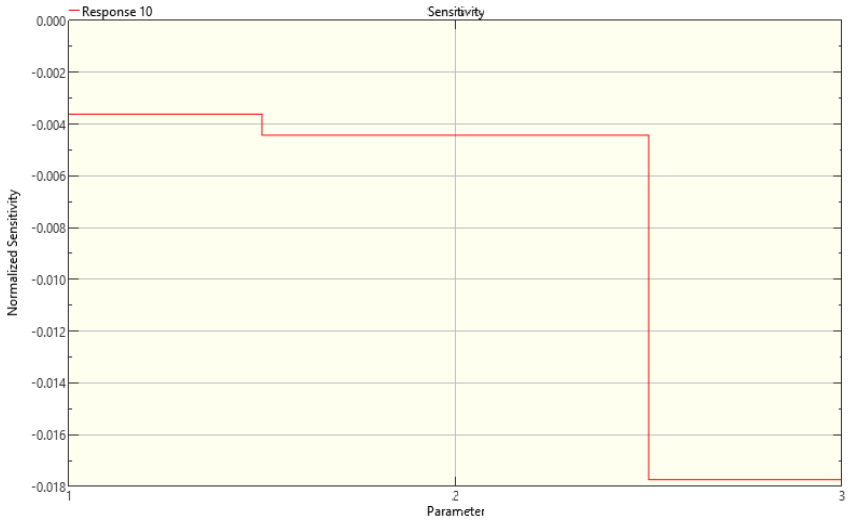

Figure 254 Sensitivity graph of the fifth mode shape to a change in spring stiffness / SS model